



Diet induced obesity model in rats: The case of high carbohydrate diet

Hamda M. Aboujassoum

A thesis submitted to University College of London for the research degree of
Doctor of Philosophy

2021

Division of Medicine
University College of London (UCL)

Declaration

I, Hamda Aboujassoum, confirm that all the work presented is my own. Where information has been derived from other sources, I confirm that this has been indicated in the thesis.

Signature:

Date:

Abstract

Global prevalence of obesity is increasing enormously and has more than doubled since 1980 as reported by World Health Organization (WHO). Currently obesity and overweight affect more than a third of the world's population, with obesity, as a disease, considered a global epidemic. Major causative factors for this epidemic are easy access to high energy-dense food, and sedentary lifestyle. Increasing body weight, associated with high fat mass, is a risk factor for metabolic syndrome (MS) affecting the function of several organs. Lifestyle intervention is a successful treatment in reversing obesity-related comorbidities. How obesity leads to the development of cardiometabolic risk and how these, in turn may be reversed with lifestyle intervention is the focus of much recent research. Therefore, the current study tested the hypothesis that high carbohydrate diet increases ectopic fat deposition, cardio-metabolic risk, and development of non-alcoholic fatty liver disease (NAFLD), which are wholly or partially reversible by diet-induced weight loss.

Male Sprague Dawley (SD) rats aged 8-9 weeks, were assigned into three groups: NC group fed with Normal chow (NC) and access to normal water *ad libitum*, CAF group fed with both diets; cafeteria style diet (CAF) and NC with 5% sugar water *ad libitum* for a period of 16 weeks, and, reversibility group (REV) fed with CAF diet and NC *ad libitum* to induce obesity and then switched to NC for three weeks duration to induce weight loss.

The CAF diet significantly increased body weight, directly related to greater consumption of this diet, compared to NC. This was associated with abnormalities in the metabolic parameters. Data from the vascular studies revealed that acetylcholine (Ach) mediated relaxation was significantly compromised following CAF feeding, suggesting endothelial dysfunction. In addition, CAF feeding induced

hepatic fat accumulation and the development of grade 3 hepatic steatosis. At the transcriptome level the CAF diet stimulated de novo lipogenesis mediated by the over-expression of sterol regulatory element binding transcription factor 1 (SREBF1) and the dysregulation of lipogenic genes. In the REV group, rats showed a trend towards weight loss, though it did not reach statistical significance (approximately 6% in three weeks). However, this decrease in weight was enough to improve metabolic parameters, to be more reflective of normal levels. Vascular studies revealed that endothelial dysfunction was not reversed by CAF withdrawal. However, great improvement was observed in hepatic steatosis. Transcriptomic analysis showed improvement in hepatic steatosis, mediated by increase in expression of genes related to fatty acid (FA) oxidation, lipid export and hepatic tissue repair.

In conclusion, the study successfully developed a diet-induced obese rat model that mimics human obesity following consumption of the regional diet (Arabian Peninsula) and demonstrated the expected metabolic changes. Further, this deterioration in metabolic function may be corrected by diet-induced weight loss. Endothelial dysfunction appeared less amenable to reversibility by short-term weight loss. However, fat accumulation around the liver decreased with slight weight loss, suggesting that lifestyle modification, especially diet is an effective strategy to address hepatic steatosis.

Impact Statement

The non-residential Ph.D. program established between the three institutes: University College London (UCL), Anti-Doping Lab Qatar (ADLQ) and Qatar University (QU) provide an opportunity for overseas student to complete their graduate studies and built a broad experience by initiating academic network and transferring scientific expertise between these institutes.

This study aimed to mimic human lifestyle and address the physiology of the development of obesity. Obesity is a disease that affects populations world-wide and resulting in increasing the rate of cardio-metabolic diseases. The evidence in this study supports the idea of the effect of diet as a significant factor in developing weight gain and obesity related comorbidities. Moreover, this study revealed that dietary intervention in association with weight loss could be a successful treatment strategy that recover obesity-related pathologies and abnormalities. Thus, lifestyle modification is the major health approach for the prevention and treatment of this condition. Highlighting the transcriptome profile of hepatic steatosis induced by obesity and reversed by weight loss, led to further insights toward developing new target molecules and biomarkers for the benefits of NAFLD treatment.

In my Ph.D. thesis I have successfully developed diet induced obesity (DIO) model using high carbohydrate diet similar to the regional diet (Arabian Peninsula). This model was the first DIO model established in the Laboratory Animal Research Center (LARC) at Qatar University. Accomplishing this study will provide me the opportunity to establish metabolic disease research studies as a researcher at LARC.

Acknowledgement

Throughout this journey, many people gave their support and encouragement toward the completion of my research project and writing my dissertation.

Firstly, I would like to deeply thank my supervisors at Qatar: Dr.Hamda Al-Naemi and Dr.Vidya Mohamed-Ali for their continuous guidance and support in my Ph.D. study. My thanks also extended to my UCL supervisors: Prof.Lucie Clapp and Prof.David Abraham for all their help.

Besides my supervisors, I would like to thank the Qatar University internal grant (QUUG-CAS-BES-13/14) for funding this project and the scholarship office at Qatar University for the financial support of my study, which helped me to build up my academic career.

My sincere thanks also go to the Laboratory Animal Research Center (LARC) at Qatar University, the Anti-Doping lab Qatar, Prof.Abraham's lab at UCL and Qatar Computing Research Center who gave me the opportunity to join their teams and access their laboratory and research facilities. Without this support and collaboration, I won't be able to conduct this research. Special thanks are extended to Dr.Nelson Orie (ADLQ) who trained me on using organ bath and supervising the contractility experiments. In Addition, I would like to express my thanks to the histopathologist at LARC Dr.Vijay Knath Govindharajan for the validation of my histology analysis.

Finally, I would like to thank my beloved family: my husband for supporting me spiritually, my three little boys and my little princess for their patience during this long journey, wishing them a successful life and bright future.

Publications and Conferences

Manuscript Ready for Publication

- **Aboujassoum H**, Mohamed-Ali V, Abraham D, Clapp L, Al-Naemi H. Cafeteria diet increased adiposity and induced hepatic steatosis in rats, are reversed with standard dietary intervention

Conference Proceedings

- **Aboujassoum H**, Orie N, Ahmed Abdi B, Clapp L, Abraham D, AlMaadheed M, Mohamed-Ali V and Al-Naemi H. A high carbohydrate diet increased adiposity and compromised vasodilation in rats. 26th European Congress on Obesity (ECO2019), 2019, Glasgow – Scotland. Obes Facts 2019;12(suppl 1):1-290.
- **Aboujassoum H**, Clapp L, Abraham D, AlMaadheed M, Mohamed-Ali V and Al-Naemi H. Cafeteria diet increased adiposity and initiated hepatic steatosis. Qatar University Annual Research Forum and Exhibition 2019. Doha – Qatar.
- **Aboujassoum H**, Orie N, Clapp L, Al-Naemi H, Mohamed-Ali V. A high carbohydrate diet increased adiposity and compromised vasodilation in rats. ARC'18, 2018, Doha, Qatar, Qatar Foundation Annual Research Conference. doi.org/10.5339/qfarc.2018.HBPD970.

Abbreviations

AALAC: American Association for Laboratory Animal Care

Abcb1a: ATP-dependent translocase

ACC1: Acetyl-CoA carboxylase 1

Ach: Acetylcholine

ACL: ATP citrate lyase

ADLQ: Anti-Doping Lab Qatar

AEE: activity-induced energy expenditure

Akt: protein kinase B

ALP: Alkaline phosphatase

ALT: Alanine aminotransferase

ANOVA: Analysis of variance

AP2: adipocyte protein 2

APE 1: apurinic/apyrimidinic endonuclease 1

Ar: Androgen receptor

AST: Aspartate aminotransferase

ATP: Adenosine triphosphate

BAT: Brown adipose tissue

BMI: Body mass index

BMR: Basal metabolic rate

BP: Blood pressure

Ca²⁺: Calcium

CaCl₂: calcium chloride

CAF: Cafeteria diet

CD36: cluster of differentiation 36

cDNA: complementary deoxyribonucleic acid

CHO: Carbohydrates

chREBP: carbohydrate regulatory element- binding protein

cm: centimeter

Cpt1a: Carnitine palmitoyltransferase 1A

cRNA: Complementary ribonucleic acid

CVDs: Cardiovascular diseases

ddH₂O: double-distilled water

DEE: diet-induced energy expenditure

dUTP: Deoxyuridine Triphosphate

DIO: diet induced obesity

DHAP: dihydroxyacetone phosphate

Dhcr7: 7-dehydrocholesterol reductase

DNA: Deoxyribonucleic acid

DNL: de novo lipogenesis

dNTP: deoxynucleotide triphosphate

DSP: Diastolic blood pressure

EC₅₀: Effective concentration 50

Ech1: Delta (3,5)-Delta (2,4)-dienoyl-CoA isomerase

ECM: Extracellular matrix

ED₅₀: Effective dose 50

EDHF: Endothelium derived hyperpolarizing factor

ELISA: enzyme-linked immunosorbent assay

eNOS: Endothelial nitric oxide synthase

ET-1: Endothelin-1

FFAs: Free fatty acids

G3P: Glyceraldehyde 3-phosphate

G6pc: glucose-6-phosphatase

Gal: Galactose

GAPDH: Glyceraldehyde 3-phosphate dehydrogenase

Gck: Glucokinase

GGT: Gamma–glutamyltransferase

GI: Gastrointestinal tract

Glc: Glucose

GLUT: Glucose transporters

gm: gram

Got1: glutamic-oxaloacetic transaminase 1

GSK: glycogen synthase kinase

Gstk1: glutathione S-transferase kappa 1

Gys2: glycogen synthase

FA: fatty acid

FABP: fatty acid binding protein

FAS: fatty acid synthase

FATP: Fatty acid transporters proteins

Fdps: Farnesyl pyrophosphate synthase

Fdft1: Farnesyl-diphosphate farnesyltransferase 1

FDR: false discovery rate

Fmo5: flavin containing dimethylaniline monooxygenase 5

Fru: Fructose

Fos: Proto-oncogene c-Fos

FOXO: Forkhead box protein O

H&E: hematoxylin and eosin

HCC: Hepatocellular cancer

HDL-c: High density lipoprotein

HFD: high fat diet

Hmgcs1: Hydroxymethylglutaryl-CoA synthase

Hmox1: Heme oxygenase 1

Hrs: Hours

Hspb1: Heat shock protein beta-1

Idh2: Isocitrate dehydrogenase w

Junb: Transcription factor jun B

Id3: inhibitor of DNA binding 3

IL-1: Interleukin 1

IL-6: Interleukin 6

IL-13: Interleukin 13

IR: Insulin receptor

IRS: insulin receptor substrate

IRS 1/2: insulin receptor substrates 1 and 2

I_{max}: Maximum relaxation effect

iNOS: Inducible nitric oxide synthase

IVC: Individual ventilation cages

IVT: *in Vitro* Transcription

LARC: Laboratory Animal Research Center

LDL: low density lipoprotein

Ldi1: Linalool dehydratase isomerase

Kcal: kilocalories

KCl: potassium chloride

KH₂PO₄: potassium dihydrogen phosphate

mg: microgram

μl: microliter

mm: micrometer

M: mole

MAP: Mean arterial pressure

Mapkapk2: MAPK activated protein kinase 2

MCP-1: monocyte chemoattractant protein 1

MgCl₂: Magnesium chloride

Mg/dL: milligrams per deciliter

Min: minutes

ml: milliliter

mm: millimeter

mM: millimole

mm Hg: millimeters of mercury

mmol/L: millimole per liter

MAPK: mitogen-activated protein kinase

MS: Metabolic syndrome

MLCK: Myosin light chain kinase

MMPs: Matrix Metalloproteinases

MNC: mononuclear cells

NA: Noradrenaline

NADH: nicotinamide adenine dinucleotide

NaCl: Sodium chloride

NaHCO₃: sodium bicarbonate

Na₂HPO₃: disodium phosphate

NAFLD: Non-alcoholic fatty liver disease

NASH: Non-alcoholic steatohepatitis

NC: Normal chow

ng: nanogram

NH₂PO₄: monosodium phosphate

nm: nanometer

nM: nanomole

nNOS: Neuronal nitric oxide synthase

NO: Nitric oxide

NOS: Nitric oxide synthase

Nqo1: NADPH quinone dehydrogenase 1

OAA: oxaloacetate

OD: optical density

PAI-1: plasminogen activator inhibitor-1

PBS: Phosphate buffered saline

PCR: Polymerase chain reaction

PDGF: Platelet-derived growth factor

PKC: 3-phosphoinositide-dependent protein kinase 1

PEP: phosphoenolpyruvate

PGI₂: Prostacyclin

PI3K: phosphatidylinositol-3-kinase

PMNC: polymorphonuclear leukocytes cells

Pnpla2: Patatin-like phospholipase domain-containing 2

PPAR γ : proliferator-activated receptor gamma

PPi: Pyrophosphate

Ppp2r5e: Protein phosphatase 2 regulatory subunit B epsilon

Prlr: Prolactin receptor

PSS: Physiological salt saline

Pygl: glycogen phosphorylase L

QCRC: Qatar Computing Research Center

QU: Qatar University

REV: Reversible group

RNA: ribonucleic acid

Rpm: revolution per minute

RT: Room temperature

RT: Reverse transcription

SAT: subcutaneous adipose tissue

SBP: Systolic blood pressure

Sc5d: Sterol-C5-desaturase

SCD1: Stearol-CoA desaturase

SD: Sprague Dawley

SEM: Standard error of the mean

sGC: Guanylyle cyclase

Socs3: Suppressor of cytokine signaling 3

Sqle: Squalene monooxygenase

SREBF1: sterol regulatory element-binding transcriptional factor 1

SST: Serum Separator Tube

TAC: Transcriptome analysis console

TCA: Tricarboxylic Acid

TDT: terminal deoxynucleotidyl transferase

TEE: Total energy expenditure

TG: Triglyceride

TGF- β 1: Transforming growth factor β 1

TIMPs: Tissue inhibitor metalloproteinases

Trib3: Tribbles pseudokinase 3

TXA₂: Thromboxane

U/ml: unit per microliter

UAE: United Arab Emirates

UDG: Uracil-DNA glycosylase

UDP: Uridine diphosphate

USA: United states of America

US: United states

UTP: Uridine triphosphate

VAT: Visceral adipose tissue

VLDL: Very low-density lipoprotein

VPR: Volume pressure recording

VSMCs: Vascular smooth muscle cells

WAT: White adipose tissue

WHO: World Health Organization

α -SMA: Alpha smooth muscle actin

Table of Contents

Declaration.....	2
Abstract.....	3
Impact Statement	5
Acknowledgement	6
Publications and Conferences	7
Abbreviations	8
List of Tables	22
List of Figures	24
CHAPTER 1: INTRODUCTION	27
1.1 Obesity.....	28
1.1.1 History	28
1.1.2 Definition.....	28
1.1.3 Epidemiology	30
1.1.4 Etiology and proposed causative factors	32
1.1.5 Adiposity and Obesity Development	34
1.2 Diet	35
1.2.1 Carbohydrates.....	35
1.2.2 Metabolism of carbohydrates	37
1.2.2.1 Glycogenesis and Glycogenolysis.....	37
1.2.2.2 Glycolysis and Glucogenesis.....	40
1.2.3 Lipids	43
1.2.3.1 Lipogenesis.....	44
1.3 Food palatability (food environment and lifestyle)	46
1.4 Sedentary lifestyle and energy metabolism.....	48
1.5 Obesity risks	50
1.5.1 Obesity and Type 2 diabetes.....	51
1.5.1.1 Insulin signaling pathway.....	51
1.5.1.2 Insulin Resistance.....	54
1.5.1.3 Inflammation	54

1.5.2	Obesity and Vascular function.....	55
1.5.2.1	Structure and function of vascular system.....	55
1.5.2.2	Vascular tone and NO signaling	56
1.5.2.3	Endothelial dysfunction.....	59
1.5.3	Obesity and Liver diseases	59
1.5.3.1	Structure and function.....	59
1.5.3.2	Liver function enzymes	61
1.5.3.3	Hepatic Lipid Metabolism.....	62
1.5.3.4	Hepatic Glucose Metabolism	63
1.5.3.5	Non-alcoholic fatty liver disease (NAFLD).....	63
1.6	Reversal of obesity related health outcomes through lifestyle intervention.....	65
1.6.1	Modifiable and non-modifiable risk factors.....	66
1.6.2	Lifestyle intervention.....	66
1.7	Aims and Objectives	69
CHAPTER 2:	MATERIALS AND METHOD	71
2.1	Animals	72
2.2	CAF Diet Preparation.....	74
2.3	Blood pressure measurements.....	76
2.4	Animal dissection and sample collection	77
2.5	Blood samples processing.....	78
2.6	Organ bath and vascular reactivity.....	78
2.7	Histological studies.....	79
2.7.1	Fixation	79
2.7.2	Sample processing.....	79
2.7.3	Embedding process.....	80
2.7.4	Sectioning.....	81
2.7.5	Staining of paraffin-embedded tissue.....	81
2.7.5.1	Hematoxylin and Eosin staining	81
2.7.5.2	Picro-sirius red staining	83
2.8	Biochemical analysis	84

2.9	Measuring insulin level using ELISA.....	84
2.10	Triglyceride quantification in liver tissue.....	85
2.10.1	Tissue samples preparation.....	85
2.10.2	Assay Procedure.....	86
2.10.3	Data Analysis	86
2.11	Transcriptome studies	87
2.11.1	RNA Extraction.....	87
2.11.2	RNA concentration and purity	88
2.11.3	Reverse Transcription	88
2.11.4	RNA Quantification using Real-Time PCR.....	89
2.11.5	Whole Transcript (WT) Expression Arrays	89
2.11.5.1	Synthesize First-Strand cDNA.....	91
2.11.5.2	Synthesize Second-Strand cDNA.....	91
2.11.5.3	Synthesis of cRNA by in Vitro Transcription.....	92
2.11.5.4	Purify cRNA	92
2.11.5.5	Assess cRNA yield and size distribution	93
2.11.5.6	Synthesis 2 nd - Cycle single-Strand cDNA.....	93
2.11.5.7	Hydrolyse RNA using RNase H.....	94
2.11.5.8	Purify 2 nd -Cycle Single-Stranded cDNA	94
2.11.5.9	Fragment and label Single-Strand cDNA	95
2.11.5.10	Using GeneTitan™ instrument	96
2.12	Statistical Analysis	97
CHAPTER 3:	RESULTS: HIGH CARBOHYDRATE DIET DEVELOPS A DIET-INDUCED	
OBESITY MODEL IN THE RAT	98	
3.1	Introduction.....	99
3.2	Body weight gain	101
3.3	Food consumption	108
3.4	Water intakes	112
3.5	Insulin and glucose levels	115
3.6	Lipid profile	117

3.7	Discussion.....	118
CHAPTER 4: RESULTS: HIGH CARBOHYDRATE DIET COMPROMISED VASODILATION AND INDUCED NAFLD IN RATS		124
4.1	Introduction.....	125
4.2	Effect of DIO on Vascular Function	128
4.2.1	Blood Pressure	128
4.2.2	Vasoconstriction with Noradrenaline (NA)	130
4.2.3	Vasorelaxation with Acetylcholine (Ach)	132
4.3	Effect of DIO on Liver	134
4.3.1	Liver weight and appearance	134
4.3.2	Liver function and lipid profile.....	137
4.3.3	Hepatic Triglycerides	137
4.3.4	Liver histological studies and the development of NAFLD.....	139
4.4	Discussion.....	142
CHAPTER 5: RESULTS: LIVER TRANSCRIPTOME ANALYSIS		148
5.1	Introduction.....	149
5.2	Gene expression studies: Microarray analysis in CAF-fed livers	153
5.2.1	Pathway Analysis	156
5.2.1.1	Effect of CAF on lipid metabolism pathways	156
5.2.1.2	Effect of CAF on inflammation, oxidative stress and cellular processes pathways	165
5.2.1.1	Effect of CAF on Glucose metabolism pathways	162
5.3	Gene expression analysis: Microarray analysis in REV livers	168
5.3.1	Pathway Analysis	171
5.3.1.1	Effect of REV on Glycolysis, Gluconeogenesis, and glycogen metabolism pathways	171
5.3.1.2	Effect of REV on adipogenesis and lipid droplet metabolism pathways	174
5.3.1.3	Effect of REV on inflammation, oxidative stress and cellular process pathways	178
5.4	Discussion.....	182
CHAPTER 6: CONCLUSION AND FUTURE DIRECTION		193
6.1	Developing DIO model of high carbohydrate diet.....	194

6.2	The prevalence of obesity-related comorbidities.....	195
6.3	Whole transcriptome analysis of liver tissue	195
6.4	Dietary intervention and reversal of body weight and changes associated with weight gain	195
6.5	Limitations of the study	196
6.6	Concluding Remarks.....	199
6.7	Future directions	199
APPENDICES.....		235

List of Tables

Table	Page
Table 1: Classification of overweight and obesity according to BMI .	29
Table 2: Obesity rates in selected countries.....	31
Table 3: Classes of Carbohydrates	36
Table 4: Criteria for Clinical Diagnosis of Metabolic Syndrome	50
Table 5: Nutritional content of NC and CAF diets.....	74
Table 6: Nutritional contents for food items.....	75
Table 7: CAF diet combinations provided to CAF group throughout the study..	75
Table 8: Histological features used in NAFLD evaluation and grading	83
Table 9: Master Mix of reverse transcriptase reaction.....	88
Table 10: Thermal cyclor incubation of reverse transcriptase reaction.....	89
Table 11: First-Strand Master Mix.....	91
Table 12: Second-Strand Master Mix.....	91
Table 13: IVT Master Mix.....	92
Table 14: 2nd-Cycle ss-cDNA Master Mix.....	94
Table 15: Fragmentation Master Mix.....	96
Table 16: Labeling Master Mix.....	96
Table 17: Lipid profile for obese and reversible rats.....	117
Table 18: Blood pressure measurements (mmHg) for NC and CAF groups.	129
Table 19: Blood pressure measurements (mmHg) for NC and REV groups.....	129
Table 20: Liver weight and body weight for obese and reversible rats.	135
Table 21: Liver function for obese and reversible rats.....	137
Table 22: Grading of hepatic steatosis.....	141
Table 23: List of differentially expressed genes related to lipid metabolism pathway in CAF vs NC.....	157
Table 25: List of differentially expressed genes related to inflammation, oxidative stress response and cellular processes pathways in CAF vs NC.	165

Table 24: List of differentially expressed genes related to Glucose metabolism pathway in CAF vs NC.....	162
Table 26: List of differentially expressed genes related to glycolysis, gluconeogenesis and glycogen metabolism pathways in REV vs NC-REV.	171
Table 27: List of differentially expressed genes related to adipogenesis and lipid droplet metabolism pathways in REV vs NC-REV.	174
Table 28: : List of differentially expressed genes related to oxidative stress pathway in REV vs NC-REV.	178

List of Figures

Figure	Page
Figure 1: Glycogenesis and Glycogenolysis.....	39
Figure 2: Glycolysis and Gluconeogenesis.	42
Figure 3: Process of De Novo lipogenesis in the liver.	45
Figure 4: Insulin signaling pathways.	53
Figure 5: Endothelial nitric oxide regulation of vascular smooth muscle cells.....	58
Figure 6: Structure of liver lobule	61
Figure 7: Pathophysiology of NAFLD.....	65
Figure 8: Spectrum of Non-alcoholic fatty liver disease (NAFLD).....	68
Figure 9: Rodent model study design.....	73
Figure 10: Timeline for blood pressure (BP) measurement.	77
Figure 11: Illustration of thoracic aorta anatomy.....	79
Figure 12: Steps of sample processing for histological studies.	80
Figure 13: Hematoxylin and Eosin staining steps.....	82
Figure 14: Insulin assay standard curve.....	85
Figure 15: Whole Transcript (WT) PLUS Amplification and Labeling Process.....	90
Figure 16: Effect of CAF diet on body weight.	102
Figure 17: Initial and final individual body weights of NC-fed rats.....	102
Figure 18: Initial and final individual body weights of CAF-fed rats.....	103
Figure 19: External body size of NC and CAF fed rats.....	104
Figure 20: Visceral organs of NC and CAF fed rats in the abdominal cavity.....	104
Figure 21: Body weights of NC and REV rats before and after reversibility.	105
Figure 22: External body size of NC and REV rats.....	106
Figure 23: Visceral organs of NC and REV rats in abdominal cavity.	107
Figure 24: Food consumption of NC group.	109
Figure 25: Food consumption of CAF group.	110
Figure 26: Food consumption of the reversible group.	111

Figure 27: Water intake for CAF and NC groups.....	113
Figure 28: Water intake for reversible group.	114
Figure 29: Effect of CAF diet and reversible diet on glucose and insulin level.....	117
Figure 30: Effect of CAF diet on vasoconstriction of aortic ring.	130
Figure 31: Diet reversible effect on vasoconstriction of aortic ring.....	131
Figure 32: Effect of CAF diet on endothelial-dependent relaxation.....	132
Figure 33: Effect of diet reversible on endothelial-dependent vasorelaxation.	133
Figure 34: Gross morphology of liver tissue.	136
Figure 35: Quantification of the TG content in the liver.	138
Figure 36: Liver histological studies.	140
Figure 37: Differentially Expressed genes between CAF and NC	154
Figure 38: Hierarchical clustering analysis of differentially expressed genes in liver of CAF vs NC.....	155
Figure 39: Effect of CAF diet on the expression of cholesterol metabolism pathway.....	159
Figure 40: Effect of CAF on the expression of cholesterol biosynthesis pathway.	160
Figure 41: Effect of CAF on the expression of Adipogenesis pathway.	161
Figure 42: Effect of CAF on the expression of glycolysis and gluconeogenesis pathways	163
Figure 43: Effect of CAF on the expression of glycogen metabolism pathway.	164
Figure 44: Effect of CAF on the expression of TGF Beta signaling pathway.	166
Figure 45: Effect of CAF on the expression of insulin signaling pathway.....	167
Figure 46: Differentially Expressed genes between REV and NC-REV Livers	169
Figure 47: Hierarchical clustering analysis of differentially expressed genes in liver of REV vs NC-REV.	170
Figure 48: Effect of REV on the expression of glycolysis and gluconeogenesis pathways.	172
Figure 49: Effect of REV on the expression of glycogen metabolism pathway.	173
Figure 50: Effect of REV on the expression of Adipogenesis pathway.	176
Figure 51: Effect of REV on the expression of lipid metabolism droplet pathway.	177
Figure 52: Effect of REV on the expression of oxidative stress pathway.	180

Figure 53: Effect of REV on the expression of MAPK signaling pathway.	181
Figure 54: Schematic summary of transcriptomic study.	192

CHAPTER 1: INTRODUCTION

1.1 Obesity

1.1.1 History

“We don’t live our own time alone, we carry our history with us” Gaarder, 1995. The obesity that is observed now is not a new phenomenon; it has its origin 50,000 years ago. History, and the study of evidence from the Stone Age, showed that human beings have always had the genetic and physiological propensity to be fat. Many artifacts have been discovered and dated the origin of obesity. Through the ages, several statues share the same figures, clear abdominal obesity and mostly females. The best known of these artifacts is the Venus of Willendorf that is now in the Vienna Museum of Natural History. Similar figures are seen all over the world and in all cultures, especially among the pre-Columbian people in North and South America. These artifacts attest to the fact that obesity has a long history (1, 2).

1.1.2 Definition

Obesity is defined as a condition of abnormal or excessive accumulation of fat or adipose tissue, which may impair human health. The American Medical Association defined obesity as a chronic, metabolic disease (3). Also, both the accumulation of fat and its distribution within the body are associated with metabolic complications. Abdominal fat deposition is a significant risk factor for developing obesity related diseases.

Obesity and overweight are assessed by Body mass index (BMI), the most commonly used procedure. It is defined as the weight in kilograms divided by the square of the height in meters (kg/m^2). Using this, people are categorized into different obesity levels: Overweight (BMI 25-30 kg/m^2), obese (BMI >30 kg/m^2) severely obese (BMI >35 kg/m^2), morbidly obese (BMI >40 kg/m^2) (Table 1) (4).

A positive correlation between BMI and various comorbidities has been observed. As BMI increased, the risk of comorbidities increased as well, which makes obesity often an independent risk factor for certain diseases. There is some evidence showed that the level of obesity leads to the related comorbidities, however may vary by geographical regions. For example, China and Japan used BMI cut-offs of 28 and 25 Kg/m² respectively for increased disease outcomes (5, 6). However, the WHO recommends a BMI > 27.5 kg/m² to be used as a cut-off for all Asian populations (7). The level of obesity has also a role in mortality and life expectancy. The lifespan of morbidly obese (BMI >40 kg/m²) individuals showed to be reduced by about 8-10 years (8).

Table 1: Classification of overweight and obesity according to BMI (4) .

Classification	BMI	Risk of comorbidities
Under weight	< 18.5	Low (but risk of other clinical problems increased)
Healthy weight	18.5 – 24.99	Average
Overweight	≥ 25	Average
Obese class I	30 – 34.99	Moderate
Obese class II	35 – 39.99	Severe
Obese class III	≥ 40	Very severe

Adapted from WHO, 2000

1.1.3 Epidemiology

The global prevalence of obesity is increasing enormously. The rate has more than doubled since 1980 as reported by World Health Organization (WHO). Both developed and developing countries are affected by this problem. Currently obesity and overweight affect more than a third of the world's population (9). Indeed, obesity, as a disease, is considered a global epidemic. If this trend continues to rise, 38% of the world's population will be overweight and 20% will be obese by 2030 (10). The current obesity epidemic is widely believed to have its origins in USA and Europe. In the USA, the trend between 1960 and 1994 increased markedly to reach 23%, making 55% of American populations overweight or obese (11). Unfortunately, in the following decade the prevalence jumped from 23% to 35% by 2011-2012 (12). In Europe, adult obesity increased from 13 to 17% between 1992 and 2005 (13).

The obesity epidemic is also sweeping across the Middle East, making obesity one of the major health concerns in the region. Kuwait had the highest obesity prevalence in the Middle East. It ranked the second most obese nation in the world after the US, with 36% in males and 48% in female (14). In the Kingdom of Saudi Arabia (KSA), the rate of obesity is increasing every year by 1.5% for women and 4.1 for men (15). A recent study reports that in the United Arab Emirates (UAE), 20% of the population suffer from obesity (16). Qatar is not exempt from this, with a prevalence of overweight and obesity reported as 70.1% in 2012, interestingly higher in males compared to females, 71.8% and 68.3% respectively (17). Obesity rates in selected countries is shown in Table 2 .

Table 2: Obesity rates in selected countries (18).

Country	Obese adults (%)	Population 2020
Nauru	61	10,903
Tonga	48.2	107,749
Samoa	47.3	202,239
Kuwait	37.9	4,380,326
United States	36.2	334,805,269
Jordan	35.5	10,300,869
Saudi Arabia	35.4	35,844,909
Qatar	35.1	2,979,915
Lebanon	33.7	6,684,849
Libya	32.5	7,040,745
Turkey	32.1	85,561,976
Egypt	32	106,156,692
United Arab Emirates	31.7	10,081,785
Iraq	30.4	42,164,965
Bahrain	29.8	1,783,983
Canada	29.4	38,388,419
Australia	29	26,068,792
Syria	27.8	19,364,809
United Kingdom	27.8	68,497,907
Algeria	27.4	45,350,148
Oman	27	5,323,993
Tunisia	26.9	12,046,656
Morocco	26.1	37,772,756
Iran	25.8	86,022,837
Ireland	25.3	5,020,199
Spain	23.8	46,719,142
Norway	23.1	5,511,370
Poland	23.1	37,739,785
Russia	23.1	145,805,947
Romania	22.5	19,031,335
Germany	22.3	83,883,596

Finland	22.2	5,554,960
Belgium	22.1	11,668,278
Iceland	21.9	345,393
France	21.6	65,584,518
Portugal	20.8	10,140,570
Sweden	20.6	10,218,971
Netherlands	20.4	17,211,447
Austria	20.1	9,066,710
Italy	19.9	60,262,770
Denmark	19.7	5,834,950
Switzerland	19.5	8,773,637
Yemen	17.1	31,154,867
Pakistan	8.6	229,488,994
Philippines	6.4	112,508,994
Afghanistan	5.5	40,754,388
Sri Lanka	5.2	21,575,842
Nepal	4.1	30,225,582
India	3.9	1,406,631,776
Bangladesh	3.6	167,885,689

Modified from data retrieved from: <https://worldpopulationreview.com/country-rankings/obesity-rates-by-country> , 2020.

1.1.4 Etiology and proposed causative factors

Obesity is a result of different factors that leads to a persistent weight gain over time. Several factors such as: genetics, diet, and lifestyle are thought to contribute to obesity development.

Obesity can potentially run-in families, suggesting a genetic component to its etiology. The genes implicated in predisposing to obesity affect different biological and physiological functions, such as regulation of food intake, metabolism of lipid and glucose, energy expenditure and finally the growth of adipose tissue (19).

Various medical conditions have also been shown to be causally associated with obesity, especially those that affect the neuroendocrine axis, such as hypothyroidism, polycystic ovarian syndrome (PCOS), hypogonadism, Cushing's syndrome, and growth hormone deficiency (7).

However, monogenic obesity is very rare, accounting for less than 5% of human common obesity, with most of the studies suggesting that the primary cause of the global obesity problem is due to energy imbalance within an organism, where energy intake is extremely high compared to energy expenditure. Energy intake is defined as all energy content of food or drinks that processed inside the body. If this energy persists in the body for long time, this state of positive energy balance leads to weight gain. Despite the other factors being of potential interest, energy output is primarily regulated by physical activity and voluntary movement.

High-energy food is readily available, due to the invasion of fast-food outlets. Indeed, the availability of healthy balanced food is more expensive, with people opting for cheaper, unhealthy fast food and snacks (20). In fact, there has been number of studies suggesting that consumption of high energy food are drastically responsible for the obesity epidemic (21). A study by Kostecka, investigated the eating habits of preschool children, and found that most children snack between meals, with the highest preference for sweets and sweetened products (22). Also, fast-food consumption among the American population was positively associated with changes in body weight, in a 15-years of prospective study (23).

Along with changes in diet, an increasingly sedentary lifestyle significantly contributes to the obesity epidemic. People have shown a preference for sedentary activities, such as using automobiles instead of walking, watching TV for a long time with unhealthy snacking during watching. Also, changes in occupation, with office bound individuals sitting for long periods during the day. In the last few decades, there has been a noticeable decrease in the occupations that require energy expenditure. Occupational physical activity has an important effect on energy

expenditure, as discussed by Church et al (24). They found a decrease in energy expenditure due to a drop in occupation physical activity since 1960 in both men and women accounting for 140 calories and 124 calories per day respectively (24).

1.1.5 Adiposity and Obesity Development

Adipose tissue is mainly consisted of adipocytes (50%), along with preadipocytes, endothelial, neuronal, epithelial, and immune cells, and has an important function in energy regulation. There are two, perhaps three, main types of adipose tissue: brown (BAT), white (WAT) and beige or 'bright' adipose tissues. As most of the publications have mainly been on BAT and WAT those are the only ones mentioned further in this thesis. The main function of BAT is heat production, which is called thermogenesis. During thermogenesis, BAT cells burn substrates such as fatty acids and glucose to produce heat and results in calorie loss (25). BAT only accounts for 1 to 2% of total fat storage in adult human subjects, found mainly in the axillary, cervical and paraspinal regions (26). In rodents, low or no BAT can lead to obesity (27), while increased BAT protects from obesity and its health consequences (28).

WAT is the main organ that contributes to adiposity and its associated comorbidities. It is an active endocrine organ that secretes numerous protein signals called adipokines. Adipokines are necessary signals to regulate physiological homeostasis. Triglycerides and lipids are stored in WAT as an energy source. Interestingly, adipocytes have the ability to change in size, nearly doubling from 60 to 120 μm , hypertrophy, as well as increase in number, hyperplasia. Both adipocyte hypertrophy and hyperplasia are the main mediators of adiposity and affect WAT function directly. Adipose tissue distribution is also an important factor in its pathology. Increased food intake leads to the expansion of both visceral and sub-cutaneous adipose tissue depots. Accumulation of visceral fat in the omental regions are most closely associated with inflammation, cytokine production and release of proinflammatory adipokines (29). Furthermore, the secretory profile of the large, hypertrophied

adipocytes is impaired, compared to smaller ones, due to high saturation of triacylglycerol within the large lipid vacuole (30). Continued high calorie intake leads to saturation of adipocyte hypertrophy and hyperplasia within the fat depots. An inability of the adipocytes to further accommodate the excess lipids leads to its ectopic fat deposition mainly in the liver, kidneys and the heart (31).

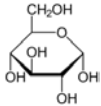
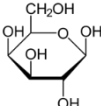
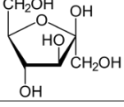
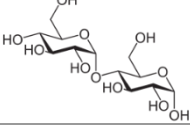
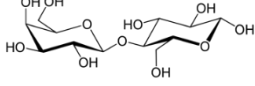
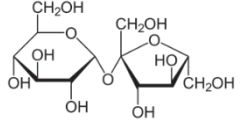
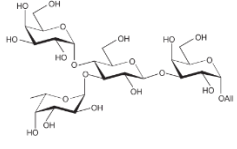
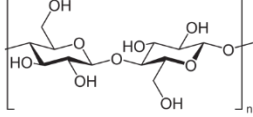
1.2 Diet

Diet is composed of organic and inorganic nutritious molecules to support the growth of living organisms and maintain their survival. These nutrients consist of macronutrients and micronutrients. Macronutrients includes carbohydrates, protein, and fats, while micronutrients are vitamins, water, and minerals. Each nutrient contains energy utilized by the body to supports body functions and metabolism. Energy is the amount of heat released through burning 1g of nutrient and expressed as kilocalories (kcal). The macronutrients are considered the major sources of energy, carbohydrates contain 4 kcal/g, proteins contain 4 kcal/g and fats contain 9 kcal/g. The balanced, recommended, dietary requirements are 45-65% carbohydrates, 20-35% fats and 10-35% proteins per day (32).

1.2.1 Carbohydrates

Carbohydrates are the most important energy source that human can get from diet. It is classified into different forms: monosaccharide, which is the simplest form of sugars, such as glucose and fructose, disaccharides, which is formed from two monosaccharide linked by glycosidic bond, such as lactose, sucrose and maltose and oligosaccharides, which are composed of 3 to 10 monosaccharides, like glycoproteins and glycolipids found in animals cell membrane. Finally, the complex form of carbohydrate are polysaccharides, composed of more than 10 monosaccharide, such as glycogen and starch (Table 3) (33).

Table 3: Classes of Carbohydrates (33)

Carbohydrates	Example	Composition	Chemical structure
Monosaccharides	Glucose (Glc)	Most abundant simple sugar	
	Galactose (Gal)	From mammalian milk	
	Fructose (Fru)	From fruits and honey	
Disaccharides	Maltose	Glc+Glc: found in malt sugar, hydrolyzed by maltase.	
	Lactose	Glc+Gal: found in milk, hydrolyzed by lactase.	
	Sucrose	Glc+Fru: found in table sugar, fruits and honey, hydrolyzed by sucrase.	
Oligosaccharides	Polymers of sugar units	Found attached to lipids (glycolipids) and proteins (glycoproteins).	
Polysaccharides	Cellulose	Polymers of Glc units, found in plants.	
	Starch	Polymers of Glc units, stored form of glucose in plant.	
	Glycogen	Polymers of Glc units, stored form of glucose in animals.	

1.2.2 Metabolism of carbohydrates

Carbohydrate metabolism refers to their breakdown and synthesis through different mechanisms to produce or release energy. This is achieved by the aid of different enzymes to induce digestion and absorption of monosaccharides. These enzymes are: α -amylase that digest polysaccharide into oligosaccharide and disaccharides. The α -amylases are produced by the saliva and pancreas. The other enzymes are lactase, sucrase and maltase, which breakdown the oligosaccharides and disaccharides into monosaccharides. The product of these breakdown processes is glucose. Glucose is the main molecular source of energy that is utilized by different tissues (34).

Carbohydrates hydrolyzed into monosaccharides through the digestion process reach the cells by glucose transporters, referred to as the GLUTs. These GLUTs are located on the surface of cell membranes and facilitate the movement of monosaccharides in and out the cells. Each member of the GLUT family function and target cells of specific tissues (33). The GLUT protein family is consisting of fourteen different isoforms, GLUT 1-14, some of them are insulin dependent and some of them are insulin independent. Each isoform has specific role(s) in maintaining glucose homeostasis (35).

1.2.2.1 Glycogenesis and Glycogenolysis

When blood glucose is high, this excess amount of glucose is converted into glycogen via a process called glycogenesis. Glycogen is stored in the liver and skeletal muscles, which regulates blood glucose and produce energy respectively. The synthesis of glycogenesis pathway requires the involvement of different enzymes. First, glucose molecules are phosphorylated by glucokinase (in liver) and hexokinase (in skeletal muscles) to produce glucose 6-phosphate. This step traps the glucose inside the cytoplasm of liver and skeletal muscle cells.

Phosphoglucomutase then converts Glucose 6-phosphate to glucose 1-phosphate. Then, uridine diphosphate (UDP)-glucose pyrophosphorylase transfers the glucose 1-phosphate to uridine triphosphate (UTP) to generate the active form of glucose UDP-glucose and released as pyrophosphate (PPi). The formation of glycogen starts from a preexisting glycogen polymer that works as a primer. The glycogen primer consists of at least four glucose units and glycogenin enzyme. Glucose units are added to the glycogen chain by an enzyme called glycogen synthase, the rate limiting enzyme of glycogenesis. As a result, α -1,4 glycosidic bonds are formed between glucose molecules (36, 37).

During starvation, the blood glucose goes down and initiates the breakdown of glycogen to release glucose molecules through glycogenolysis. The pathway starts with the rate-limiting enzyme glycogen phosphorylase. This enzyme cleaves the free end of glucose molecules at the α -1,4 glycosidic bond and releases glucose-1-phosphate, which is then converted into glucose in the liver and to pyruvate (by glycolysis) in the muscles. The action of the glycogen phosphorylase stops within four glucose residues from a branch point. Glycogen metabolism then continues by utilizing another enzyme called the debranching enzyme. This enzyme has a transferase (4:4) activity to move the four remaining glucose residues to non-reducing free end of the main chain. Then the α -1,6 galactosidase activity of this enzyme, hydrolyzes the α -1,6 bond and releases free glucose, not glucose 1-phosphate (36, 38) (Figure 1).

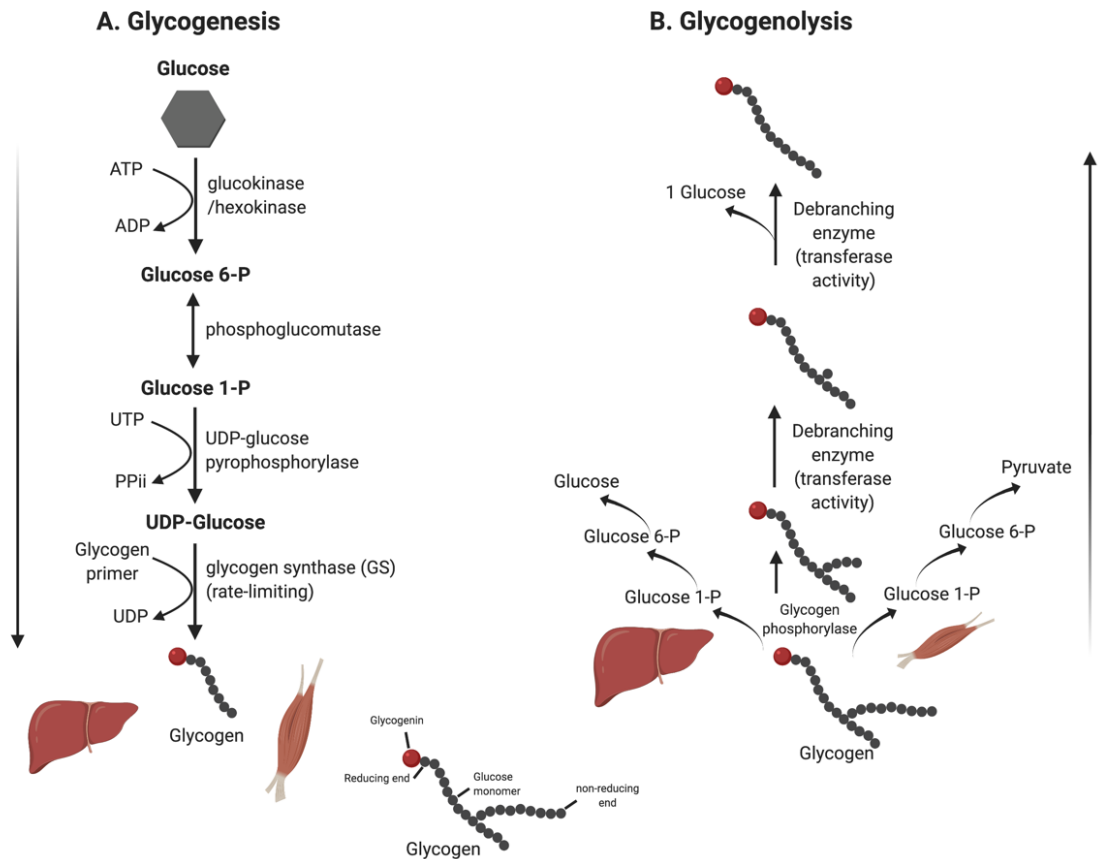


Figure 1: Glycogenesis and Glycogenolysis.

(A) Glycogenesis: Begins with glucose phosphorylation into glucose-6-phosphate, which is isomerized to glucose 1-phosphate. Glucose 1-phosphate is then transferred onto uridine triphosphate (UTP) to produce uridine diphosphate glucose (UDP) and release pyrophosphate. UDP-glucose aids glucose to reach the non-reducing end of glycogen. (B) Glycogenolysis: Glycogen branch is break down by glycogen phosphorylase to yield one glucose 1-P molecule at a time. Glucose 1-P is then converted into glucose in the liver or pyruvate in the muscle. ATP: adenosine triphosphate; ADP: adenosine diphosphate (36, 39).Created with BioRender.com.

1.2.2.2 Glycolysis and Glucogenesis

Glycolysis is the process of glucose breakdown to generate energy. When the systemic blood glucose is elevated, the glucose is acquired by the cells through glucose transporters (GLUTs). Once the glucose gets into the cytoplasm, the glycolytic pathway starts with a series of enzymatic reactions. This series is started with the phosphorylation of glucose into glucose 6-phosphate by hexokinase (in all cell types) or glucokinase (in liver and pancreatic β cells). The phosphoglucose isomerase enzyme is then isomerize glucose 6-phosphate into fructose 6-phosphate. Then the phosphofructokinase-1 is converted to fructose 6-phosphate and fructose 1,6-biphosphate. After this step, aldolase A enzyme leads the reaction and splits the fructose 1,6-biphosphate from 6-carbon molecule into two three-carbon molecules which are glyceraldehyde 3-phosphate (G3P) and dihydroxyacetone phosphate (DHAP). The last phase of the glycolysis reaction is the conversion of G3P into pyruvate via five enzymatic reactions. This phase requires the involvement of the following enzymes: 1) phosphoglycerate kinase (converts 1,3-bisphosphoglycerate into 3-phosphoglycerate), 2) glyceraldehyde 3-phosphate dehydrogenase (converts G3P into 1,3-bisphosphoglycerate), 3) Pyruvate kinase converts phosphoenolpyruvate into pyruvate. The yield of this pathway is two pyruvate molecules, two ATP and two NADH (Figure 2) (40, 41).

Glucogenesis refers to the production of glucose from noncarbohydrate sources. It occurs primary in the liver, with less amount in the kidney and small intestine. This process begins when the dietary glucose is insufficient to supply organs that utilize glucose as a main energy source like the brain, nervous system etc. The precursors of glucogenesis are lactate, amino acids, and glycerol. Glucogenesis using pyruvate as a precursor, is the reversal reaction of glycolysis. Glucogenesis first starts in the mitochondria, pyruvate carboxylase activity converts mitochondrial pyruvate (product of glycolysis) to oxaloacetate (OAA). OAA cannot cross the mitochondrial membrane directly; the movement is facilitated indirectly by mitochondrial malate

dehydrogenase which converts OAA into malate. Once malate passes the mitochondrial membrane, it is then converted to oxaloacetate by the cytosolic malate dehydrogenase via oxidation. The phosphoenolpyruvate carboxykinase catalyzes the cytosolic oxaloacetate and forms phosphoenolpyruvate (PEP). The PEP then creates fructose 1,6-biphosphate via glycolysis reversal reaction. Fructose 1,6-biphosphatase is a glucogenesis rate limiting enzyme, which dephosphorylates fructose 1,6-biphosphate into fructose 6-phosphate. Fructose 6-phosphate is isomerized into glucose 6-phosphate (by another glycolysis reversal reaction). Finally, glucose is produced from the dephosphorylation of glucose 6-phosphate. Once glucose is synthesized, it is transported by the blood to the targeted cells to maintain their function. Glucogenesis is a costly process because it consumes more energy to produce glucose (Figure 2) (40, 42).

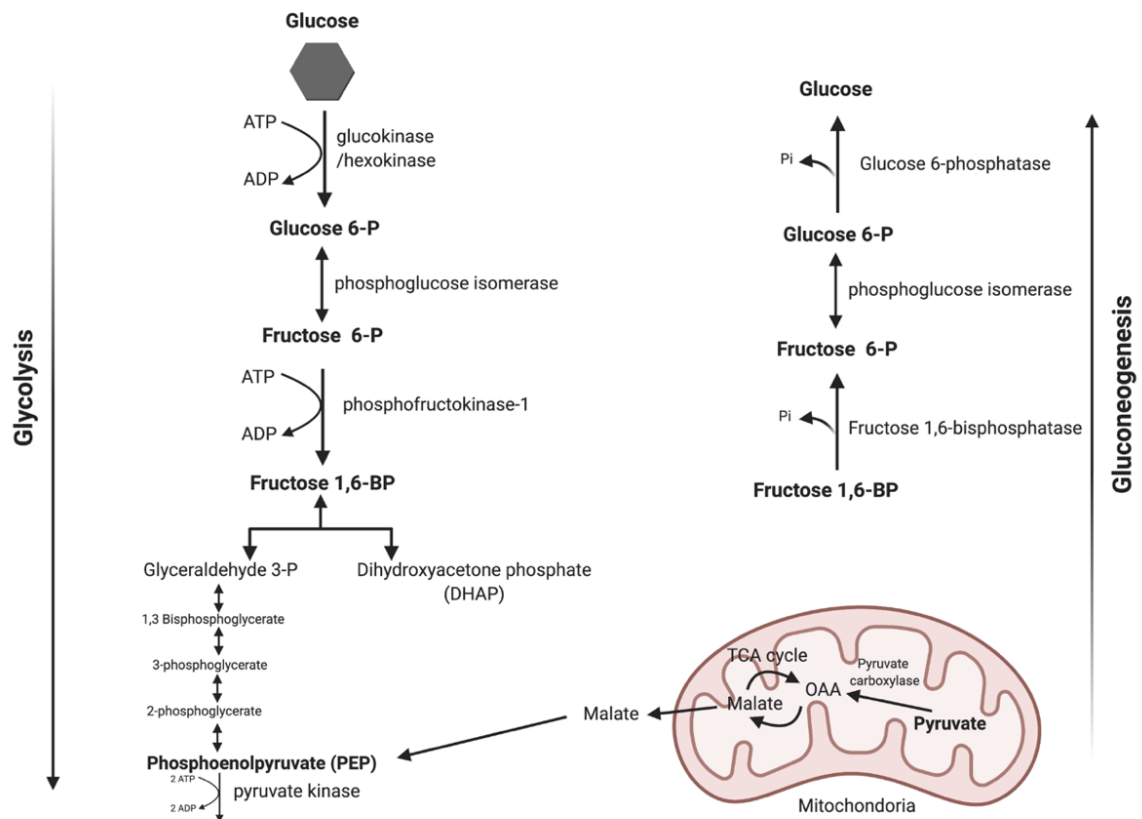


Figure 2: Glycolysis and Gluconeogenesis.

Schematic diagram represents the metabolic pathways of glycolysis vs gluconeogenesis. Lines with single arrowhead represents irreversible reaction, arrowhead with two ends represents reversible reactions. ATP: adenosine triphosphate; ADP: adenosine diphosphate; BP: biphosphate; Pi: phosphate; OAA: oxaloacetate; TCA: tricarboxylic acid (40). Created with BioRender.com

1.2.3 Lipids

Lipids (fats) are heterogenous organic compounds that are known to be poorly water solubility. Lipids are amphipathic, which means they can be polar or nonpolar. They have various functions in the body: serve as energy storage (triglycerides), structural components of cell membrane (glycolipids, phospholipids, and cholesterol), signaling molecules (hormones and vitamins) and other functions, such as thermogenesis in brown adipose tissue and emulsifying agent in digestion and absorption. Dietary lipids include a mixture of compounds. These compounds are fatty acids, triacylglycerol, cholesterol, and cholesterol esters. FA are composed of monocarboxylic acids with hydrocarbon chains. FA can be found in three different forms: saturated (no double bond), monounsaturated (one double bond) or polyunsaturated (two or more double bonds). Triacylglycerols are the stored form of fat in the body, which consist of three fatty acids attached to a glycerol backbone. Cholesterol and cholesterol ester consist of free cholesterol and cholesterol esterifies to FA. Once lipids are digested, they are catalyzed by lipase enzyme which target and hydrolyze the ester bonds (39). FA then enters the targeted tissue through FA transporters (FATP), or FA translocase CD36, or by diffusion (43). Following the uptake, FA is broken down in the cytoplasm via β -oxidation process. This process occurs in the cytoplasm and aims to convert FA into fatty acyl CoA molecules. In order to facilitate the transportation of fatty acid across the mitochondria, the fatty acyl CoA and carnitine are combined together and produce a fatty acyl carnitine molecule. In the mitochondrial matrix, fatty acyl carnitine molecule is converted back into fatty acyl CoA. Fatty acyl CoA then enters a multiple enzymatic step ending with the formation of Acetyl CoA. This molecule enters the Tricarboxylic Acid cycle (TCA) and produce energy. Excess FA are stored as source of energy in the form of TG by esterification reaction which require 3 FA and 1 glycerol molecule.

1.2.3.1 Lipogenesis

FA can also be produced from non-lipid sources through the *de novo* lipogenesis process (DNL). Lipogenesis is an important metabolic process that is switched on at energy sufficient states, when carbohydrate is at a high level. This process appears mainly in the liver and adipose tissue, where fatty acid is synthesized from carbohydrate (non-lipid source) (44). Excess glucose is metabolized by DNL, a metabolic step that occurs in the cytoplasm of hepatocytes and adipocytes. This step is aimed at converting glucose into FA and esterified into triglyceride (45) as an energy for long-term storage. Uptake of circulating glucose activates glycolysis to yield pyruvate. This pyruvate is transported to the mitochondria and enters the TCA cycle to form citrate. Then citrate is traveled back to the cytoplasm and converted into Acetyl-CoA by the enzyme ATP citrate lyase (46). DNL begins with Acetyl-CoA, which is converted by the enzyme acetyl-CoA carboxylase 1 (ACC1) into Malonyl-CoA. Malonyl-CoA substrate produces 16-carbon palmitic acyl-CoA through the action of fatty acid synthase (FASN), forming palmitate. Palmitate is the first outcome of DNL process, which is then undergoes elongation and desaturation to generate more complex fatty acids, such as palmitoleic acid, stearic acid, and oleic acid. These fatty acids are precursors of TG formation through the esterification process. These TG serve as an energy source by β -oxidation (47) (Figure 3).

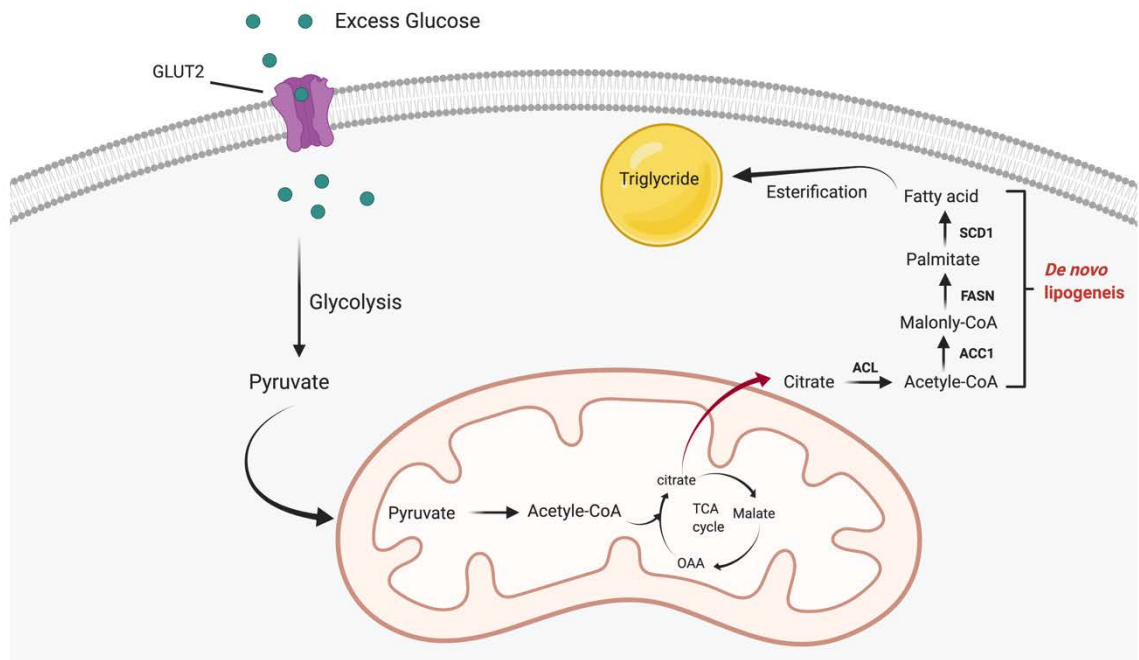


Figure 3: Process of De Novo lipogenesis in the liver.

De novo lipogenesis is a complicated metabolic process that alters extra carbohydrate into fatty acids, which are then converted into TG. The process starts in the cytoplasm, when Acetyl-CoA is converted to Malonyl-CoA by ACC1, Malonyl-CoA to palmitate, which is esterified into TG. GLUT2: Glucose transporter 2. TCA: Tricarboxylic acid cycle; OAA: Oxaloacetate; ACL: ATP citrate lyase; ACC1: Acetyl-CoA carboxylase 1; FASN: fatty acid synthase enzyme; SCD1: Stearoyl-CoA desaturase. Created by BioRender.com.

1.3 Food palatability (food environment and lifestyle)

In the 19th century, the food industry transitioned towards an increase in the production of ready-to-consume products such as, cakes, biscuits, sauces, pies and meat products (48). Consequently, this led to a nutrition turn, by shifting the consumption from staple crops and whole grains to partially or highly processed food, especially seen in the developing countries (49). Ready-to-eat food refers to food items that are processed or highly processed and made from cheap ingredients and additives, which make it more palatable, such as burgers, nuggets, sugary drinks, pasta, pizza, cereal bars and other sweetened products (48). These palatable foods produce a hedonic reward and sensory state that goes beyond just stimulating further food intake (50).

Globally, most communities witnessed a shift in the food system and the displacement of healthy/unrefined/whole food to ready-to-eat ultra-processed products. The NOVA food classification system has been used to classify food into four groups based on the following criteria: nature, purpose and extent of processing as reported by Pan American Health Organization (51) :

- 1- **Unprocessed or minimal processed food:** is food items that originated from plant or animals and did not undergo industrial process. They are characterized by minimal removal of part of the food, without replacement with any additives.
- 2- **Processed culinary ingredients:** are ingredients extracted from nature through industrial processing and used mainly to prepare food and make it more palatable (fats, oils, sugar and salts).
- 3- **Processed food:** are produced by adding culinary ingredients such as sugar, salt, and oil to make the food more durable and palatable. This includes simple bread, cheese, and preserved food.
- 4- **Ultra-processed:** include food stuff formulated from industrial manufacturing derived from food or organic sources. These products are ready-to-consume

but has less or no whole food. Ultra-processed food are all sugary, salty, and fatty packed snacks, such as chocolate, cookies, pastries, cakes, carbonated drinks, energy drinks, sugar-sweetened drinks, fruit drinks, fruit yoghurt and sweetened cereals. Ready meals that are commonly found at home and fast-food outlet such as: pre-prepared meat, seafood, vegetables, burgers, nuggets, French fries, packet soup, noodles, and desserts.

The main purpose of food processing is to make it more desirable, enjoyable, diverse and palatable. Food palatability is defined by McCrickerd and Forde as “a positive hedonic evaluation of food’s sensory characteristics, which reflects previously learned knowledge that a food’s sensory quality is nutritional and safe to eat” (50). Palatable and high dense food are high in glycemic load, salt, and fat and low in nutritional contents (52). Marketing strategy has a significant role in promoting and selling these kind of food items and make it desirable for the consumer (48). Ready-to-eat food change eating behaviors and tend to be more convenient, because it requires less preparation and can be consumed while involved with other activities such as watching TV (53). Purchasing and consuming of ultra-processed food is increasing in high income countries compared to middle and low-income countries (54). These kinds of food started causing problems in terms of human health due to its low nutritional contents and usually hyper-palatable. Also, it has been shown that such palatable and hyper-palatable food may lead to food addiction through activation of the reward system (55).

Several studies have assessed the association between consumption of high palatable, ultra-processed and high dense food and the risk of developing obesity and its related comorbidities. An increase in body weight was observed within 4 years due to the consumption of specific types of ultra-processed food like, fast-food, potato chips, fried potato and sweets (56). Asfaw suggested that consuming

processed food has a high impact on body weight and could be considered as a major risk of developing obesity (49). Eating out frequently is clearly linked with weight gain and obesity over time (57). This evidence supports the correlation between type of consumed food and the obesity epidemic. Eating ultra-processed food showed an increase in metabolic syndrome characterized with abdominal adiposity, elevated fasting plasma glucose, blood pressure, TAG and lower HDL (58). Triglyceride and glucose are the most significant MS components due to the consumption of ultra-processed food, while consumption of unprocessed food is considered as a protective diet against metabolic syndrome (MS) (59). Along with the health consequences of ultra-processed food consumption, some studies showed the reversible effect of consuming unprocessed or less processed food (60).

1.4 Sedentary lifestyle and energy metabolism

Food is the main fuel for energy and the maintenance of body functions. Energy is measured by kilocalories (Kcal) and it represents the capacity to do work. Energy is obtained from food macronutrients which are: Carbohydrates (4 Kcal/g), proteins (4 Kcal/g) and fats (9 Kcal/g), these macronutrients supply the body with immediate energy molecule known as Adenosine Triphosphate (ATP). Excess energy obtained from food is stored in the body as fat (main storage of energy) or glycogen (short-term energy storage) or protein (used only in severe starvation). Energy expenditure is the number of calories required to meet the body needs. It depends on age, sex, weight, physical activity, diet, and overall health. It consists of three components. The main and largest component is known as basal metabolic rate (BMR), which refers to the amount of food consumed and utilized to maintain the basic body functions such as, respiration, muscle contraction and heartbeat. BMR accounts for 60-70% of total energy expenditure. The main determinant of the BMR is the body size. A larger body size means larger lean fat mass or fat-free mass (the mass of muscles and organs) which require more BMR compared to small body size (61).

Another component of energy expenditure is the diet-induced energy expenditure (DEE), which is around 10% of total energy expenditure (TEE). It is associated with food ingestion and is the energy utilized for digestion, metabolism, and storage of consumed micronutrients. The third component is the physical activity-induced energy expenditure (AEE), which is produced from exercise and the movement of skeletal muscles. AEE is a variable component of TEE because it depends mainly on an individual's lifestyle. The main factors disturbing energy expenditure are food intake and physical activity (62).

Energy balance is attained when the energy intake is equal to energy expenditure, which result in maintenance of body weight. When this balance is interrupted by increased food intake relative to energy expenditure, positive energy balance occurs and resulting in weight gain. On the other hand, negative energy balance occurs when the energy intake is less relative to energy expenditure, resulting in weight loss.

Food is consumed as a mixture of all the macronutrients, and each macronutrient varies in its capacity to be stored as energy. Fat is the easiest and preferred form of energy storage that can be extended for long term energy usage. While carbohydrates and proteins have a limited storage capacity. Excess carbohydrate is converted to glycogen (a short-term energy storage molecule) stored in the liver and skeletal muscles.

Nowadays, sedentary lifestyle has a direct effect on energy balance. There is a noticeable decline in physical activity due to the increased motorization and mechanization in the first half of 20th century (63), such as: using automobiles instead of walking and cycling, elevators, washing machines, entertainment in front of television and video games, using electronic mails and computers at work.

1.5 Obesity risks

Obesity is of major concern when considering public health. It is a risk of developing a collection of diseases described as the MS (64). MS is a collection of risk factors that influence the development of diseases such as cardiovascular disease, type 2 diabetes, non-alcoholic fatty liver disease (NAFLD) and cancer (65). Different criteria are used to diagnose MS: waist circumference: ≥ 102 cm in men and ≥ 88 cm in women, High Density Lipoprotein Cholesterol level (HDL-c): in men < 40 mg/dL, in women < 50 mg/dL, Triglyceride level: ≥ 150 mg/dL, fasting glucose: ≥ 100 mg/dL blood pressure (BP): $\geq 130/\geq 85$ mmHg (66). American Heart Association diagnoses the MS if the patient suffers from three of five criteria shown in Table 4 (67).

Table 4: Criteria for Clinical Diagnosis of Metabolic Syndrome (67)

Measure (any 3 of 5 constitute diagnosis of metabolic syndrome)	Categorical Cut-points
Elevated waist circumference	≥ 102 cm (≥ 40 inches) in men ≥ 88 cm (≥ 35 inches) in women
Elevated fasting glucose	≥ 100 mg/dL Or on drug treatment for elevated glucose
Elevated blood pressure	≥ 130 mm Hg systolic blood pressure or ≥ 85 mm Hg diastolic blood pressure Or on antihypertensive drug treatment in a patient with a history of hypertension
Reduced HDL-c	< 40 mg/dL (1.03 mmol/L) in men < 50 mg/dL (1.3 mmol/L) in women Or on drug treatment for reduced HDL-C
Elevated triglycerides	≥ 150 mg/dL (1.7 mmol/L) Or on drug treatment for elevated triglycerides

1.5.1 Obesity and Type 2 diabetes

1.5.1.1 Insulin signaling pathway

Insulin is a hormone that is produced and secreted by the pancreatic β -cells in response to stimuli, such as increased circulating glucose level. Normally, insulin acts as glucose regulator, reducing its plasma levels by enhancing cellular uptake in peripheral tissues such as adipose tissues, skeletal muscles, and liver. Beside its effect on regulating glucose, insulin can act also on adipose tissue as an inhibitor of lipolysis by inhibiting lipase enzyme. Lipase hydrolyzes triglycerides into free fatty acids (FFAs) and glycerol as end products (68). Insulin also stimulates adipogenesis, the process of differentiation of pre-adipocytes into mature functioning adipocytes (65).

In order to trigger the function of insulin, this process requires the binding of insulin-to-insulin receptor on the cell membrane. Insulin receptor (IR) is a heterotetrametric transmembrane protein, which has a structure of two parts, two extracellular α -subunits and two transmembrane β -subunits. Once insulin binds to its receptor, this triggers a cascade of phosphorylation events inside the targeted cell, leading to different actions occurring at different time points. Initially insulin binds to the extracellular α subunit, leading to the stimulation of tyrosine kinase and β -subunits phosphorylation. Subsequently, this event phosphorylates the insulin receptor substrates 1 and 2 (IRS1/2). The activation of these substrates triggers two masters downstream signaling pathways: the mitogen-activated protein kinase (MAPK) pathway and the phosphatidylinositol-3-kinase (PI3K) pathway. MAPK cascade activation (Raf, MEK and ERK1/2) regulates proliferation, differentiation, and survival of the cell. The stimulation of PI3k pathway activates 3-phosphoinositide-dependent protein kinase 1 (PDK1), leading to protein kinase B (Akt) phosphorylation. Akt phosphorylation is responsible for the phosphorylation of several downstream signaling cascades such as: glycogen synthase kinase (GSK)-

3, translocation of glucose transporter receptor (GLUT4), Forkhead box protein O (FOXO) and mammalian target of rapamycin (69) (Figure 4).

Defects in insulin signaling leads to metabolic dysregulation and chronic diseases, such as type 2 diabetes, hypertension, hyperlipidemia and atherosclerosis or cardiovascular dysfunction.

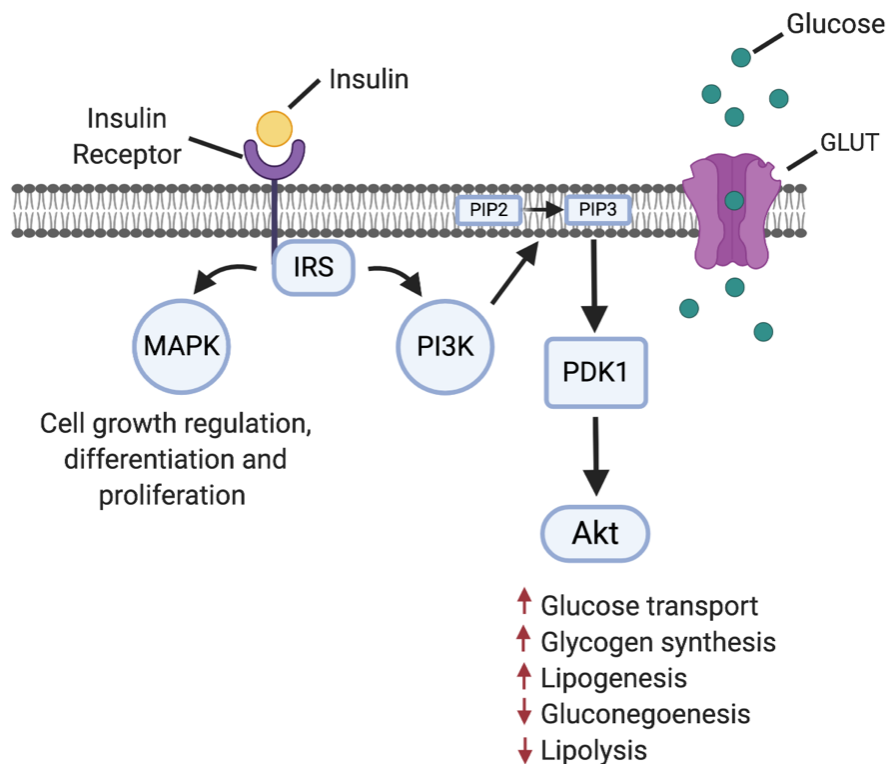


Figure 4: Insulin signaling pathways.

Insulin signaling begins when insulin binds to its receptor and activates IRS. IRS activates PI3K, which converts PIP2 to PIP3. PIP3 a second messenger activates PDK1 to recruit Akt. Consequently, Akt signaling pathway regulates different metabolic process; ↑ up-regulation, ↓ down-regulation. The stimulation of the other pathway, MAPK induces the activation of genes responsible for the regulation of cell growth. PIP2: phosphatidylinositol 4,5-bisphosphate; PIP3: phosphatidylinositol 3,4,5-trisphosphate; GLUT: Glucose transporter; IRS: insulin receptor substrate; MAPK: mitogen-activated protein kinase, PI3K: phosphatidylinositol-3-kinase; PDK1: 3-phosphoinositide-dependent protein kinase 1; Akt: protein kinase B. Adapted from: Int. J. Mol. Sci. 2014, 15, 6184-6223; doi:10.3390/ijms15046184 (69). Created with BioRender.com

1.5.1.2 Insulin Resistance

High levels of circulating Insulin, hyperinsulinemia, is the main contributor to MS associated diseases. In the pathological condition called “insulin resistance” peripheral tissues fail to respond to insulin and consequently prevent the uptake of glucose from the blood stream. The sensitivity of muscles, adipose tissue and liver to insulin is decreased with insulin resistance (70). Insulin resistance leads to increase in the systemic glucose levels and end with type 2 diabetes mellitus. Moreover, it affects adipose tissue by increasing lipolysis, which consequently increase free fatty acids (FFAs) in the circulation and impair adipose tissue to uptake and store the excess FFAs. Hypertrophic adipocytes are insulin resistant at least in part due to decreased insulin receptor phosphorylation, which reduces the tissue glucose uptake leading to greater release of pancreatic insulin ultimately causing hyperinsulinemia (29). As a result, excess FFAs start to accumulate in the abdominal organs to form ectopic fat deposition. Thus, the liver takes up the excess circulating FFA's causing hepatic steatosis (fatty liver) which has an impact on hepatic insulin sensitivity (71).

1.5.1.3 Inflammation

Chronic and low-grade inflammation is usually associated with obesity and obesity-related pathologies (72). Inflammation is a physiological action that requires an increase in the circulating white blood cells, and elevation of proinflammatory cytokines in the circulation and tissues. Inflammation is also marked by infiltration of macrophages in the tissues, and elevation of interleukin 6 (IL-6), tumor necrosis factor (TNF- α), interleukin 1 (IL-1), monocyte chemoattractant protein 1 (MCP-1), plasminogen activator inhibitor-1 (PAI-1). This inflammation also appears to target insulin signaling and reduce tissue and cellular sensitivity to it. It induces the inhibition of different insulin signaling pathways in both adipose and liver tissues. These mechanisms include first, inhibition of insulin receptor and IRS-1 (insulin

receptor substrate). Second, inhibition of the peroxisome proliferator-activated receptor gamma (PPAR γ), PPAR γ is a nuclear receptor and mainly presented in adipose tissue. It regulates fatty acid storage, adipocyte differentiation and glucose metabolism. Third, inflammation stimulates lipolysis through blocking of TG synthesis and release FFA in the plasma.

Thus, insulin has a complex signaling pathway and it regulates glucose and fat metabolism, insulin resistance disrupts the insulin-signaling cascade and compromises its normal physiological actions.

1.5.2 Obesity and Vascular function

1.5.2.1 Structure and function of vascular system

The vascular system is made up of vessels that transport blood through the body in order to maintain body function. Blood is pumped out from the heart to move through blood vessels starting with the artery, capillary and ending with the veins. The vascular wall is consisted of three different layers surrounding the lumen of the blood vessel. Tunica intima (inner layer) is a single layer of endothelial cells lining the lumen of all blood vessels and has a direct contact with the blood. Tunica media (middle layer) is the vascular part of the vascular wall which consist of vascular smooth muscle cells (VSMCs). This layer is the main part of the vascular reactivity. The sympathetic nervous system and neurochemicals control vascular smooth muscle cells to maintain the vascular tone. The last layer is tunica externa which form the outer part of the blood vessel. This layer is important to support and protect the blood vessel, because it is made of collagen fibers. The function of the vascular layer is very critical in regulating the circulation system, any small changes in the vessel diameter directly affects the blood flow and pressure.

Arteries are at the top of the vascular tree, which supply the organs of the body with oxygenated blood. They are characterized by thicker walls compared to the other vessels due to the thick layer of VSMCs. Arteries can be divided into three types based on their position: conducting arteries, conduit arteries and resistance arteries (64). Conducting arteries which includes aorta, pulmonary artery and carotid artery are the largest among the others. They contain high number of elastic fibers to allow the vessel to expand and contract as a result of the intermittent ventricular ejection (73). Conduit arteries such as the brachial, femoral, and radial artery are branched from the conducting artery. These arteries act as a distributor that pump the blood to specific body regions (74). Further branching of the conduit artery leads to the resistance arteries, which are responsible for the perfusion of blood through organs and tissues (64).

1.5.2.2 Vascular tone and NO signaling

Vascular tone is the balance between constriction and dilation of blood vessels that change the vessel diameter. Vascular tone is regulated by distinct stimulators leading to the constriction and dilation of the VSMCs layer. The endothelium has the ability to release various vasoactive factors that act directly on the VSMCs layer function. These factors exhibit vasodilatory effects, such as nitric oxide (NO), prostacyclin (PGI₂) and endothelium derived hyperpolarizing factor (EDHF), or vasoconstrictive effects such as thromboxane (TXA₂) and endothelin-1 (ET-1) (75).

NO is an endothelial-dependent vasorelaxation agent and plays a critical role to maintain the vasodilator tone of blood vessel. NO released when nitric oxide synthase (NOS) is triggered and converts the amino acid L-arginine to NO (76). NOS has three different isoforms: neuronal isoform (nNOS) produce NO as a neuronal messenger to regulates neurotransmitter release (77), inducible isoform (iNOS) which induce the release of NO in response to inflammation or injury to activate macrophages (78). The third isoform is the endothelial nitric oxide synthase (eNOS)

that release NO to regulate the vasculature (79). Vascular relaxation is highly dependent on the activity of the eNOS isoform.

eNOS is bound to the endothelial cell membrane proteins called caveolins, which is regulated by the level of intercellular calcium (Ca^{2+}) (80). Increased levels of intercellular Ca^{2+} enhance the formation of calcium calmodulin complex that attach to the eNOS calmodulin-binding domain, causing NO production (81). NO diffuses to adjacent VSMCs and stimulates its signaling cascade through guanylyl cyclase (sGC), cyclic guanosine monophosphate or protein kinase G leading to reduce VSMCs tension (75) (Figure 5).

The contraction of VSMCs is also regulated by changes in the intracellular Ca^{2+} concentration. High levels of cytoplasmic Ca^{2+} results in the formation of Ca^{2+} - calmodulin complex, which consequently activates the enzyme myosin light chain kinase (MLCK) (82). MLCK activation leads to the phosphorylation of myosin light chain, causing cross bridges between actin and myosin and result in VSMCs contraction (82) (Figure 5). VSMCs contraction shortens the long axis of VSMCs and decreases the diameter of the blood vessel. Vascular tone depends significantly on the level free Ca^{2+} in the cytoplasm of VSMCs.

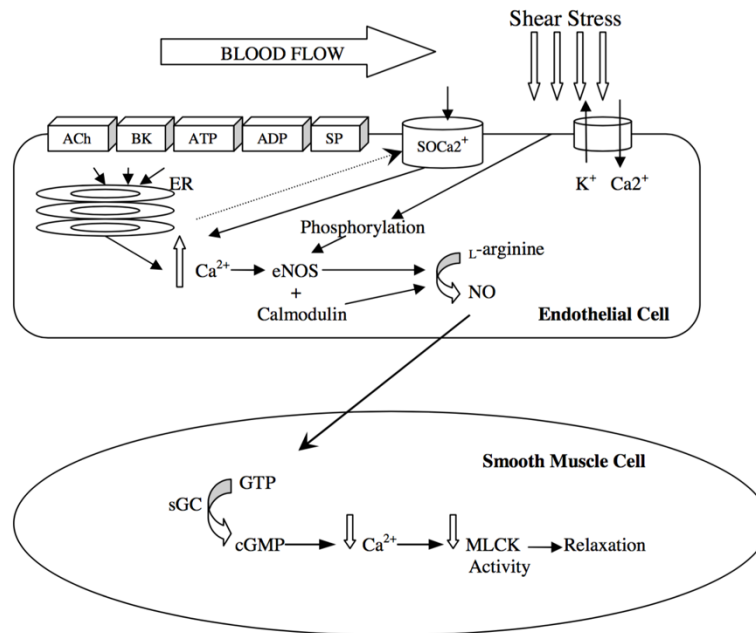


Figure 5: Endothelial nitric oxide regulation of vascular smooth muscle cells.

ACh=acetylcholine; BK= bradykinin; ATP= adenosine triphosphate; ADP= adenosine diphosphate; SP= substance P; SOCa2+= store-operated Ca2+ channel; ER= endoplasmic reticulum; NO= nitric oxide; sGC= soluble guanylyl cyclase; cGMP= cyclic guanosine-3', 5-monophosphate; MLCK= myosin light chain kinase (64).

The mechanism of the VSMCs contractile function is very complex and carefully regulated. It is triggered by the activity of ion channels and membrane receptors located on the cell membrane of VSMCs and endothelial cells. Mechanical sensors also respond to changes that occur due to the blood flow and intravascular pressure. In addition, the gaseous signaling molecule that directly activates the second messenger system once it diffuses inside the VSMCs. All these activities have a major role in controlling blood vessels and the changes in the vascular tone.

1.5.2.3 Endothelial dysfunction

Obesity is associated with medical complications related to vascular dysfunction, such as hypertension, dyslipidemia, atherosclerosis, and vascular alterations (83). As mentioned earlier obesity is associated with MS which may be responsible for increasing the risk of CVDs by 50% (84). A key feature of endothelial dysfunction is the dysregulation in the ratio between vasoconstriction and vasodilation. Defects in endothelial cells affects the release of NO and other vasodilatory agents, and consequently compromise the vasodilatory capacity of blood vessels. A variety of pathophysiological stimulus can alter the normal function of endothelium, such as oxidative stress and inflammation (85). The decline in NO bioavailability can be due to different factors including decreased expression of eNOS, alteration in eNOS cellular signaling and NO degradation (86). Alteration in metabolic parameters causes lipid deposition on the vascular wall and induces oxidative stress, thus triggering inflammatory reaction to release chemoattractant and cytokines and finally end with endothelial dysfunction (87). Endothelial cells are shown to be more vulnerable to damage by inflammation in metabolic stress (88).

1.5.3 Obesity and Liver diseases

1.5.3.1 Structure and function

The liver is the second largest organ in the body. It is located inferior to the diaphragm extends across the entire abdominal cavity. It is made of pinkish-brown soft tissue that has the ability to regenerate following tissue damaged. The liver is an essential organ that is responsible for multiple physiological and biological functions related to digestion, metabolism, immunity, and storage of nutrients within the body. These functions include protein production, glycogen synthesis, lipid formation (triglycerides and cholesterol), blood clotting factors and bile secretion.

The liver is divided into two lobes, the right and the left. Each lobe is made of smaller functional units called lobules. Histologically the lobule is hexagonal in cross section, with a central vein, located in the center, and the portal triads are located in its

angles. The portal triads are composed of branches of the portal vein, hepatic artery, and bile ducts. The liver consists of three main cell types: hepatocytes (forms approximately 75% of the liver mass), Sinusoidal lining cells (stellate cells, Kupffer cells, and endothelial cells) and the bile duct cells (89).

Hepatocytes are arranged and extend from the central vein to the portal edges (90). Instead of capillaries, large spaces are found between the hepatocyte's plates lined with endothelial cells called sinusoids. Kupffer cells are permanent phagocytes found in the sinusoids and responsible for fighting any foreign substance that drain into the liver (91). The blood from portal vein and artery drains into the sinusoid. Once the blood enters the sinusoid, the flow slows down to facilitate the exchange of oxygen and nutrients between the blood and hepatocytes. Then the blood leaves the sinusoid and drains into the central vein. Based on the blood flow the hepatic lobule is divided into three zones. The layer nearest the central vein is called zone 3 and is the most oxygen-poor zone. The middle layer of the lobule is zone 2 and the outer layer near to the portal triad is called zone 1. Zone 1 and zone 2 are richer in oxygen compared to zone 3 (92) (Figure 6).

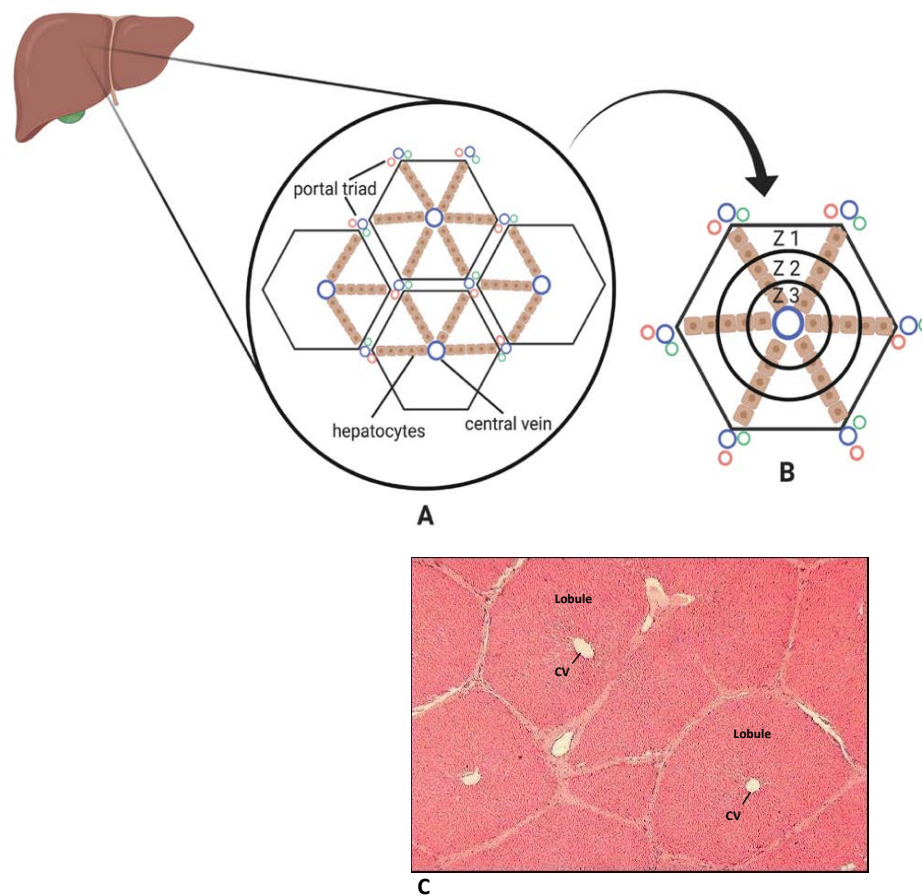


Figure 6: Structure of liver lobule

A: The hexagonal structure of liver lobule composed of three main parts: central vein, hepatocytes, and the portal triad. B: The three zones of the liver lobule based on the blood flow, Z1: zone 1, Z2: zone 2, Z3: zone 3. Created with BioRender.com. C: Liver histological image showing the hexagonal lobules and the arrangements and hepatocytes outer the central vein (93). Retrieved from: http://www.vivo.colostate.edu/hbooks/pathphys/digestion/liver/histo_lobule.html

1.5.3.2 Liver function enzymes

Liver is the main site of protein production. Normally liver produces 10-12 g of albumin per day. Albumin is a carrier protein that carries hormones, fatty acids, and

steroids. It has also a major role in stabilizing the intracellular fluid volume because it has a contribution in the osmotic pressure. Liver dysfunction negatively affects albumin production and secretion. To assess the liver function, clinical tests are applied to measure the levels of liver enzymes including alanine aminotransferase (ALT), aspartate aminotransferase (AST), alkaline phosphatase (ALP), and γ -glutamyl transferase (GGT). Serum or plasma albumin is also a useful parameter to assess the liver function (94).

ALT is an enzyme found in the hepatocyte cytoplasm, and it is considered a specific marker of liver health, with high levels marking injury. AST is a mitochondrial enzyme that can be found in other tissues, such as brain, heart, muscle, and kidney. ALP is found in the canicular and sinusoidal membrane of the liver. This enzyme can be found also in the intestine, placenta, and bone. GGT is a glycoprotein located in the cell surface of hepatocytes and most other cells. GGT elevation is a significant indicator for alcohol consumption (95).

Liver injury causes breakdown of the hepatocytes and the release of aminotransferases enzymes in the blood. In addition, liver enzymes can be affected by other factors such as liver disease, environmental factors, and toxins.

1.5.3.3 Hepatic Lipid Metabolism

The liver is the main regulator of lipid metabolism in the body. The normal physiological function of the liver is the uptake of circulating FFAs derived mainly from lipids released from dietary intake and the adipose tissue. FFAs can also be synthesized from non-lipid sources, such as glucose, by DNL. DNL is a process that require enzymes to convert excess glucose to FFAs in the liver. The FFAs pool inside the liver is utilized for energy, membrane synthesis, or stored as triglycerides (96). Excess triglycerides are released to the circulation in the form of very low-density

lipoprotein (VLDL). FFAs are normally generated from distinct sources: diet, DNL and lipolysis of visceral fat tissue or subcutaneous fat.

1.5.3.4 Hepatic Glucose Metabolism

Along with the role of the liver in lipid metabolism, it is also responsible for the regulation of endogenous glucose levels. Carbohydrates are ingested from food and absorbed by the gastrointestinal tract (GI) to reach the bloodstream. Glucose is the major fuel utilized by cells for energy production. Excess glucose is taken up by the liver and stored as glycogen through a process called glycogenesis. In the fasting state, the glucose level starts to decline. In such situations, the liver becomes an active source for the glucose production to compensate hypoglycemia. Hepatocytes breakdown the stored glycogen to release glucose in the circulation through the process of glycogenolysis. In hyperglycemic conditions the liver converts excess glucose into triglycerides for long-term storage, which induces fat accumulation in hepatocytes.

1.5.3.5 Non-alcoholic fatty liver disease (NAFLD)

Non-alcoholic fatty liver disease (NAFLD) is the most common chronic liver disease widely attributed to the obesity epidemic. It is defined as the accumulation of excessive fat in the liver with the presence of >5% steatosis in individuals with no history of alcohol abuse (97). Fatty liver is associated with obesity; It has been reported that 80% of NAFLD patients are obese with BMI > 30 Kg/m² (98). Epidemiological data shows that NAFLD affects many populations globally as follows: United States – 30%, Middle East – 32%, South America – 30%, Asia – 27%, Europe – 24% and Africa – 13% (99). The disease starts with the development of fatty liver and may progress to non-alcoholic steatohepatitis (NASH) with hepatic inflammation (100). Approximately 10-25% of patients who suffer from fatty liver end

up with NASH, and within 5 years an estimated 5-8% of those patients develop liver cirrhosis (101). In advanced stages liver cirrhosis may develop to liver hepatocellular cancer (HCC) that make NAFLD/NASH a risk factor for liver cancer (102). Excess FFAs is the main contributor in the progression of fatty liver disease.

Obese individuals exhibit high levels of circulating FFAs, which accounts for the majority of lipids in the NAFLD liver (103). Diet is an independent risk factor for the development of NAFLD (104). Western diet rich in refined grains, red meat, pastries, and beverages high in sugar are associated with the development of metabolic syndrome and NAFLD (104). Liver takes up the FFAs and stores them in the form of triglycerides. When the liver is overwhelmed, these triglycerides are exported to the circulation in the form of VLDL (Figure 7). High hepatic VLDL increases the concentration of circulating triglycerides and low density lipoprotein (LDL) and lower the concentrations of HDL (100). The majority of NAFLD cases are asymptomatic (105). Clinically, liver enzymes are used to assess the presence of liver disease. However, liver enzymes are elevated in only 20% of NAFLD patients (105). Indeed, Marchesini *et al* reported that 21% out of 799 obese patients showed increased level of ALT and AST (106). ALT, AST, ALP and GGT correlated with liver fat (107, 108). However, aminotransferases are more helpful in the diagnosis of NASH (109). High serum levels of hepatic enzymes are associated with obesity, and reversed with weight loss, with marked improvement in steatosis (110) (Figure 7).

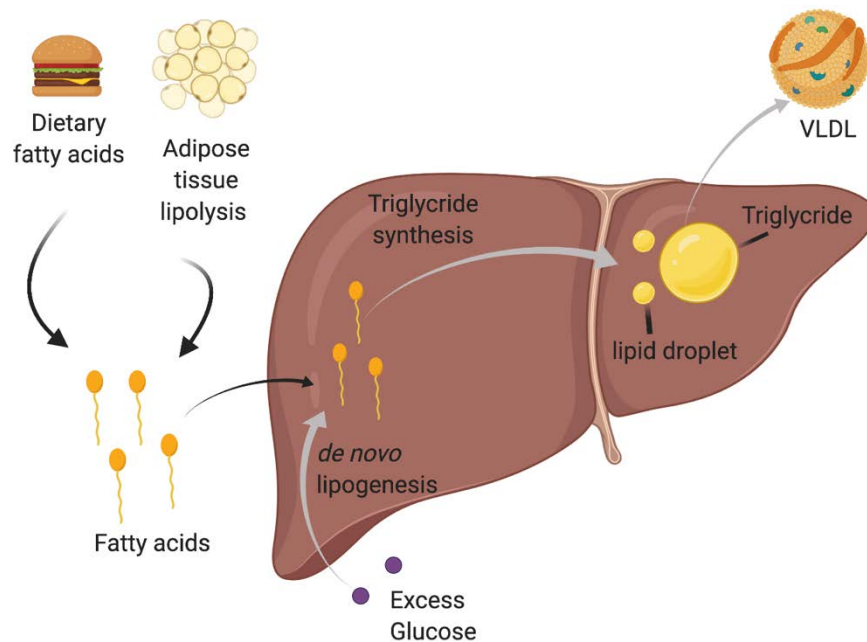


Figure 7: Pathophysiology of NAFLD.

High fat diet and lipolysis of adipose tissue increase FFAs in the circulation. FFAs are taken up by the liver from circulation or synthesized from *de novo* lipogenesis. Excess FFAs in the liver are used to synthesize triglyceride. Excess triglycerides are released to the blood stream as VLDL. Created with BioRender.com

1.6 Reversal of obesity related health outcomes through lifestyle intervention

Gaining weight is combined with increase in fat mass, and the induction of the secretion of biochemical products from adipose tissue, adipokines, that disrupt the metabolic signaling pathways (111). These abnormalities include abnormal lipid profile, insulin resistance and ectopic fat deposition.

1.6.1 Modifiable and non-modifiable risk factors

Obesity and overweight as a disease develop due to interaction between different risk factors. Generally, risk factors are divided into modifiable and non-modifiable. Modifiable risk factors are related to those, which can be changed, such as overweight, physical inactivity, diabetes, high blood pressure, and high blood cholesterol. Whereas the non-modifiable risk factors cannot be changed because they are related to genetic traits such as: age, ethnic background, and family history.

Lifestyle intervention is an influencing factor of modifiable risk factors that has a positive impact on obesity and obesity-related diseases. It has been reported that weight loss has a beneficial effect on obesity related disease. Different treatments are recommended to achieve successful weight loss. The recommendation of the proper treatment is dependent on the severity of obesity and its related diseases (co-morbidities).

1.6.2 Lifestyle intervention

Achieving weight loss via lifestyle intervention is an efficient and safe approach to treat obesity-associated diseases (112). This strategy depends on restriction, inclusion, or exclusion of different foods. Recently, Freire classified dietary intervention strategies into three main programs based on: 1) diet, changes in the macronutrients (lipid, protein, and carbohydrate) such as low-carbohydrate, low-fat and high-protein diets. 2) restriction of specific foods, like the Mediterranean diet, gluten-free, vegan, vegetarian etc. 3) timing of food intake, such as fasting, prolonged, intermittent etc. (113). Manipulation of dietary macronutrients has been reported to affect gene expression, metabolic pathways, hormones that affect fat storage and deposition (114). Carbohydrate is the most effective macronutrients that

induce the secretion of insulin, and consequently increase the fat deposition in adipose tissue as the ultimate fat storage destination (114).

Weight loss of 5% to 10% is highly recommended for individuals with MS due to its impact on metabolic parameters (115). The diabetes prevention program showed an effective improvement in glucose level with lifestyle intervention associated with weight loss (116). The withdrawal of CAF feeding in an animal study was able to return the circulating glucose level to its basal level (117). Studies also support the reversal of lipid profile with weight loss associated with dietary intervention. Changes in systemic triglycerides (45) and HDL cholesterol are the significant outcomes of overweight and obesity. Lifestyle intervention is able to manage the abnormal levels of TG and HDL cholesterol and return them back to their normal levels (118). Weight reduction directly affects TG, because it is the most sensitive lipid parameter and result in more favorable levels (119). Consequently, favorable levels of lipid parameters and glucose reduce the risk of CVDs (118). Weight loss has positive effects on blood pressure in hypertensive patients (120). Modest weight loss (5-10%) of initial weight showed to be able to reverse obesity related comorbidities with lifestyle intervention as reported in human studies (121). The degree of improvement depends on the obesity level; morbid obesity for example requires greater weight loss to achieve a satisfactory clinical improvement (122).

NAFLD is another complication of diet-induced obesity. It has been suggested that dietary and lifestyle intervention is a good strategy to recover NAFLD and NASH. NAFLD recovery depends on the severity of the diseases (Figure 8). Liver damage ranges from simple steatosis to fibrosis and cirrhosis. Histological assessment showed that as the severity is increased, the chance of reversing healthy liver is decreased (123). Supporting evidence showed that weight reduction markedly improved steatosis and liver enzymes (110). To date weight loss is the best option to treat NAFLD and NASH (124).

Non-alcoholic fatty liver disease (NAFLD) spectrum

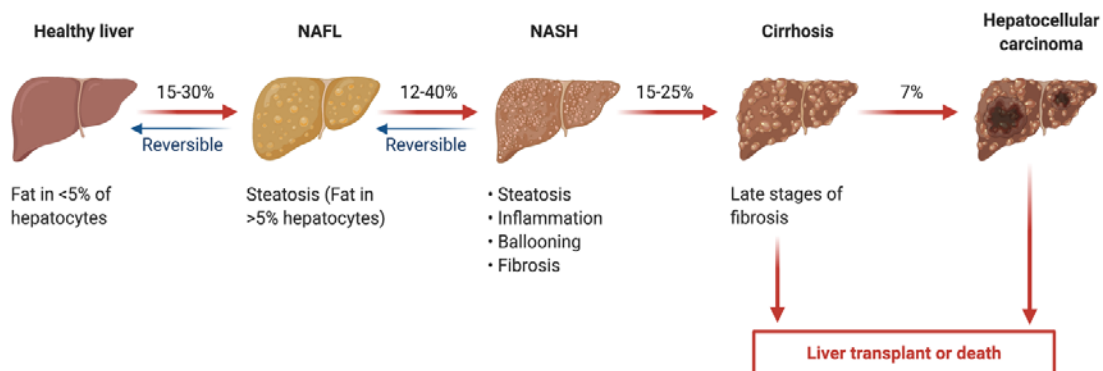


Figure 8: Spectrum of Non-alcoholic fatty liver disease (NAFLD)

The reversal of liver damage caused by steatosis is dependent on the severity of the disease, as the severity increased the chance of liver recovery decreased. Created with BioRender.com.

1.7 Aims and Objectives

Obesity and obesity related co-morbidities are pathological phenomenon that threatens global population. Although the disease has a possible genetic susceptibility, however it is mainly related to lifestyle features, such as diet and physical activity. Most DIO rodent models of obesity are based on high fat intake. However, human diets are more likely to be composed of increased calorie intake as carbohydrates, and, to a slightly lower extent, fat.

Hypothesis:

Therefore, the current study tested the hypothesis that high carbohydrate diet increases ectopic fat deposition, cardio-metabolic risk, and development of NAFLD, which are reversible with weight loss induced by dietary restriction.

To test the above hypothesis, the study aimed to:

- 1- Establish a diet-induced obesity rat model using high carbohydrate diet (CAF diet), followed by dietary restriction (REV) to induce weight loss.
- 2- Assess the extent to which CAF diet induced body weight gain, changes in fat distribution, metabolic parameters, and determined the effectiveness of CAF withdrawal on reversing these changes.
- 3- Determine whether CAF diet-induced obesity increased cardiometabolic risks and affected the vascular function in the DIO model. Moreover, to assess the extent to which diet switch could reverse these abnormalities.
- 4- Investigate if this DIO model developed NAFLD, and the degree of NAFLD progression. In addition, to assess the efficiency of dietary intervention in reversing NAFLD.
- 5- Explore the alterations in hepatic transcriptome and determine the mechanistic pathways associated with both weight gain and weight loss.

This study would contribute to the existing knowledge of diet-induced obesity, and, assess the extent to which CAF withdrawal could induce weight loss and reverse obesity-associated abnormalities. In addition, the transcriptomic analysis could help in discovering biomarkers that have disease management and therapeutic potential.

CHAPTER 2: MATERIALS AND METHOD

2.1 Animals

Seventy-nine male Sprague-Dawley rats (purchased from Charles River-UK) aged 4-5 weeks were housed in individual ventilation cages (IVC). Following the Guide for the care and use of Laboratory Animals, environmental conditions were maintained as follows: temperature ($20-26^{\circ}\text{C}\pm 1^{\circ}\text{C}$), Humidity ($30-70\%\pm 5\%$), 12:12 light/dark cycle and given *ad libitum* access to Normal Chow (NC). Rats were maintained under control conditions until they reached adult age (8 weeks). At 8 weeks old, rats were weighed and randomly assigned to the following diet groups: Normal chow (NC) as a control group, Cafeteria diet (CAF) and Reversible (REV) (Figure 1). In each group, the animals were housed at 3 animals/cage. The NC group had *ad libitum* access to NC diet and plain water without additives (Table 5), while the CAF group had *ad libitum* access to NC diet, a highly palatable Cafeteria style diet with known nutritional contents (Table 5) and water with 5% added sugar to represent the soda drinks (the total carbohydrate content represented the food and the sugary water). CAF diet was provided freshly every day. Animals in the CAF group could select and consume freely the diet between NC and CAF, which were provided in excess. CAF feeding was performed for 16 weeks until rats gained 20-30% of body weight compared to their control. In order to induce weight loss, part of CAF group was assigned as REV group, and their diet was changed from CAF to NC by the end of week 18 (Figure 9). The gap between the end of obesity period and the start of recovery period was two weeks. In this gap the dissection for CAF group and the blood pressure measurement for the REV (before reversibility) was performed. The dissection and sample collection of CAF group was performed in weeks 16 and 17, while the blood pressure measurement for the REV group was done on week 18.

Food intake, water intake and body weight were measured weekly throughout the study. For the body weight, a cutoff point (threshold) at 580 gm was set, and any rat that exceeded this threshold considered as obese. Animals and cages were observed daily for any abnormal conditions or behavioral changes.

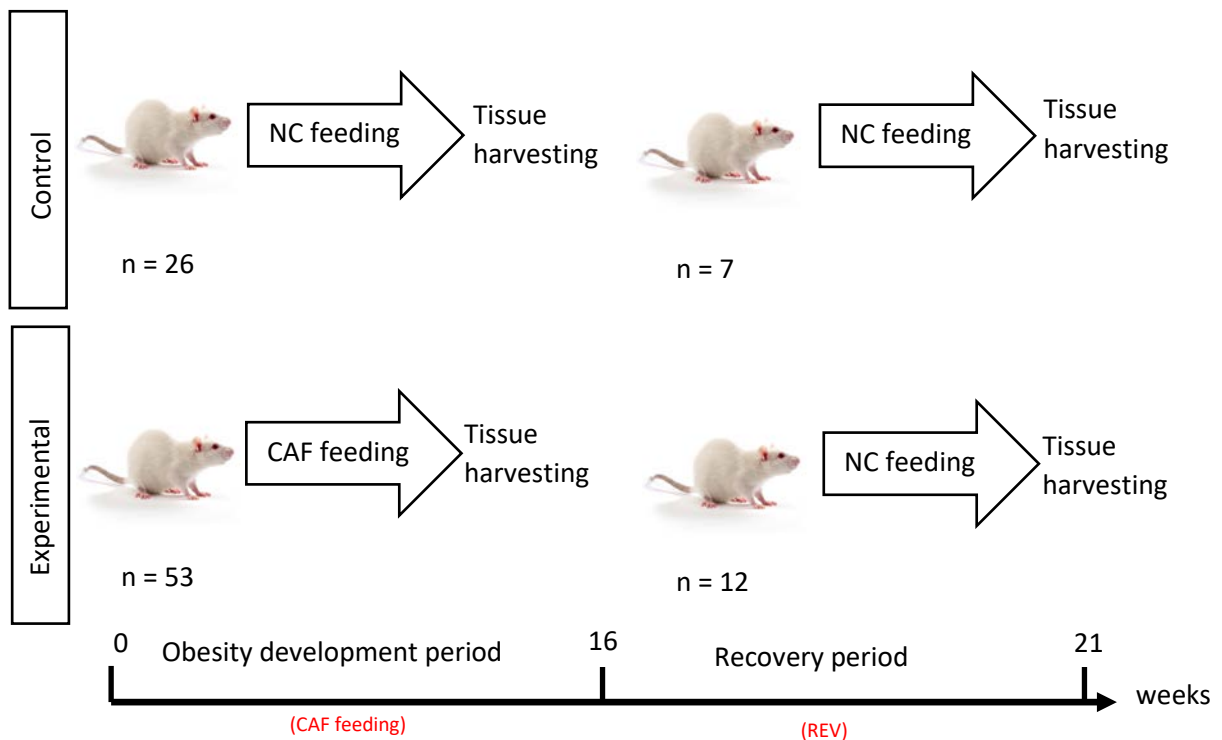


Figure 9: Rodent model study design.

Rats were grouped into 2 groups: NC; fed with normal chow, and CAF; fed with normal chow and cafeteria diet. When CAF-fed rats gained around 20-30% of their body weight at week 16, tissues were harvested along with their control from NC-fed group. Part of CAF-fed rats group was shifted to normal chow (REV) until weight loss was observed. Tissues were harvested as an end point of the study.

Table 5: Nutritional content of NC and CAF diets.

Diet	Fat (%)	Protein (%)	Carbohydrate (%)
NC	2.71	14.37	49
CAF	10	9-12	60-70

The table represents the percentage of carbohydrates (CHO), protein and fat for both diets: Normal chow (NC) and Cafeteria-style diet (CAF).

2.2 CAF Diet Preparation

CAF diet characterized by high carbohydrates was used in this study. The food items used in the study were available in the local market and consumed by human subjects. The selection was initially based on the food label, and then these food items were sent to the food analysis laboratory (Central Food Laboratories, Public Health Department, Ministry of Health -Qatar) to confirm the nutritional contents. The final selection of the food items was based on the lab analysis results except the Macaroni, because it was added in the middle of the study. Despite the other nutritional contents of the diet, in this study we focused only on the percentage of macronutrients: Carbohydrate, fat and protein.

Diet was prepared freshly every day using the following food items: frozen burger, sliced bread, macaroni, mini croissant and refined sugar (Table 6). These items were grouped into 3 mixtures (Table 7). Items in mixture 1 and 2 were mixed and served as a homogenized meal, while items in mixture 3 were served separately without mixing. The carbohydrate content was completed by adding refined sugar to each mixture. All mixtures were provided equally (every day) in a raw form without cooking in a sterilized plate inside the cage. Rats were offered the three food mixtures in different duration. In the beginning of the study the food was changed in week 9, then food was changed between the 3 combinations every 2 weeks throughout the study to sustain increased food consumption.

Table 6: Nutritional contents for food items.

Table represents the nutritional content for each food item used in the study from lab analysis and the commercial label.

Parameter	Americana beef burger		Al Arabiya Beef burger		Mini Croissant		Milk slice bread		Macaroni	
	Lab analysis (%)	Commercial label (%)	Lab analysis (%)	Commercial label (%)	Lab analysis (%)	Commercial label (%)	Lab analysis (%)	Commercial label (%)	Lab analysis (%)	Commercial label (%)
Moisture content	24	-	19	-	24.6		34.5		NA	-
Ash content	5.8	-	4	-	1.20		1.2		NA	-
Fat content	20	16.16	6	9.7	15	15	1.4	1.8	NA	1.7
Fiber content	2.2	-	4	-	3.8	4.5	3	2.9	NA	2
Protein	12		14.4	15.6	8	10	6.3	8.9	NA	12
Carbohydrate	36.0	40	52.6		47.4	52	53.6	56.4	NA	71

Table 7: CAF diet combinations provided to CAF group throughout the study. Three varieties of diet combinations were offered to CAF group to induce the diet consumption.

Mixture 1	Mixture 2	Mixture 3
Milk slice bread and Americana beef burger	Mini croissant and Al Arabiya beef burger	Pasta and Americana beef burger

2.3 Blood pressure measurements

Systolic (SBP) and diastolic (DBP) blood pressure were measured by using the CODA tail-cuff blood pressure system (CODA™, Kent Scientific Corporation, Torrington, CT, USA) (126). Initial blood pressure was measured one week before the study began. Final blood pressure for CAF group was measured before dissection and sample collection. For the REV group, blood pressure was measured after CAF feeding before starting reversibility, and after reversibility before dissection and sample collection (Figure 10). Procedure was performed following the system user guide. Rats were randomly picked from the cage and restrained in the rat holder. Once rat was restrained it was placed on a warming pad to induce the blood flow in the tail. The occlusion cuff was placed close to the base of the tail, and the Volume Pressure Recording (VPR) cuff placed 2mm away from the occlusion cuff. Before starting the measurement of the blood pressure, tail temperature was measured using non-contact infrared thermometer. The tail temperature should be between 32-35°C. Five cycles were set as acclimation cycles and fifteen as regular cycles. The average of five accepted cycles was calculated for each rat readings.

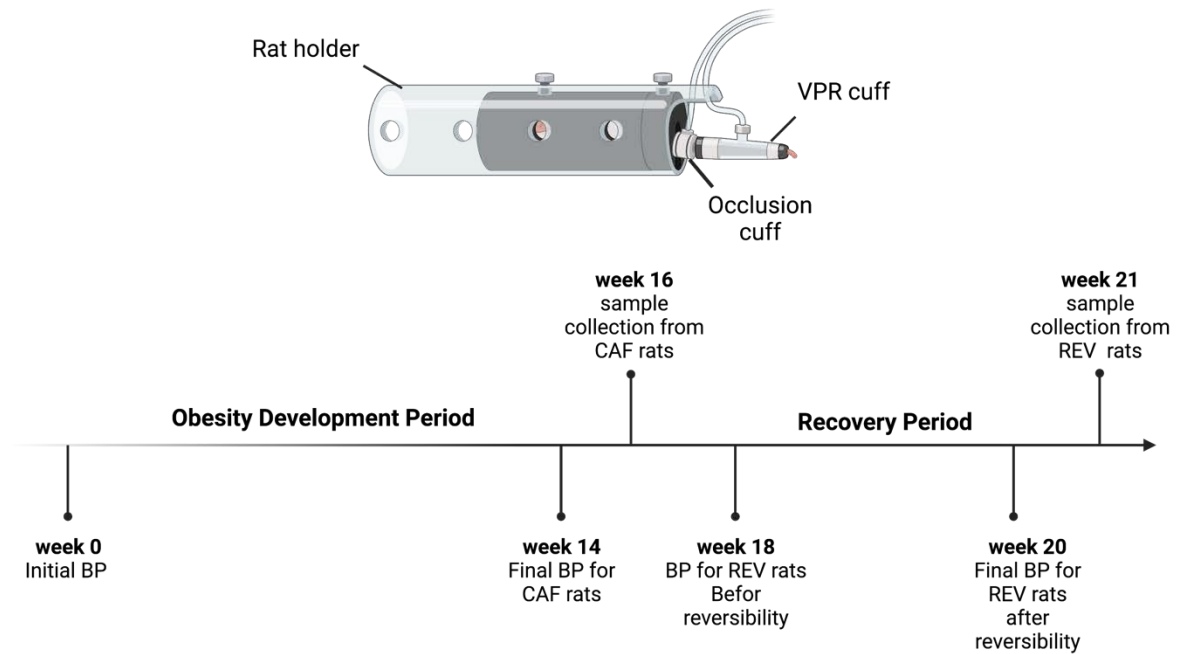


Figure 10: Timeline for blood pressure (BP) measurement.

Blood pressure was measured initially before the CAF feeding, 14 weeks post- CAF feeding (final BP for CAF group). For REV group, BP was measured before reversibility (week 18) and after reversibility (week 20).

2.4 Animal dissection and sample collection

Animals were fasted for 12 hrs prior to dissection. Animals were anesthetized with 20mg/kg pentobarbital. Blood was collected by cardiac puncture as a terminal procedure in three different tubes. After blood collection animals were dissected immediately to collect the following organs: Thoracic aorta ring (ascending aorta) and liver. Tissue samples were washed with 1X phosphate buffered saline (PBS) (NaCl 0.137M; KCl 2.7mM; Na₂HPO₃ 0.01M; NH₂PO₄ 1.8mM; PH 7.4) before processing, except the thoracic ring; it was placed directly on 1X physiological salt saline (PSS) (NaCl 112 mM; KCl 5 mM; CaCl₂ 1.8 mM; MgCl₂ 1mM; NaHCO₃ 25 mM; KH₂PO₄ 0.5 mM; glucose 10 mM). Tissue weight was recorded for liver.

2.5 Blood samples processing

Blood samples were collected in K₂EDTA tube and Serum separator Tube (SST) to separate plasma and serum samples respectively. Samples were centrifuged at 600 xg for 10 min. Serum and plasma samples were collected in aliquots in 1.5ml Eppendorf tubes and stored at -80°C until analysis.

2.6 Organ bath and vascular reactivity

The ascending thoracic aorta was trimmed from fat and connective tissue. Aortic rings were cut (~4 mm in length) (Figure 11) and mounted at the optimal length for isometric tension recording in tissue organ bath (model 750TOBS, DMT Systems, Aarhus, DK). Organ baths contained 20 ml of PSS solution. The solution was kept at 37 ± 0.5 °C, and saturated with gas mixture of 95% O₂, 5% CO₂. The aortic rings were allowed to normalize and equilibrate for at least 30 min under a resting tension of 1.5 g. After this period, the vessel was stimulated with 90mM KCl to test for viability. Cumulative concentration-effect curves were constructed from the response of the tissue to noradrenaline (NA) (10^{-9} – $10^{-4.5}$) to assess the contractile function of each aortic segment. Endothelial function was assessed by studying the relaxing effects of cumulative concentration of Acetylcholine (Ach) (10^{-9} – $10^{-4.5}$) on arteries contracted with the effective dose of NA (ED₅₀ 100 nM). Each dose-response curve was established and separated by a washout period of 30-60 min.

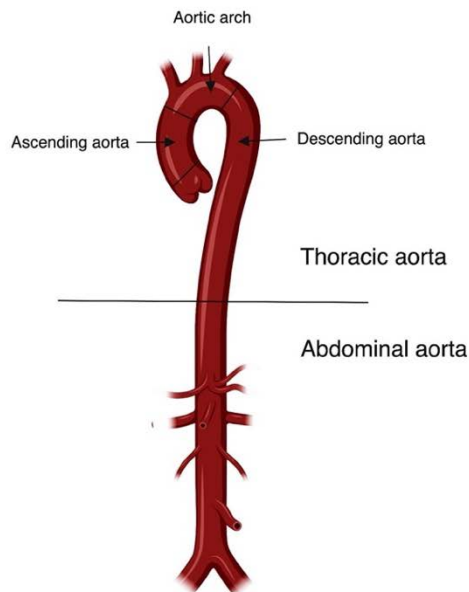


Figure 11: Illustration of thoracic aorta anatomy.

Different parts of thoracic aorta are shown; ~ 4mm aortic ring of thoracic aorta was used to run the vascular studies using organ bath system. Created with BioRender.com

2.7 Histological studies

Histological examination are a standard and powerful technique using microscopy to visualize structural changes in tissue sections. It is a well-established technique widely used in medicine, especially in disease diagnosis. This was done on the liver tissue sections.

2.7.1 Fixation

All tissue samples of liver were fixed in 10% buffered formalin immediately after harvesting and washed with PBS. Fixation was performed for 24 to 48 hrs. After fixation, samples were washed with tap water and then stored in 70% ethanol.

2.7.2 Sample processing

Samples were trimmed and placed in a cassette with proper labeling. All labelled cassettes were loaded in the automated processor (HISTO-PRO 300 VACCUM TISSUE PROCESSOR, Histo-Line Laboratories, Italy) chamber. Samples were

processed starting with dehydration in a serial concentration of alcohol, then alcohol was cleared by processing the samples in xylene solvent to facilitate the paraffin infiltration (Figure 12).

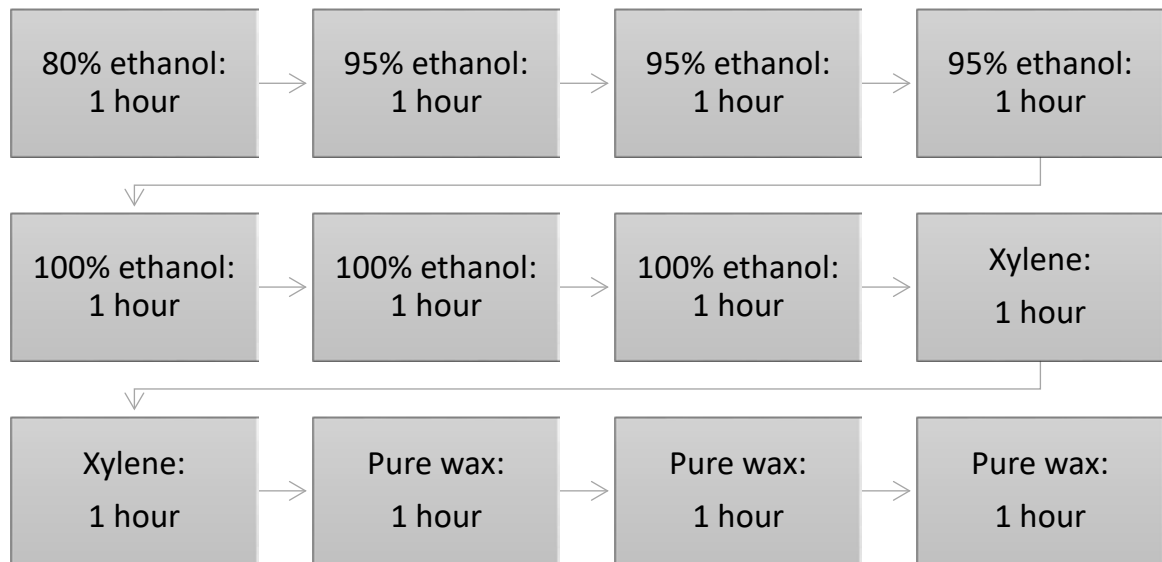


Figure 12: Steps of sample processing for histological studies.

Chart illustrates the tissue processing steps from tissue dehydration to wax infiltration.

2.7.3 Embedding process

Embedding tissue into paraffin supports the tissue structure and helps sectioning tissue into very thin slices. After tissue processing, tissue samples were embedded into paraffin wax using embedding workstation (TEC2900 Embedding Center, Histo-Line Laboratories, Italy). The stainless-steel base mold was taken from the storage compartment and placed on the hot spot of the station. Warm tissue sample was positioned in the desired position, and paraffin wax was poured on the tissue. The mold was immediately covered by the cassette. The full assembly; the wax and cassettes; was placed on the cold plate until solidified. After wax solidification, the mold removed carefully, and wax block left on cold plate for more solidification.

2.7.4 Sectioning

Paraffin-embedded tissue blocks were chilled on ice. Cold wax gives more support to the tissue and allows thinner sections during sectioning. First the wax block was trimmed at 10-30mm until tissue surface was exposed and showed representative sections to cut. Second, the exposed surface was soaked in very cold water for a couple of hours, this step allows the moisture to penetrate the tissue and make the sectioning easier. Third, the paraffin block was inserted and oriented in the microtome to start sectioning. Fourth, sectioning was performed at 4-5mm, and the ribbon formed was floated on the pre-heated water bath at 37°C. Sections were separated using tweezers. Finally, sections were picked out from the water bath using microscopic slides and placed upright in a slide rack. Slides were dried at 37°C overnight.

2.7.5 Staining of paraffin-embedded tissue

At this level histological sections were stained to visualize the cells and tissue structure. Staining can be performed either by non-specific stain, to show the general structure within a tissue section, or specific staining to show specific changes within a tissue section.

2.7.5.1 Hematoxylin and Eosin staining

Hematoxylin and eosin are the most commonly used non-specific stain. This stain is a combination of acidic and basic dyes. Hematoxylin is a basic dye stains acidic structures of stained tissue such as nucleus which turned into purple. While the eosin is acidic dye that targets basic structures of the cell and turn it to pink color such as cytoplasm, intracellular membrane and fibers. Staining steps started with dewaxing, hydration with decreasing serial concentration of alcohol, hematoxylin staining, dehydration with increasing serial concertation of alcohol to remove excess water

from tissue section, eosin staining, more dehydration and finally clearing with xylene (Figure 13).



Figure 13: Hematoxylin and Eosin staining steps.

Sections were dewaxed with xylene, hydrated with decreasing serial concentration of alcohol before hematoxylin staining, dehydrating with increasing serial concentration of alcohol before eosin staining. Ensure dehydration after eosin stain to remove any excess water before clearing with xylene.

Once slide staining was performed, one drop of DPX (mounting media) was added on the slide and coverslip was loaded gently on the slide and allow the DPX to spread beneath the coverslip. H&E stained slides were used to examine the development of non-alcoholic fatty liver diseases. The analysis of stained sections was performed from 5 independent control animals and 6 independent treated animals and each animal had five liver sections. Histological evaluation for liver sections was performed blindly. Five fields were randomly selected from each section to evaluate the grade of hepatic steatosis as described previously (127). The degree of steatosis was graded 0-3 based on the average percent hepatic fat-accumulation per field at 20X magnification. The following histological features were examined: hepatocyte ballooning, micro-vesicular steatosis, macro-vesicular steatosis, polymorphonuclear

leukocytes cells PMNC and mononuclear cells MNC (Table 8). Validation of NAFLD grading was performed blindly by a trained histopathologist.

Table 8: Histological features used in NAFLD evaluation and grading (124).

Hepatic steatosis	0	1	2	3	
Hepatocyte ballooning	absent	mild	Moderate	Severe	
Microvesicular steatosis	=>5%	5-33%	33-66%	>60%	
Macrovesicular steatosis	=>5%	5-33%	33-66%	>60%	
Inflammation	0	1	2	3	4
PMNC infiltration (foci/field)	absent	minimal	Mild	Moderate	severe
MNC infiltration (foci/field)	absent	minimal	Mild	Moderate	severe

2.7.5.2 Picro-sirius red staining

Picro-sirius red is a specific stain that detects collagen networks in normal and pathological tissue sections. Sections were dewaxed in xylene for 10 min, and rehydrated in serial concentration of alcohol (100%, 90% and 70%). On a tissue section circled with paraffin pen, drops of Weigert's iron hematoxylin (Merk, cat # HX73929273, Germany) was added for 10 min to stain the nucleus. After 10 min slides were washed with running tap water for 5 min. Once washing was performed, picro-sirius red (Direct Red 80, Sigma, cat # 365548-5G, USA) drops were added to each slide and left for 1 hour. Then slides were dipped in 1% acid alcohol 2 to 3 times and immediately transferred to 100% ethanol for 10 dips. Finally, slides were dipped in xylene and mounting with a drop of DXP and coverslip. Slides were examined under light microscope and assessed for abnormal collagen deposition.

2.8 Biochemical analysis

Serum samples were used for the assessment of biochemistry parameters that had changed, perhaps due to the diet. These parameters include glucose level, lipid profile (cholesterol, triglycerides, high-density lipoprotein cholesterol (HDL) and low-density lipoprotein cholesterol (LDL)) and liver function (ALT, AST and ALP). Measurements were performed using a clinical chemistry analyzer (COBAS INTEGRA 400 plus).

2.9 Measuring insulin level using ELISA

Plasma insulin level was measured using rat insulin enzyme-linked immunosorbent assay (ELISA) commercially available kit (Alpco Immunoassays; catalog #80-INSRT-E01) according to manufacturer instructions. All reagents, samples and standards were prepared as instructed. Ten μl of standards, control and samples were added into their respective wells of 96-well plate (provided by the kit). In addition 75 μl of working strength conjugate was added into each well. The plate was sealed and incubated for 2 hours at room temperature with shaking at 700-900 rpm on a microplate shaker. After incubation, washing was performed 6 times for each well with 350 μl of washing buffer. Residual wash buffer and bubbles were removed by inverting and tapping the plate on absorbent paper. Then 100 μl of TBM substrate was added to each well, plate was sealed, and incubation was performed at room temperature for 15 minutes with shaking at 700-900 rpm on a microplate shaker. 15 minutes later, 100 μl of stop solution was added into each well and shake gently to mix the contents. Microplate was analyzed using a microplate reader (Biochrom EZ Read 400, Galapagos Software, UK) at 450nm within 30 min of adding the stop solution. By the end of the assay, standard curve was contracted from the standards and samples concentrations were determined (Figure 14).

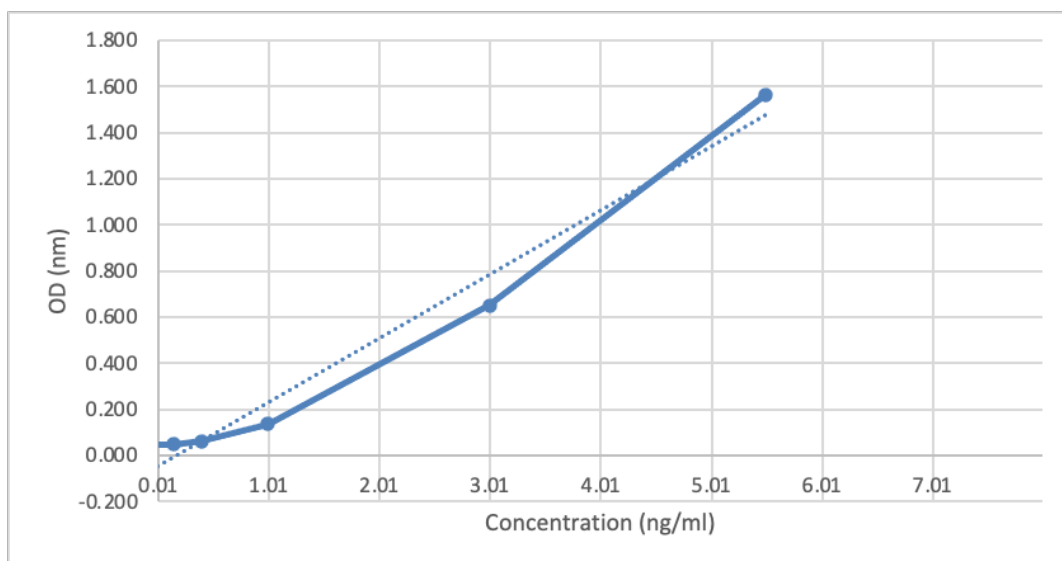


Figure 14: Insulin assay standard curve.

Standard curve of concentration versus absorbance. The concentration of insulin in ng/ml was determined using the equation $y=0.2766x-0.0455$ with an R^2 value of 0.987. Where y is absorbance and x is concentration.

2.10 Triglyceride quantification in liver tissue

Triglyceride Quantification assay kit (Colorimetric/Fluorometric) (abcam, cat# ab65336) was used to determine TG levels in liver tissue. It is a sensitive assay to measure triglyceride concentration. In this assay triglyceride is converted to free fatty acids and glycerol, then glycerol is oxidized and generates a product which reacts with the triglyceride probe to form a color at 570nm. The detection range of assay was between 2 μ M – 10mM. The colorimetric procedure was followed to perform this assay.

2.10.1 Tissue samples preparation

Tissues were prepared by grinding 100 mg of liver sample using mortar and pestle with liquid nitrogen. Homogenized samples were re-suspended in 1ml of 5% NP-40 (Thermo Scientific, cat # 85124, Switzerland)/ddH₂O solution using pestle for 10-15

passes. Then samples were heated slowly to 80-100°C in a water bath for 2-5 minutes or until the NP-40 solution becomes cloudy. Following the heating step, samples were cooled down at room temperature (heating and cooling step was repeated to solubilize all the triglycerides). Once triglycerides were solubilized, samples were centrifuged at top speed (24,000 g) for 2 min to remove any insoluble materials. Finally, samples were diluted 10-fold.

2.10.2 Assay Procedure

All assay materials and prepared reagents were equilibrated at room temperature. Standard dilutions were prepared following the assay protocol. All standards and samples were assayed in duplicate. 50µl of standard dilutions were added into each well. 25µl of samples were added into each well, and volume was adjusted to 50µl/well with triglyceride assay buffer. One sample background control was applied in the assay by adding 25µl of sample background control in the well (volume adjusted to 50µl with triglyceride assay buffer). 2µl of lipase (provided with the kit) were added to standard and samples wells, and 2µl of triglyceride assay buffer were added to the sample background control. Reaction was incubated for 20 min at room temperature to convert triglyceride to glycerol and fatty acid. 50µl of reaction mix were added to each standard, sample and sample background control. Reaction was incubated for 60min at room temperature and protected from light. The output was measured using a multiplate reader (VERSAmax Tunable Multiplate Reader, Molecular Devices, USA) at 570nm. Standards, control and samples were assayed in duplicate.

2.10.3 Data Analysis

The average of duplicate readings was calculated. The average absorbance was corrected by subtracting the mean value of the blank from standards, control and samples. The standard curve then was constructed from the corrected values of the standards. After plotting the standard curve, the corrected sample OD readings were

applied to get the amount of triglyceride in each sample in nmol. Finally, the concentration of the triglyceride was calculated using the following formula:

$$\text{Triglyceride concentration} = B / V * D$$

Where:

B = amount of triglyceride in the sample well calculated from standard curve in nmol.

V = sample volume added in the sample wells (μL).

D = sample dilution factor if sample is diluted to fit within the standard curve range

2.11 Transcriptome studies

2.11.1 RNA Extraction

Total RNA was extracted from tissues following TRIzol® Reagent, protocol. Tissue was powdered using mortar and pestle under frozen condition with liquid nitrogen. Powdered samples were homogenized using 1ml TRIzol® Reagent (Invitrogen, Cat#: 15596026) and followed vortexing 10 times for 5 sec each and sit for 5 sec on ice in between spin. Homogenized samples were centrifuge for 5 min at 18,660 xg at 4°C. After centrifugation, supernatant was removed from each sample and transferred to a new cold tube. 100μl of chloroform was added in each tube, then samples were vortexed for 15 sec and left on ice for 15 min. After that, samples were centrifuged for 15 min at 18,660 xg and 4°C . Clear aqueous phase was collected into a new tube, and an equal volume of isopropanol was added. All samples were incubated at -20°C for 1hour and 30 min or overnight to allow precipitation.

After incubation, samples were centrifuged at 18,660 xg for 15 min at 4°C and isopropanol was removed carefully. The remaining pellet from each sample was washed twice with 0.8ml of 75% ethanol. Washing was performed twice by resuspension and centrifugation of the sample at 18,660 xg for 5min at 4°C. Then ethanol was removed carefully. Remaining pellets were dried on ice for 10 min. The

dried pellets were re-suspended with 45ml RNase free water. All sample were incubated at room temperature for 10min, then samples were vortexed and incubated on ice for 10 min. Samples were stored in -80°C for long term storage.

2.11.2 RNA concentration and purity

RNA concentration and purity were measured for all extracted RNA samples using NanoDrop spectrophotometer (NanoDrop 2000, Thermo Fisher, USA) at 260nm and 280nm, and the UV light peak absorbance for nucleic acid is at 260nm. NanoDrop calculates the RNA concentration in ng/ml. the ratio of 260nm and 280nm is used to assess the purity of RNA. A ratio of ~2 is generally accepted as pure. In this study, all RNA samples within the ratio between 1.7 to 2 A₂₆₀/A₂₈₀ ratio were used for downstream applications.

2.11.3 Reverse Transcription

The cDNA kit used in this procedure was High Capacity cDNA Reverse Transcription kit (200 reactions, cat #: 4368814, Thermo Fisher Scientific). The procedure was performed following the kit protocol. Prior to start the protocol, all kit reagents were thawed at room temperature except the enzyme it was thawed on ice. After thawing, 2X Master Mix was prepared (Table 9).

Table 9: Master Mix of reverse transcriptase reaction.

Component	Volume
10X RT Buffer	2.0 ml
25X dNTP Mix (100 mM)	0.8 ml
10X RT Random Primers	2.0 ml
MultiScribe Reverse Transcriptase	1.0 ml
Nuclease-free water	4.2 ml
Total per reaction	10.0 ml

10ml of 2X master mix pipetted into each well of 96-well reaction plate. Then 10ml of 200ng RNA sample was added to the master mix and mixed by pipetting. The plate was sealed centrifuged to spin down the content and eliminate air bubbles. The plate was loaded in the thermal cycler (Applied Biosystems™, USA) with the following program (Table 10):

Table 10: Thermal cycler incubation of reverse transcriptase reaction.

Setting	Step 1	Step 2	Step 3	Step 4
Temperature	25°C	37°C	85°C	4°C
Time	10 minutes	120 minutes	5 minutes	∞

2.11.4 RNA Quantification using Real-Time PCR

Quantitative real time PCR for rat GAPDH (Thermo Fisher Scientific Cat# Rn01775763_g1) was performed using SYBR green.

2.11.5 Whole Transcript (WT) Expression Arrays

Whole transcriptome profiling for isolated liver tissues was carried out on GeneChip WT PLUS Reagent Kit (Clariom™ S Assay HT, Rat, ThermoFisher Scientific, Cat#: 902974). This assay is a second-generation transcriptome-wide gene-level expression profiling tool, to generate a comprehensive expression profile and biomarker. Total RNA (50 - 500 ng) were processed for hybridization of Rat Clariom S Assay kit (Figure 15).

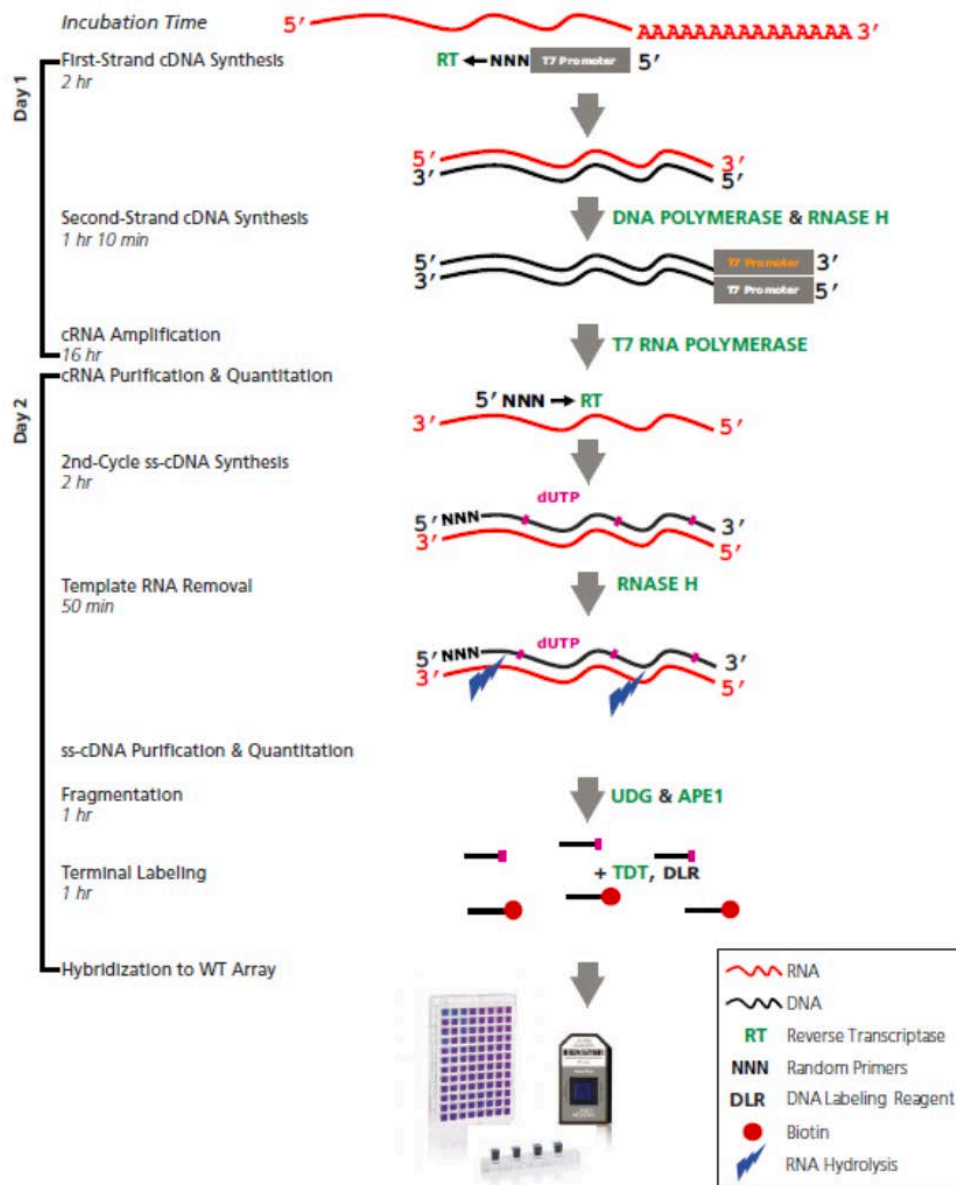


Figure 15: Whole Transcript (WT) PLUS Amplification and Labeling Process.
(WT Reagent Kit Manual)

2.11.5.1 Synthesize First-Strand cDNA

The first-strand master mix was prepared on ice for all total RNA samples in the experiment (Table 11):

Table 11: First-Strand Master Mix

Component	Volume for one reaction
First-strand buffer	4 ml
First strand enzyme	1 ml
Total volume	5 ml

Master Mix was mixed by gentle vortexing and centrifuged; 5ml of first-strand master mix was added to each well of 96-well plate (this step performed on ice). Then total RNA samples were added to each master mix aliquots (final reaction volume; 10 ml), mixed and centrifuged. Finally, the first-strand synthesis reaction was incubated in the thermal cycler for 1 hr at 25°C, then for 1 hr at 42°C, then at least for 2 min at 4°C. After incubation, immediate centrifugation was performed, and samples placed on ice for 2 min before proceeding with next step.

2.11.5.2 Synthesize Second-Strand cDNA

Second-strand cDNA master mix was prepared for all first-strand cDNA samples (Table 12):

Table 12: Second-Strand Master Mix

Component	Volume for one reaction
Second-strand buffer	18 ml
Second-strand enzyme	2 ml
Total volume	20 ml

Master mix was mixed by gentle vortexing and centrifuged, 20ml of second-strand master mix was added to each 10ml first-strand cDNA sample (this step performed on ice) mixed and centrifuged. Finally, reaction was incubated 1 hr at 16°C, 10 min at 65°C, 2 min at 4°C. After incubation, immediate brief centrifugation was performed, and samples placed on ice.

2.11.5.3 Synthesis of cRNA by *in Vitro* Transcription

In this step, complementary RNA was synthesized by *in Vitro* Transcription (IVT) of the second-strand cDNA template using T7 RNA polymerase. Master mix was prepared at room temperature for all second-strand cDNA (Table 13):

Table 13: IVT Master Mix

Component	Volume for one reaction
IVT buffer	24 ml
IVT enzyme	6 ml
Total volume	30 ml

Master mix was mixed by gentle vortexing and centrifuged, 30ml of the IVT master mix was transferred to each 30ml second-strand cDNA sample (this step performed at room temperature), mixed and centrifuged. Finally, reaction was incubated for 16 hr at 40°C, then at 4°C. After incubation, immediate brief centrifugation was performed, and samples were placed on ice.

2.11.5.4 Purify cRNA

In this step, cRNA purification was performed by removing enzymes, salts, inorganic phosphates, and unincorporated nucleotides to prepare it for 2nd-cycle single-stranded cDNA synthesis.

First the purification beads were mixed well by vortexing to re-suspend any settled particles. Then 100ml of the purification beads was added to each 60ml of cRNA and mixed by up and down pipetting. After mixing, the samples were transferred to a U-bottom plate and mixed again by pipetting. Incubation was performed for 10 min, cRNA binds to the purification beads during the incubation. Once incubation finished, the plate was moved to a magnetic stand to capture the Purification beads. The purification beads then formed pellets due to the effect of the magnets in the magnetic stand. Supernatant was discarded without disturbing the Purification beads. Washing was performed for the purification beads pellets with 200ml of 80% ethanol 3times/3sec each. The plate exposed to air-dry for 5min. The plate then was removed from the magnetic stand and 27ml of preheated nuclease free water was added to each well and incubated for 1 min to elute cRNA. It was mixed well by pipetting 10 times and then the plate was moved again to the magnetic stand for ~5 min to capture the purification beads. The produced supernatant contained the eluted cRNA. The purified cRNA was transferred to nuclease free water and placed on ice. All cRNA samples yielded from this step were assessed by NanoDrop spectrophotometer (NanoDrop 2000, Thermo Fisher, USA) at 260nm and 280nm.

2.11.5.5 Assess cRNA yield and size distribution

Concentration of cRNA was determined by measuring its absorbance at 260 nm using NanoDrop spectrophotometer (NanoDrop 2000, Thermo Fisher, USA).

2.11.5.6 Synthesis 2nd- Cycle single-Strand cDNA

In this step, the synthesis of cDNA was performed by reverse transcription of cRNA. On ice, 24ml of cRNA (15mg) were combined with 4ml of 2nd-Cycle Primers. Centrifugation was applied to collect the mix from bottom of the tube. The cRNA Primers mix was then incubated in a thermal cycler at 70°C for 5 min, then at 25°C

for 5 min, and then at 4°C for 2 min. Following incubation, the cRNA/Primers mix was centrifuged and placed on ice. 12ml of the 2nd-Cycle ss-cDNA Master mix (Table 14) was added to each cRNA/2nd-Cycle Primers sample, mixed gently and centrifuged. The reaction was incubated in at 25°C for 10 min, then at 42°C for 90 min, then at 70°C for 10 min, then at 4°C for 2 min. After incubation, samples were immediately placed on ice.

Table 14: 2nd-Cycle ss-cDNA Master Mix

Component	Volume for one reaction
2 nd -Cycle ss-cDNA buffer	8 ml
2 nd -Cycle ss-cDNA enzyme	4 ml
Total volume	12 ml

2.11.5.7 Hydrolyse RNA using RNase H

This step aimed to use RNase H to hydrolyze cRNA template to form single-stranded cDNA. First 4 ml of RNase H was added to each 2nd-Cycle ss-cDNA sample, mixed gently and centrifuged. Second, incubation was performed at 37°C for 45 min, then at 95°C for 5min and then at 4°C for at least 2 min. After incubation samples were centrifuged and immediately placed on ice. 11ml of nuclease-free water was added to each hydrolyzed 2nd-cycle ss-cDNA sample, mixed gently and centrifuged. The hydrolyzed ss-cDNA samples were stored overnight at -20°C.

2.11.5.8 Purify 2nd-Cycle Single-Stranded cDNA

This step aimed to purify the 2nd ss-cDNA to remove enzymes, salts and unincorporated dNTPs. After this step, the cDNA is ready for fragmentation and labeling. 100 ml of purification beads was added to each 2nd-cycle ss-cDNA sample, mixed well by pipetting and transferred to a U-bottom plate wells. 150ml of absolute ethanol was added to each ss-cDNA/Beads sample, mixed 10 times by pipetting and incubated for 20 min. during this incubation, the ss-cDNA in the samples bind to the

purification beads. Then the plate was moved to a magnetic stand to capture the purification beads. The capture finished within ~5 min until the mixture is transparent and purification beads formed a pellet in the bottom of each well. The clear supernatant was discarded without moving the plate from the magnetic stand and disturbing the purification beads. Washing of the purification beads was followed by adding 200ml of 80% ethanol wash solution to each well and incubated for 30s. Then the 80% ethanol was aspirated and discarded without disturbing the purification beads. Washing step was performed 3 times. After final wash, the plate was left to air-dry on the magnetic stand for 5 min. The plate was removed from the magnetic stand to elute the ss-cDNA. 30ml of preheated (65°C) Nuclease-free water was added to each well and incubated for 1 min. It was mixed well 10 times by pipetting. After mixing, the plate was moved again to the magnetic stand and incubated for ~5min to capture the purification beads. The supernatant of each well, eluted ss-cDNA, was transferred to nuclease free tube and placed on ice. Finally, the concentration of the ss-cDNA was measured at 260nm using NanoDrop spectrophotometer (NanoDrop 2000, Thermo Fisher, USA).

2.11.5.9 Fragment and label Single-Strand cDNA

In this step, the purified ss-cDNA that resulted from the previous step was fragmented by the enzymes uracil-DNA glycosylase (UDG) and apurinic/apyrimidinic endonuclease 1 (APE 1) at the unnatural dUTP residues and breaks the DNA strand. This resulted in a fragmented cDNA which was labeled by terminal deoxynucleotidyl transferase (TdT) with the assistance of the proprietary DNA labeling Reagent that is covalently linked to biotin.

In this procedure 5.5mg of ss-cDNA was prepared. On ice the fragmentation master mix was prepared by combining the components in Table 15, mixed well by gentle vortexing and centrifuged. On ice, 16.8ml of the fragmentation master mix was added to each purified ss-cDNA sample, mixed by gentle vortexing and centrifuged.

The reaction was incubated using thermal cycler for 1 hr at 37°C, then for 2 min at 93°C, then for at least 2 min at 4°C.

Table 15: Fragmentation Master Mix

Component	Volume for one reaction
Nuclease-free water	10 ml
10X cDNA Fragmentation Buffer	4.8 ml
UDG, 10U/ml	1ml
APE 1, 1000 U/ml	1ml
Total volume	16.8 ml

On ice, 45ml of the fragmented ss-cDNA was transferred to each well. 15ml of labeling master mix (Table 16) was added to each 45ml fragmented ss-cDNA and mixed by gentle vortexing and centrifugation. The reaction was incubated for 1 hr at 37°C, then for 10 min at 70°C, then for at least 2 min at 4°C.

Table 16: Labeling Master Mix

Component	Volume for one reaction
5X TdT Buffer	12 ml
DNA Labeling Reagent, 5 mM	1 ml
TdT, 30 U/ml	2 ml
Total volume	15 ml

2.11.5.10 Using GeneTitan™ instrument

The array plates were prepared and assembled as instructed in the protocol. The fragmented and labeled SS-cDNA samples were transferred to the array plates with well labeling of each sample. Proper alignment and loading of plates were performed in the GeneTitan drawer as instructed in the instrument manual. After finishing the set-up of the array plates and instrument, the scanning was started using the GeneChip™ Command Console™ Software (AGCC) as described in the protocol.

2.12 Statistical Analysis

Statistical analysis of the data was carried out using Prism® software version 8 for Mac (GraphPad, La Jolla, CA). Body weight, food consumption and water intake were analyzed by two-way analysis of variance (ANOVA) followed by a Sidak's multiple comparison test as the recommended test by the software. Blood pressure (BP) was analyzed by taking the average of at least 5 readings/animal in the initial measurements. The final BP followed the analysis of initial, in addition each rat represented the average readings of three or four consecutive days. Then data of BP, biochemical parameters (lipid profile, liver function, glucose level, insulin level and hepatic triglycerides) were analyzed by unpaired *t*-test.

For dose–response curves, vessel force at the peak values for contractile agent and lowest value for the relaxant were recorded; change in force was measured as value for each dose minus the basal vessel force (g/mg) or the peak contraction before adding the vasorelaxant divided by vessel weight. The curves of agonist concentration-response were created on log scale and data fitted using the sigmoidal (variable slope) fitting routine in Prism. The dose of agonist, which caused 50% of maximum response, was expressed as the mean log EC₅₀, and used as an effective value of sensitivity to the agonist. Maximum relaxation effect (I_{max}) in percentage was calculated as an effective value of relaxation. Comparisons were made using two-way ANOVA (with Mann-Whitney test).

Transcriptome data analysis using Transcriptome Analysis Console software (TAC) 4.0.2. The differences in gene expression were determined when genes were upregulated or downregulated with 2-fold change in the expression. The statistically significant difference was determined at $P \leq 0.05$ using one-way analysis of variance (ANOVA), followed by multiple correction for false discovery rate (FDR) with a cut-off of 0.05. All data were shown as mean \pm standard error of mean (SEM). Significance was defined as $P \leq 0.05$, n = number of samples.

CHAPTER 3: RESULTS: HIGH CARBOHYDRATE DIET DEVELOPS A DIET-INDUCED OBESITY MODEL IN THE RAT

3.1 Introduction

Animal models are widely used to investigate the development of obesity and its associated co-morbidities. Interestingly, several of the characteristics of obesity are common in most mammalian species, making animal models an important tool for understanding the disease, its mechanisms and also in the investigation of treatment interventions. Rodent models, both rats and mice, have been extensively used in the study of human obesity. In mice, the leptin-deficient ob/ob mouse and the leptin receptor deficient db/db mouse are commonly used models of obesity. The Zucker rat is the MC4 receptor deficient genetic model of obesity. However, rats are often used to investigate diet induced obesity (DIO) (129). The choice of obesity model always depends on the goal of the study. In addition, choosing a proper diet that induces obesity is also another important factor. A huge number of studies have been published using high fat diets to induce obesity. However, the current study was interested in the obesogenic effect of CAF diet, characterized by high carbohydrate, which more closely mimics the regional (Arabian Peninsula) diet. For better understanding of obesity-associated pathologies, an experimental model of DIO was developed in this study. It is generally accepted that food intake has a critical role in influencing body adiposity. It is therefore important to understand the relationship between diet, obesity and its consequences. Sprague Dawley rats have been used frequently as DIO models because they share many of the common forms of human obesity (129). SD rats are an outbred strain that are susceptible to DIO with individual variations (130).

This chapter presents the results of the following aims:

- 1- Establish a diet-induced obesity rat model using high carbohydrate diet (CAF diet) followed with dietary intervention to induce weight loss.

- 2- Assess the extent to which CAF diet can induce body weight gain, fat distribution, metabolic parameters, and determine the effectiveness of CAF withdrawal on reversing these changes.

3.2 Body weight gain

To determine the effect of the CAF diet on body weight, rats were fed with a palatable high carbohydrate diet for 16 weeks. Results showed that all CAF-fed rats gained significant levels of weight (20-30% weight gain) starting from week 5, compared to the NC-fed rats ($P < 0.001$; Figure 16). Individual body weight gains were analyzed and expressed with the results as shown below (Figure 17 & Figure 18). There is no threshold that has been established to diagnose obesity in animal models, such as those established for human. Thus, in this study an animal that gained 20-30% weight compared to control was considered an obese animal, as described previously (131). Based on that a threshold for expected body weight gain of 580 gm was established. This threshold was represented by a red line in the graphs in figures 16 & 17. The graph showed CAF-fed rats gained more weight compared to their control NC-fed rat. The body weight gained by CAF-fed rats exceeded the cut-offline (98% rats). The majority (77 %) of the NC-fed rats were below this threshold. Conversely 3.7 % of the CAF fed animals were below this threshold. By comparing the body appearance of NC and CAF-fed rats, NC-fed rats were leaner than CAF-fed rats (Figure 19). CAF-fed rats showed clear adiposity in the abdominal area, which was absent in NC-fed rats (Figure 20).

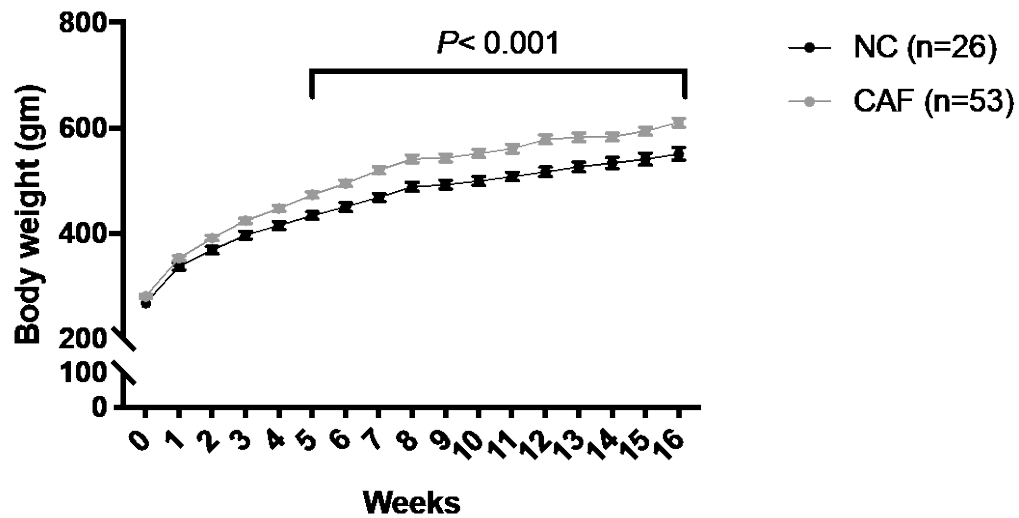


Figure 16: Effect of CAF diet on body weight.

The graph represents the body weight of both groups NC and CAF. CAF diet significantly increased body weight (gray curve) compared to NC-fed rats (black curve), $P < 0.001$. Data expressed as mean \pm SEM.

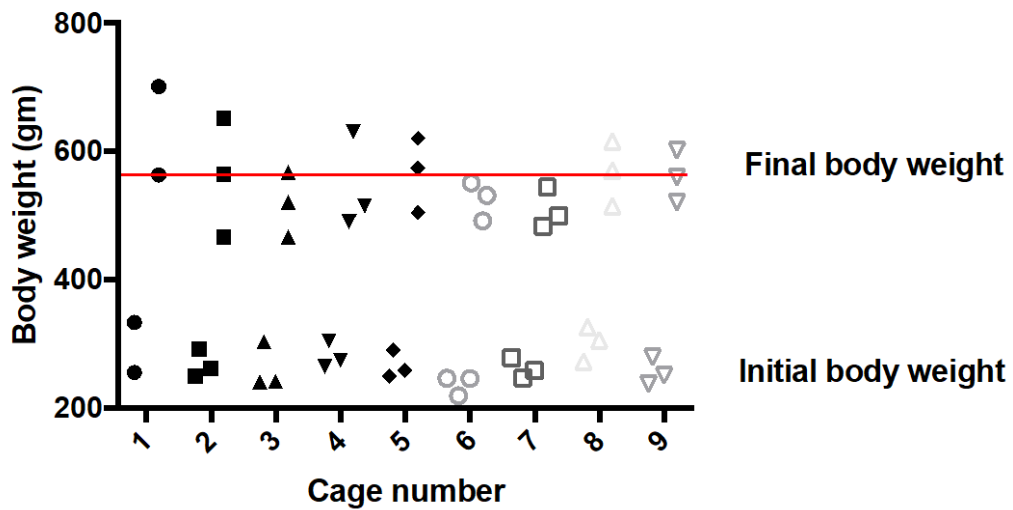


Figure 17: Initial and final individual body weights of NC-fed rats.

The graph represents the initial and final body weights of all NC-fed rats. Red line represents threshold animal body weight (580 gm), 77% of NC-fed rats body weight were below the threshold line.

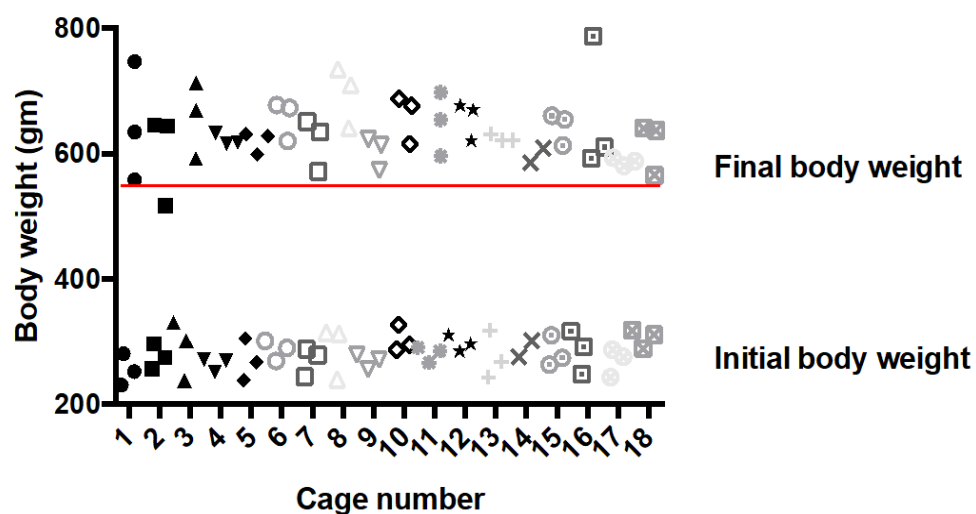


Figure 18: Initial and final individual body weights of CAF-fed rats.

The graph represents the initial and final body weights of all CAF-fed rats. Red line represents the body weight threshold (580 gm), and the body weight of all CAF-fed rats exceeded this threshold.

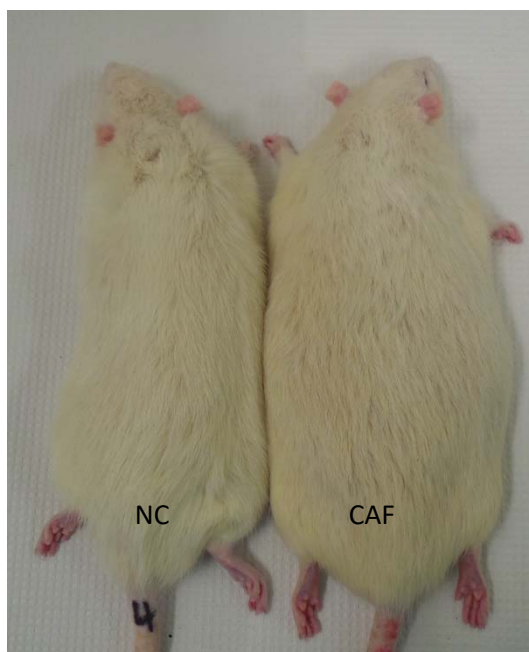


Figure 19: External body size of NC and CAF fed rats.

Figure showed external body size of representative animals from the NC and CAF groups.

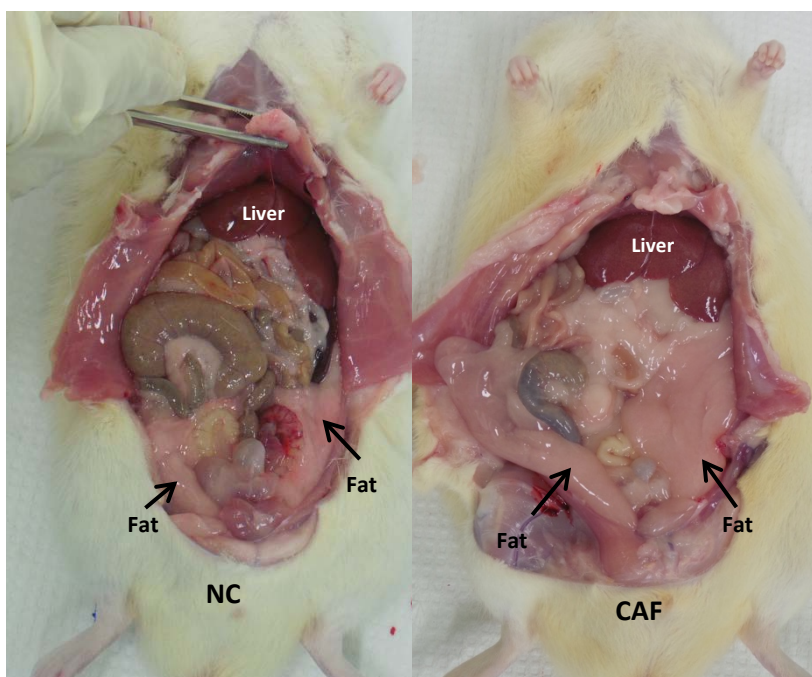


Figure 20: Visceral organs of NC and CAF fed rats in the abdominal cavity.

CAF-fed rats showed clear ectopic fat deposition in the abdominal cavity, compared to NC-fed rat. Black arrows are pointing at the fat tissues in the abdominal cavity.

In the studies that investigated the effect of the reversal of the body weight gain by changing from the CAF to NC for three weeks, a slight loss (6%) in body weight was observed (Figure 21). This slight loss did not show any changes in the accumulated fat amount in the abdominal area as observed during dissection (Figure 22 & Figure 23). Conversely, NC rats continued to gain weight as a part of the animal's normal growth and aging (Figure 21).

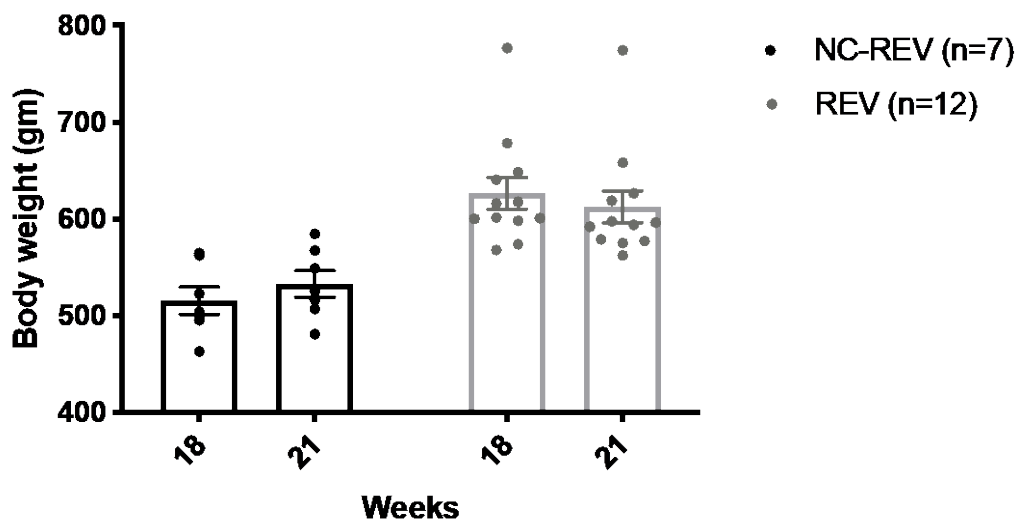


Figure 21: Body weights of NC and REV rats before and after reversibility.

REV rats lost 6% of their initial weight when diet was changed to normal chow. NC rats continue to gain weight as part of their physiological growth. None of the changes in either NC or REV groups were statistically significant ($P < 0.05$). NS: not significant. . Data expressed as mean \pm SEM.

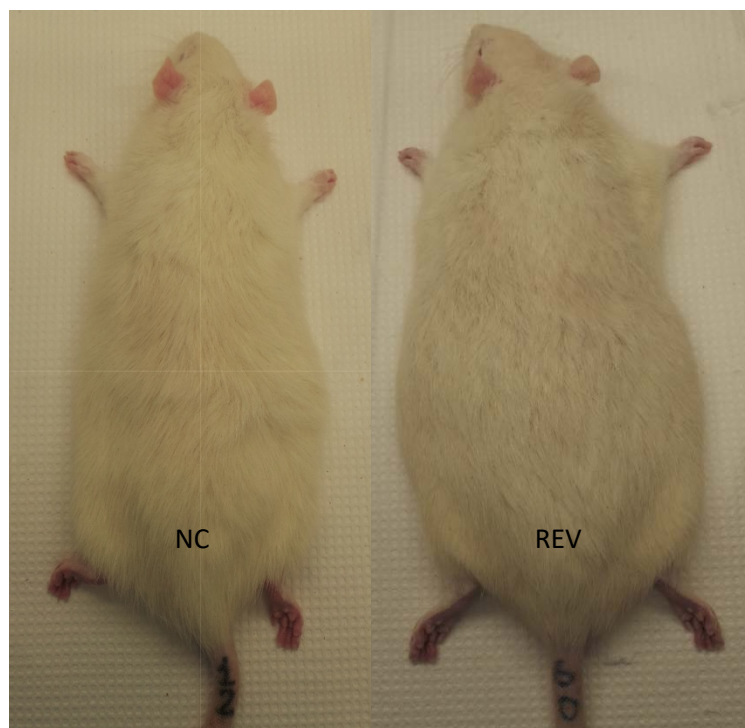


Figure 22: External body size of NC and REV rats.

The graph showed the external body size of representative animals from NC and REV groups. When diet was changed from CAF to NC, REV rat still appeared bigger, compared to the NC fed rat.

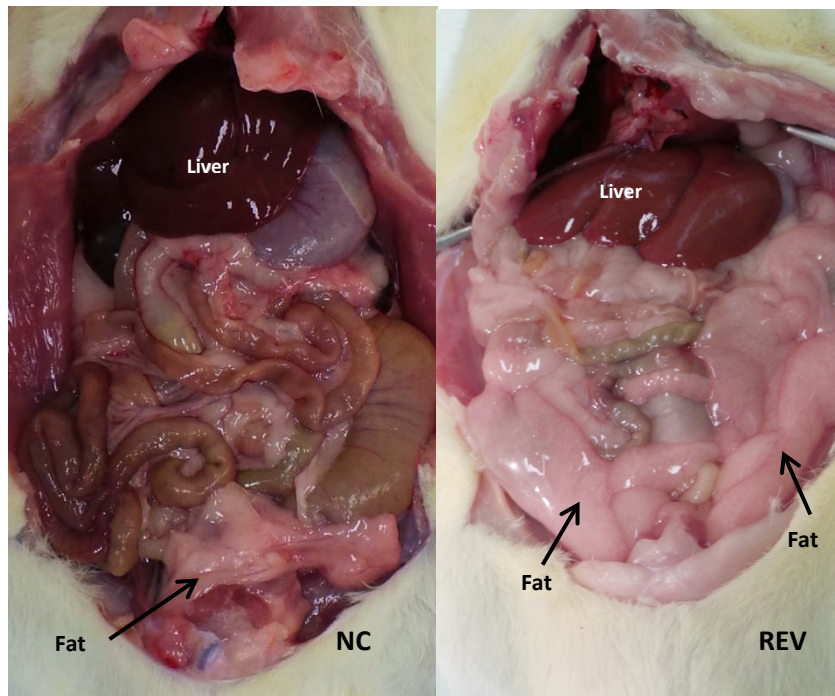


Figure 23: Visceral organs of NC and REV rats in abdominal cavity.

REV rats showed ectopic fat deposition, apparent in the abdominal cavity, compared to the NC fed rats. Black arrows are pointing at the fat tissues in the abdominal cavity.

3.3 Food consumption

To determine if CAF diet induced hyperphagia, both diets (CAF and NC) were offered to the CAF group, while NC group received only the NC diet. In the beginning of the study, particularly in the first week, rats consumed the highest amount of CAF, approximately 39 gm/rat/day. This amount started to decrease gradually to reach 20gm/rat/day and stabilize throughout the study. Slight peaks were observed in weeks 9 and 13, these peaks were due to change in diet variety (Figure 25). CAF-fed rats preferred to consume more CAF diet (20 gm/rat/day) than NC diet, which was around 5 gm/rat/day. This difference in consumption was statistically significant. However, the control group, which represents the NC-fed rats, showed a constant NC consumption around 25 gm/rat/day throughout the study (Figure 24).

In order to study the reversible effects of food consumption on body weight, diet was changed from CAF to NC for three weeks. The consumption dropped in the beginning of the experiment, however, consumption increased gradually over time until by the end of the 4 weeks the REV rats consumed the same amount as the control animals (Figure 26).

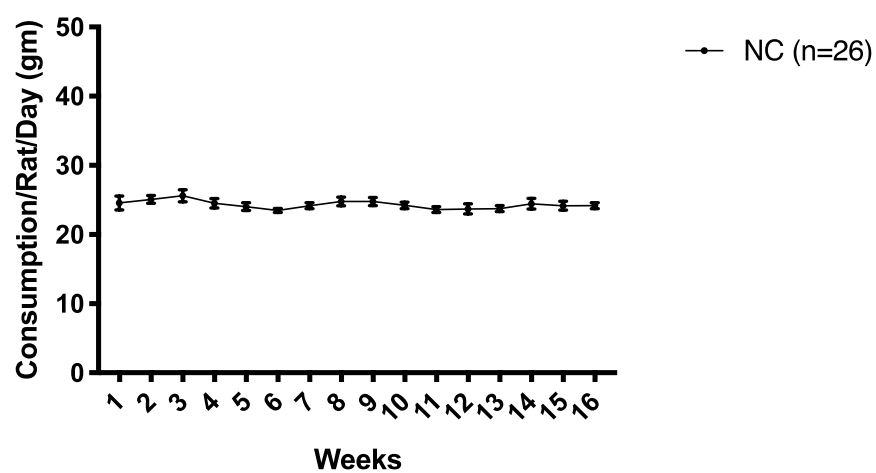


Figure 24: Food consumption of NC group.

The curve illustrated constant food consumption by NC group throughout the study. The consumption was approximately 25 gm/rat/day. Data expressed as mean \pm SEM.

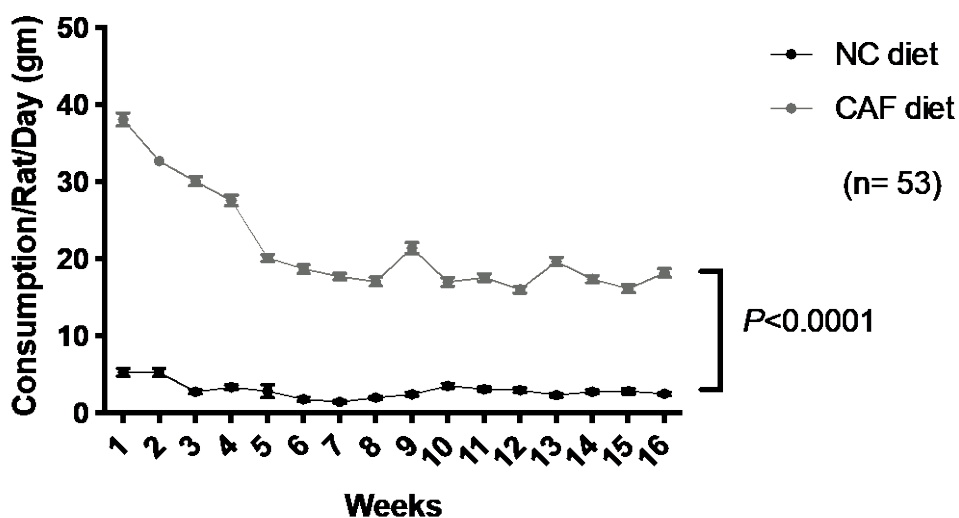


Figure 25: Food consumption of CAF group.

The graph represents the consumption of both diets (NC and CAF) offered for CAF group (n=53) in the same cage. CAF-fed rats consumed a large quantity of CAF diet (gray curve) in the beginning of the study, the consumption declined dramatically to reach approximately 20gm/rat/day by week 5. NC consumption (black curve) for the same group was very low approximately 5gm/rat/day. The difference between the curves was significant $P<0.0001$. Data expressed as Mean \pm SEM.

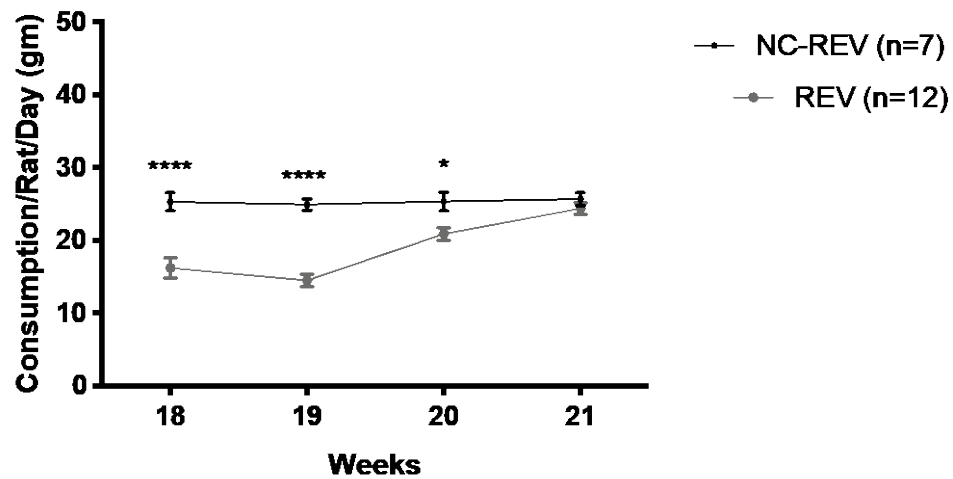


Figure 26: Food consumption of the reversible group.

A significant decline in food consumption was observed in the REV rats when diet was changed from CAF to NC, $P < 0.0001$. However, in weeks 2 (week 19) and 3 (week 20) food consumption by the REV rats increased to equal those of NC rats, approximately 25gm/rat/day, by week 4 (week 21). $*P \leq 0.05$, $****P \leq 0.0001$. Data expressed as Mean \pm SEM.

3.4 Water intakes

CAF-fed rats were supplied with sugared-water to increase the carbohydrate component of their diets (analogous to human consumption of sugary drinks), while NC-fed rats were supplied with normal untreated water. NC-fed rats showed steady water intake throughout the study. Initially CAF-fed rats consumed less water compared to NC, which increased significantly later on as shown in week 6. The increment in the water intake among CAF-fed rats was due to addition of sugar in the water to induce the consumption (Figure 27).

In order to study the reversible effects on body weight and also the contribution of sugary drink consumption to this, water was supplied without sugar. Data showed a drop in the intake by REV rats in the first week of reversibility period due to the replacement of sugar water with just water. Then water intake increased until the end of the study. The NC rats showed stable water intake. Unexpectedly, sudden, unexplained increase of water intake was observed in week 21 (Figure 28).

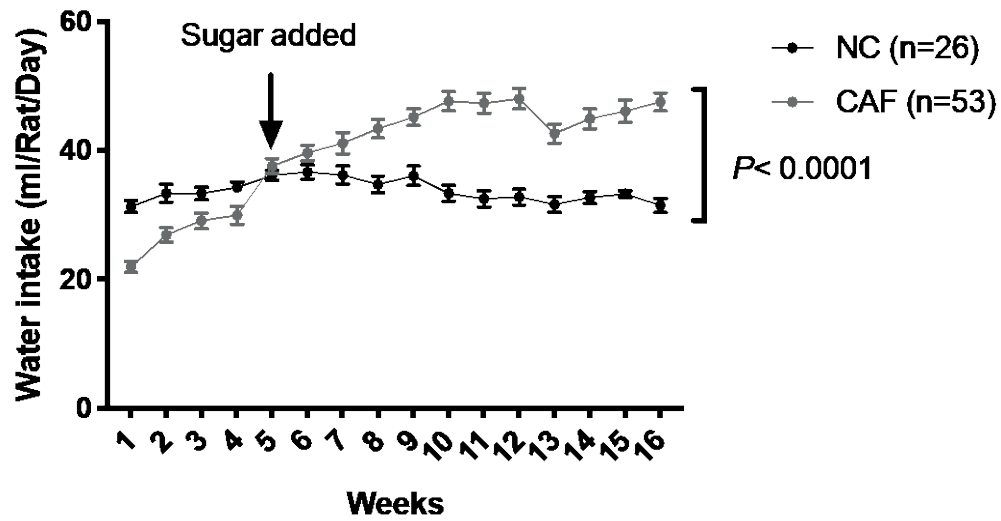


Figure 27: Water intake for CAF and NC groups.

The grey curve represents the water intake for CAF-fed rats, and the black curve represents the control NC-fed rats. Sugar was added to the water of CAF group only at week 5. CAF-fed rats showed dramatic increase in the water intake, however NC showed steady intake. The difference between the curves was significant with P value < 0.001 at weeks 8 and 9, and with P value < 0.0001 starting from week 9 to week 16. Data expressed as Mean \pm SEM.

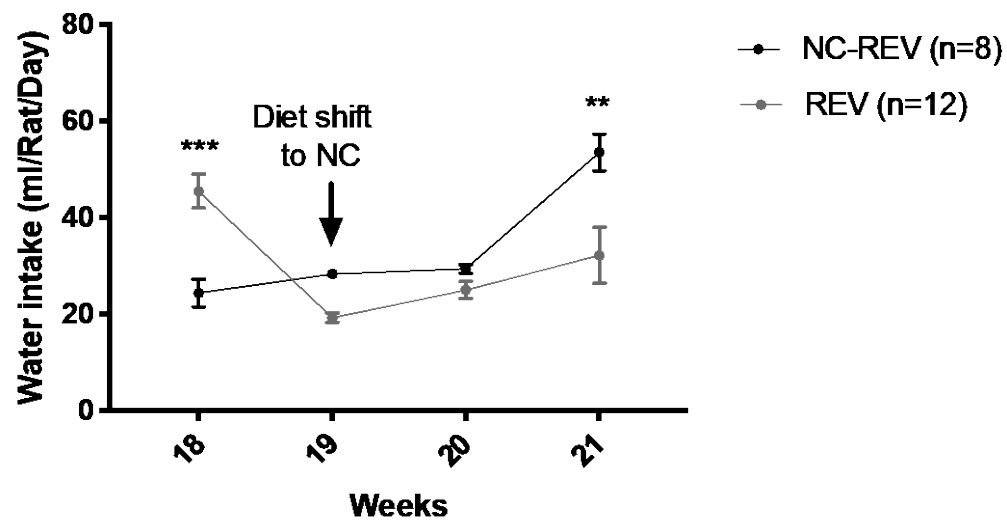


Figure 28: Water intake for reversible group.

REV rats witnessed a significant drop in the water intake at week 19; this drop was returned by week 21. NC rats consumed equal amount of water with unexpected significant rise by week 21. ** $P \leq 0.01$, *** $P \leq 0.001$. Data expressed as Mean \pm SEM.

3.5 Insulin and glucose levels

To determine if CAF feeding altered glucose and insulin levels, systemic glucose and insulin were measured. Serum glucose level did not differ between all the groups (Figure 29). Although NC-REV showed an increase in glucose level (before reversibility) compared to other groups, but this increment was not statistically significant. 16 weeks of CAF feeding lead to a significant increase in plasma insulin level in CAF group compared to NC (Figure 29). Diet reversal from CAF to NC caused slight decrease in insulin level but was not statistically significant.

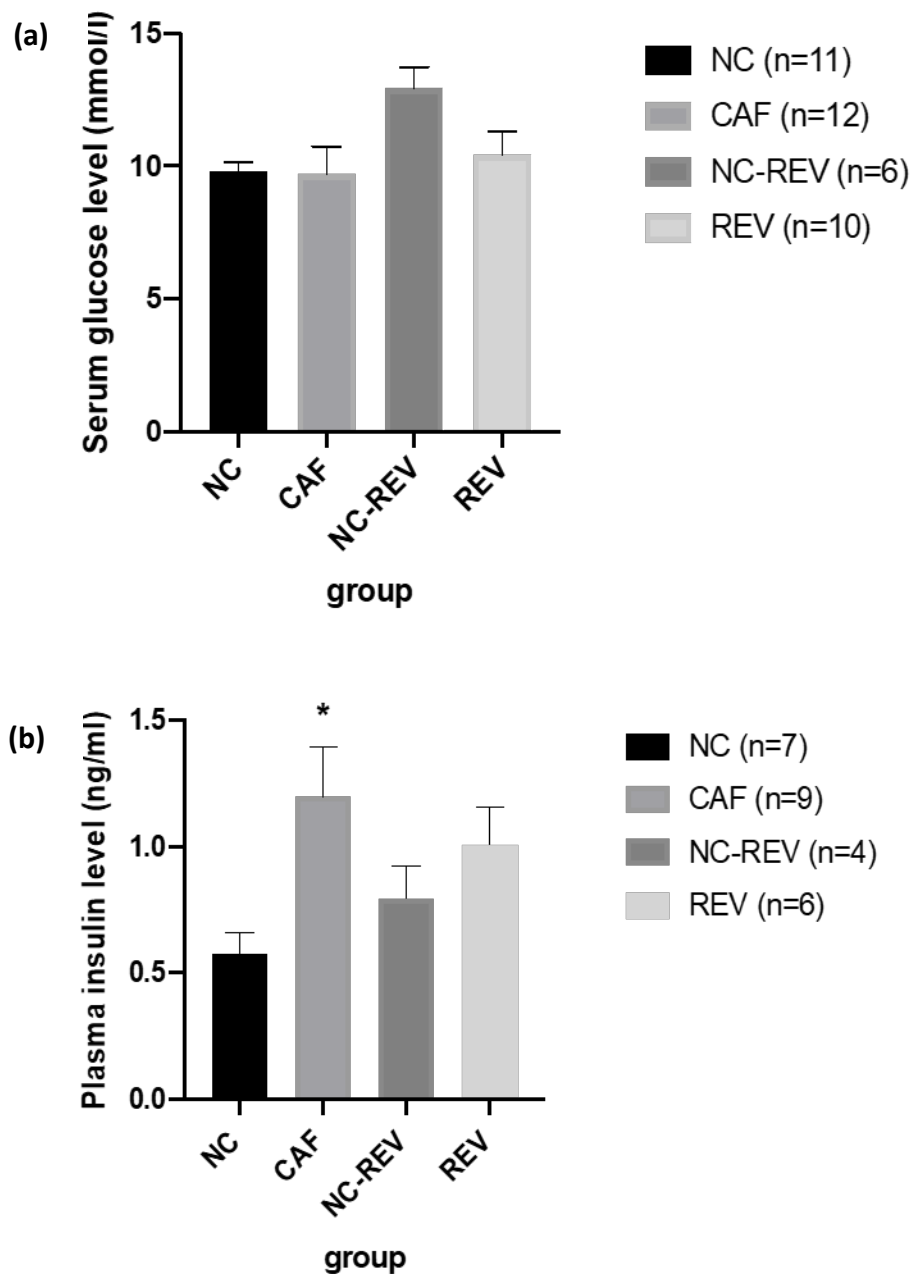


Figure 29: Effect of CAF diet and reversible diet on glucose and insulin levels.

(a) No significant change was seen in serum glucose level when rats fed with CAF diet as well as reversible diet, compared to their controls NC and NC-REV respectively. (b) Plasma insulin level was significantly increased when rats fed with CAF diet for 16 weeks ($P < 0.01$) compared to NC, this increment showed slight decrease (not significant) in REV rats compared to NC-REV. Data expressed as mean \pm SEM.

3.6 Lipid profile

CAF-fed rats had elevated serum triglycerides and lower HDL-cholesterol level compared to NC-fed rats. Interestingly the unfavorable lipid profile was reversed to normal levels when the animals were shifted to normal diet (Table 17).

Table 17: Lipid profile for obese and reversible rats.

Parameter	Obese		Reversible	
	NC (control) (n=11)	CAF (n=12)	NC (control) (n=6)	REV (n=10)
Cholesterol (mmol/L)	1.77± 0.13	1.77± 0.11	1.88± 0.13	2.1± 0.15
HDL (mmol/L)	1.44±0.11	1.11 ± 0.08 *	1.58± 0.13	1.66± 0.12
LDL (mmol/L)	0.29± 0.04	0.26± 0.04	0.35± 0.06	0.35± 0.04
Triglycerides (mmol/L)	0.90± 0.13	1.75± 0.19 ***	0.82± 0.2	1.1± 0.12

Data expressed as mean ± SEM and statistically evaluated using unpaired t-test. *P≤ 0.05, *** P≤ 0.001

3.7 Discussion

Diet and lifestyle are the major modulators when trying to curb the high prevalence of obesity. There is a huge take-up of the Western style diet and high-energy dense and processed diets, such as exemplified by many fast foods. Consequently, eating habits have changed among populations all over the world. Several studies have been published addressing obesity and its health consequences by developing DIO models. The CAF diet is a robust model of MS that is capable of inducing weight gain, hyperglycemia, and inflammation in rats (132). The present study addressed this concept. The study investigated whether a diet similar to one consumed by human subjects in the region (Arabian Peninsula), consisting of high carbohydrate intake, could induce obesity and its associated co-morbidities. Furthermore, the study also assessed the extent to which a reduction in calories could reverse body weight gain after switching from the CAF diet to NC.

In the current rat model, CAF diet (characterized with high carbohydrates) significantly induced weight gain. As a result of weight gain, high accumulation of adipose tissue was observed in the abdominal cavity, suggesting that the CAF diet induced ectopic fat deposition. Fat deposition in this study was assessed by observation only without measuring the fat weight or size. The CAF diet was successful in its ability to produce an obese animal that closely mimics human model of obesity development and evolution. This data supported the idea that CAF model was a robust DIO model (132). These findings were in line with previous studies that revealed CAF feeding for 15 weeks and for 45 days induced obesity in male Sprague Dawley rats (133). CAF diet was also more effective in inducing adiposity in Wistar rats compared to high fat (HF) diet (134). This model was also successfully developed in a mouse model and showed that CAF diet had a significant impact on

body weight compared to HF diet (135). These findings are encouraging in building up other studies of DIO using CAF diet.

In order to assess weight loss, the diet was changed to NC for three weeks, which had a lower caloric content. A slight weight loss was observed ~6% over a 3-week period. Although the weight loss was small, this is a good indicator that dietary intervention could be a strategy to induce weight loss. Longer periods of dietary intervention could have a greater positive impact on weight loss. Moreover, adding exercise along with dietary intervention, or calories restriction, may increase the degree of weight loss. In this study, a huge fat deposition in the abdominal area was observed. Unfortunately, the amount of fat deposition did not decrease with weight loss. This could be due to the short duration of the recovery period. Fat tissue accumulated over 16 weeks of CAF feeding, perhaps half of this period at least might be needed to be able to get a significant level of recovery. That the degree of recovery may depend on the CAF-feeding time has also been suggested by Rynes et al, where it was shown that 1.5 months was required to recover from the body weight gain and fat tissue accumulation induced by 2 months of CAF feeding (117). Along with that, in the current study energy intake was lowered without increasing energy expenditure. Perhaps additionally increasing energy expenditure could have been more effective in the short duration of recovery. Abdominal obesity was detected from observational assessment only, by comparing obese rats with lean rats at the same time point. Due to study limitations abdominal obesity assessment by measuring body width or using MRI techniques, as done by other studies, was not possible (136, 137).

This study showed that CAF feeding induced adiposity at a significantly high rate, suggesting that weight gain was accompanied with increased CAF consumption and water (sugary drinks) intake. Although both diets were offered in the cage (CAF and

NC), the consumption of the CAF diet was significantly higher than consumption of NC in the same cage. This observation indicated that rodents prefer high dense food, suggesting greater palatability. Palatability is one of the significant determinants of food intake, as reported in several studies which showed the preference of more palatable CAF diet over other types of diet (132). The CAF consumption was high in the beginning of the study, after which it gradually decreased and then maintained at a constant level throughout the study. The food intake peaked at weeks 5, 9 and 13, due to the change in the diet variety to induce consumption. Despite the slight difference in the food items, relative intake of macronutrients (fat, carbohydrate and protein) was controlled throughout the study. Interestingly, the amount of food consumed by CAF group was equal to amount consumed by NC group ~25 gm/rat/day (Figures 21 & 22), however the type of diet was different. The CAF-fed rats revealed a dramatic increase in water consumption by week 5. This increment was due to the introduction of sucrose in the water to induce the consumption and to represent the fizzy/soda/ sugar containing drinks in human diet. The preference of CAF over NC led to an increase in the energy intake as a result of food palatability. The food items used in this study (frozen burgers, bread and croissants) can be categorized as processed foods, which contained additives such as fat, sugar and salt to make it more enjoyable and desirable. The presence of these additives, specially salt and sugar, enhance the preference of CAF over NC (134). Indeed, good taste of food trigger the appetite in rats for the CAF diet (138). Collectively, the high intake of sugar-containing water and CAF diet might be linked to the changes in the appetite hormone production or the stimulation of the reward system leading to food addiction (139).

When diet was shifted from CAF to NC to start the recovery period, REV group witnessed a dramatic drop in food consumption. Compared with a previous study, this drop could be related to either: 1) low palatability of the NC diet or to 2) the switch to a diet with different nutritional composition (140). Along with the drop in the

diet consumption, a slight drop in the water consumption was also noticed at the beginning of the recovery period. This is probably due to the removal of sucrose from water. Although there was drop in the consumption of food and water during the recovery period, this drop did not show a significant effect on body weight.

Adiposity is highly associated with the development of MS. One of the key players of metabolic syndrome is the disruption of the glucose and insulin levels, as risk factors for type 2 diabetes. Our results revealed that CAF diet induced a partial hyperglycemia in only 33% of CAF-fed rats and 67% of the same group exhibited hyperinsulinemia (Figure 29). These findings suggest that our DIO rodent model represent early features of metabolic disorders that could lead to diabetes. Similar findings have been suggested by Sampey et al. and showed that 3 of 10 CAF fed rats were hyperglycemic after 15 weeks of CAF diet feeding suggesting a pre-diabetic state (132). Although data from several sources have identified that accumulation of adipose tissue is associated with glucose intolerance and insulin sensitivity, this was not observed in the current study. This observation may be related to the study period or the type of diet. Contradictory to the findings of the current study, SD rats fed with CAF diet were hyperinsulinemic after 20 weeks of feeding, with no change in glucose levels (136).

Another important feature of MS is disturbance in lipid profile. Maintaining normal lipid profile plays a role in preventing the development of cardiovascular diseases. HDL for example, is a 'good' cholesterol that should be at optimal level. In this study, the lipid profile revealed a significant increase in the TG and a decrease in HDL-C levels, which is an indicator of MS. Similar effects of CAF feeding were observed previously (140, 132). Dyslipidemia was probably evident due to CAF feeding which is rich in carbohydrate. The type of diet used in this study characterized with high CHO, appears to have a critical role in metabolic changes. Excess ingested lipids

are broken down and delivered to adipose cells as FFAs, once these adipocytes are saturated, excess FFAs are transferred to the liver to be utilized or stored in the form of TGs. TGs can also be synthesized from non-lipid sources, such as carbohydrates. Excess circulating glucose is stored in the liver as glycogen or converted to FFAs through de novo lipogenesis. Ultimately FFAs can be converted to triglycerides for longer storage. TG has an inverse correlation with HDL. Different mechanisms have been suggested in the literature for this being a direct causal factor for TG lowering HDL. Indeed, the metabolic data here showed a significant increase in TG and decrease in HDL, but not glucose.

Visceral adiposity is hypothesized to be linked with insulin resistance, as a result it potentiates the release of FFA to supply the liver resulting in hypertriglyceridemia (136). Interestingly, TG and HDL-C levels were reversed with diet within three weeks. Consistent with these findings, CAF withdrawal completely reversed metabolic implications, including triglycerides, in young rats (141). These findings are highly associated with the type of diet used in this study. The high dietary carbohydrate appears to be metabolized and may contribute to the elevated TG levels.

Switching diet from CAF to NC showed a slight improvement in the insulin and glucose levels. 80% of rats in REV group showed a decrease in glucose level and 50% showed a decrease in glucose level (Figure 29). This slight improvement also could be related to the short duration of recovery period. In addition, this improvement was achieved only with dietary intervention under sedentary situation. Adding exercise completely reversed insulin resistance after CAF feeding in rats (142), analogous to that shown in human subjects, which showed an improvement in insulin sensitivity when exercise was added along with dietary intervention (143). Ectopic fat deposition is a common characteristic of obesity. When adipose tissue is overwhelmed with lipids, excess lipids start to accumulate in the organs, such as

liver and skeletal muscles (144). When lipids accumulate in skeletal muscles, this causes mitochondrial dysfunction and end with insulin resistance (145). Exercise induces the utilization of lipids, therefore activates glucose transporter (GLUT4) (146). Collectively, the variation in the glucose and insulin levels in the studied population is due to the strain used in this study. An outbreed rat strain was used in this study which has a genetic diversity within population and highly representative of a human population (147). This could also explain the current ongoing studies on metabolically healthy obese population that are considered as obese, but with no signs of MS (148).

CHAPTER 4: RESULTS: HIGH CARBOHYDRATE DIET COMPROMISED VASODILATION AND INDUCED NAFLD IN RATS

4.1 Introduction

Hypertension is a common and severe disease related to obesity. Excessive adiposity raises blood pressure which is a risk factor for the development of other CVD complications (149). Several human and animal studies revealed the association between obesity and various arterial and microvascular abnormalities (150, 151). The prevalence of hypertension within obese individual is ranging between 60%-77% (152).

The fat distribution has a significant effect on cardiometabolic risk factors and hypertension, for example visceral fat (VAT) showed a higher risk of developing hypertension compared to subcutaneous adipose tissue (SAT) (149).

Vascular relaxation is controlled mainly by the endothelium via the production of NO as a vasorelaxant. Defects in the endothelium directly affects the rhythm of the vascular tone. It has been shown that vasorelaxation mediated by NO was attenuated with adiposity (153). Many factors have been reported to be responsible for endothelial dysfunction, these factors include insulin resistance (153), hypercholesterolemia (154), hypertriglyceridemia (155), raised non-esterified free fatty acids, and high blood pressure (149). All these factors are common characteristics of MS which is highly associated with obesity.

Liver diseases are another common and serious health issue that is usually addressed in obesity studies. NAFLD and NASH cases have seen a rapid increase mainly due to environmental factors. The prevalence of NAFLD in non-obese individuals is low (15%). On the other hand, the prevalence within obese and extremely obese individual is 65% and 85% respectively (156). These percentages support the evidence that obesity is a risk factor of NAFLD. What makes NAFLD a major health concern is that the disease operates over a wide spectrum, progressing from hepatic steatosis to NASH, with the worsening situation being fibrosis or cirrhosis and ultimately leading to life-threatening hepatic carcinoma (HCC) (157).

NAFLD is characterized by hepatic lipid accumulation. There are different sources of hepatic lipid accumulation: high level of fatty acids delivered to the liver, production of hepatic FA from de novo lipogenesis (DNL) and reduced lipid excretion from the liver. The liver is the major site of metabolism in the body, and the input and output of hepatic lipids has a significant role in lipid accumulation. NAFLD is initiated when the rate of lipid input exceeds the rate of lipid output. Hepatic lipid inputs include the lipid synthesis through de novo lipogenesis from carbohydrate ingestion and other precursor, FA derived from adipocyte lipolysis, or from lipoprotein-triglycerides (158). On the other hand, the output mechanisms include the utilization of hepatic lipid through β -oxidation or the secretion of TG into the circulation in the form of very low-density lipoprotein (VLDL) (158).

In NAFLD patient, the percentage of hepatic lipid is around 26% from DNL and 15% from dietary carbohydrate (159). High consumption of carbohydrates is considered a main trigger of DNL and consequently seen to make a higher contribution to NAFLD compared to dietary fat (159). Diet enriched in carbohydrates is able to stimulate the hepatic fatty acid synthesis, shifting carbohydrates toward fat biosynthesis in the liver (160). In addition overconsumption of fructose elevates the TG level in plasma (161).

Taken together, observations and evidence from cell, animal and human support the contention that overconsumption of carbohydrates has a lipogenic potential.

Histopathological evaluation remains the dominant method of NAFLD assessment and diagnosis. Each stage of the disease has its own unique histopathological characteristics. Simple steatosis is characterized with fat droplet accumulation in the hepatocytes (123). The progression to NASH is characterized with hepatocyte injury,

ballooning and initiation of inflammation. Advanced stage of NASH encompasses sever inflammation, fibrosis and consequently cirrhosis (162).

Several studies showed the positive association between weight loss and the recovery of obesity-related comorbidities by applying diet and lifestyle intervention. Interestingly, most studies showed a significant improvement in both BP and hepatic steatosis with diet and lifestyle intervention. This strategy is a good approach to be applied to obese hypertensive patients, because it could delay the use of antihypertensive drugs (163). The degree of weight loss has a positive impact in reducing the CVDs risks, weight loss of 2-5% can improve triglycerides level and systolic BP as reported (122). Indeed, more weight loss resulted in more improvement (122). An improvement also observed in the endothelial dysfunction as reported in different models (164, 165).

This chapter provides the results of the following aim:

To determine whether CAF diet-induced obesity increased cardiometabolic risk and affected the vascular function in the DIO model developed.

In addition, to investigate whether the current DIO model developed NAFLD, and the extent of this pathology.

The study also assessed the efficiency of switching diet to a lower calorie diet in reversing these abnormalities.

4.2 Effect of DIO on Vascular Function

4.2.1 Blood Pressure

To determine the effect CAF-induced obesity and dietary weight loss on blood pressure, blood pressure was recorded. Initial blood pressure was recorded for all animals before starting the experiment, the readings were comparable in both groups, NC versus CAF. Interestingly, 16 weeks post CAF feeding, data showed significant elevation in the trend of systolic blood pressure (SBP) as well as mean arterial pressure (166) in CAF-fed group compared to NC-fed group (Table 18). In the REV group the measurements were performed before starting the REV and at the end of REV period. Although REV group showed higher SBP and mean arterial pressure (MAP) before reversibility was started compared to their control NC-REV, however this difference was not statistically significant. No change was observed in all parameter readings after reversibility in REV vs NC-REV. (Table 19).

Table 18: Blood pressure measurements (mmHg) for NC and CAF groups.

Initial and final SBP, DBP and MAP.

Parameter/ Group	Initial (mmHg)			Final (mmHg)		
	SBP	DBP	MAP	SBP	DBP	MAP
NC (n=16)	166.8 ± 3.8	134.7 ± 4.0	145.1 ± 3.9	148.8 ± 3.5	106.3 ± 3.1	120.2 ± 3.22
CAF (n=19)	164.2 ± 4.7	126.1 ± 4.7	138.5 ± 4.7	162.7 ± 3.3**	115.6 ± 3.4	131.0 ± 3.3*

Data expressed as mean ± SEM and statistically evaluated using unpaired t-test to compare NC vs CAF initial and final readings of SBP, DBP and MAP. *P ≤ 0.05, ** P ≤ 0.01, *** P ≤ 0.001.

Table 19: Blood pressure measurements (mmHg) for NC and REV groups.

Initial and final SBP, DBP and MAP.

Parameter / Group	Before (mmHg)			After (mmHg)		
	SBP	DBP	MAP	SBP	DBP	MAP
NC-REV (n=7)	138.03 ± 5.29	98.70 ± 7.77	106.30 ± 5.32	141.69 ± 3.83	98.72 ± 3.76	112.69 ± 3.74
REV (n=12)	150.53 ± 2.22*	105.18 ± 2.31	119.93 ± 2.24*	147.62 ± 5.33	102.41 ± 4.39	117.15 ± 4.67

Data expressed as mean ± SEM and statistically evaluated using unpaired t-test to compare NC-REV vs REV before and after reversibility. *P ≤ 0.05, ** P ≤ 0.01.

4.2.2 Vasoconstriction with Noradrenaline (NA)

To determine the contractile function of the large vessel (ascending thoracic aorta) when fed with CAF diet, arteries were assessed using cumulative concentrations of NA (10^{-9} – $10^{-4.5}$). The noradrenergic contractions in the CAF-fed rats showed less vasoconstriction compared with the control NC-fed rats. However, the sensitivity of both curves to NA were not significant (LogEC_{50} $-7.709 \pm$ vs. $-7.704 \pm$ M respectively) (Figure 30). Comparable contraction effect was shown between NC rats and REV rats when CAF diet was stopped for three weeks (Figure 31).

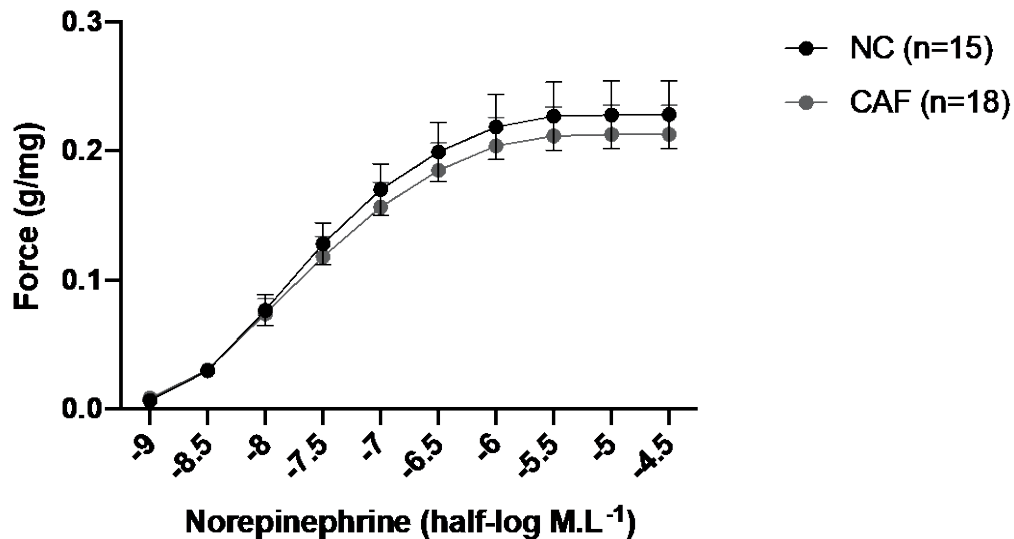


Figure 31: Effect of CAF diet on vasoconstriction of aortic ring.

In response to a vasoconstrictor, noradrenaline, curves illustrated a slight downward shift in the curve in CAF-fed rats, compared to NC-fed rats, however the difference between the curves was not significant. Data expressed as mean \pm SEM.

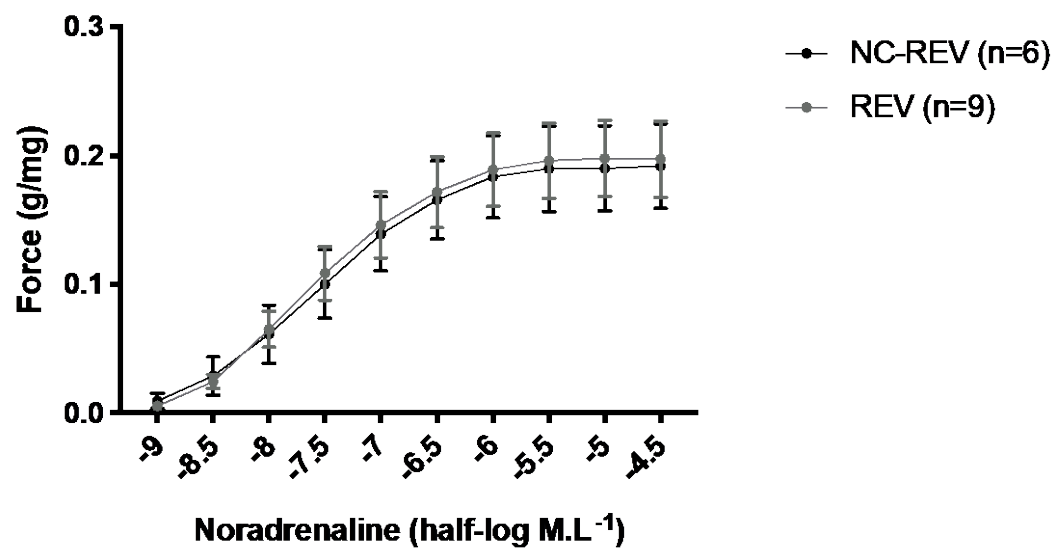


Figure 32: Diet reversible effect on vasoconstriction of aortic ring.

The curves showed comparable vasoconstrictive effects in response to noradrenaline when diet was changed to normal chow for three weeks. Data expressed as mean \pm SEM.

4.2.3 Vasorelaxation with Acetylcholine (Ach)

To assess endothelial function, Ach relaxation was recorded in aortic segments pre-constricted with 100nM NA. Ach relaxation was attenuated in the CAF compared to NC; CAF curve was significantly shifted to the right of NC curve ($P<0.001$) with I_{\max} 80.9 ± 3.4 and 70.5 ± 6.4 respectively. These data revealed that CAF-fed rats had less vasodilation compared to NC-fed rats (Figure 32). This effect continued to be significant and was not reversed when the diet changed to NC ($P<0.001$) (Figure 33).

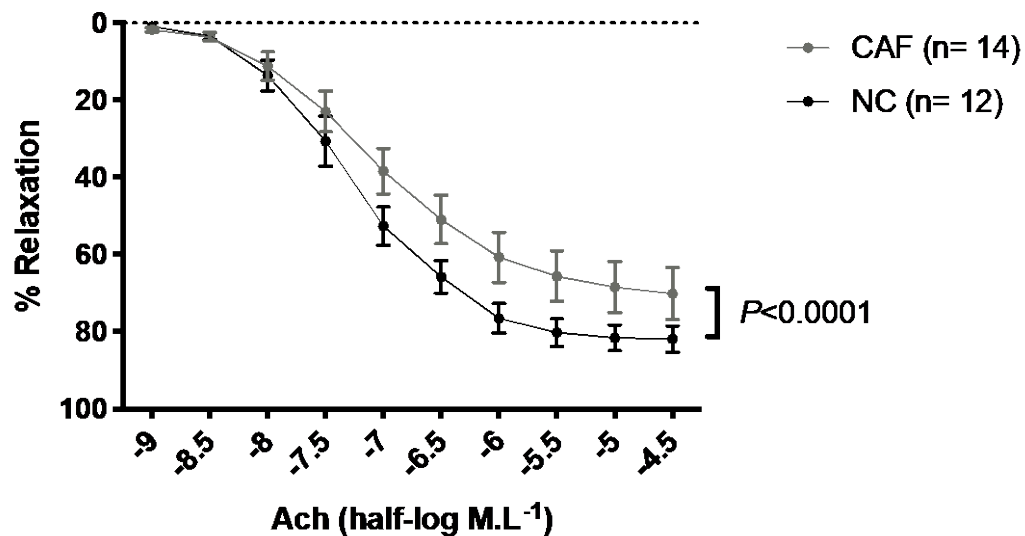


Figure 33: Effect of CAF diet on endothelial-dependent relaxation.

Ach relaxation was greater in NC arteries compared to CAF arteries with a significant difference between the curves ($P<0.0001$). Data expressed as mean \pm SEM.

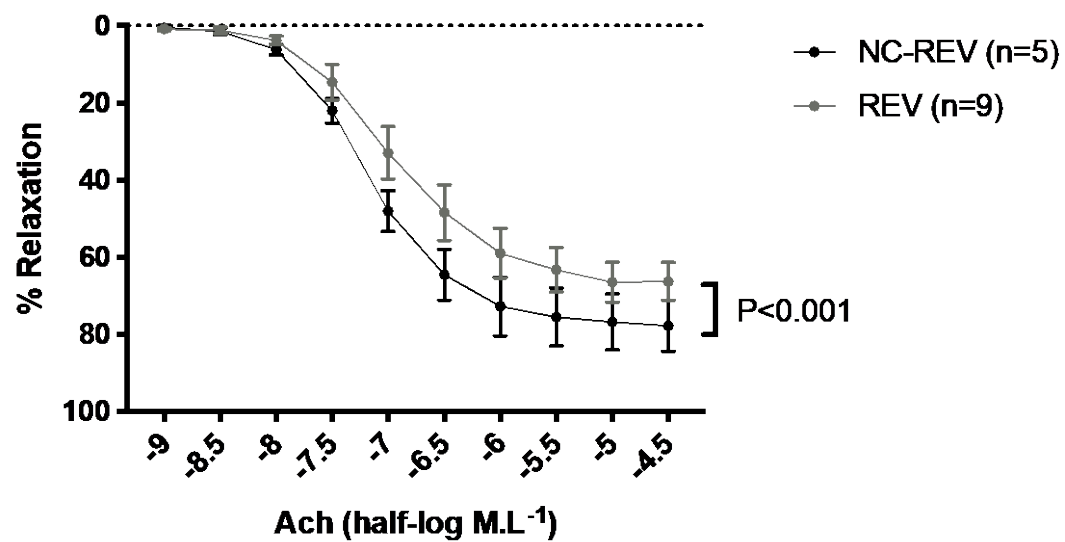


Figure 34: Effect of diet reversible on endothelial-dependent vasorelaxation.

Ach relaxation caused rightwards shift of the NC-REV curve compared with the REV curve. The change between the curves was significant $P < 0.001$. Data expressed as mean \pm SEM.

4.3 Effect of DIO on Liver

4.3.1 Liver weight and appearance

To determine changes in the appearance and weight of the liver due to CAF feeding, liver weight was recorded immediately after dissection and photographs were taken. Liver weight was significantly associated with body weight. CAF-fed rat livers were significantly heavier ($P < 0.001$) than those of NC-fed rats. Slight reduction in liver weight was observed compared to CAF-fed liver weight, which is still significantly higher when compared to its control NC-REV (Table 20).

As shown in Figure 34, change was observed in the appearance of CAF-fed liver, compared to NC-fed liver. CAF-fed rat liver showed to be discolored compared to the NC-fed rat liver. When the diet was changed to NC, the liver weight decreased (17.36 ± 0.87 vs 15.62 ± 0.74) compared to the CAF-fed animals and their appearance started to return to its normal dark coloring, comparable to those of the NC rats.

Table 20: Liver weight and body weight for obese and reversible rats.

Parameter	CAF		REV	
	NC (n= 11)	CAF (n= 15)	NC-REV (n=7)	REV (n= 12)
Body wt (gm)	555.4 ± 14.3	646.6 ± 16.5***	532.9±13.7	612.5 ± 16.5*
Liver (gm)	12.7 ± 0.4	17.4±0.8***	12.7 ± 0.8	15.6 ± 0.7 *
Ratio (%)	2.3 ± 0.1	2.7 ± 0.1 **	2.4 ± 0.1	2.6 ± 0.1

Data expressed as mean ± SEM and statistically evaluated using unpaired t-test to compare NC vs CAF and NC-REV vs REV. *P≤ 0.05, ** P≤ 0.01, *** P≤ 0.001.

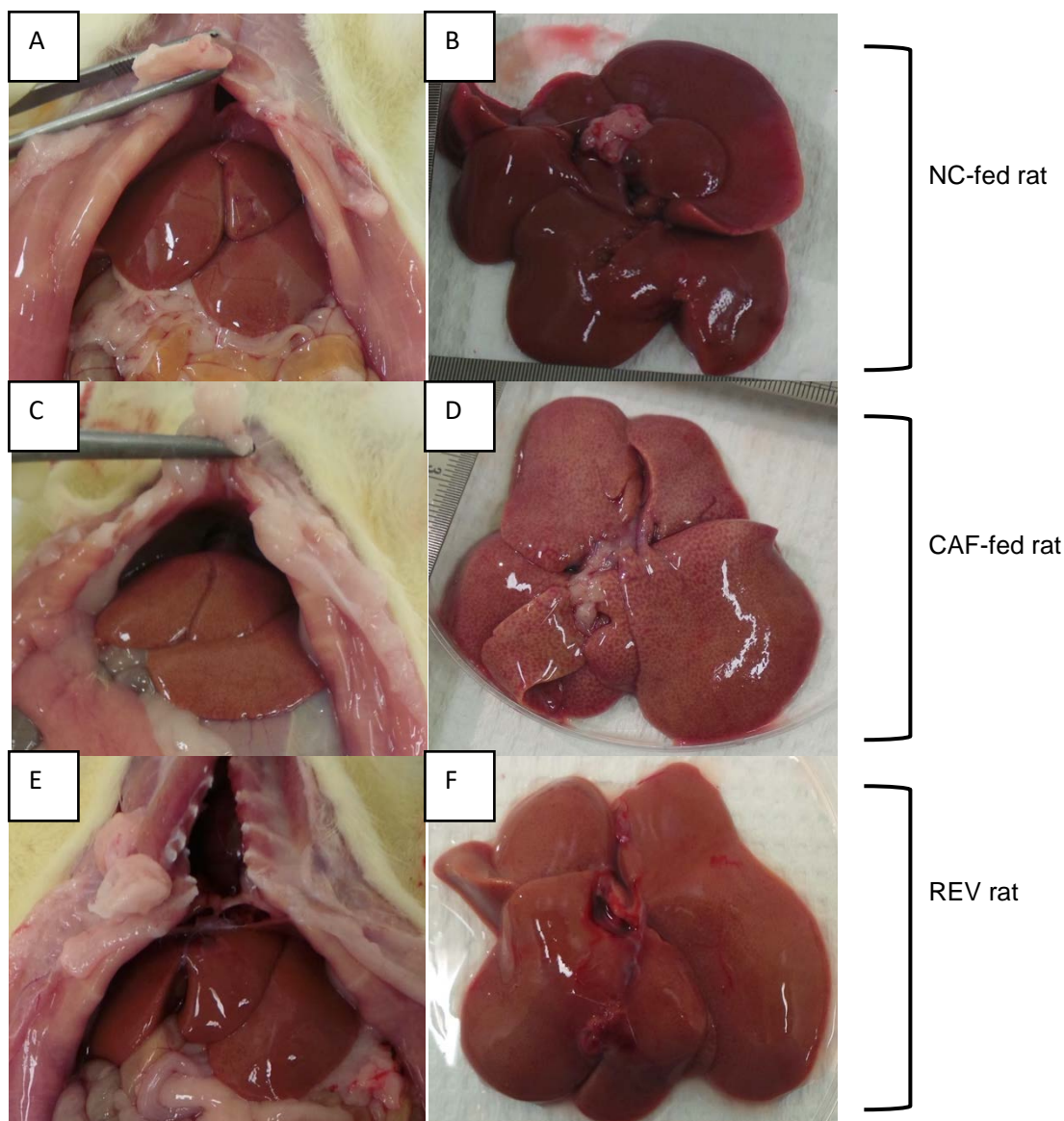


Figure 35: Gross morphology of liver tissue.

The figure showed a representative liver tissue from NC, CAF, and REV. The NC-fed rat liver appeared brown in color with a smooth surface (A and B), discolored appearance was observed in CAF-fed rats (C and D), discoloration was reduced in REV rat (E and D), when diet was changed to normal chow.

4.3.2 Liver function and lipid profile

In order to determine if CAF diet induced changes in the biochemical parameters, serum samples were analyzed. The liver function profile showed a significant increase in Alkaline Phosphatase (ALP) and albumin in CAF-fed rats compared to their control, which was returned to normal level in the reversible group (Table 21).

Table 21: Liver function for obese and reversible rats.

Parameter	Obese		Reversible	
	NC (n=11)	CAF (n=12)	NC (n=6)	REV (n=10)
ALP (U/L)	68.9 ± 4.6	89.9 ± 5.4 ***	71.9 ± 7.5	62.0 ± 3.9
ALT (U/L)	79.7 ± 9.8	83.5 ± 28.8	123.3 ± 16.8	83.2 ± 9.2
AST (U/L)	362.8 ± 56.2	295.6 ± 52.7	372.7 ± 70.3	293.0 ± 35.2
ALBUMIN (g/L)	37.1 ± 0.7	42.7 ± 0.8 **	38.7 ± 0.9	38.8 ± 0.9

Data expressed as mean ± SEM and statistically evaluated using unpaired t-test. *P≤ 0.05, ** P≤ 0.01, *** P≤ 0.001.

4.3.3 Hepatic Triglycerides

To determine if the CAF diet exerted any effect of TG deposition in the liver, liver tissue samples were homogenized and TG content was evaluated using the TG assay kit. The TG content of the harvested hepatic tissue in the CAF group was significantly higher ($P \leq 0.01$) compared to NC group. Interestingly, the TG content was significantly decreased ($P \leq 0.001$) in the REV group, when the diet was changed to NC for three weeks duration (Figure 35).

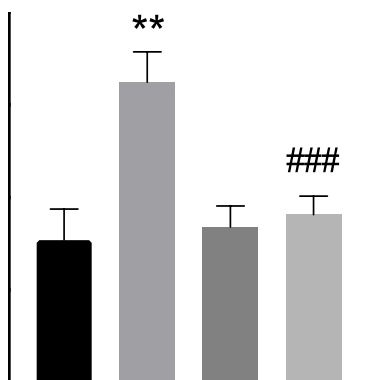


Figure 36: Quantification of the TG content in the liver.

CAF group showed a significant increase in TG content compared to NC. TG content significantly decreased with partial weight loss in REV group when diet changed from CAF to NC. * Represent the statistical difference between NC vs CAF, # represent the statistical difference between CAF vs REV. *or # $P \leq 0.05$, ** or ## $P \leq 0.01$, *** or ### $P \leq 0.001$. Data expressed as mean \pm SEM

4.3.4 Liver histological studies and the development of NAFLD

To determine if CAF feeding induced hepatic histological changes H&E stained liver sections were examined under light microscope. Results showed normal structure of hepatocytes in the NC group. CAF fed group showed micro-vesicular fatty change in most hepatocytes, with initial macro-vesicular development in some rats (between score 1 and score 2). More changes were observed around periportal region, portal triad and centrilobular region (Figure 36). The steatosis grade (refer to chapter 2 for hepatic steatosis grading methodology) ranged between grade 2 and 3 for CAF group (Table 22). The absence of PMNC and MNC infiltration indicates no signs of inflammation occurred in the same rats. A strong reversal effect was observed in the REV group when diet was changed to NC only micro vesicular steatosis was observed with grade 1. In order to confirm the absence of inflammation, more sections from the same rats were stained with Sirius red (specific stain for collagen deposition, as a marker of tissue fibrosis). Results revealed that normal distribution of collagen fibers in all the studied groups (Figure 36).

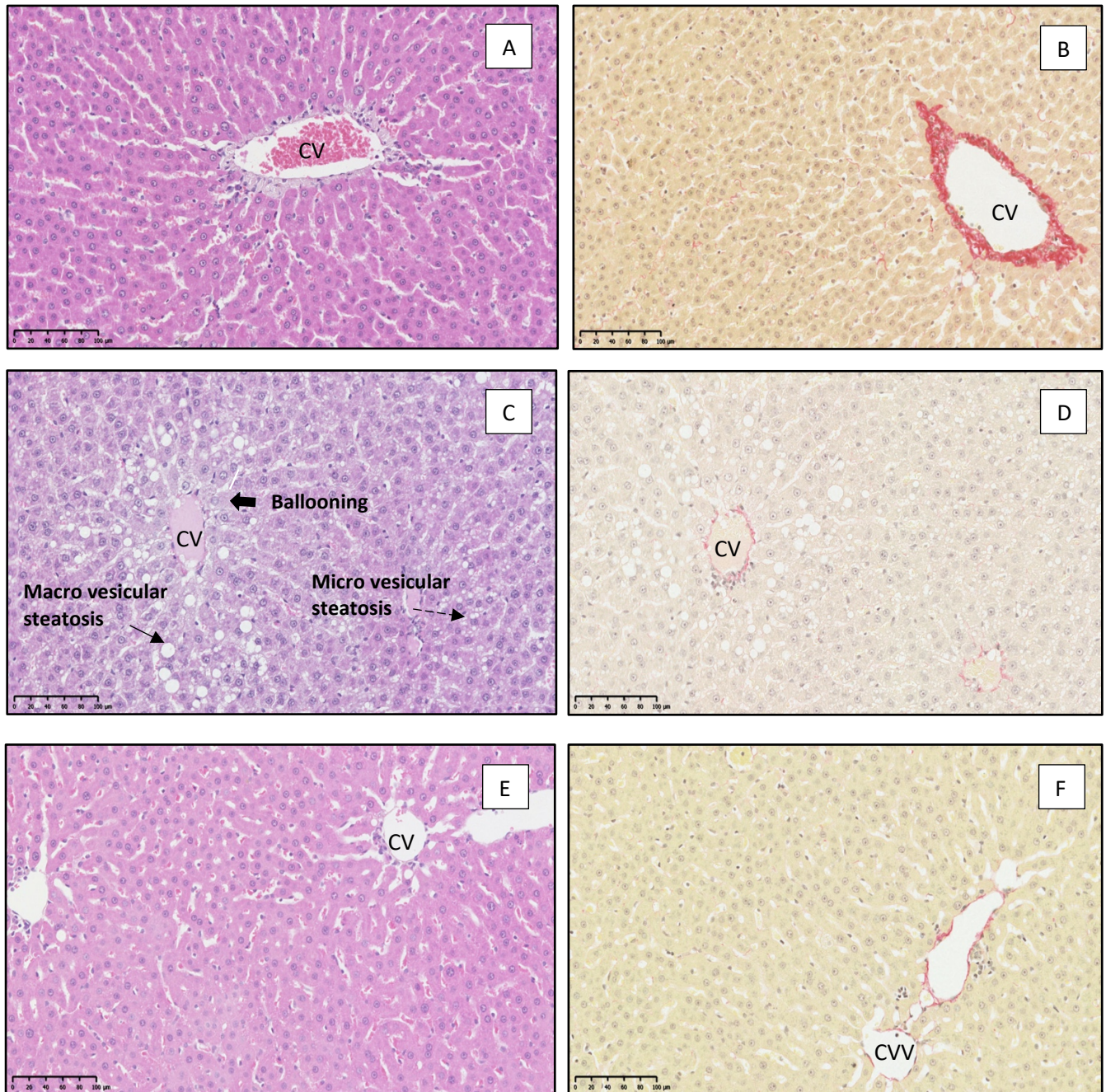


Figure 37: Liver histological studies.

(A) NC, normal hepatic cells, (B) NC (Sirius red), normal collagen fibers distribution. (C) CAF, rats reveal hepatocyte ballooning, micro-vesicular steatosis and some macro-vesicular steatosis around the central vein (CV) (grade 3 hepatic steatosis). (D) CAF, no changes were observed in the collagen distribution. (E) REV, liver showed normal hepatocytes when diet was changed from CAF to NC. (F) REV, no changes were observed in the collagen distribution. Images in the left panel stained with Hematoxylin and eosin, and images in the right panel stained with Sirius red. Images were analyzed using 20X objective (bar= 100µm).

Table 22: Grading of hepatic steatosis

group	Animal #	Score				
		Hepatocyte Ballooning	Microvesicular steatosis	Macrovesicular steatosis	PMNC	MNC
NC	1	0	1	0	0	0
	2	0	0	0	0	0
	3	0	1	0	0	0
	4	0	2	0	0	0
CAF	1	1	1	0	0	0
	2	1	3	1	0	0
	3	1	3	2	0	0
	4	1	1	0	0	0
	5	1	3	1	0	0
	6	0	2	0	0	0
REV	1	0	0	0	0	0
	2	0	1	0	1	1
	3	0	1	0	0	0
	4	0	2	0	0	0
	5	0	0	1	0	0
	6	0	1	0	0	0

4.4 Discussion

Central obesity is considered an independent risk factor for the development of CVDs and associated with MS (167). While overall obesity is largely linked to impaired vasoreactivity, as seen in reports comparing obese to lean individuals (168), dietary components may also affect vascular function.

Data from this study showed that CAF diet significantly increased SBP, as shown in the final blood pressure readings when comparing CAF to NC. The risk of developing hypertension is strongly associated with body mass index (BMI) (169). Elevated SBP, DBP and MAP readings were observed in the initial measurements for both groups. This could be due to the first experience for rats to be exposed to the tail-cuff system. It is recommended to do adaptation trials before starting the actual readings. REV rats showed high SBP before shifting diet from CAF to NC, which was lowered after reversibility but did not reach a statistical significance. Several human studies, observational and interventional, showed that weight loss through dietary intervention lowered blood pressure (170). Collectively, this support the published guidelines that dietary intervention combined with weight loss is the first step in treating hypertension (46).

Rats fed with CAF diet or NC for 16 weeks showed a comparable effect of vasoconstriction in response to noradrenaline. These results are supported by another study that showed that reactivity to noradrenaline was similar in rats fed with high fat diet for 30 weeks (83), and in Wistar rat fed with CAF diet (171).

Endothelial cells have a significant role in vascular smooth muscle relaxation by acetylcholine. Acetylcholine is an endothelial-dependent relaxant, which triggers the production of NO. Therefore, the noradrenaline-precontracted aortic rings from CAF group revealed a significant decrease in vasorelaxation. These findings suggest that endothelial function was impaired by the CAF diet. Impaired arterial relaxation due to endothelial dysfunction with dietary obesity in rats was reported by Naderali EK *et*

al (172). The induction of endothelial dysfunction by a CAF diet is consistent with previous data suggesting the same in animal models with high levels of circulating FFAs and obesity (168, 173). Several factors have an effect on vascular function such as: hyperinsulinemia, hyperglycemia, lipotoxicity and inflammation. In the current model data showed that not all animals suffered from hyperinsulinemia nor hyperglycemia. Inflammation also was examined by measuring systemic IL-6 and TNF-alpha (results not shown) and no inflammation was detected in all samples. So, these factors have been neglected as the global causative factors of vascular dysfunction. Lipotoxicity might be the most likely causative factor of endothelial dysfunction in this model. The same has been suggested in another study using Wistar rats fed with CAF diet, that plasma TG may have a significant effect on vascular function independently of insulin resistance (171). Therefore, the vascular dysfunction could be mediated by diet-induced hypertriglyceremia independently from diet-induced obesity (174). Moreover, the Zucker fatty rat exhibited high level of FFA and TG, this model showed an impairment in acetylcholine-stimulated vasodilation via oxidative stress (175). Oxidative stress is referred to the production of reactive oxygen species (ROS) that suppress the antioxidant defense (176). High level of plasma lipids leads to oxidative stress which produce superoxide, as a result, hydrogen peroxide interacts with NO, affecting its bioavailability (177). This evidence strongly suggest that oxidative stress is a mechanism that can induce endothelial dysfunction.

This effect was similar with the REV group. Impairment in endothelial function persists even when the CAF diet is withdrawn and replaced with NC. Studies suggest that diet-induced weight loss significantly improved plasma biomarkers of endothelial function, but endothelial dysfunction was not as readily repaired (178). Conversely, a complete restoration of endothelial dysfunction was observed with reduction in energy intake (179). The improvement of endothelial function could be related to the withdrawal duration of the palatable food, where it was almost the same duration of palatable food feeding (179). In addition, exercise could also help in opposing

endothelial dysfunction via upregulation of NO-dilation system (180). The possible underlying mechanisms that mediate the improvement of endothelial dysfunction are suggested to be increase in the expression of endothelial nitric oxide synthase (eNOS), leading to increase in bioavailability of NO (181), in addition to reduction in the oxidative stress (165) and lipid peroxidation (182).

Endothelial dysfunction observed in the current study could be either due to a damage to the endothelial cells, or defect in the pathway that mediates vasorelaxation such as lack of NO production and expression of eNOS. Transcriptome analysis has the potential to address this question.

Abnormal fat deposition in hepatocytes results in hepatic steatosis, a pathological condition that leads to liver abnormality, such as NAFLD and NASH. NAFLD is the most common chronic liver disease associated with obesity and MS. Liver steatosis is strongly associated with visceral adiposity (183).

The results here suggested that the CAF diet induced liver discoloration, which was clearly apparent from the liver appearance. The pale color of CAF-fed rat liver is likely to be a consequence of fat accumulation in the organ. Consistent with this finding, liver of the human hepatic lipase (hHL)-expressing mice was pale in color after 16 week feeding regimen (184). This appearance was improved when the diet was switched to normal chow for 4 weeks.

A positive correlation between body weight and liver weight was observed, when body weight increased liver weight was increased. This finding is similar to previous studies (135, 184). These findings suggest that liver weight was increased due to hepatic fat accumulation.

Liver enzymes activities are a reflective marker for liver damage. It happens when the hepatocyte injury occurs and increase the leakage of the enzymes into the blood stream. Liver fat accumulation is accompanied by disturbances in the liver function. The current data showed a significant elevation of ALP and albumin levels. It has been shown that clinical diagnosis of liver steatosis includes the elevation of ALT and AST, however, the efficiency of these enzymes in diagnosis of NASH is limited due to their low specificity, sensitivity, and prognostic value (185). Indeed, most of NAFLD patients showed a normal level of liver enzymes (105). Another clinical marker used in the process of NAFLD diagnosis is the evaluation of lipid profile (186). The current results revealed a significant higher TG in CAF-fed rats and a significant lower HDL in the same group. Additionally, as expected the CAF-fed livers exhibited higher TG content compared to NC-fed livers. These finding are in line with other studies, TG was significantly increased in rats fed with high carbohydrate diet containing 70% CHO (187). Same findings were also observed in rat-fed with high carbohydrate/high fat diet in 8 weeks of feeding (188). The discoloration observed in this study is evident by the disturbance in the liver enzymes and the elevation in systemic and hepatic TG, thereby highlighting the role of CAF diet in inducing the synthesis of liver lipids which distributes to other tissues through circulation. It appears that liver is adapting to the metabolic changes induced by the new nutritional condition. Interestingly, 6% weight loss was able to reverse all these changes to its normal level.

The main hepatic feature of NAFLD is hepatic steatosis, which was confirmed by histopathological analysis of liver tissue. In the histological studies to assess the severity of hepatic steatosis, H&E stain analysis showed signs of mild steatosis associated with ballooning degeneration scored with grade 3 steatosis. Usually, NAFLD is accompanied with inflammation. However, hepatic steatosis of CAF-fed

livers was not associated with lobular inflammation, as confirmed by inflammation scoring. The hepatic steatosis grading was further confirmed by the specific stain Picro-sirius red used to diagnose the fibrotic changes. No changes were occurred in the stained sections, which means this model did not induce collagen deposition and did not show any fibrotic changes among all the groups. Thus, cumulative evidence supports the fact that diet is an important mediator of the development of NAFLD. The literature showed different diets were tested in order to induce NAFLD with different animal models, such as the case of high fat diet which revealed short-term feeding caused damage of the liver tissues (189), and high fructose drinking water induced simple steatosis within 8 weeks (190).

The interesting part of this section is the effectiveness of the dietary intervention in reversing the abnormal changes induced by CAF diet. Lifestyle intervention with diet modification is not only effective with weight reduction, but also improving liver steatosis and NAFLD recovery. The dietary modification by switching from CAF to NC was able to achieve 6% weight loss in 4 weeks. Although 6% seems not to be sufficient to recover all the changes developed in 16 weeks of overfeeding, it showed clear improvement in the liver appearance, a significant reduction in the liver weight, and recovery of lipid profile and liver function enzymes. Additionally, the elevation of TG content was diminished. This led to the main finding of this study that hepatic steatosis was completely reversed from grade 3 to grade 1 (almost normal healthy liver). This could be due to the severity of the steatosis, where this model did not reach the severe condition, which is recognized by inflammation and fibrosis. It is well known that liver tissue has the capability to repair itself (191). Histological assessment revealed that NAFLD and NASH recovery depends on the degree of severity of the hepatic steatosis, as the severity is increased, the chance of recovering healthy liver is decreased (123).

After shifting the diet from CAF to NC, the rats remained obese, but there was a clear improvement in the hepatic steatosis. These findings match those observed in earlier studies in mice (192), and rat (193) models, which were fed with trans-fat diet and high carbohydrate/ high fat diets respectively. Both models were subjected to natural recovery by dietary standardization. Although the current model revealed a modest weight loss (6%), however it has a high impact in reversing the liver steatosis. This supports a previous study that showed weight reduction markedly improved steatosis (110), suggesting that even slight weight loss is an effective treatment for NAFLD and NASH (124).

It has been suggested that high carbohydrate enhances DNL in the liver, while high fat diet decreases the DNL. This could be also applicable to this model. The present findings suggest that hepatic DNL increase due to high load of carbohydrates from CAF diet leading to hepatic TG accumulation and consequently the formation of NAFLD. Therefore, the leading mechanisms for the development of hepatic steatosis will be further explored by the transcriptome analysis and presented in the next chapter.

CHAPTER 5: RESULTS: LIVER TRANSCRIPTOME ANALYSIS

5.1 Introduction

Hepatic lipids homeostasis is regulated by four major pathways to optimize the balance between acquisition and disposal of lipids (194). First, DNL is one of the common pathways that uses non-lipid sources (carbohydrate) and converted to lipid. Second pathway is the uptake of fatty acids from the circulation, by specific FA transporters located on the cell membrane of hepatocytes. Third, oxidation of FA, especially when there is low level of glucose in the circulation. Fourth, lipids are exported to the circulation by VLDL. The dysregulation of one of these pathways results in lipid retention and the development of NAFLD. The molecular mechanisms underlying the disruption of these pathways in disease warrants greater investigation (194). Thus, there are a number of molecular transcriptional factors extensively studied and well known in regulating the carbohydrate and lipid metabolism in the liver (195).

De novo lipogenesis. DNL pathway is considered as a significant contributor in intrahepatic lipid accumulation in fatty liver diseases, and suggested to be the major pathway in NAFLD progression (196). Recently, studies showed that DNL play a major role in utilizing glucose as a response of overfeeding. In addition, fructose has a significant role in upregulating DNL enzymes (ACC1: Acetyl-CoA carboxylase, FAS: fatty acid synthase and SCD1: stearoyl-CoA desaturase-1) than HFD (197). At the transcriptional level, DNL is regulated by the transcriptional factors: sterol regulatory element-binding protein 1 (SREBP-1), carbohydrate regulatory element-binding protein (ChREBP). SREBP-1 is involved in lipogenesis which regulates the cholesterol and triglyceride synthesis (198). It was clearly shown that hepatic TG level is higher under the overexpression of SREBP-1 in transgenic mice model (199). Insulin has a significant role in regulating the activation of SREBP-1, it stimulates SREBP-1 under insulin resistance (IR) condition and increase the FA production through de novo lipogenesis (200, 201). ChREBP is a main regulator of carbohydrate

metabolism involved in glycolysis, fructolysis, gluconeogenesis and contribute to DNL pathway (202, 203). Fructose administered to mice, activates ChREBP and lead to metabolic disturbances such as glucose intolerance, hyperinsulinemia hypertriglyceridemia resulting in hepatic steatosis (204). Thus, ChREBP require the upregulation of lipogenic and glycolytic genes (204).

Fatty acid uptake. FA diffusion through the lipid bilayer exhibited less contribution to the FA uptake process (205). Thus, the uptake of circulating FA is mediated by FA transporters (FATP) located on the cell membrane of hepatocytes, these transporters are called: cluster of differentiation 36 (CD36) and caveolins (43). The master regulator of this process is peroxisome proliferators-activated receptor-gamma (PPAR-g). It increases the uptake of FA by mediating the expression of adipocyte protein 2 (Ap2) and CD36 (206). FA are traveled between organelles via certain fatty acid binding protein Because of FA hydrophobic properties, (FABP) (207). FABP1 is the major isoform in the liver (207). FABP1 has a role in the utilization of FA either through oxidation to generate energy or conversion into TG (208). FABP1 is used as a pharmacological target in order to suppress hepatic steatosis, where FABP1 knockdown mice showed a significant protection against TG accumulation (209). Hepatic FABP expression is increased in obese patients with hepatic steatosis compared to obese patient without steatosis (210). Therefore, inhibition of FA uptake has a potential role in improving the hepatic fat accumulation and NASH development (211).

Fatty acid oxidation. It is the utilization of FA as an energy source during glucose depletion or fasting. Fatty acids are delivered to hepatocytes through 3 different sources, from the hydrolysis of stored TG in hepatocytes, lipids imported from circulation or from DNL (212). Fatty acid oxidation mainly takes place in the mitochondria and called β -oxidation. Other pathways of FA oxidation are α -oxidation

and ω -oxidation, which take place in endoplasmic reticulum (ER) in the presence of cytochrome P450 enzymes (213). Peroxisome proliferator-activated receptor α (PPAR- α) is the transcriptional factor that control fatty acid oxidation to produce energy in absence of glucose (214). Upregulation of PPAR- α lead to the expression of targeted genes responsible for fatty acid oxidation in different organelles such as: mitochondria (medium-and long-chain acyl-CoA dehydrogenases), peroxisome (Acyl-CoA oxidase (ACOX) 1 and enoyl-CoA hydratase) and endoplasmic reticulum mediated through cytochrome (CYP4A1 and CYP4A3) (166). Thus, differential expression of PPAR- α could be related to different aspects of the NAFLD pathogenesis. Evidence showed the negative correlation between PPAR- α expression and the severity of hepatic steatosis (215), proposing the critical role of PPAR- α expression in fatty acid oxidation and protection from liver steatosis.

Lipid export is mediated by VLDL, which plays an essential role in the lipid metabolism process in the liver. The function of this lipoprotein is to carry endogenous hepatic TG, mainly synthesized from dietary carbohydrate to other tissues such as adipose tissues and skeletal muscles. Consequently, TG is utilized by these tissues for energy production or esterified and stored as fat (216). Normally export of TG is increase based on the hepatic TG content. However, in steatosis the TG export reaches a plateau independently from the TG level accumulated in hepatocytes (217). Impairment in the VLDL-TG export is potentially inducing the NAFLD and NASH (218).

Transcriptome analysis is a well-established method to explore gene expression profiles and is a powerful tool used to investigate the mechanistic pathways involved in specific functions and pathological conditions. Understanding the mechanistic pathways mediating liver steatosis is a potential tool in discovering therapeutic intervention and protection against hepatic lipotoxicity.

This chapter provides the results from the aim to:

Explore the alteration in hepatic transcriptome and determine the differential expression of genes related to mechanistic pathways associated with both weight gain and weight loss.

5.2 Gene expression studies: Microarray analysis in CAF-fed livers

To identify the expression of genes associated with CAF-diet induced hepatic steatosis, microarray analysis was performed. CAF livers showed that out of 23188 genes studied, 218 genes (0.94%) were differentially expressed (corrected P-value, false discovery rate (FDR) P-value <0.05). Of these, 70 (32.11%) genes were upregulated, and 148 (67.89%) genes were downregulated (Figure 37). These genes were subjected to hierarchical clustering (Figure 38). All NC samples were clustered in 1 branch, and all CAF samples were clustered in another branch. In each group the tree represents the relationship among samples and the branch length reflects the degree of similarity between samples based on their gene expression profile. These results showed that CAF diet induced the changes of genes in a variety of biological processes, with the largest number of altered genes being associated with glucose, lipid metabolism and liver injury (Appendix 1).

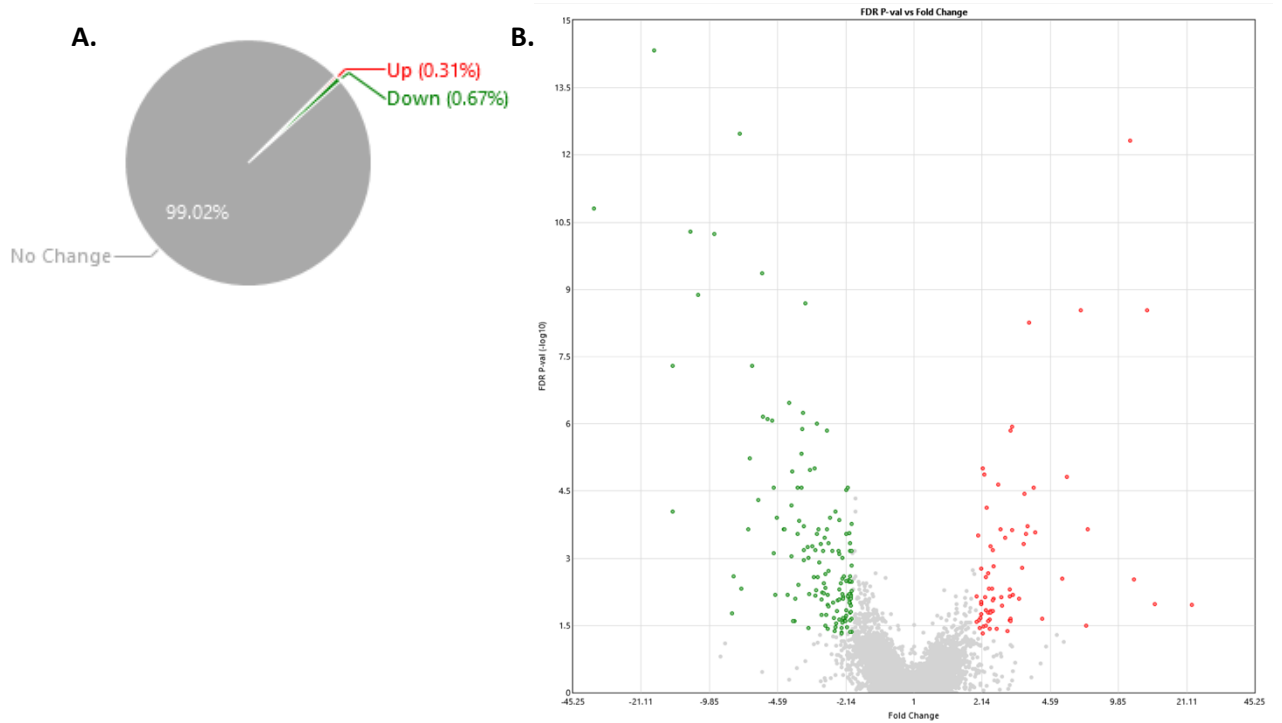


Figure 38: Differentially Expressed genes between CAF and NC (FDR P-value < 0.05; RMA).

(A) Pie chart representing the percentages of differentially expressed genes. (B) Volcano plot of gene expression fold change vs. FDR P-Value. Red color indicates the 70 up-regulated genes, green color indicates the 148 down-regulated genes. Gray indicates genes that were not different.

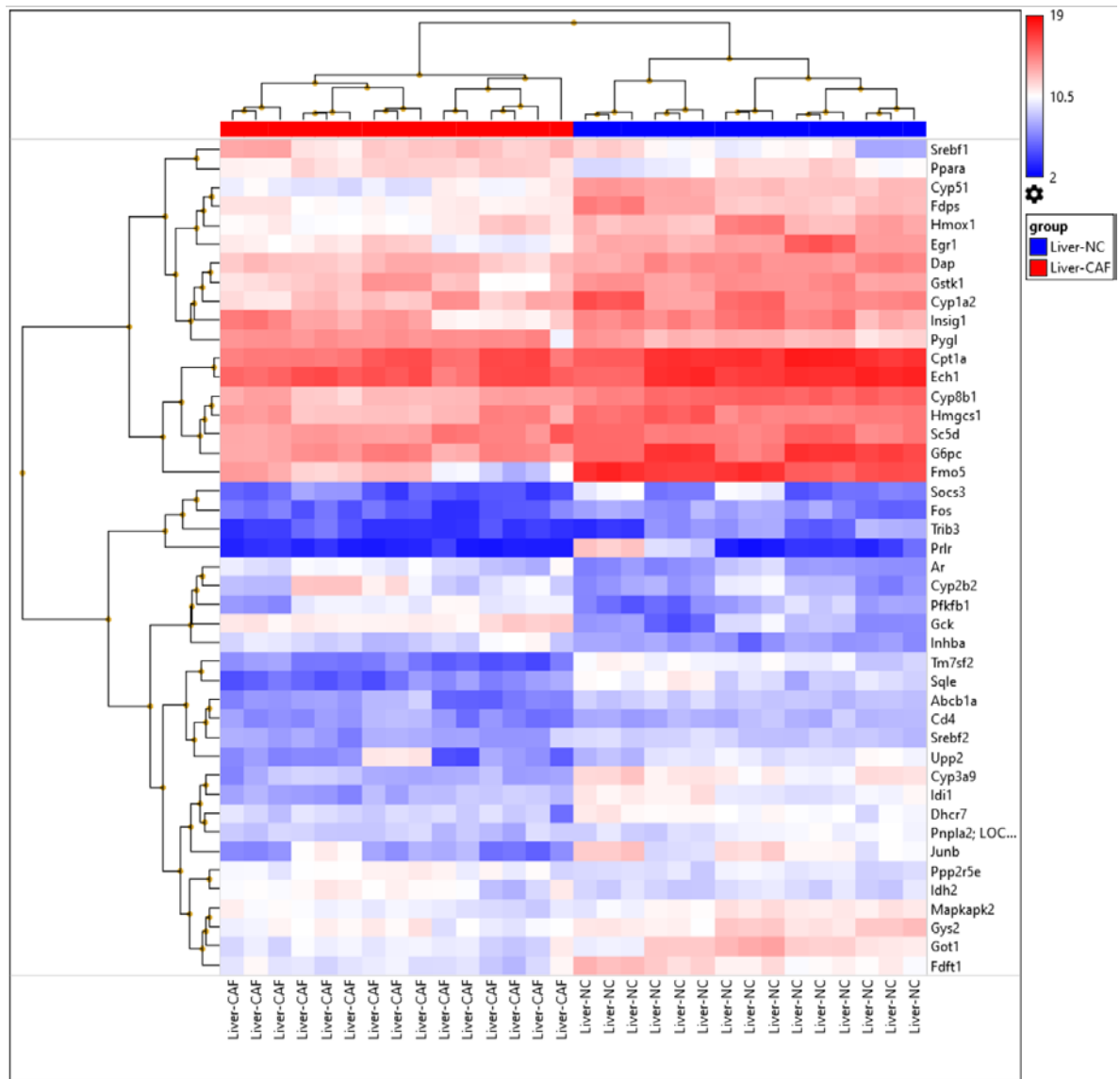


Figure 39: Hierarchical clustering analysis of differentially expressed genes in liver of CAF vs NC.

The columns represent different samples, and the rows represents measurements from different genes. Right portion represent NC group, and left portion represent CAF group. Samples from both groups (15 NC and 15 CAF) with expression values for 44 genes were subjected to hierarchical clustering. Blue color denotes the high expression in CAF compared to NC, Red color denote low expression in CAF compared to NC.

5.2.1 Pathway Analysis

5.2.1.1 Effect of CAF on lipid metabolism pathways

The key transcriptional regulators of lipid metabolism such as *Srebf1* and *Ppara-a* were upregulated (Figure 39 & 41). Other genes related to lipid synthesis and cholesterol biosynthesis were decreased in CAF-fed rats compared to NC-fed rats (Figure 39 & 40). Lipid export and excretion showed a down-regulation in ATP-dependent translocase (*Abcb1a*). The genes encoding for fatty acid oxidation such as Carnitine palmitoyltransferase 1A (*Cpt1a*) was decreased while Isocitrate dehydrogenase (*Idh2*) was increased. Moreover, CAF-induced liver steatosis was also associated with the reduction in the expression of multiple cytochrome P450 family genes such as *Cyp1a2*, *Cyp8b1* and *Cyp51*. In contrast *Cyp2b2* was upregulated (Table 23).

Table 23: List of differentially expressed genes related to lipid metabolism pathway in CAF vs NC.

Gene symbol	Fold change	FDR P-value	Regulation	Outcomes*
SREBF1	2.99	0.0002	Up-regulated	Transcription factor involved in lipogenesis. Facilitates FFA accumulation and TG formation.
Ppara- α	2.32	0.0006	Up-regulated	Transcriptional factor involved in lipid metabolism. Enhances FA uptake, utilization and catabolism.
Idh2	2.91	0.0003	Up-regulated	Enzyme involved in citric acid cycle. Catalyzes the oxidation decarboxylation of isocitrate to 2-oxoglutarate.
Cyp2b2	5.22	0.0029	Up-regulated	Cytochrome P450 enzyme involved in NADPH-dependent electron transport pathway. Oxidizes steroids, fatty acids, and xenobiotic.
Idi1	-4.88	8.39E-07	Down-regulated	Enzyme involved in cholesterol biosynthesis. Catalyzes the interconversion of isopentenyl diphosphate (IPP) to its highly electrophilic isomer, dimethylallyl diphosphate (DMAPP).
Fdps	-3.53	4.73E-06	Down-regulated	Enzyme involved in cholesterol biosynthesis. Catalyzes the production of geranyl pyrophosphate and farnesyl pyrophosphate from isopentenyl pyrophosphate and dimethylallyl pyrophosphate.
Hmgcs1	-3.67	0.0003	Down-regulated	Enzyme involved in cholesterol synthesis pathway. Catalyzes the reaction in which acetyl-CoA condenses with acetoacetyl-CoA to form 3-hydroxy-3-methylglutaryl-CoA (HMG-CoA)
Fdft1	-3.48	1.29E-06	Down-regulated	Enzyme involved in cholesterol biosynthesis (mevalonate pathway). Catalyzes the condensation of 2 farnesyl pyrophosphate (FPP) moieties to form squalene.
Sqle	-12.19	1.11E-14	Down-regulated	Rate-limiting enzyme in steroid biosynthesis. Catalyzes the first oxygenation step in sterol biosynthesis.
Sc5d	-2.23	0.0004	Down-regulated	Enzyme involved in cholesterol biosynthesis. Catalyzes the conversion of lathosterol into 7-dehydrocholesterol.
Pnpla2	-2.23	0.0029	Down-regulated	Enzyme involved in hydrolysis. Hydrolyzes triacylglycerol to diacylglycerol.

Ech1	-2.64	0.0066	Down-regulated	Enzyme involved in mitochondrial fatty acid beta-oxidation pathway. Catalyzes the hydration of 2-trans-enoyl-coenzyme A (CoA) intermediates to L-3-hydroxyacyl-CoAs.
Dhcr7	-2.64	0.0002	Down-regulated	Enzyme involved in sterol biosynthesis. Converts 7-dehydrocholesterol (7-DHC) to cholesterol.
Abcb1a	-3.28	0.0006	Down-regulated	Protein belongs to ATP-binding cassette (ABC) transporters. Pumps xenobiotic out of the cells.
Cpt1a	-2.05	0.0173	Down-regulated	Mitochondrial enzyme involved in beta-oxidation of long chain fatty acids. Catalyzes the transfer of the acyl group of a long-chain fatty acyl-CoA from coenzyme A to L-carnitine.
Cyp1a2	-5.15	7.96E-07	Down-regulated	Cytochrome P450 enzyme. Metabolizes polyunsaturated fatty acids into signaling molecules.
Cyp8b1	-3.88	0.004	Down-regulated	Cytochrome P450 enzyme. Converts 7 alpha-hydroxy-4-cholesten-3-one into 7-alpha,12-alpha-dihydroxy-4-cholesten-3-one.
Cyp51	-7.05	4.74E-13	Down-regulated	Cytochrome P450 enzyme involved in cholesterol biosynthesis. Removes the 14alpha-methyl group from lanosterol.

*Outcomes generated from www.genecards.org or www.uniprot.org.

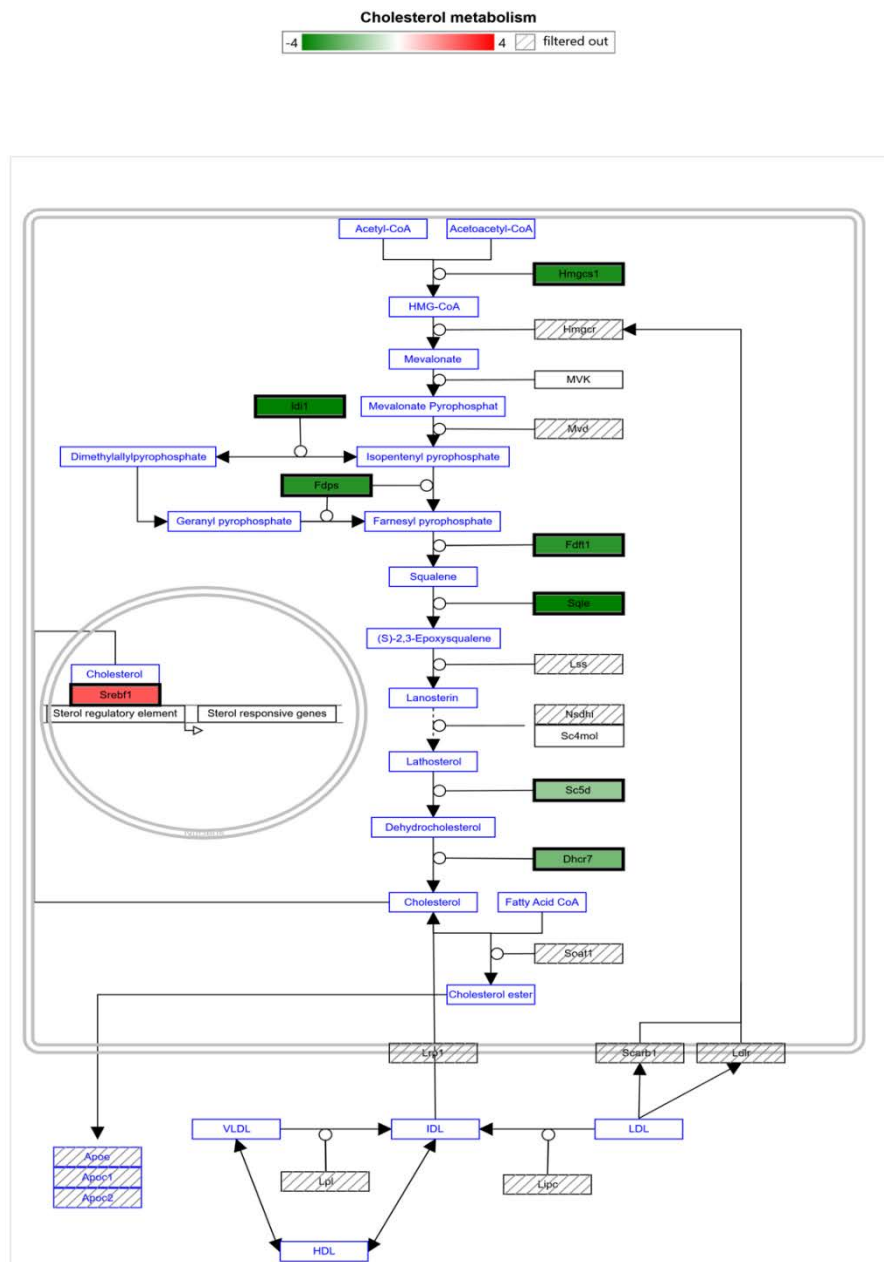


Figure 40: Effect of CAF diet on the expression of cholesterol metabolism pathway.

SREBF1 was the significant mediator in this pathway. Red color represents the upregulated genes, and the green color represent the down-regulated genes. Pathway analysis performed using TAC 4.0 software.

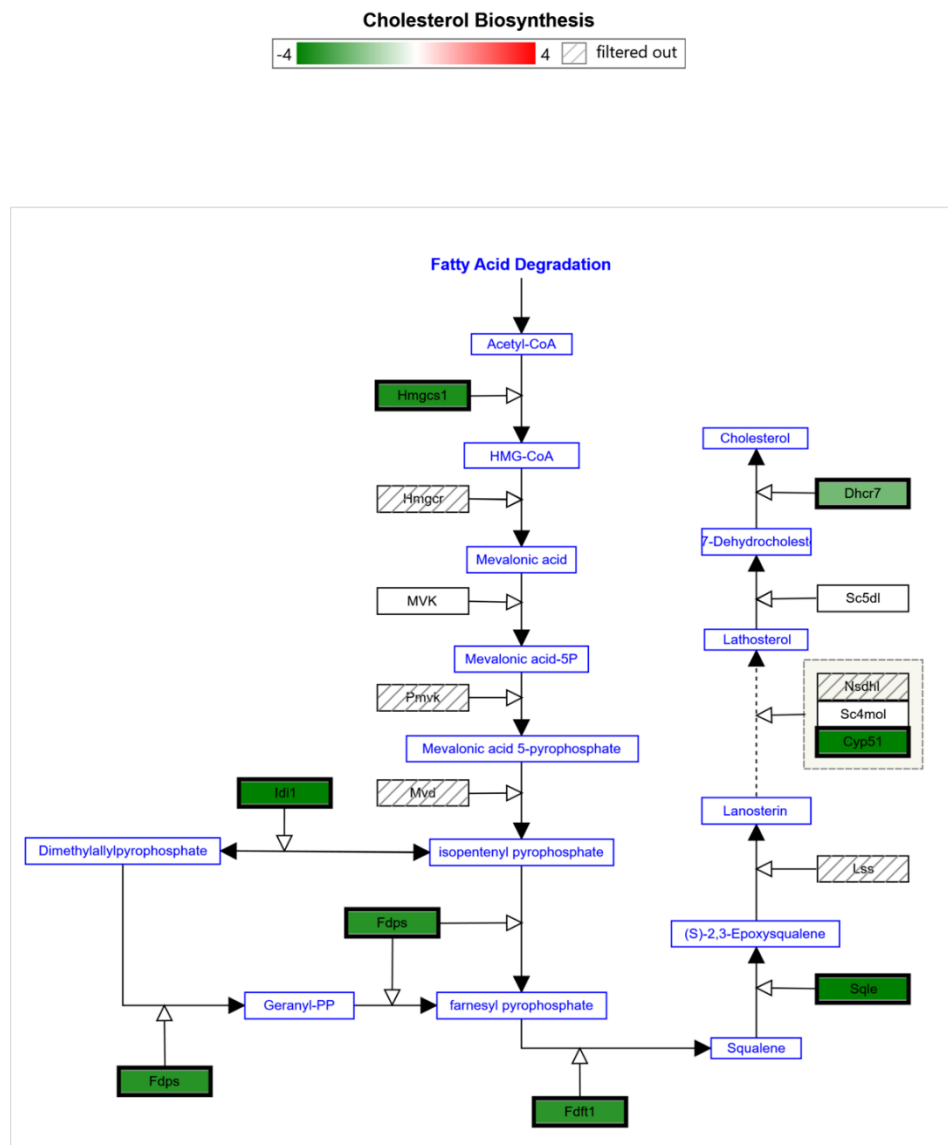


Figure 41: Effect of CAF on the expression of cholesterol biosynthesis pathway.

The chart represents the differential expression of genes related to cholesterol metabolism. Red color represents the up-regulated genes, and the green color represent the down-regulated genes. Pathway analysis performed using TAC 4.0 software.

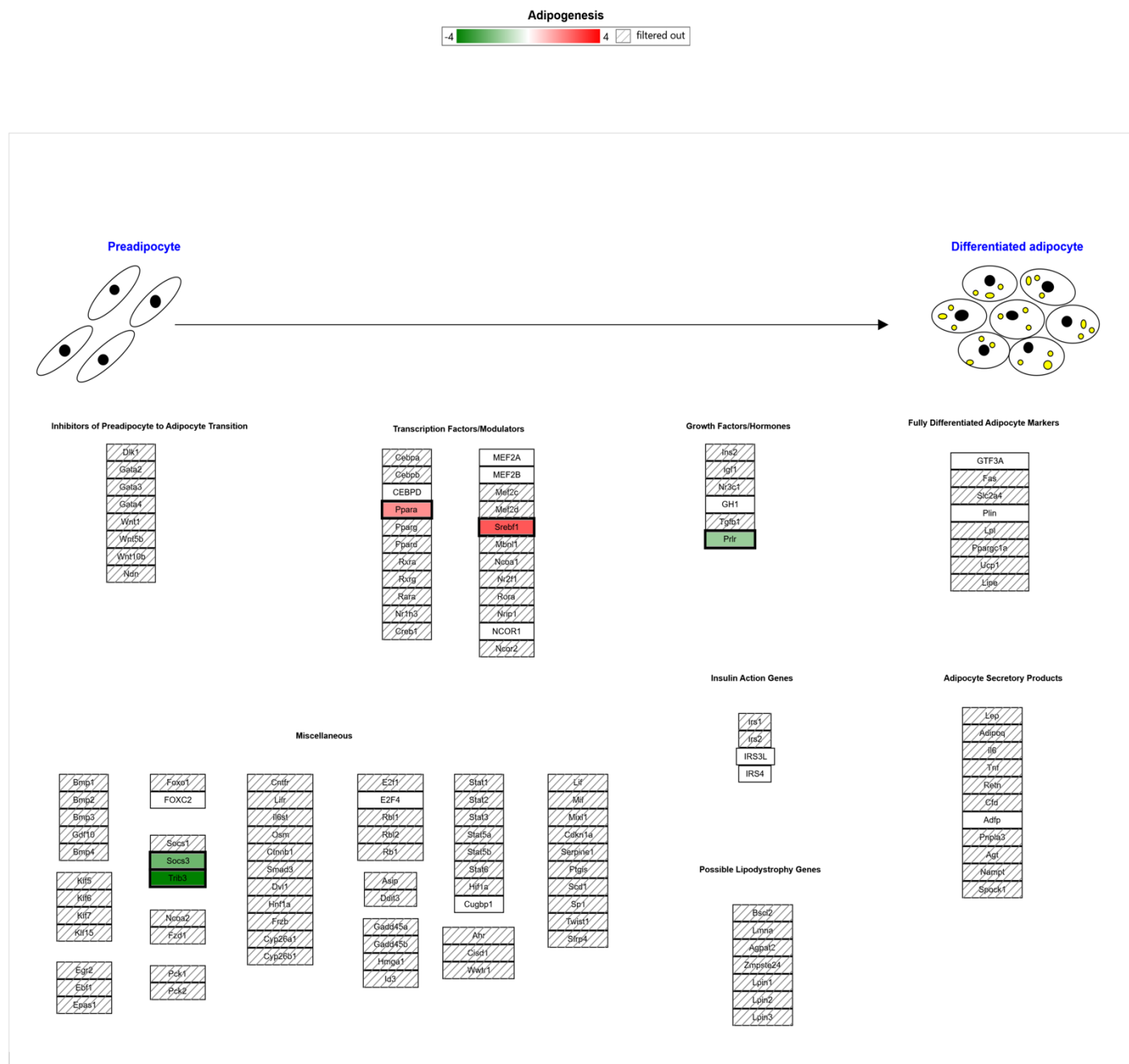


Figure 42: Effect of CAF on the expression of Adipogenesis pathway.

The chart represents the significant involvement of the transcriptional factors PPAR and SREBF1 that mediates the adipogenesis pathway. Red color represents the upregulated genes, and the green color represent the down-regulated genes. Pathway analysis performed using TAC 4.0 software.

5.2.1.1 Effect of CAF on Glucose metabolism pathways

The transcriptome analysis revealed that hepatic genes related to glucose metabolisms such as: glucokinase (Gck), glycogen phosphorylase L (Pygl) and protein phosphatase 2 regulatory subunit B epsilon (Ppp2r5e) were upregulated in response to CAF diet. Conversely, other genes such as glucose-6-phosphatase (G6pc), glutamic-oxaloacetic transaminase 1 (Got1) and glycogen synthase (Gys2) were down regulated (Table 24) (Figures 42 & 43).

Table 24: List of differentially expressed genes related to Glucose metabolism pathway in CAF vs NC.

Gene symbol	Fold change	FDR P-value	Regulation	Outcomes*
Gck	13.51	2.97E-09	Up-regulated	Enzyme involved in glycolysis pathway. Phosphorylates glucose to produce glucose-6-phosphate.
Pygl	2.29	0.025	Up-regulated	Enzyme involved in glycogen metabolism. Catalyzes the cleavage of alpha-1,4-glucosidic bonds of glycogen to release glucose-1-phosphate.
Ppp2r5e	2.02	0.0071	Up-regulated	Enzyme involved in the negative control of cell growth and division.
G6pc	-5.4	7.00E-07	Down-regulated	Key enzyme involved in glucose hemostasis (gluconeogenesis and glycogenolysis) .Catalyzes the hydrolysis of D-glucose 6-phosphate to D-glucose and orthophosphate.
Got1	-4.29	0.0002	Down-regulated	Involved in amino acid metabolism tricarboxylic acid cycles. Converts aspartate into oxaloacetate.
Gys2	-2.07	0.0084	Down-regulated	Key enzyme in glycogenesis. Catalyzes the reaction of UDP-glucose and (1,4- α -D-glucosyl) _n to produce UDP and (1,4- α -D-glucosyl) _{n+1} .

*Outcomes generated from www.genecards.org or www.uniprot.org.

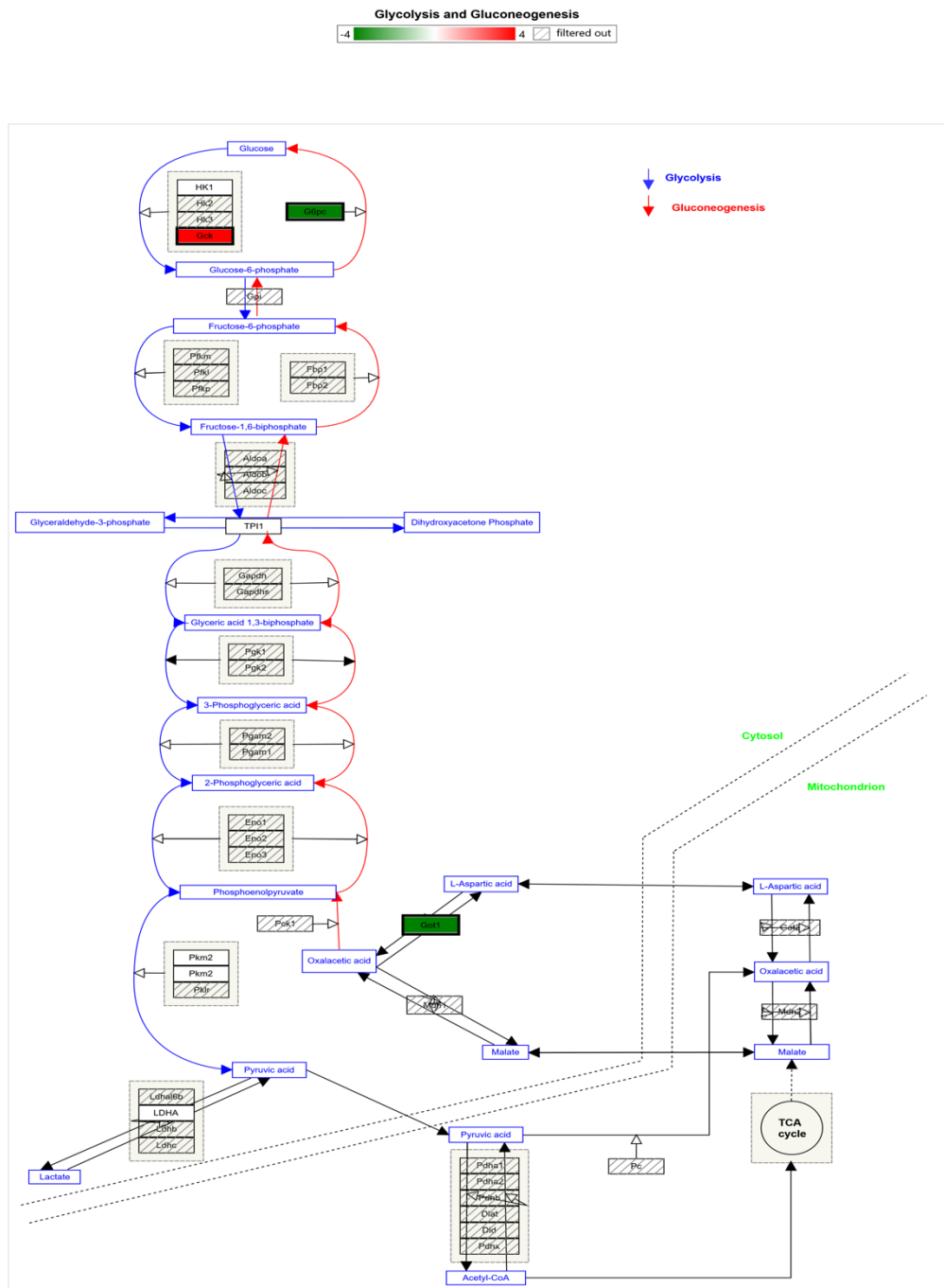


Figure 43: Effect of CAF on the expression of glycolysis and gluconeogenesis pathways.

The results represent a significant increase in Gck to stimulate glycolysis and significant decrease in G6pc to suppress gluconeogenesis. Red color represents the upregulated genes, and the green color represent the down-regulated genes. Pathway analysis performed using TAC 4.0 software.

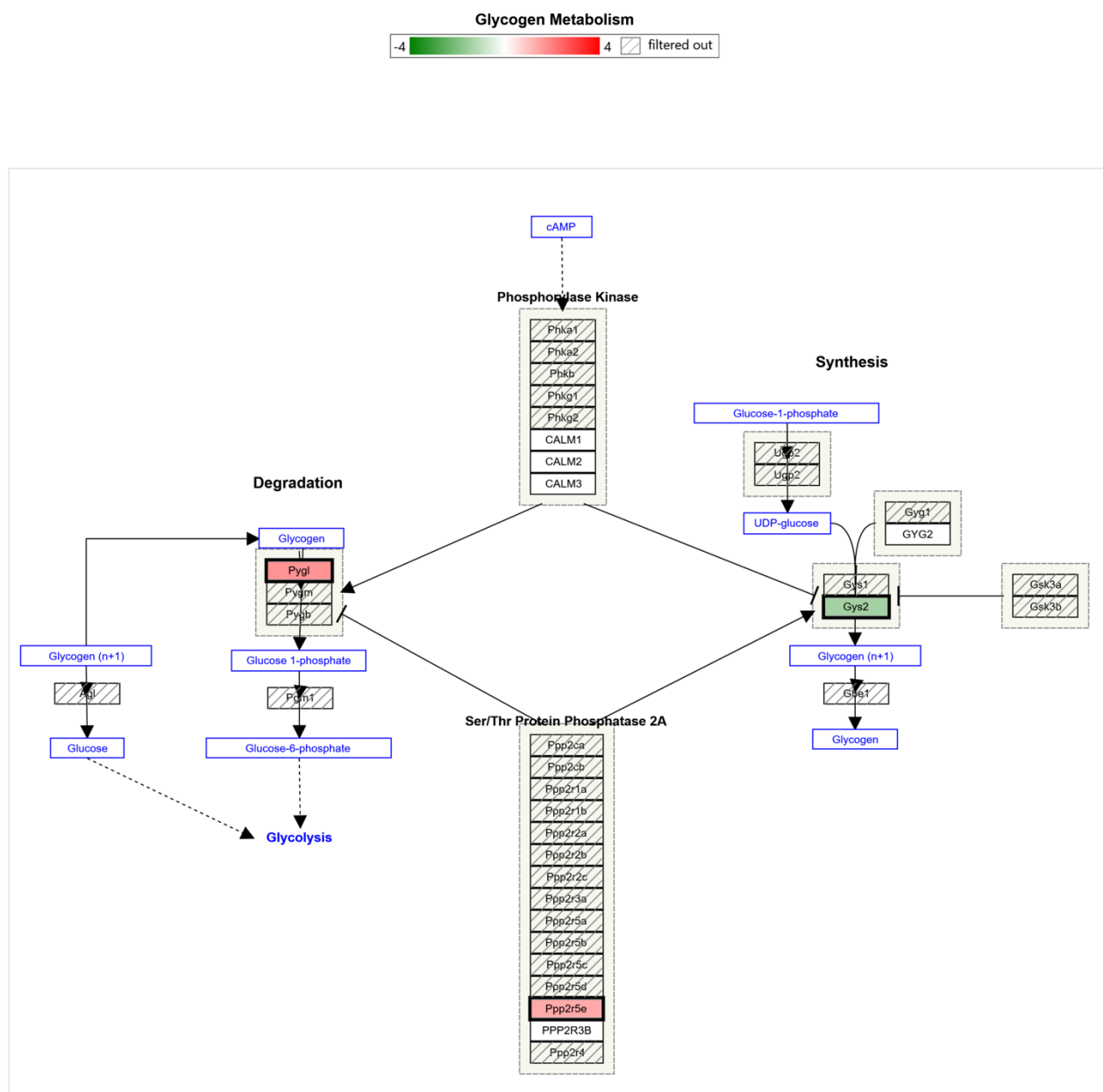


Figure 44: Effect of CAF on the expression of glycogen metabolism pathway.

The chart represents the differential expression of genes that suppress the glycogen degradation (Pygl, Ppp2r5e and Gys2). Red color represents the upregulated genes, and the green color represent the down-regulated genes. Pathway analysis performed using TAC 4.0 software.

5.2.1.1 Effect of CAF on inflammation, oxidative stress and cellular processes pathways

Expression of Hepatic genes related to inflammation and oxidative stress response were decreased in response to CAF feeding. In addition, genes involved in cellular proliferation and differentiation pathways also showed a decrease in their expression in response to CAF feeding (Table 25) (Figures 44 and 45).

Table 25: List of differentially expressed genes related to inflammation, oxidative stress response and cellular processes pathways in CAF vs NC.

Gene symbol	Fold change	FDR P-value	Regulation	Outcomes*
inhba	3.61	5.64E-09	Up-regulated	Member of TGF- β superfamily. Regulates divers functions including insulin secretion.
Gstk1	-3.43	0.0009	Down-regulated	Enzyme belongs to glutathione transferase superfamily, involved in cellular detoxification. Catalyzes the transfer of the thiol of GSH to electrophilic substrates.
Junb	-14.85	5.15E-08	Down-regulated	Transcription factor involved in regulating gene activity. Positive regulator of transcription by RNA polymerase II.
Fos	-3.87	0.025	Down-regulated	Transcription factor involved in cell proliferation, differentiation and transformation.
Hmox1	-4.26	0.0002	Down-regulated	Enzyme involved in heme catabolism. Cleaves heme to form biliverdin.
Trib3	-6.88	0.0048	Down-regulated	Negative regulator of NF-kappaB.
Fmo5	-35.93	1.57E-11	Down-regulated	NADPH-dependent flavoenzymes. Involved in cholesterol biosynthesis and glucose hemostasis.
Mapkapk2	-2.22	0.008	Down-regulated	Kinase enzyme, Involved in many cellular process such as cell proliferation, stress and inflammatory responses. Phosphorylates mitogen-activated protein kinase (MAPK).
Egr1	-6.28	5.93E-06	Down-regulated	Transcription factor regulates cell proliferation, survival and death.
Socs3	-2.71	0.0025	Down-regulated	Belongs to SOCS family protein, negative regulator of cytokines signal through the JAK/STAT pathway.

*Outcomes generated from www.genecards.org or www.uniprot.org.

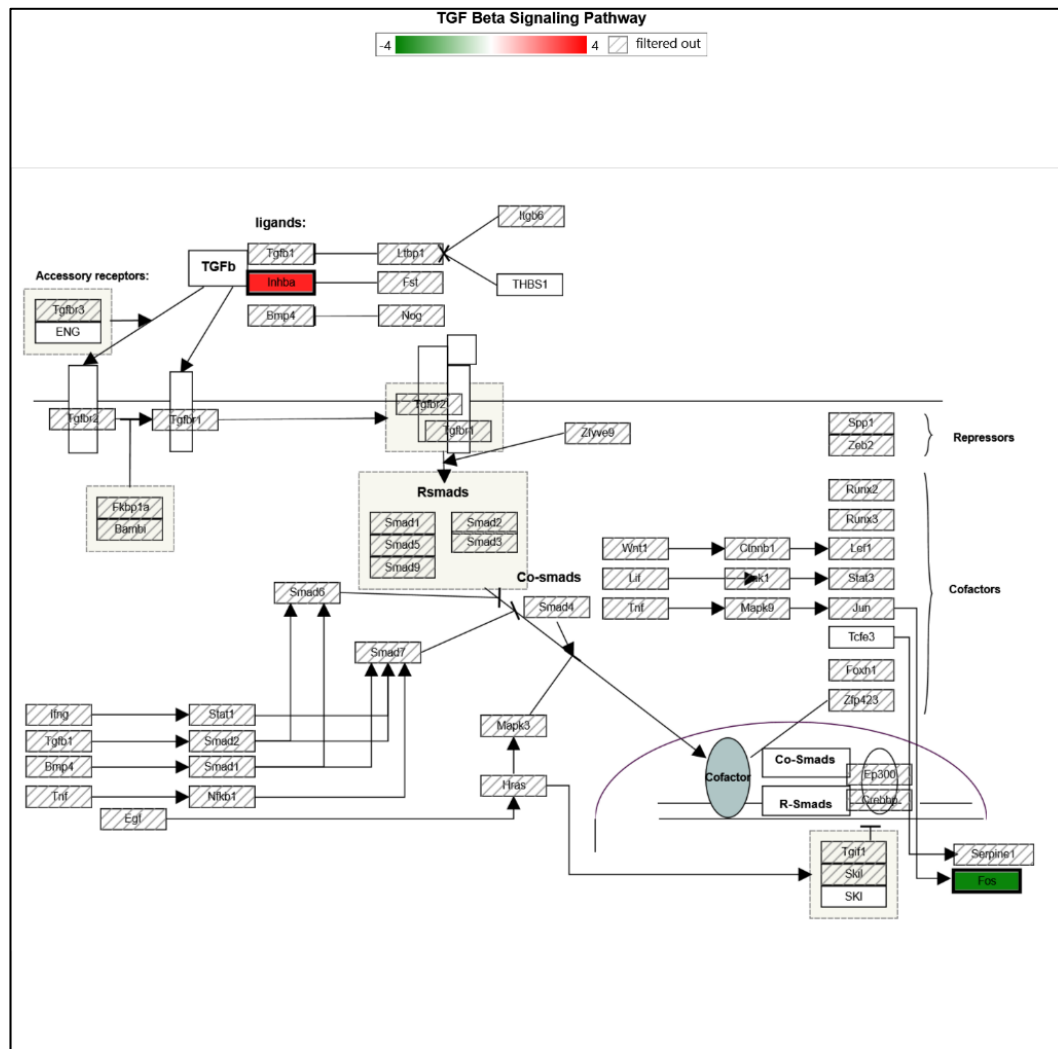


Figure 45: Effect of CAF on the expression of TGF Beta signaling pathway.

The data showed upregulation of *Inhba* and down regulation of *Fos*. Red color represents the upregulated genes, and the green color represent the down-regulated genes. Pathway analysis performed using TAC 4.0 software.

5.3 Gene expression analysis: Microarray analysis in REV livers

To identify the differential expression associated with CAF withdrawal in REV group, microarray analysis of REV livers revealed a total of 414 genes (1.79%) out of 23188 studied were differentially expressed (corrected P-value, FDR P-value <0.05). 334 genes (80.68%) were upregulated, and 80 genes (19.32%) were downregulated (Figure 46).

The hierarchal clustering showed a clear alteration in the expression of genes related to lipid, glucose and tissue repair mechanisms (Figure 47). All NC-REV samples were clustered in 1 branch, and all REV samples were clustered in another branch. In each group the tree represent the relationship among samples and the branch length reflect the degree of similarity between samples based on their gene expression profile (Appendix 2).

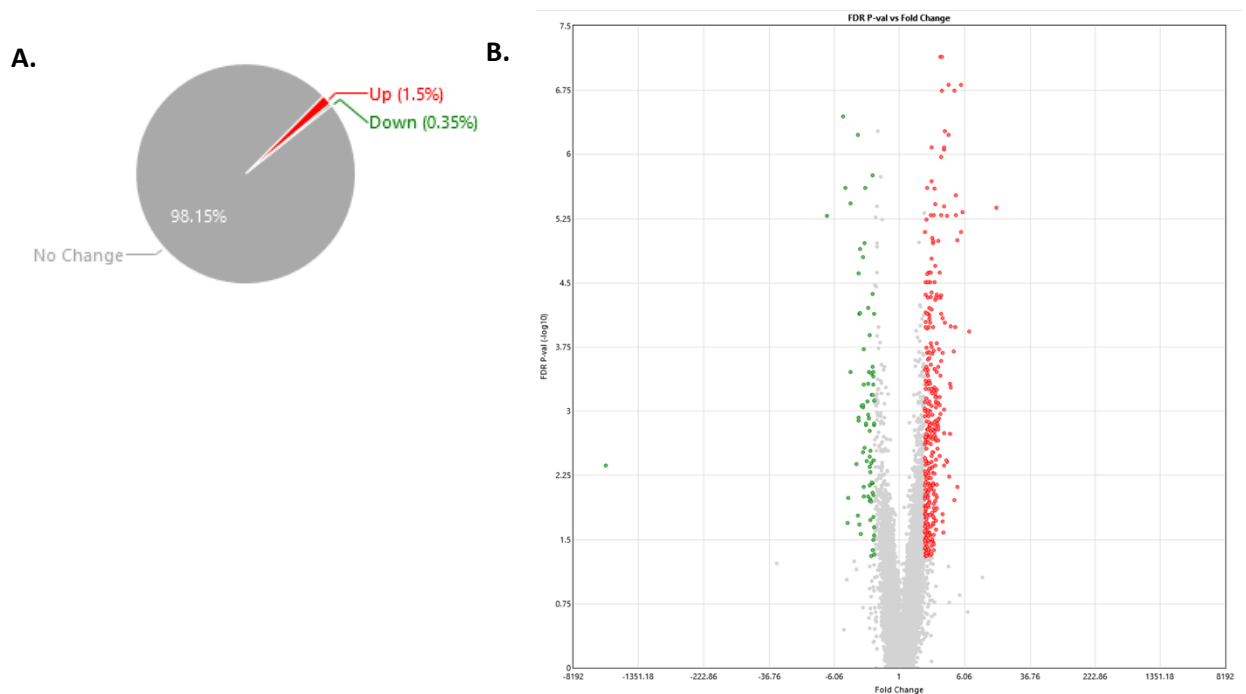


Figure 47: Differentially Expressed genes between REV and NC-REV Livers (FDR P-value < 0.05; RMA).

(A) Pie chart representing the percentages of differentially expressed genes. (B) Volcano plot of gene expression fold change vs. FDR P-Value. Red color indicates the 334 up-regulated genes, green color indicates the 80 down-regulated genes. Gray indicates genes that were not different.

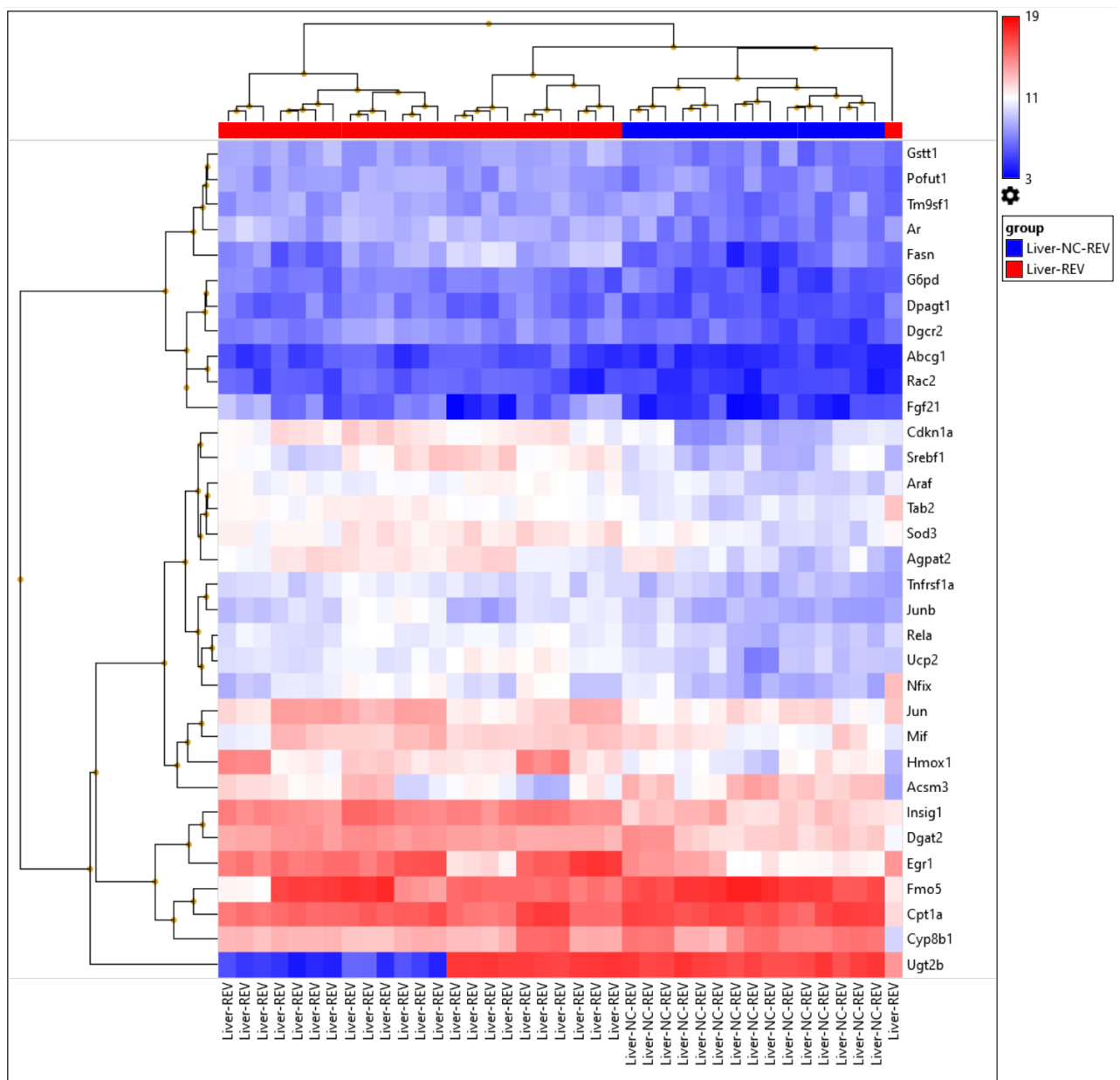


Figure 48: Hierarchical clustering analysis of differentially expressed genes in liver of REV vs NC-REV.

The columns represent different samples, and the rows represent measurements from different genes. Right portion represent NC-REV group, and left portion represent REV group. Samples from both groups (15 NC-REV and 24 REV) with expression values for 33 genes were subjected to hierarchical clustering. Blue color denotes the high expression in REV compared to NC-REV, Red color denotes low expression in REV compared to NC-REV.

5.3.1 Pathway Analysis

5.3.1.1 Effect of REV on Glycolysis, Gluconeogenesis, and glycogen metabolism pathways

Pathway analysis revealed an upregulation in pyruvate kinase isoenzyme R/L (Pklr) that catalyze phosphoenolpyruvate into pyruvic acid (rate limiting step in glycolysis) (Figure 48). Glycogen metabolism pathway showed an increase in the expression of phosphorylase kinase (Phkg2) (Table 26) (Figure 49).

Table 26: List of differentially expressed genes related to glycolysis, gluconeogenesis and glycogen metabolism pathways in REV vs NC-REV.

Gene symbol	Fold change	FDR- P value	Regulation	Outcomes*
Pklr	2.45	0.032	Up-regulated	Enzyme involved in glycolysis/gluconeogenesis pathway. Catalyzes the production of pyruvate and ATP from phosphoenolpyruvate.
Phkg2	2.28	0.026	Up-regulated	Enzyme involved in glycolysis/gluconeogenesis. Mediates glycogen breakdown.

*Outcomes generated from www.genecards.org or www.uniprot.org.

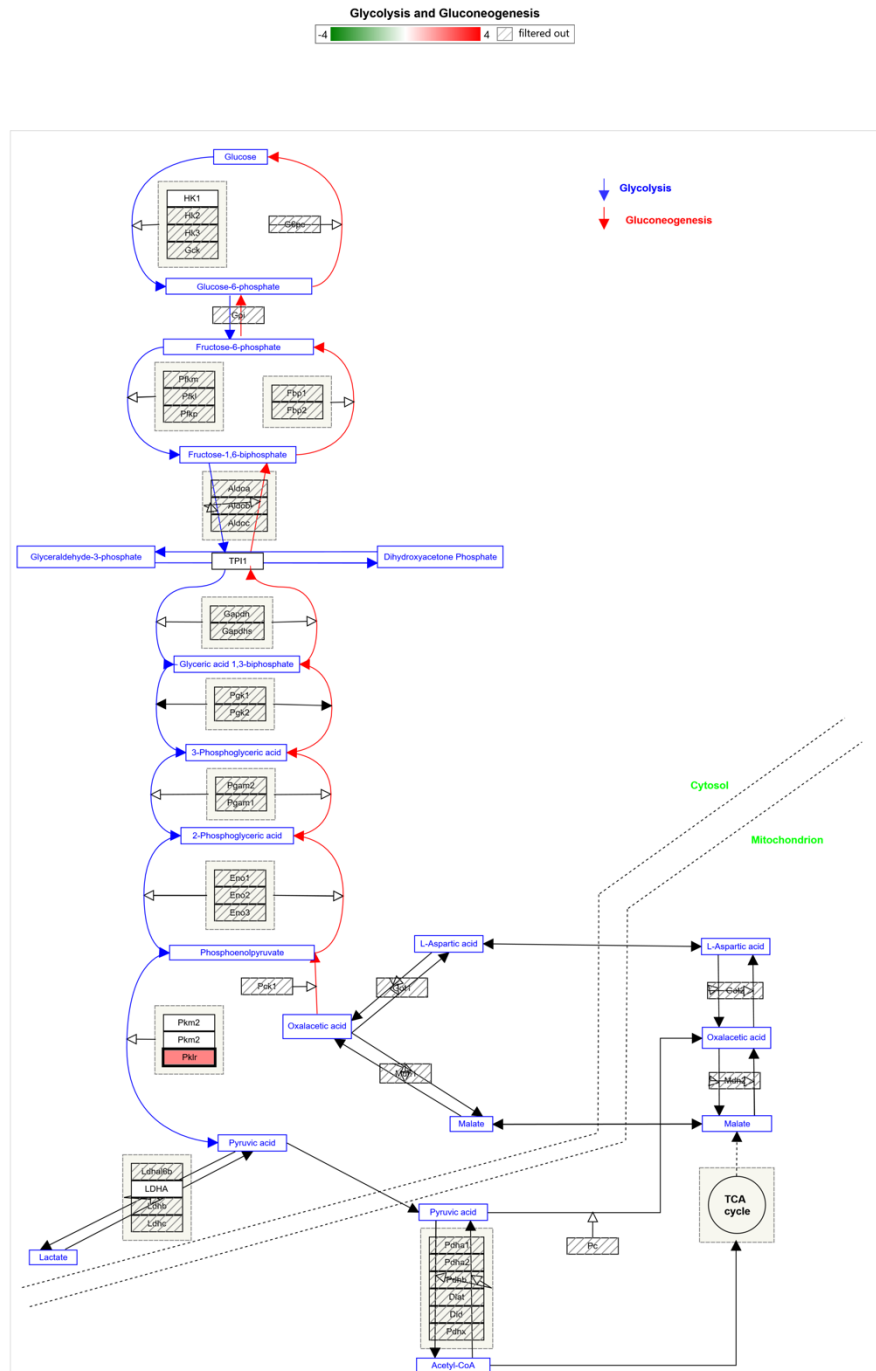


Figure 49: Effect of REV on the expression of glycolysis and gluconeogenesis pathways.

The results represent a significant increase in Pklr. Red color represents the upregulated genes, and the green color represent the down-regulated genes. Pathway analysis performed using TAC 4.0 software.

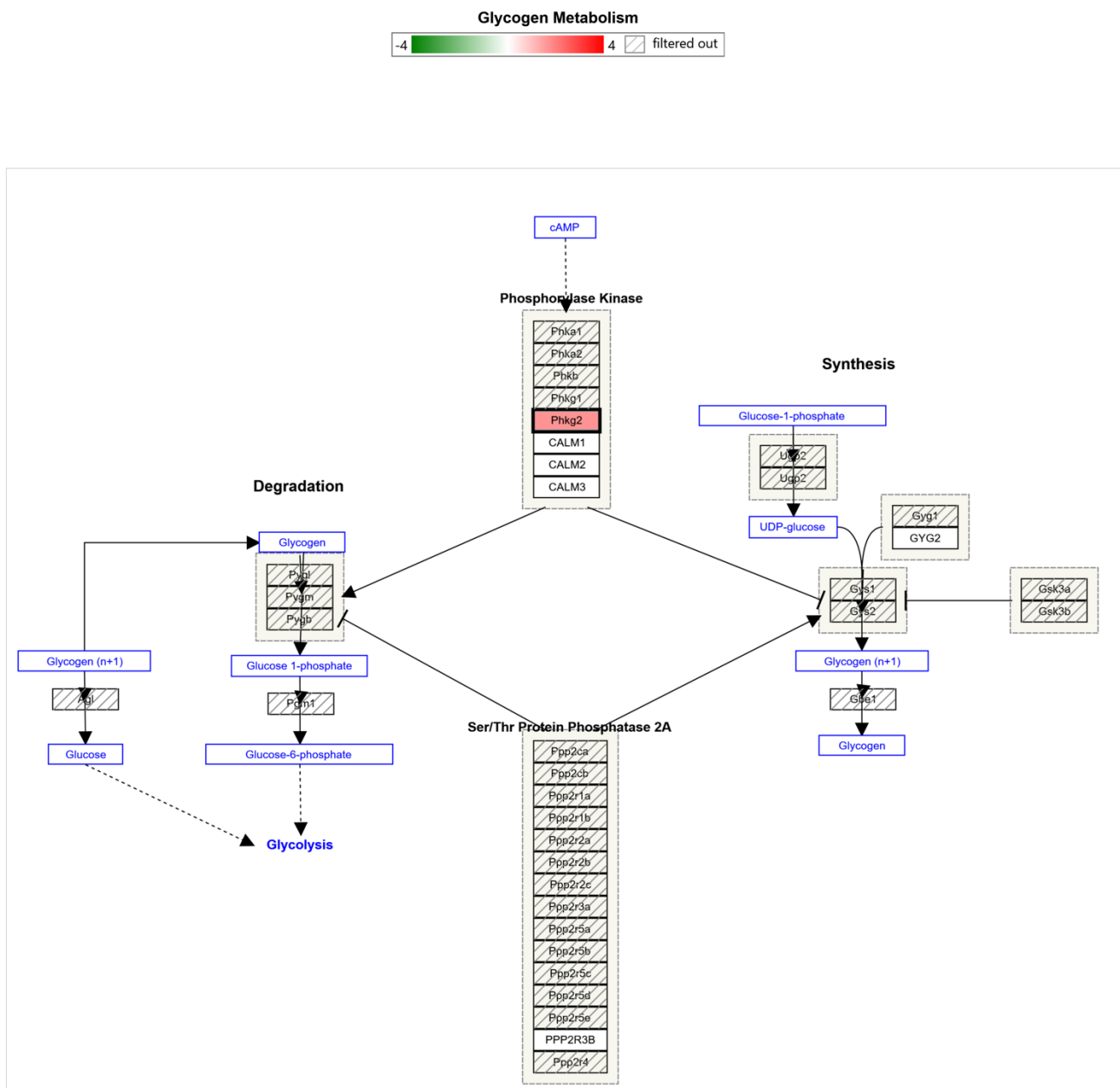


Figure 50: Effect of REV on the expression of glycogen metabolism pathway.

The chart represents the high expression of Phkg2. Red color represents the upregulated genes, and the green color represent the down-regulated genes. Pathway analysis performed using TAC 4.0 software.

5.3.1.2 Effect of REV on adipogenesis and lipid droplet metabolism pathways

Pathway analysis showed different genes over-expressed in adipogenesis pathway including: Srebf1, Nuclear Receptor Subfamily 1 Group H Member 3 (Nr1H3), macrophage migration inhibitory factor (Mif), Cyclin Dependent Kinase Inhibitor 1A (Cdkn1a), Endothelial PAS Domain Protein 1 (Epas), 1-Acylglycerol-3-Phosphate O-Acyltransferase 2 (Apgat2) and Diacylglycerol O-acyltransferase 2 (DGAT2) (Table 27) (Figures 50 & 51).

Table 27: List of differentially expressed genes related to adipogenesis and lipid droplet metabolism pathways in REV vs NC-REV.

Gene symbol	Fold change		Regulation	Outcomes*
SREBF1	3.42	0.001	Up-regulated	Transcription factor involved in lipogenesis. Facilitates FFA accumulation and TG formation.
Nr1H3	2.01	0.0263	Up-regulated	Nuclear receptor involved in cholesterol homeostasis and inflammation. Regulates cholesterol uptake through MYLIP-dependent ubiquitination of LDLR, VLDLR and LRP8.
Mif	2.13	0.081	Up-regulated	Inflammatory cytokine, involved in innate immunity regulation. Regulates macrophages function in host defense, interacts with Cd74 to activates pro-survival and proliferative pathways to protect during injury.
Cdkn1a	5.7	4.79E-06	Up-regulated	Regulator of cell cycle progression at G1. Inhibits cyclin-dependent kinase activity, preventing phosphorylation of critical cyclin-dependent kinase substrates and blocking cell cycle progression.
Epas	2.09	0.0005	Up-regulated	Transcriptional factor involved in the physiological response to oxygen concentration. Induces genes regulated by oxygen under hypoxia condition.
Apgat2	2.6	0.0176	Up-regulated	Enzyme involved in de novo phospholipid biosynthesis. Converts lysophosphatidic acid to phosphatidic acid.
DGAT2	2.84	0.0014	Up-regulated	Enzyme involved in TG synthesis. Catalyzes the final step of TG formation by covalently binding diacylglycerol to long chain fatty acyl-CoAs.

Ucp2	2.33	3.14E-05	Up-regulated	Mitochondrial uncoupling protein, involved in β -oxidation pathway.
------	------	----------	--------------	---

*Outcomes generated from www.genecards.org or www.uniprot.org.

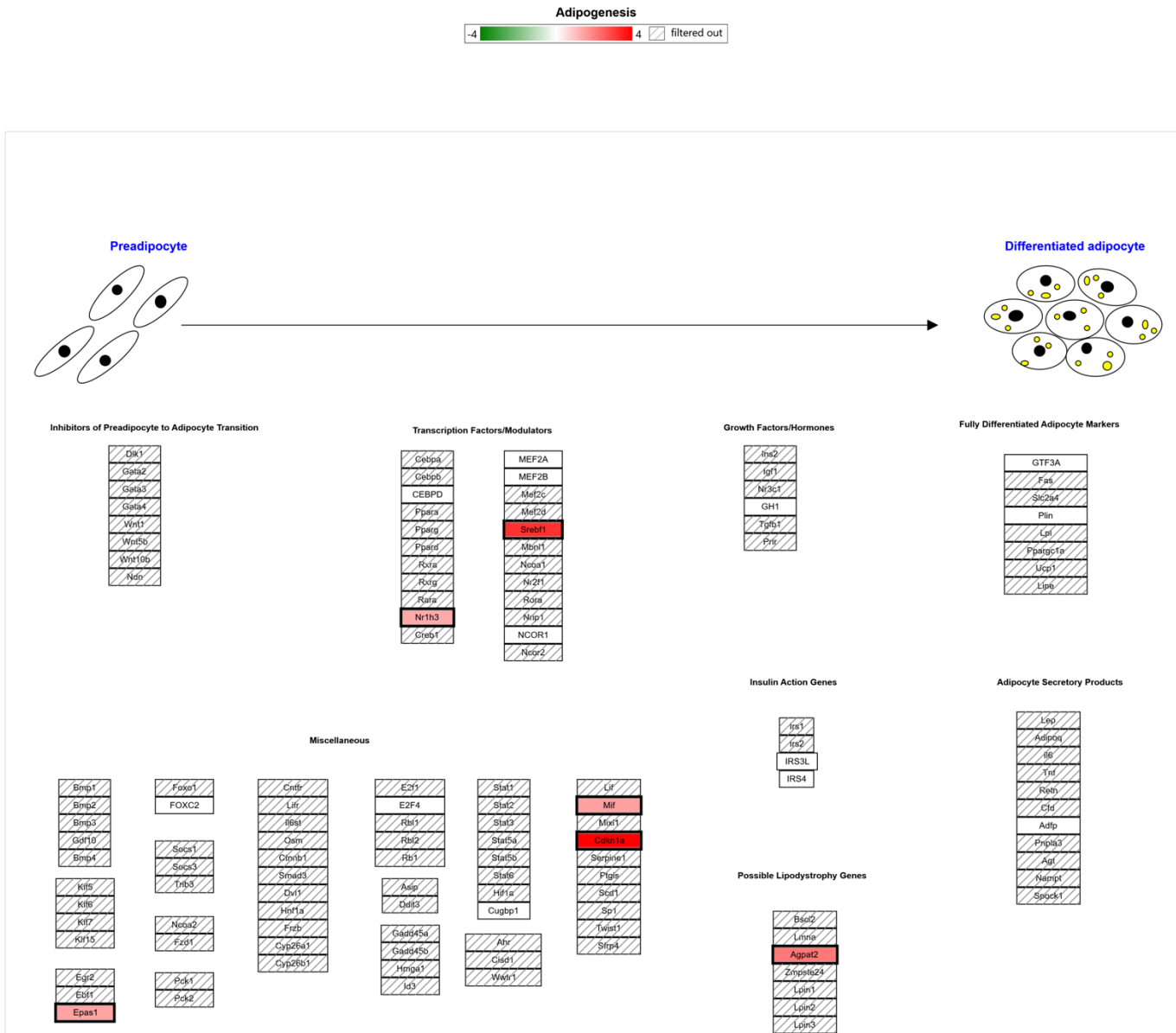


Figure 51: Effect of REV on the expression of Adipogenesis pathway.

The chart represents the significant increase in the expression of gene related to adipogenesis. Red color represents the upregulated genes, and the green color represent the down-regulated genes. Pathway analysis performed using TAC 4.0 software.

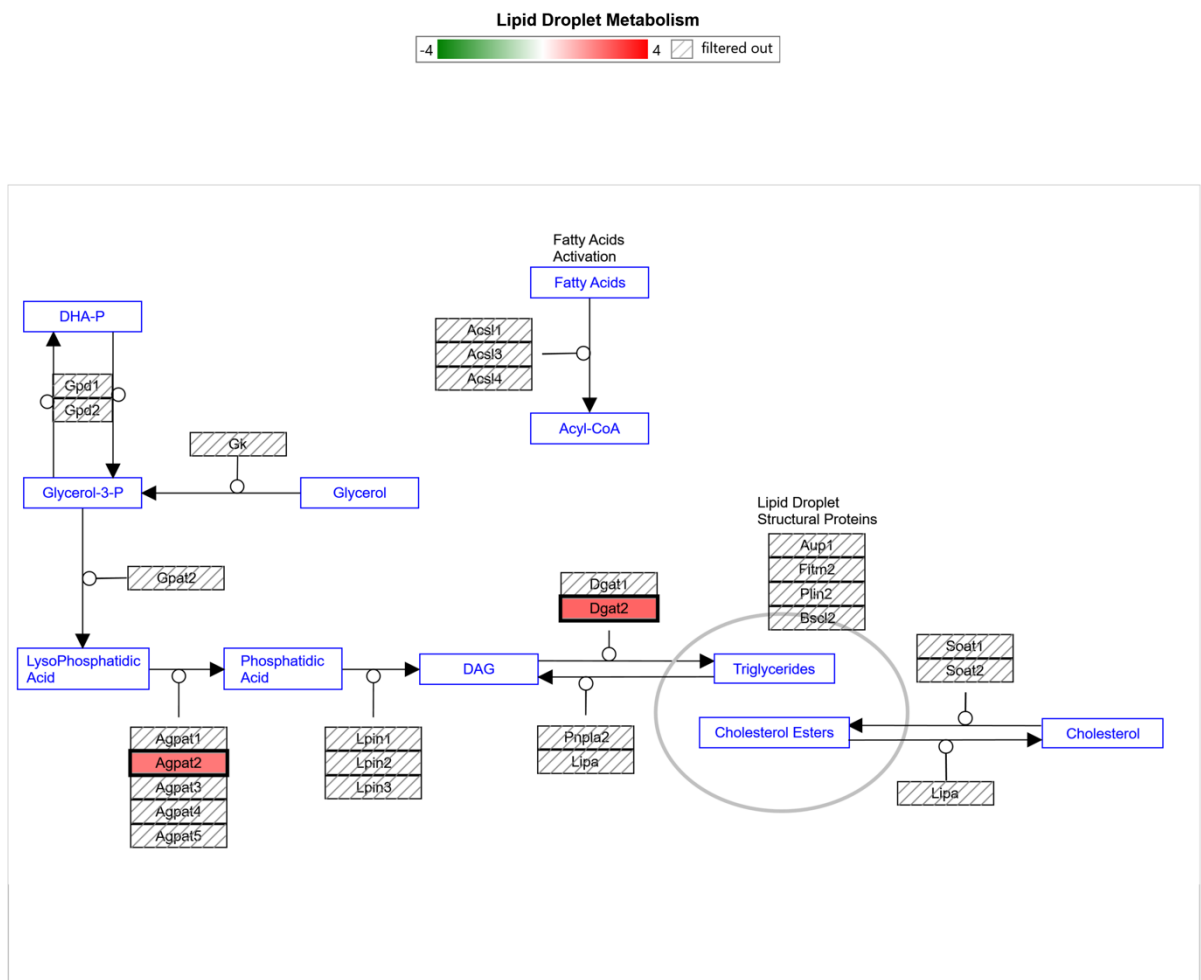


Figure 52: Effect of REV on the expression of lipid metabolism droplet pathway.

The chart represents the significant increase in Dgat2 and Agpat2. Red color represents the upregulated genes, and the green color represent the down-regulated genes. Pathway analysis performed using TAC 4.0 software.

5.3.1.3 Effect of REV on inflammation, oxidative stress and cellular process pathways

In the oxidative stress related pathway, it was found that there is an overexpression of transcriptional factor jun b proto-oncogene (Junb), Heme oxygenase 1 (Hmox1) an essential enzyme in heme catabolism, superoxide dismutase 3 (Sod3) an enzyme that catalyze superoxide radicals into hydrogen peroxide and oxygen and Nuclear factor I X (Nfix) (Figure 52) (Table 28). In addition, MAPK pathway was also showed an upregulation in a couple of genes as shown in table 28 and figure 53.

Table 28: List of differentially expressed genes related to oxidative stress pathway in REV vs NC-REV.

Gene symbol	Fold change	FDR P-value	Regulation	Outcomes*
Junb	2.42	0.0464	Up-regulated	Transcription factor involved in regulating gene activity. Positive regulator of transcription by RNA polymerase II.
Hmox1	2.02	0.0011	Up-regulated	Enzyme involved in heme catabolism. Cleaves heme to form biliverdin.
Sod3	2.27	8.46E-05	Up-regulated	Antioxidant enzyme involved in oxidative stress. Catalyzes the conversion of superoxide radicals into hydrogen peroxide and oxygen to protect tissues from oxidative stress.
Nfix	2.9	0.0016	Up-regulated	Transcription factor activates transcription and replication.
Jun	2.89	0.0015	Up-regulated	Transcriptional factor involved in cellular proliferation and apoptosis.
Dusp1	5.51	1.54E-07	Up-regulated	Enzyme involved in different cellular processes. Dephosphorylates MAP kinase MAPK1/ERK2.
Dusp7	4.65	0.0001	Up-regulated	Enzyme involved in different cellular processes. Dephosphorylates MAP kinase MAPK1/ERK2.
Rac2	2.04	0.0134	Up-regulated	Small G protein belongs to Ras superfamily. Regulates different cellular processes.
Tab2	2.07	3.14E-05	Up-regulated	Involved in the activation of JNK and NF-kappa-B signaling pathways
Tnfrsf1a	2.19	0.0016	Up-regulated	Receptor of TNF- α . Activates the transcription factor NF- κ B, and regulates inflammation.

Fgf1	2.61	0.0013	Up-regulated	Growth factor involved in a variety of biological processes such as cell growth and tissue repair.
Fgf21	4.05	0.0018	Up-regulated	Member of the fibroblast growth factor (FGF) family. Regulates glucose hemostasis and insulin sensitivity.

**Outcomes generated from www.genecards.org or www.uniprot.org.*

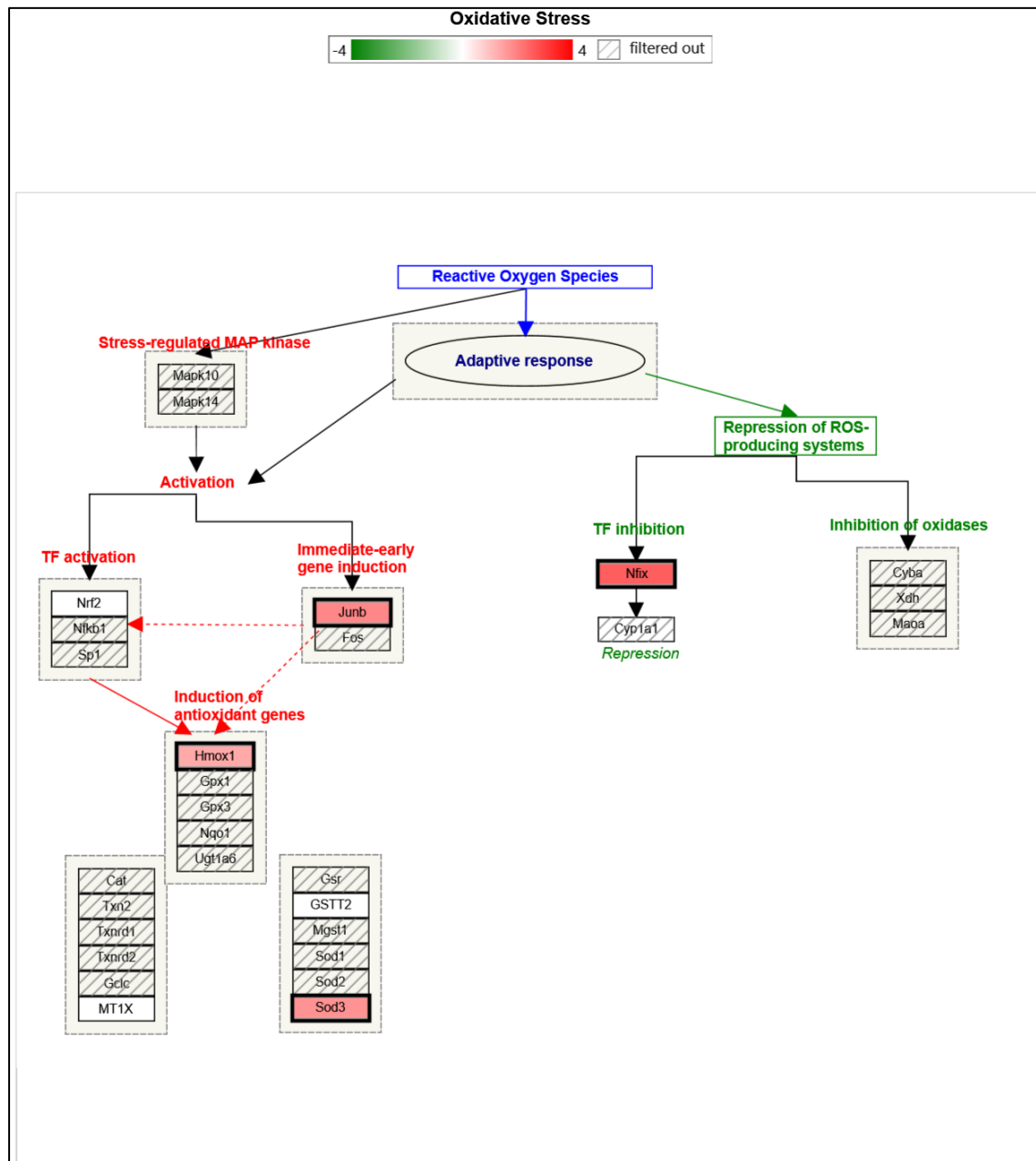


Figure 53: Effect of REV on the expression of oxidative stress pathway.

The chart represents the significant increase in Junb, Nfix, Hmox1 and Sod3. Red color represents the upregulated genes, and the green color represent the down-regulated genes. Pathway analysis performed using TAC 4.0 software.

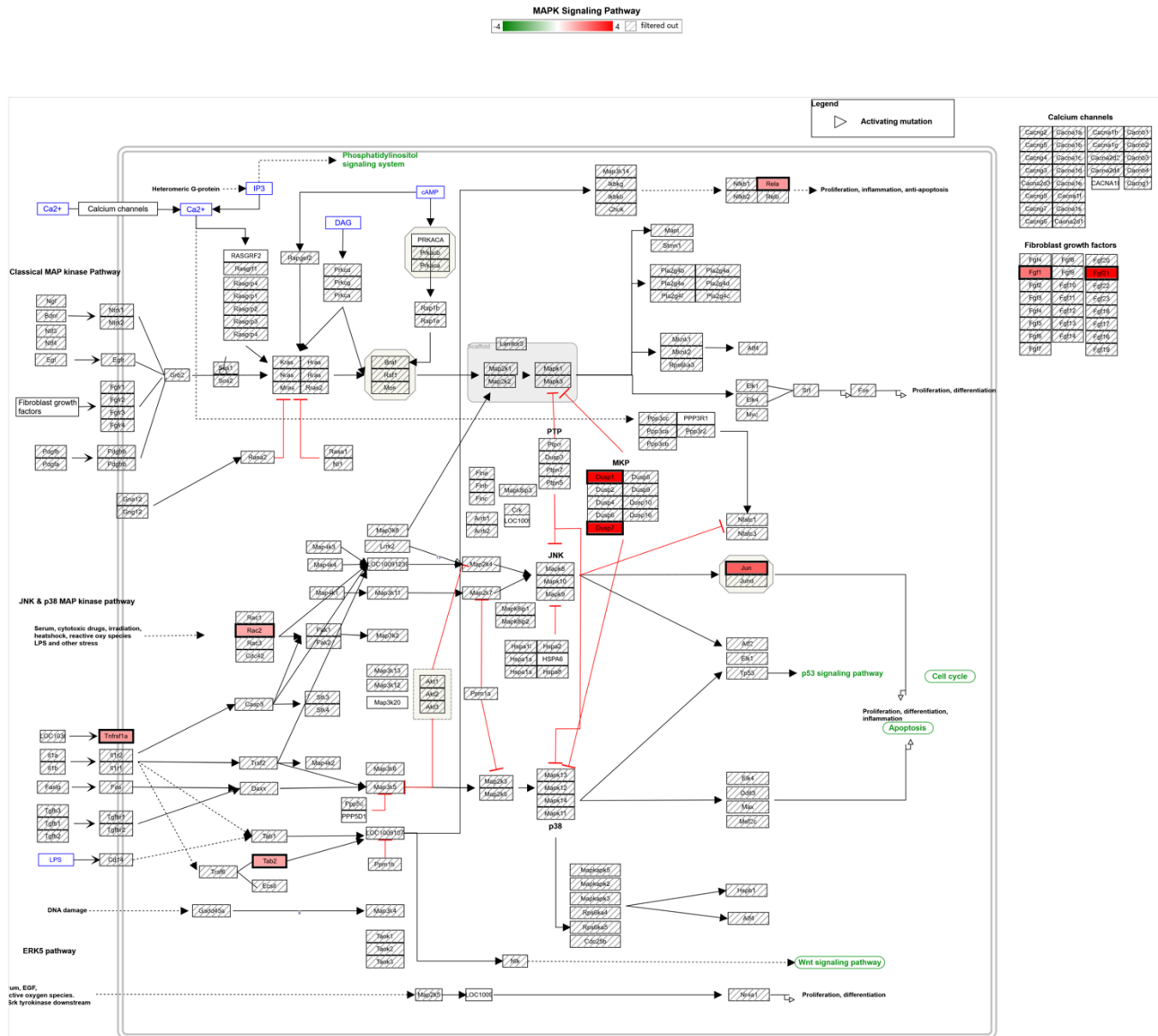


Figure 54: Effect of REV on the expression of MAPK signaling pathway.

The chart represents the induction of MAPK signaling pathway including: Dusp1, Dusp7, Jun, Rac2, Tab2, Tnfrsf1a, fgf1, fgf21. Red color represents the upregulated genes, and the green color represent the down-regulated genes. Pathway analysis performed using TAC 4.0 software

5.4 Discussion

NAFLD is a pathologic condition of hepatic fat accumulation. Increased fat accumulation is attributed to different mechanisms, mostly increased de novo lipogenesis and fatty acid uptake or decreased lipid export through fatty acid oxidation. The results presented here demonstrated that long time feeding with high carbohydrate diet can affect lipid and carbohydrate metabolism leading to fat accumulation. However, the mechanisms that mediate these actions are not fully understood. Recently, microarray data has become an effective tool to investigate the pathogenesis of NAFLD. Whole transcriptome of the liver has been analyzed to investigate the differential expression of genes mediates the development of hepatic steatosis under the condition of CAF feeding and CAF withdrawal.

The current results revealed that CAF diet induced hepatic steatosis has a strong correlation with de novo lipogenesis. CAF feeding resulted in increased expression of number of glucose metabolism genes. Gck, has a central role in hepatic glucose disposal (glycolysis). It was significantly upregulated with 13.5-fold-increase, to facilitate the breakdown of the high load of carbohydrate as a non-lipid source. In agreement with these findings, chronic Gck overexpression was shown to lead to hepatic TG accumulation in transgenic mice (220). These findings may be a good indicator of this being an insulin driven process, because the transcription of Gck is dependent on insulin (221). Therefore, the hyperinsulinemia shown in this study appears to induce the hepatic uptake of glucose. In addition, G6pc is an important enzyme that has a dual effect in gluconeogenesis and glycogenolysis. These results showed that this enzyme was suppressed in response to CAF feeding. These findings suggested that the liver is regulating the hemostasis of glucose by suppressing production of glucose from noncarbohydrate sources (gluconeogenesis) and the breakdown of glycogen to release glucose (glycogenolysis).

The current results also showed a significant up-expression of SREBF1. SREBF1 is the gene that encodes for SREBP1-c. It is one of transcriptional factor that is involved in cholesterol and fatty acid metabolism (222). The induction of de novo lipogenesis has been shown to be regulated by the upregulation of SREBF1. SREBF1 was suggested to be the predominant regulator of DNL (218). The role of SREBP1-c in the pathogenesis of NAFLD is supported by several studies. Enhanced expression of SREBP1-c in a mouse model induced fat accumulation and resulted in mild fatty liver (223). Moreover, studies of diet-induced obesity support this finding in rats fed on high fat diets (224), and high fat\high carbohydrate diets (225). Activation of SREBP-1c lead to the expression of downstream targets such as ACC and FAS, these two targets are upregulated in NAFLD (226). These findings were not confirmed in the current study, which showed no changes in the expression of these genes. This could be related to the type of diet used here. The stimulation of SREBPs expression can be mediated by different nutritional and hormonal stimuli (227). One of these stimuli is insulin, the activation of SREBF1 is enhanced by insulin to activate insulin-responsive genes in the liver (228).

The gene expression profile of CAF group showed low expression in Insig1 gene. Insig1 is highly expressed in hepatocytes and it is widely thought to be involved in intercellular lipid metabolism homeostasis (229). There is an opposite relationship between Insig1 and SREBF1 in inducing hepatic fat deposition. It inhibits the activity of SREBF1 (230), whereas in the NAFLD condition, hepatic Insig1 is significantly decreased (231). This suggest that overexpression of SREBF1 is mediated by suppression of Insig1 and consequently results in hepatic steatosis. The transcriptome analysis of the current study showed an absence of differential expression of FA uptake regulating genes such as (FATP, CD36 and FABP). Collectively, these observations suggest that the leading pathway of hepatic lipid accumulation is de novo lipogenesis, not through FA uptake from the circulation.

PPAR-alpha is another transcriptional factor that is highly associated with lipid metabolism, and regulates the expression of a number of genes that has a critical role in lipid metabolism (232), especially with fatty acid uptake and β -oxidation (233). Fatty acid β -oxidation is the process of breaking down fatty acid to produce energy. It is known that FA β -oxidation is decreased in NAFLD patients (234). Consequently, this led to the activation of downstream genes. This data showed that PPAR-alpha was up-regulated in response to CAF feeding. Although PPAR-alpha has a direct effect on fatty acid β -oxidation, the current data showed genes of FA β -oxidation process such as *Ech1* and *Cpt1a* were down-regulated after CAF feeding.

Cpt1a is a β -oxidation process rate limiting enzyme, that mediate the entrance of long-chain FA into the mitochondria (235). Increase in hepatic de novo lipogenesis overwhelms the capacity of β -oxidation process, leading to fat accumulation and consequently development of NAFLD (236). Perhaps, the suppression of β -oxidation in current model was not regulated by PPAR-alpha. The literature reveals conflicting reports regarding FA β -oxidation in NAFLD and NASH, some reports showed enhanced FA β -oxidation, while others showed that it is unchanged or decreased (237, 238, 239). The over-expression of PPAR-alpha could explain its relation to the hepatic steatosis score because it has been revealed that PPAR-alpha expression is reduced with higher NAFLD score and progression of NAFLD to NASH (240). In addition, these results showed a decrease in *Abcb1a* gene. *Abcb1a* belongs to ABC transporters family that regulates lipid transport in the liver (241).

One of the significant genes that plays a role in intracellular fat accumulation is *Pnpla2*. *Pnpla2* encodes the enzyme triglyceride lipase that catalyze the hydrolysis of triglyceride from lipid droplet to release fatty acids and glycerol (242). The current transcriptomic analysis showed a down-regulation of *Pnpla2* which supports its involvement in the mechanism for fat accumulation in the liver.

Taken together, the decrease in FA β -oxidation and lipid transport appear to mediate the increase in hepatic fat accumulation.

Liver is the major site of detoxification and drug metabolism, Cytochrome P450 enzymes are highly involved in this process and regulate the metabolism of endogenous substrate such as FA, vitamins and steroids (243). The current data showed a significant decrease in the activity of Cyp51, Cyp8b1, Cyp1a2, Cyp2b2 and Cyp3a9. The Cyp51 and Cyp8b1 are contributor enzymes in the cholesterol hemostasis. Cyp51 is a responsive gene and critical enzyme involved in de novo synthesis of cholesterol. It has been observed that Cyp51 is correlated with the circulating VLDL, HDL and LDL levels (244). High levels of cholesterol suppress the expression of Cyp51 in hamster fed with HF diet (244), as well as rat model fed with high cholesterol diet (245). Similar findings have been reported for Cyp8b1 in rat fed with western-diet (125). In addition, these data showed a downregulation in Hmgcr and Fdps genes, which are also involved in cholesterol de novo lipogenesis. These findings are in line with the another study using diet-induced obese mice (246). The current data is consistent with previous findings and suggest the dysregulation of cholesterol metabolism.

Inflammation is a hallmark of hepatic steatosis progression from NAFLD to NASH. Although liver enzyme levels were significantly increased, markers of inflammation were not induced in response to CAF diet. In this study the observation showed that most of the genes related to inflammation were in fact downregulated. In addition to the role of PPAR-alpha in lipid metabolism, it has an anti-inflammatory effect by the regulation of NF-kB expression (247). These findings suggest that PPAR-alpha may protect the liver from inflammation. These findings are consistent with a previous report which showed the protective effect of PPAR-alpha against diet-induced liver inflammation in mice model (248).

Tm7sf2 was the most downregulated gene. It has been shown that Tm7sf2 is linked with NF- κ B, mice lacking Tm7sf2 revealed increase in NF- κ B, which initiate inflammation signaling (249). Moreover, Trib3 which is considered as a negative regulator of NF- κ B was also suppressed. These findings suggest the activation of NF- κ B. However, these findings also showed a significant decrease in the expression of Junb, a significant transcriptional regulator of the NAFLD progression to NASH (250). Egr1 is another transcriptional factor that has a significant role in developing fatty liver (251). It has been suggested that Egr1 participate in the transcription regulation of Socs3 and Fos (251).

Taken together, the expression profile of the inflammatory markers showed a protective effect against the progression of fatty liver from score 3 (as showed in histological assessment) to NASH.

Dietary intervention implicated in the withdrawal of CAF diet for three weeks (REV) were associated with different gene expression compared to its control NC-REV. The literature showed that hepatic steatosis improvement is regulated by decrease FA uptake and de novo lipogenesis, increase FA oxidation and lipid export. It was interesting that CAF withdrawal caused variations in the gene expression that were relatively different from those expressed with CAF diet.

When diet was changed from CAF to NC, REV group showed a decrease in Gck expression, which might be due to low carbohydrate load. The expression of Phkg2 was increased with dietary intervention. Phkg2 is a key enzyme that regulates glycogen breakdown and metabolism. It catalyzes the cleavage of glucosyl unit from glycogen and release of glucose 1-phosphate. This finding could explain that the Phkg2 overexpression which may be due to low load of carbohydrate, with glycogen breaking down to compensate and maintain glucose homeostasis. Patients who exhibited Phkg2 deficiency required glucose dietary intervention to maintain glucose

homeostasis (252). Phkg2 deficiency also is a risk factor for increasing serum transaminases and circulating TG (252). In addition, it causes abnormal liver histology that may progress into cirrhosis (253). Thus, this data suggested that the overexpression of Phkg2 with dietary intervention might be a protective mechanism against hypoglycemia and hepatic steatosis progression.

The level of SREBF1 activity and its targeted genes responsible for de novo lipogenesis remained upregulated when diet was shifted from CAF to REV. The activation of hepatic de novo lipogenesis through SREBF1 required the presence of glucose (254), the data presented here indicates that de novo lipogenesis in REV group was not activated due to low carbohydrate. Downstream targets of SREBF1 such as FASN showed to be up regulated, suggesting that FA synthesis induced through SREBF1. These findings conflict with what has been reported in the literature. Studies showed that herbal and traditional intervention inhibited the activity of SREBF1, FAS and consequently decrease fat accumulation (255, 256). This observation suggests that activation of FASN could impact glucose and lipid metabolism, which was impaired during CAF feeding. Beside the function of FAS in FA production via de novo lipogenesis and FA synthesis for energy storage, it also has critical role in membrane assembly and repair (236). Perhaps, increased expression of FASN could be involved in FA production, to be utilized for tissue repair. This is evident by the improvement of lipid profile, as indicated by normal systemic TG. Interestingly, REV modulates the expression of Insig1 that is involved in cholesterol biosynthesis. This is consistent with previous findings in dietary treatment of hepatic steatosis (257). Surprisingly, genes related to TG biosynthesis were up regulated, such as Dgat2. Dgat2 is a fundamental enzyme that plays role in TG synthesis and crucial for survival (258). Thus, the upregulation of Dgat2 may be due to low dietary glucose that induce hepatocytes to switch on the TG synthesis as a backup source of energy.

FA oxidation is the most significant lipid clearance mechanism that reduces hepatic lipid accumulation. The transcriptome profile showed an increase in the expression of Ucp2. Ucp2 has a role in lipid and glucose metabolism and mediating energy expenditure (259). This finding indicates the involvement of this gene in mediating the FA oxidation, perhaps mediating the β -oxidation catabolism of the FA stored in lipid droplets and TGs. Similar observations were reported with drug intervention in Wistar rat that received 1-triple TTA (260), and in mice fed with very low carbohydrate diet (261), indicating the effect of drug and lifestyle intervention in inducing FA oxidation. Increased FA oxidation is considered as one of the significant pathways to improve lipid metabolism in NAFLD with carbohydrate restriction (262).

The other mechanism that attenuates the lipid accumulation is the lipid export and excretion. Lipid transporter ABCs significantly modulate lipid metabolism and excretion route. Abcg1 is an ABCs transporter that was overexpressed in REV group. It is recognized by its role in controlling tissue lipids and transferring cholesterol to HDL to prevent lipid accumulation (263). The anti-oxidative enzyme Sod3 was also upregulated, which enhance the expression of genes related to energy expenditure such as Ucp2 (264). Taken together, these findings suggest that the clearance of accumulated lipids in hepatocytes was facilitated by FA oxidation and lipid excretion.

Interestingly, Gstm1 was up regulated with dietary intervention. This gene belongs to Glutathion-S-transferase and has an important role in suppressing oxidative stress (265), and detoxification of xenobiotics (266). In DIO model, Gstm1 expression was reduced (266), indicating the effect of REV diet in improving hepatic steatosis through the activity of drug metabolizing enzymes. On the other hand, Ugt2b which exhibited the same role of detoxification was significantly downregulated in the

current study. However, a decrease in the expression of this enzyme was seen another DIO model as well (266).

Liver is a highly sensitive organ that responds immediately to regeneration and recovery after injury. The present results showed that the majority of overexpressed genes due to dietary intervention were related to inflammation and tissue repair. The upregulation of these genes indicates the activation of reparative mechanism of the damage caused by CAF diet. Among these genes, Egr1 showed to have the highest expression in REV group, with 14.5-fold increase compared to the REV-NC. Egr1 is a transcriptional factor that regulates the hepatocellular mitotic progression (267). It is part of a list of genes that are induced in the early phase of liver regeneration. Egr1 deficient mice showed an impairment in liver regeneration (267). Jun is another significant gene involved in the proliferative response, but to a lesser extent compared to Egr1 (268). It is also a transcriptional factor that has a critical role in early response to hepatic regeneration after injury (269). Jun activation is involved in multiple pathways related to liver physiology and pathophysiology (270). One of the common pathways that regulate the expression of Jun is TNF-alpha, by triggering its receptor Tnfr1, which is associated with cell survival and proliferation (270). While sustained activation of Jun induced ROS accumulation and consequently lead to apoptosis and cell death (271). This dual effect of Jun expression could explain the involvement of Jun in the NAFLD progression to NASH (272). Tnfrsf1a was seen to be upregulated in the current study.

Surprisingly, Mif expression was increased in the current data. Although Mif has been identified as a pro-inflammatory cytokine that has a pathogenic role (273), however a recent study showed that it has a protective function against lipid accumulation, with exercise intervention (274). It has been shown that Mif has a dual function to ameliorate hepatic lipid accumulation. This may be either by suppressing lipogenesis through decreasing SREBP1-c expression, or by activating lipid

oxidation (274). Comparing these findings with the current study, it appears that Mif may participate in improving hepatic steatosis through lipid oxidation, not SREBF1. In addition, Fgf21 expression was increased, another factor that could protect the liver from inflammation (275). Thus, Fgf21 has a potential therapeutic effect due to its multiple action in treating obesity and fatty liver (276). In addition, to regulating the role of Sod3 role in FA oxidation and thereby increasing energy expenditure, it may also regulate the recovery of tissue injury (277). Taken together, the transcription profile for the REV group showed a clear alteration in the inflammation and tissue repair genes, indicating that the mechanisms by which CAF withdrawal may be reversing the hepatic damage caused by CAF feeding.

It is interesting to note that despite the massive abdominal obesity and the development of hepatic steatosis in the current model, no alteration was observed in inflammatory response at different levels: serum level, histological examination, and gene expression. This revealed that the current stage of hepatic steatosis did not convert to the severe stage, with the involvement of the inflammatory reaction. Interestingly, this level of hepatic steatosis appears to be reversible with modest lifestyle modification. These observations were reflected in the REV group. Thus, dietary intervention might be considered as an effective treatment at a certain level of obesity that can be recommended clinically.

In summary, CAF feeding for 16-weeks was sufficient to significantly alter the gene expression profile of lipid metabolism. This alteration was enriched in DNL gene expression, especially SREBF1 which was the most sensitive gene in the current model. These changes indicate the extent to which carbohydrate, the main component of the CAF diet used in this study, in attenuating hepatic lipogenesis. Interestingly, even modest dietary intervention, for a short period with only a small weight loss (6%), was effective in improving the lipogenic pathway by increasing FA

oxidation and tissue repair. These results suggest that liver is very sensitive to dietary modulation, which might be useful in reducing the pathogenesis and prevalence of NAFLD. This is the first study to investigate the full transcriptomic profile of liver steatosis induced by high carbohydrate diet, and the differential expression of liver recovery with dietary interventions in rats (Figure 54).

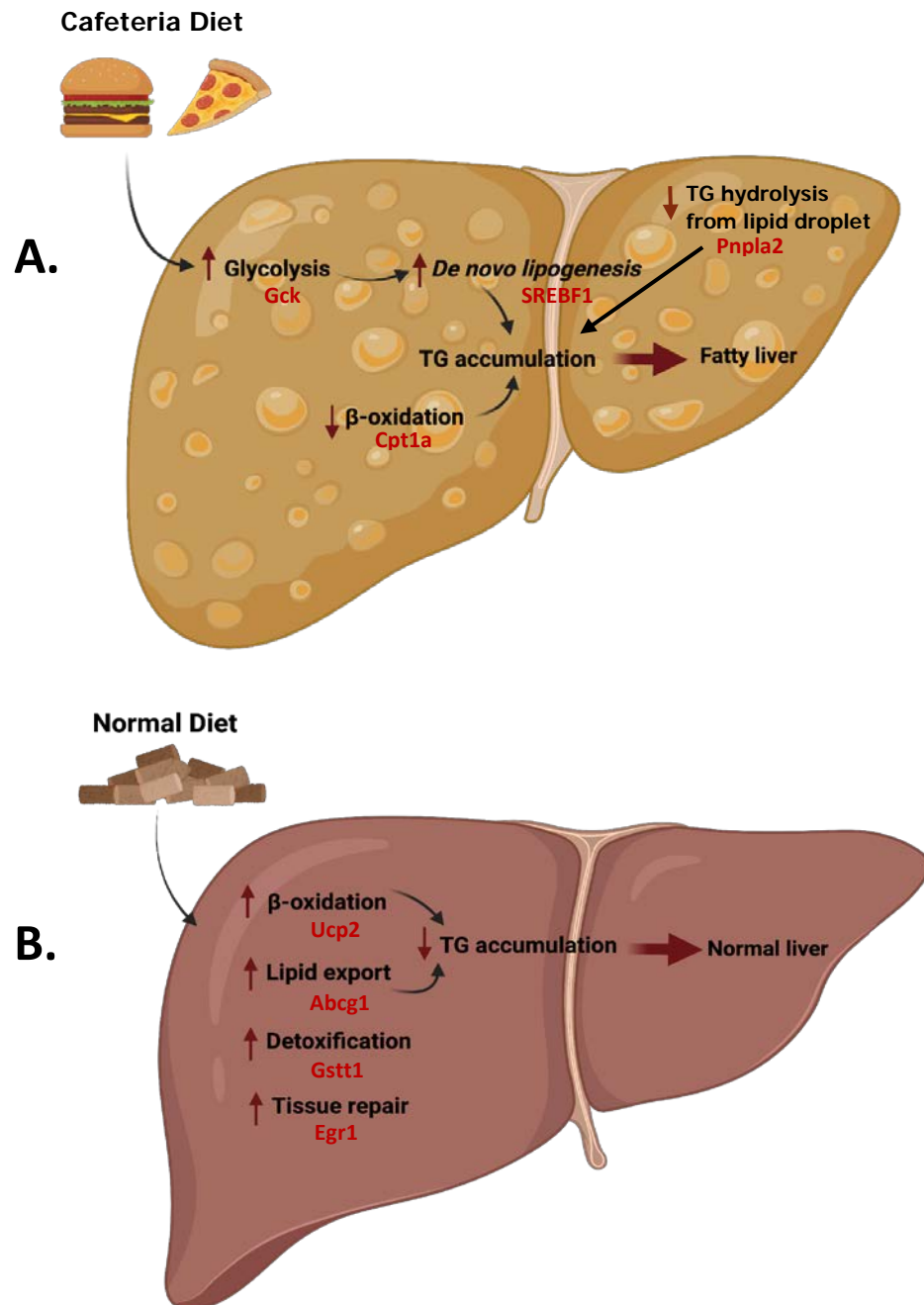


Figure 55: Schematic summary of transcriptomic study.

A) The main mechanisms involved in the development of hepatic steatosis in CAF-fed rats, include increase Glycolysis, and *De novo lipogenesis*, decrease in β-oxidation and hydrolysis of TG from lipid droplet. All these events lead to hepatic steatosis and eventually NAFLD. B) The main mechanisms involved in reversible group when diet change from CAF to NC include increase in β-oxidation, lipid export, detoxification and tissue repair leading to decrease in TG accumulation and consequently reversing the fatty liver to normal liver.

CHAPTER 6: CONCLUSION AND FUTURE DIRECTION

The objectives and specific aims of this research work were: 1) Establish a diet-induced obesity rat model using high carbohydrate diet (CAF diet) followed with dietary intervention to induce weight loss. 2) Assess the extent to which CAF diet can induce body weight gain, fat distribution, metabolic parameters, and determine the effectiveness of CAF withdrawal on reversing these changes. 3) Determine whether CAF diet-induced obesity increase cardiometabolic risks and affects the vascular function in my DIO model. Moreover, to assess the extent to which diet switch may reverse these abnormalities. 4) Investigate if this DIO model developed NAFLD, and the degree of NAFLD progression. In addition, to assess the efficiency of dietary intervention in reversing NAFLD. 5) Explore the alterations in hepatic transcriptomes and determine the mechanistic pathways associated with both weight gain and weight loss. Overall, these objectives were achieved effectively. In addition, the whole transcriptome analysis generated an abundance of data which will provide a basis for further studies.

6.1 Developing DIO model of high carbohydrate diet

The present study successfully developed the DIO model, using a high carbohydrate diet (125), that more closely reflected the regional diet and lifestyle. Exposing the rat model to an obesogenic diet instead of using an obese rat model was challenging. The challenge was implicit in the rat's eating behavior and choices, and this meant the offered CAF diet type had to be changed every week or two weeks in order to induce food consumption, and ensuring the animals reached the weight gain target (20-30%). The advantage of the current model is the use of outbred rats, which considers any heterogeneity, and mimics the human obese model.

The data showed that CAF feeding of adult rats significantly induced adiposity and body weight gain. Weight gain was associated with some changes in MS features, such as abdominal adiposity, disturbances in glucose and insulin levels, elevation of systemic triglycerides, low HDL-cholesterol, high SBP and abnormal levels of liver

function enzymes. These abnormal metabolic changes are likely to predispose these animals to obesity-related comorbidities.

6.2 The prevalence of obesity-related comorbidities

This study addressed the comorbidities commonly associated with diet-induced obesity. As disturbances in metabolic parameters is a risk factor of cardiovascular disease, the vascular reactivity of this model was assessed. The data showed that CAF diet did not affect vascular contraction. However, the CAF diet induced endothelial dysfunction which affected vascular dilation.

NAFLD was another outcome of DIO in this study. Excess fat induced hepatic fat deposition leading to liver steatosis. The livers of CAF-fed animals exhibited higher weight, with elevated triglyceride contents, compared to NC-fed rats. A clear hepatic steatosis was developed in CAF-fed rats which diagnosed with grade 3 hepatic steatosis. Interestingly, hepatic steatosis was not associated with inflammation which is a hallmark of NAFLD progression to NASH.

6.3 Whole transcriptome analysis of liver tissue

The investigation of the hepatic transcriptome pointed to lipid accumulation, triggered through the over-expression of SREBF1 as a master transcriptional regulator of hepatic lipid metabolism. Furthermore, DNL appeared to have a significant role in the suggested mechanism that led to the pathological changes in the pathological changes in liver due to the nutritional insult.

6.4 Dietary intervention and reversal of body weight and changes associated with weight gain

Dietary and healthy lifestyle intervention was the focus of this study. The aim of this part of the study was to assess the extent to which modest, short-term, calorie restriction could reverse changes induced by DIO. The dietary intervention involved

the replacement of CAF diet to NC diet for three weeks. The shift in diet only revealed a slight loss of body weight. Interestingly, this slight weight loss completely reversed the metabolic parameters, but not endothelial dysfunction. In addition, NAFLD was reversed from grade 3 to normal liver. This was supported by the findings of the transcriptome analysis, which showed that recovery was mediated by increasing FA oxidation pathway, lipid export and tissue repair mechanisms. These improvements were achieved without changes in physical activity. Increased physical activity could have resulted in greater improvements in metabolic and vascular health. These interesting findings need to be validated and could provide the basis for guidance for the public to maintain healthier lifestyle and avoid the progression of obesity related comorbidities.

Taken together, modest calorie restricted diet, low in carbohydrate especially, had a beneficial effect on weight loss and successfully reversed some of the metabolic pathologies of obesity related comorbidities.

6.5 Limitations of the study

There were several issues that may be seen as limitations of the current study. Firstly, the study used only male rats, which is not a complete representation of a whole population. While previously it was thought that males were more at risk for developing cardiometabolic diseases more recent evidence suggests that the protective effect, perhaps of the sex hormones, specifically estrogen, seems to be disappearing. The evidence now suggests that females have the same risk as males, especially amongst South Asian and Arab populations (278, 279). This may be because of the increased prevalence of obesity, sedentary lifestyle and/or components of the modern diet. In addition, the body composition between men and women are different, men exhibit less fat mass and more muscle mass compared to women (280). In adipose tissue, sex differences have significant impact on fat distribution. Although women have more fat mass compared to men, its distribution

generally protects from cardiometabolic risk. In women adiposity is concentrated at SAT depots in the mammary and gluteofemoral areas, while it is more in the abdominal region and VAT in men. This kind of female fat distribution is referred to as pear-shape and suggested to be a protective phenotype (281). Increased SAT, as well as VAT, in the abdominal areas is also found in women, but mainly in the postmenopausal period (282).

Thus, sex differences have a potent effect on fat distribution and as different fat depots vary in their metabolic health and contribution to disease this needs to be addressed, but, was not in this study.

Second issue is the diet. this study used a custom-made diet that focused on its palatability. The diet was tested on the animals before starting the study. Then selection was based on their preference and considered to be more palatable. Thus, this study focused more on the percentages of the macronutrient composition, more than energy. Many DIO studies have used CAF diet, with assorted ingredients being fed to the animals. Moreover, the CAF diet usually consists of high carbohydrate/high fat, which is different from the current study that focused on high carbohydrate. Other studies used additives, such as honey and bacon, to induce the consumption. Therefore, making the diet more palatable is challenging for all researchers. In DIO studies the diet differs in the composition and the source of each composition, thus the results observed might differ from each study, which make the comparison between studies more challenging (130). The main concern in the diet selection for DIO studies is to make it more palatable in order to make the model more robust and reproducible to study obesity.

In addition to the previous limitations, the short reversibility period used in this study may not have been adequate to fully realize the complete benefits of the calorie restrictive part. Although the period was short, it showed a positive effect on the

adverse metabolic parameters. Expanding the recovery time may have greater effects specially with weight loss. A weight loss of at least 15 to 20% of the gained weight would have been ideal. In order to achieve that, adding other intervention such as physical activity might have helped achieve the study goals, as physical activity has a beneficial effect on restoring metabolic parameters, as well as mRNA expression of genes involved in hepatic lipogenesis (283).

Another limitation of the transcriptome studies was that there was no further validation to confirm the involvement of the suggested pathways. Additional analysis of the related proteome or metabolome would have also helped confirm the importance of the pathway/gene in the various phases of weight gain and loss. However, it is a powerful approach in investigating the causative pathways of various diseases and finding novel therapeutic targets. Many other technologies “omics” have been developed in order to achieve the same target. These omics (genomics, transcriptomics, metabolomics and proteomics) are capable of showing the integration and modeling of biological networks (284). Although transcriptomics showed an abundance of differentially expressed genes, however, they may not be reflected at the protein or physiological/functional level. This phenomenon was raised by Feder and Walser (2005) and said, “The probability of predicting whether a particular protein's concentration increases or decreases under stress would seem to be greater for a flip of a coin (50%) than for transcriptomics (typically <50%)”. Therefore, further studies suggest that only little is known about the protein function and activity evoked from transcriptomic data (285). Only approximately 40% of transcripts are shown to be expressed at the protein level, due to the post-translational and translational modifications and degradation of proteins (286). Taken together, these suggest the importance of further steps required to validate the transcriptome data.

6.6 Concluding Remarks

Overall, the objectives and specific aims of this study were achieved and a provided a well-established new DIO model for future studies. The transcriptome analysis provided a broad list of lipogenic genes involved in the development of NAFLD, suggesting a key role of therapeutic targets.

6.7 Future directions

Data generated from the current study afforded the opportunity to think about future direction and answer ambiguous research question, with the first task being validation of the transcriptome results. The current study only presents the differential expression of whole liver transcriptome, which now requires further steps to confirm the suggested pathways. These investigations, using RT-PCR and western blots, of selected genes and proteins, are planned.

Other future direction is to apply the same study on females and look at the sex difference in developing obesity, cardiometabolic risks and obesity related comorbidities. Moreover, to investigate the sex differences of the differential gene expression in hepatic lipogenesis. This will help in assessing the efficiency of developing DIO model in females.

The reversibility period needs to be extended and the increased physical activity added, as a complete lifestyle modification. Increased physical activity intervention is planned, with the animals either using treadmill or voluntary running wheels, which has been recently added to the lab facilities at LARC. This is for the purpose of inducing weight loss and restoring all the changes to the normal level.

In the current study, other tissues have been collected such as adipose tissues and skeletal muscles. These tissues will be used to establish other studies, such as looking at the differential gene expression of adipose tissues and FA efflux among the three types of adipose tissues collected.

Despite many studies having been developed and published on various DIO models, there is a lack of comparison between these diets and their effects on cardiometabolic risks and the development of NAFLD. Evidence showed that the high carbohydrate diet has a particularly detrimental effect on the liver, compared to high fat diet (287). These direct comparisons between high carbohydrate and HF diets are currently underway in the laboratory. These will allow further exploration of the macronutrient components of the diet on cardiometabolic and vascular function, their mechanisms, best ways of combating them and therapeutic interventions.

References

1. Bray GA. A Guide to Obesity and the Metabolic Syndrome. U.S: Taylor and Francis Group; 2011.
2. Bouchard GABaC. Handbook of Obesity (Epidemiology, Etiology and Physiopathology. Third Edition ed. U.S: Taylor and Francis Group; 2014.
3. POLLACK A. A.M.A. Recognizes Obesity as a Disease. 2013.
4. Consultation W. Obesity: preventing and managing the global epidemic. World Health Organization technical report series. 2000;894:1-253.
5. Zhou BF. Predictive values of body mass index and waist circumference for risk factors of certain related diseases in Chinese adults--study on optimal cut-off points of body mass index and waist circumference in Chinese adults. Biomedical and environmental sciences : BES. 2002;15(1):83-96.
6. Kanazawa M, Yoshiike N, Osaka T, Numba Y, Zimmet P, Inoue S. Criteria and classification of obesity in Japan and Asia-Oceania. World Rev Nutr Diet. 2005;94:1-12.
7. Fock KM, Khoo J. Diet and exercise in management of obesity and overweight. J Gastroenterol Hepatol. 2013;28 Suppl 4:59-63.
8. Whitlock G, Lewington S, Sherliker P, Clarke R, Emberson J, Halsey J, et al. Body-mass index and cause-specific mortality in 900 000 adults: collaborative analyses of 57 prospective studies. Lancet. 2009;373(9669):1083-96.
9. Ng M, Fleming T, Robinson M, Thomson B, Graetz N, Margono C, et al. Global, regional, and national prevalence of overweight and obesity in children and adults during 1980-2013: a systematic analysis for the Global Burden of Disease Study 2013. Lancet. 2014;384(9945):766-81.

10. Kelly T, Yang W, Chen CS, Reynolds K, He J. Global burden of obesity in 2005 and projections to 2030. *International journal of obesity* (2005). 2008;32(9):1431-7.
11. Flegal KM, Carroll MD, Kuczmarski RJ, Johnson CL. Overweight and obesity in the United States: prevalence and trends, 1960-1994. *International journal of obesity and related metabolic disorders : journal of the International Association for the Study of Obesity*. 1998;22(1):39-47.
12. Ogden CL, Carroll MD, Kit BK, Flegal KM. Prevalence of childhood and adult obesity in the United States, 2011-2012. *Jama*. 2014;311(8):806-14.
13. von Ruesten A, Steffen A, Floegel A, van der AD, Masala G, Tjonneland A, et al. Trend in obesity prevalence in European adult cohort populations during follow-up since 1996 and their predictions to 2015. *PLoS One*. 2011;6(11):e27455.
14. Khoja T. Health Care in Gulf Cooperation Council Countries: A Review of Challenges and Opportunities.9(8).
15. Ng SW, Zaghoul S, Ali HI, Harrison G, Popkin BM. The prevalence and trends of overweight, obesity and nutrition-related non-communicable diseases in the Arabian Gulf States. *Obesity reviews : an official journal of the International Association for the Study of Obesity*. 2011;12(1):1-13.
16. Vats MG, Mahboub BH, Al Hariri H, Al Zaabi A, Vats D. Obesity and Sleep-Related Breathing Disorders in Middle East and UAE. *Can Respir J*. 2016;2016:9673054.
17. Qatar Health Report. 2012.
18. Review WP. Obesity Rates by Country 2020 [updated 2020. Available from: <https://worldpopulationreview.com/country-rankings/obesity-rates-by-country>.
19. Mutch DM, Clement K. Unraveling the genetics of human obesity. *PLoS Genet*. 2006;2(12):e188.

20. Vanhoutte PM. Obesity and vascular dysfunction: the fat-e of rich and poor. *British journal of pharmacology*. 2012;165(3):541-3.
21. Lavie CJ, De Schutter A, Parto P, Jahangir E, Kokkinos P, Ortega FB, et al. Obesity and Prevalence of Cardiovascular Diseases and Prognosis—The Obesity Paradox Updated. *Progress in Cardiovascular Diseases*. 2016;58(5):537-47.
22. Kostecka M. Eating habits of preschool children and the risk of obesity, insulin resistance and metabolic syndrome in adults. *Pak J Med Sci*. 2014;30(6):1299-303.
23. Pereira MA, Kartashov AI, Ebbeling CB, Van Horn L, Slattery ML, Jacobs DR, Jr., et al. Fast-food habits, weight gain, and insulin resistance (the CARDIA study): 15-year prospective analysis. *Lancet*. 2005;365(9453):36-42.
24. Timothy S. Church DMT, Catrine Tudor-Locke, Peter T. Katzmarzyk, Conrad P. Earnest, Ruben Q. Rodarte, Corby K. Martin, Steven N. Blair, Claude Bouchard. Trends over 5 Decades in U.S. Occupation-Related Physical Activity and Their Associations with Obesity. *PLoS ONE*. 2011;6(5).
25. Wang W, Seale P. Control of brown and beige fat development. *Nat Rev Mol Cell Biol*. 2016;17(11):691-702.
26. Chait A, den Hartigh LJ. Adipose Tissue Distribution, Inflammation and Its Metabolic Consequences, Including Diabetes and Cardiovascular Disease. *Front Cardiovasc Med*. 2020;7:22-.
27. Lowell BB, V SS, Hamann A, Lawitts JA, Himms-Hagen J, Boyer BB, et al. Development of obesity in transgenic mice after genetic ablation of brown adipose tissue. *Nature*. 1993;366(6457):740-2.
28. Stanford KI, Middelbeek RJ, Townsend KL, An D, Nygaard EB, Hitchcox KM, et al. Brown adipose tissue regulates glucose homeostasis and insulin sensitivity. *The Journal of clinical investigation*. 2013;123(1):215-23.

29. Poddar M, Chetty Y, Chetty VT. How does obesity affect the endocrine system? A narrative review. *Clin Obes*. 2017;7(3):136-44.
30. Bluher M, Michael MD, Peroni OD, Ueki K, Carter N, Kahn BB, et al. Adipose tissue selective insulin receptor knockout protects against obesity and obesity-related glucose intolerance. *Developmental cell*. 2002;3(1):25-38.
31. Bjorndal B, Burri L, Staalesen V, Skorve J, Berge RK. Different adipose depots: their role in the development of metabolic syndrome and mitochondrial response to hypolipidemic agents. *Journal of obesity*. 2011;2011:490650.
32. Manore MM. Exercise and the Institute of Medicine recommendations for nutrition. *Curr Sports Med Rep*. 2005;4(4):193-8.
33. Panini SR. Carbohydrate Metabolism. *Medical Biochemistry*. U.S: Thieme Medical Publishers; 2013. p. 166.
34. C.Elliott WHEaD. Digestion of Carbohydrates. *Biochemistry and Molecular Biology*. Third Edition ed. U.S: Oxford University Press; 2005. p. 155-7.
35. Thorens B, Mueckler M. Glucose transporters in the 21st Century. *American journal of physiology Endocrinology and metabolism*. 2010;298(2):E141-E5.
36. Panini SR. Carbohydrate Metabolism. *Medical Biochemistry*. U.S: Thieme Medical Publishers; 2013. p. 178-80.
37. C.Elliott WHEaD. Mechanism of Glycogen Synthesis. *Biochemistry and Molecular Biology*. Third ed. U.S: Oxford University Press; 2005. p. 168-71.
38. C.Elliott WHEaD. Breakdown of Glycogen to release Glucose into the blood. *Biochemistry and Molecular Biology*. Third ed. U.S: Oxford University Press; 2005. p. 171-3.
39. Panini SR. Fatty Acid Metabolism. *Medical Biochemistry*. U.S: Thieme Medical Publishers; 2013. p. 202-3.

40. Panini SR. Carbohydrate Metabolism Medical Biochemistry. U.S: Thieme Medical Publishers; 2013. p. 169-73.
41. C.Elliott WHEaD. Glycolysis, the citric acid cycle and the electron transport system: reactions involved in these pathways. Biochemistry and Molecular Biology. U.S: Oxford University Press; 2005. p. 196-201.
42. C.Elliott WHEaD. Synthesis of glucose (gluconeogenesis). Biochemistry and Molecular Biology. U.S: Oxford University Press; 2005. p. 247-50.
43. Nguyen P, Leray V, Diez M, Serisier S, Le Bloc'h J, Siliart B, et al. Liver lipid metabolism. J Anim Physiol Anim Nutr (Berl). 2008;92(3):272-83.
44. Liu X, Wang H, Liang X, Roberts MS. Chapter 30 - Hepatic Metabolism in Liver Health and Disease. In: Muriel P, editor. Liver Pathophysiology. Boston: Academic Press; 2017. p. 391-400.
45. Naaktgeboren WR, Linschoten M, de Graeff A, v Rhenen A, Cramer MJ, Asselbergs FW, et al. Long-term cardiovascular health in adult cancer survivors. Maturitas.
46. Whelton PK, Carey RM, Aronow WS, Casey DE, Jr., Collins KJ, Dennison Himmelfarb C, et al. 2017 ACC/AHA/AAPA/ABC/ACPM/AGS/APhA/ASH/ASPC/NMA/PCNA Guideline for the Prevention, Detection, Evaluation, and Management of High Blood Pressure in Adults: A Report of the American College of Cardiology/American Heart Association Task Force on Clinical Practice Guidelines. J Am Coll Cardiol. 2018;71(19):e127-e248.
47. Ameer F, Scandiuzzi L, Hasnain S, Kalbacher H, Zaidi N. De novo lipogenesis in health and disease. Metabolism. 2014;63(7):895-902.

48. Monteiro CA, Moubarac J-C, Cannon G, Ng SW, Popkin B. Ultra-processed products are becoming dominant in the global food system. *Obesity Reviews*. 2013;14(S2):21-8.
49. Asfaw A. Does consumption of processed foods explain disparities in the body weight of individuals? The case of Guatemala. *Health Econ*. 2011;20(2):184-95.
50. McCrickerd K, Forde CG. Sensory influences on food intake control: moving beyond palatability. *Obesity reviews : an official journal of the International Association for the Study of Obesity*. 2016;17(1):18-29.
51. Pan American Health Organization. Washington DC. Ultra-processed food and drink products in Latin America: Sales, sources, nutrient profiles, and policy implications. PAHO. 2019.
52. Gearhardt AN, Davis C, Kuschner R, Brownell KD. The addiction potential of hyperpalatable foods. *Curr Drug Abuse Rev*. 2011;4(3):140-5.
53. Poti JM, Braga B, Qin B. Ultra-processed Food Intake and Obesity: What Really Matters for Health-Processing or Nutrient Content? *Curr Obes Rep*. 2017;6(4):420-31.
54. Monteiro CA, Moubarac JC, Cannon G, Ng SW, Popkin B. Ultra-processed products are becoming dominant in the global food system. *Obesity reviews : an official journal of the International Association for the Study of Obesity*. 2013;14 Suppl 2:21-8.
55. Kalon E, Hong JY, Tobin C, Schulte T. Psychological and Neurobiological Correlates of Food Addiction. *Int Rev Neurobiol*. 2016;129:85-110.
56. Mozaffarian D, Hao T, Rimm EB, Willett WC, Hu FB. Changes in diet and lifestyle and long-term weight gain in women and men. *N Engl J Med*. 2011;364(25):2392-404.

57. Nago ES, Lachat CK, Dossa RA, Kolsteren PW. Association of out-of-home eating with anthropometric changes: a systematic review of prospective studies. *Crit Rev Food Sci Nutr*. 2014;54(9):1103-16.
58. Lavigne-Robichaud M, Moubarac JC, Lantagne-Lopez S, Johnson-Down L, Batal M, Laouan Sidi EA, et al. Diet quality indices in relation to metabolic syndrome in an Indigenous Cree (Eeyouch) population in northern Québec, Canada. *Public Health Nutr*. 2018;21(1):172-80.
59. Rinaldi AE, Gabriel GF, Moreto F, Corrente JE, McLellan KC, Burini RC. Dietary factors associated with metabolic syndrome and its components in overweight and obese Brazilian schoolchildren: a cross-sectional study. *Diabetol Metab Syndr*. 2016;8(1):58.
60. Bertioia ML, Mukamal KJ, Cahill LE, Hou T, Ludwig DS, Mozaffarian D, et al. Changes in Intake of Fruits and Vegetables and Weight Change in United States Men and Women Followed for Up to 24 Years: Analysis from Three Prospective Cohort Studies. *PLoS Med*. 2015;12(9):e1001878.
61. Webb P. Energy expenditure and fat-free mass in men and women. *The American journal of clinical nutrition*. 1981;34(9):1816-26.
62. Westerterp KR. Control of energy expenditure in humans. *European Journal of Clinical Nutrition*. 2017;71(3):340-4.
63. Swinburn BA, Sacks G, Hall KD, McPherson K, Finegood DT, Moodie ML, et al. The global obesity pandemic: shaped by global drivers and local environments. *The Lancet*. 2011;378(9793):804-14.
64. Sandoo A, van Zanten J, Metsios GS, Carroll D, Kitas GD. The Endothelium and Its Role in Regulating Vascular Tone. *The Open Cardiovascular Medicine Journal*. 2010;4:302-12.

65. Lam DW, LeRoith D. Metabolic Syndrome. In: De Groot LJ, Chrousos G, Dungan K, Feingold KR, Grossman A, Hershman JM, et al., editors. Endotext. South Dartmouth (MA)2000.
66. Alberti KG, Eckel RH, Grundy SM, Zimmet PZ, Cleeman JI, Donato KA, et al. Harmonizing the metabolic syndrome: a joint interim statement of the International Diabetes Federation Task Force on Epidemiology and Prevention; National Heart, Lung, and Blood Institute; American Heart Association; World Heart Federation; International Atherosclerosis Society; and International Association for the Study of Obesity. *Circulation*. 2009;120(16):1640-5.
67. Grundy SM, Cleeman JI, Daniels SR, Donato KA, Eckel RH, Franklin BA, et al. Diagnosis and management of the metabolic syndrome: An American Heart Association/National Heart, Lung, and Blood Institute scientific statement. *Circulation*. 2005;112(17):2735-52.
68. Gallagher EJ, Leroith D, Karnieli E. The metabolic syndrome--from insulin resistance to obesity and diabetes. *The Medical clinics of North America*. 2011;95(5):855-73.
69. Jung U, Choi M-S. Obesity and Its Metabolic Complications: The Role of Adipokines and the Relationship between Obesity, Inflammation, Insulin Resistance, Dyslipidemia and Nonalcoholic Fatty Liver Disease. *International journal of molecular sciences*. 2014;15:6184-223.
70. White MF. Insulin signaling in health and disease. *Science (New York, NY)*. 2003;302(5651):1710-1.
71. Lanthier N, Leclercq IA. Adipose tissues as endocrine target organs. *Best practice & research Clinical gastroenterology*. 2014;28(4):545-58.
72. Ye J. Mechanisms of insulin resistance in obesity. *Frontiers of Medicine*. 2013;7(1):14-24.

73. McEniery CM, Wilkinson IB, Avolio AP. Age, hypertension and arterial function. *Clinical and experimental pharmacology & physiology*. 2007;34(7):665-71.
74. Pugsley MK, Tabrizchi R. The vascular system. An overview of structure and function. *Journal of pharmacological and toxicological methods*. 2000;44(2):333-40.
75. Sandoo A, van Zanten JJ, Metsios GS, Carroll D, Kitas GD. The endothelium and its role in regulating vascular tone. *The Open Cardiovascular Medicine Journal*. 2010;4:302-12.
76. Palmer RM, Ashton DS, Moncada S. Vascular endothelial cells synthesize nitric oxide from L-arginine. *Nature*. 1988;333(6174):664-6.
77. Prast H, Philippu A. Nitric oxide as modulator of neuronal function. *Progress in neurobiology*. 2001;64(1):51-68.
78. Michel T, Feron O. Nitric oxide synthases: which, where, how, and why? *The Journal of clinical investigation*. 1997;100(9):2146-52.
79. Lamas S, Marsden PA, Li GK, Tempst P, Michel T. Endothelial nitric oxide synthase: molecular cloning and characterization of a distinct constitutive enzyme isoform. *Proceedings of the National Academy of Sciences of the United States of America*. 1992;89(14):6348-52.
80. Bucci M, Gratton JP, Rudic RD, Acevedo L, Roviezzo F, Cirino G, et al. In vivo delivery of the caveolin-1 scaffolding domain inhibits nitric oxide synthesis and reduces inflammation. *Nature medicine*. 2000;6(12):1362-7.
81. Bae SW, Kim HS, Cha YN, Park YS, Jo SA, Jo I. Rapid increase in endothelial nitric oxide production by bradykinin is mediated by protein kinase A signaling pathway. *Biochemical and biophysical research communications*. 2003;306(4):981-7.
82. Pfitzer G. Invited review: regulation of myosin phosphorylation in smooth muscle. *Journal of applied physiology (Bethesda, Md : 1985)*. 2001;91(1):497-503.

83. Nascimento TB, Baptista Rde F, Pereira PC, Campos DH, Leopoldo AS, Leopoldo AP, et al. Vascular alterations in high-fat diet-obese rats: role of endothelial L-arginine/NO pathway. *Arquivos brasileiros de cardiologia*. 2011;97(1):40-5.
84. Boden-Albala B, Sacco RL, Lee HS, Grahame-Clarke C, Rundek T, Elkind MV, et al. Metabolic syndrome and ischemic stroke risk: Northern Manhattan Study. *Stroke*. 2008;39(1):30-5.
85. Ghosh A, Gao L, Thakur A, Siu PM, Lai CWK. Role of free fatty acids in endothelial dysfunction. *Journal of biomedical science*. 2017;24(1):50.
86. Cai H, Harrison DG. Endothelial Dysfunction in Cardiovascular Diseases: The Role of Oxidant Stress. *Circulation research*. 2000;87(10):840.
87. Cersosimo E, DeFronzo RA. Insulin resistance and endothelial dysfunction: the road map to cardiovascular diseases. *Diabetes/metabolism research and reviews*. 2006;22(6):423-36.
88. Kim F, Pham M, Maloney E, Rizzo NO, Morton GJ, Wisse BE, et al. Vascular inflammation, insulin resistance, and reduced nitric oxide production precede the onset of peripheral insulin resistance. *Arteriosclerosis, thrombosis, and vascular biology*. 2008;28(11):1982-8.
89. Trowers E, Tischler M. Physiology of the Liver, Gallbladder and Pancreas: "Getting By" with Some Help from Your Friends. *Gastrointestinal Physiology: A Clinical Approach*. Cham: Springer International Publishing; 2014. p. 81-97.
90. Dancygier H. Microscopic Anatomy. *Clinical Hepatology: Principles and Practice of Hepatobiliary Diseases*. Berlin, Heidelberg: Springer Berlin Heidelberg; 2010. p. 15-51.
91. Tortora GJ. Principles of Human Anatomy. In: Roesch B, editor. US: John Wiley & Sons, Inc.; 2005. p. 784-7.

92. Hiatt LPGaJL. Color Textbook of Histology. In: Mahon IOaJ, editor. Third Edition ed. US: Elsevier; 2007. p. 425-6.
93. Funk LM, Jolles SA, Greenberg CC, Schwarze ML, Safdar N, McVay MA, et al. Primary care physician decision making regarding severe obesity treatment and bariatric surgery: a qualitative study. *Surgery for Obesity and Related Diseases*. 2016;12(4):893-901.
94. Dasgupta A. Chapter 5 - Liver Enzymes as Alcohol Biomarkers. In: Dasgupta A, editor. *Alcohol and its Biomarkers*. San Diego: Elsevier; 2015. p. 121-37.
95. Dancygier H. Basic Laboratory Parameters. *Clinical Hepatology: Principles and Practice of Hepatobiliary Diseases*. Berlin, Heidelberg: Springer Berlin Heidelberg; 2010. p. 319-31.
96. Gong Z, Tas E, Yakar S, Muzumdar R. Hepatic lipid metabolism and non-alcoholic fatty liver disease in aging. *Mol Cell Endocrinol*. 2017;455:115-30.
97. Ahmed M. Non-alcoholic fatty liver disease in 2015. *World journal of hepatology*. 2015;7(11):1450-9.
98. Bellentani S, Saccoccio G, Masutti F, et al. PRevalence of and risk factors for hepatic steatosis in northern Italy. *Annals of Internal Medicine*. 2000;132(2):112-7.
99. Carr RM, Oranu A, Khungar V. Nonalcoholic Fatty Liver Disease. *Gastroenterology Clinics*. 45(4):639-52.
100. Pappachan JM, Babu S, Krishnan B, Ravindran NC. Non-alcoholic Fatty Liver Disease: A Clinical Update. *J Clin Transl Hepatol*. 2017;5(4):384-93.
101. Milic S, Lulic D, Stimac D. Non-alcoholic fatty liver disease and obesity: biochemical, metabolic and clinical presentations. *World J Gastroenterol*. 2014;20(28):9330-7.

102. White DL, Kanwal F, El-Serag HB. Non-Alcoholic Fatty Liver Disease and Hepatocellular Cancer: A Systematic Review. *Clinical gastroenterology and hepatology : the official clinical practice journal of the American Gastroenterological Association*. 2012;10(12):1342-59.e2.
103. B Savage D, K Semple R. Recent insights into fatty liver, metabolic dyslipidaemia and their links to insulin resistance 2010. 329-36 p.
104. Satapathy SK, Sanyal AJ. Epidemiology and Natural History of Nonalcoholic Fatty Liver Disease. *Seminars in liver disease*. 2015;35(3):221-35.
105. Gao X, Fan JG. Diagnosis and management of non-alcoholic fatty liver disease and related metabolic disorders: consensus statement from the Study Group of Liver and Metabolism, Chinese Society of Endocrinology. *J Diabetes*. 2013;5(4):406-15.
106. Marchesini G, Avagnina S, Barantani EG, Ciccarone AM, Corica F, Dall'Aglio E, et al. Aminotransferase and gamma-glutamyltranspeptidase levels in obesity are associated with insulin resistance and the metabolic syndrome. *Journal of endocrinological investigation*. 2005;28(4):333-9.
107. Kotronen A, Westerbacka J, Bergholm R, Pietilainen KH, Yki-Jarvinen H. Liver fat in the metabolic syndrome. *The Journal of clinical endocrinology and metabolism*. 2007;92(9):3490-7.
108. Thamer C, Tschritter O, Haap M, Shirkavand F, Machann J, Fritsche A, et al. Elevated serum GGT concentrations predict reduced insulin sensitivity and increased intrahepatic lipids. *Hormone and metabolic research = Hormon- und Stoffwechselforschung = Hormones et metabolisme*. 2005;37(4):246-51.
109. Angulo P, Lindor KD. Non-alcoholic fatty liver disease. *J Gastroenterol Hepatol*. 2002;17 Suppl:S186-90.

110. Parker BM, Wu J, You J, Barnes DS, Yerian L, Kirwan JP, et al. Reversal of fibrosis in patients with nonalcoholic steatohepatosis after gastric bypass surgery. *BMC obesity*. 2017;4.
111. Sikaris KA. The clinical biochemistry of obesity. *Clin Biochem Rev*. 2004;25(3):165-81.
112. Hohenester S, Christiansen S, Nagel J, Wimmer R, Artmann R, Denk G, et al. Lifestyle intervention for morbid obesity: effects on liver steatosis, inflammation, and fibrosis. *American Journal of Physiology-Gastrointestinal and Liver Physiology*. 2018;315(3):G329-G38.
113. Freire R. Scientific evidence of diets for weight loss: Different macronutrient composition, intermittent fasting, and popular diets. *Nutrition*. 2020;69:110549.
114. Ludwig DS, Ebbeling CB. The Carbohydrate-Insulin Model of Obesity: Beyond "Calories In, Calories Out". *JAMA Intern Med*. 2018;178(8):1098-103.
115. Ferland A, Eckel RH. Does sustained weight loss reverse the metabolic syndrome? *Curr Hypertens Rep*. 2011;13(6):456-64.
116. Knowler WC, Barrett-Connor E, Fowler SE, Hamman RF, Lachin JM, Walker EA, et al. Reduction in the incidence of type 2 diabetes with lifestyle intervention or metformin. *N Engl J Med*. 2002;346(6):393-403.
117. Reynés B, García-Ruiz E, Díaz-Rúa R, Palou A, Oliver P. Reversion to a control balanced diet is able to restore body weight and to recover altered metabolic parameters in adult rats long-term fed on a cafeteria diet. *Food Research International*. 2014;64:839-48.
118. Brown JD, Buscemi J, Milsom V, Malcolm R, O'Neil PM. Effects on cardiovascular risk factors of weight losses limited to 5-10. *Transl Behav Med*. 2016;6(3):339-46.

119. Wadden TA, Anderson DA, Foster GD. Two-year changes in lipids and lipoproteins associated with the maintenance of a 5% to 10% reduction in initial weight: some findings and some questions. *Obes Res.* 1999;7(2):170-8.
120. Fantin F, Giani A, Zoico E, Rossi AP, Mazzali G, Zamboni M. Weight Loss and Hypertension in Obese Subjects. *Nutrients.* 2019;11(7).
121. Members EP, Jensen MD, Ryan DH, Donato KA, Apovian CM, Ard JD, et al. Executive summary: Guidelines (2013) for the management of overweight and obesity in adults. *Obesity.* 2014;22(S2):S5-S39.
122. Ryan DH, Yockey SR. Weight Loss and Improvement in Comorbidity: Differences at 5%, 10%, 15%, and Over. *Curr Obes Rep.* 2017;6(2):187-94.
123. Hubscher SG. Histological assessment of non-alcoholic fatty liver disease. *Histopathology.* 2006;49(5):450-65.
124. Zivkovic AM, German JB, Sanyal AJ. Comparative review of diets for the metabolic syndrome: implications for nonalcoholic fatty liver disease. *The American journal of clinical nutrition.* 2007;86(2):285-300.
125. Gabbia D, Roverso M, Guido M, Sacchi D, Scaffidi M, Carrara M, et al. Western Diet-Induced Metabolic Alterations Affect Circulating Markers of Liver Function before the Development of Steatosis. *Nutrients.* 2019;11(7):1602.
126. Mishra JS, Hankins GD, Kumar S. Testosterone downregulates angiotensin II type-2 receptor via androgen receptor-mediated ERK1/2 MAP kinase pathway in rat aorta. *J Renin Angiotensin Aldosterone Syst.* 2016;17(4):1470320316674875.
127. Li X, Lian F, Liu C, Hu K-Q, Wang X-D. Isocaloric Pair-Fed High-Carbohydrate Diet Induced More Hepatic Steatosis and Inflammation than High-Fat Diet Mediated by miR-34a/SIRT1 Axis in Mice. *Scientific reports.* 2015;5:16774-.

128. Madika A-L, Devos P, Delsart P, Boudghène F, Polge A-S, Bauters C, et al. Evaluation of screening for myocardial ischaemia in women at cardiovascular risk. *Archives of Cardiovascular Diseases*.
129. Lutz TA, Woods SC. Overview of animal models of obesity. *Curr Protoc Pharmacol*. 2012;Chapter 5:Unit5 61.
130. Buettner R, Schölmerich J, Bollheimer LC. High-fat Diets: Modeling the Metabolic Disorders of Human Obesity in Rodents. *Obesity*. 2007;15(4):798-808.
131. Fernandez CDB, Bellentani FF, Fernandes GSA, Perobelli JE, Favareto APA, Nascimento AF, et al. Diet-induced obesity in rats leads to a decrease in sperm motility. *Reproductive Biology and Endocrinology*. 2011;9(1):32.
132. Sampey BP, Vanhoose AM, Winfield HM, Freemerman AJ, Muehlbauer MJ, Fueger PT, et al. Cafeteria Diet Is a Robust Model of Human Metabolic Syndrome With Liver and Adipose Inflammation: Comparison to High-Fat Diet. *Obesity (Silver Spring, Md)*. 2011;19(6):1109-17.
133. Martire SI, Maniam J, South T, Holmes N, Westbrook RF, Morris MJ. Extended exposure to a palatable cafeteria diet alters gene expression in brain regions implicated in reward, and withdrawal from this diet alters gene expression in brain regions associated with stress. *Behavioural brain research*. 2014;265:132-41.
134. Buyukdere Y, Gulec A, Akyol A. Cafeteria diet increased adiposity in comparison to high fat diet in young male rats. *PeerJ*. 2019;7:e6656.
135. Zeeni N, Dagher-Hamalian C, Dimassi H, Faour WH. Cafeteria diet-fed mice is a pertinent model of obesity-induced organ damage: a potential role of inflammation. *Inflammation research : official journal of the European Histamine Research Society [et al]*. 2015;64(7):501-12.
136. Lewis AR, Singh S, Youssef FF. Cafeteria-diet induced obesity results in impaired cognitive functioning in a rodent model. *Heliyon*. 2019;5(3):e01412.

137. Gomez-Smith M, Karthikeyan S, Jeffers MS, Janik R, Thomason LA, Stefanovic B, et al. A physiological characterization of the Cafeteria diet model of metabolic syndrome in the rat. *Physiology & behavior*. 2016;167:382-91.
138. Oliva L, Aranda T, Caviola G, Fernández-Bernal A, Alemany M, Fernández-López JA, et al. In rats fed high-energy diets, taste, rather than fat content, is the key factor increasing food intake: a comparison of a cafeteria and a lipid-supplemented standard diet. *PeerJ*. 2017;5:e3697.
139. Lindqvist A, Baelemans A, Erlanson-Albertsson C. Effects of sucrose, glucose and fructose on peripheral and central appetite signals. *Regul Pept*. 2008;150(1-3):26-32.
140. Gomez-Smith M, Karthikeyan S, Jeffers MS, Janik R, Thomason LA, Stefanovic B, et al. A physiological characterization of the Cafeteria diet model of metabolic syndrome in the rat. *Physiology & behavior*. 2016;167:382-91.
141. Lalanza JF, Caimari A, del Bas JM, Torregrosa D, Cigarroa I, Pallas M, et al. Effects of a post-weaning cafeteria diet in young rats: metabolic syndrome, reduced activity and low anxiety-like behaviour. *PLoS One*. 2014;9(1):e85049.
142. Brandt N, De Bock K, Richter EA, Hespel P. Cafeteria diet-induced insulin resistance is not associated with decreased insulin signaling or AMPK activity and is alleviated by physical training in rats. *American journal of physiology Endocrinology and metabolism*. 2010;299(2):E215-24.
143. Mora-Rodriguez R, Ortega JF, Ramirez-Jimenez M, Moreno-Cabañas A, Morales-Palomo F. Insulin sensitivity improvement with exercise training is mediated by body weight loss in subjects with metabolic syndrome. *Diabetes & Metabolism*. 2019.
144. Sethi JK, Vidal-Puig AJ. Thematic review series: adipocyte biology. Adipose tissue function and plasticity orchestrate nutritional adaptation. *Journal of Lipid Research*. 2007;48:1253-62.

145. SIMONEAU J-A, VEERKAMP JH, TURCOTTE LP, KELLEY DE. Markers of capacity to utilize fatty acids in human skeletal muscle: relation to insulin resistance and obesity and effects of weight loss. *The FASEB Journal*. 1999;13(14):2051-60.
146. Di Meo S, Iossa S, Venditti P. Improvement of obesity-linked skeletal muscle insulin resistance by strength and endurance training. *J Endocrinol*. 2017;234(3):R159-r81.
147. Lohmiller JJ, Swing SP. Chapter 6 - Reproduction and Breeding. In: Suckow MA, Weisbroth SH, Franklin CL, editors. *The Laboratory Rat (Second Edition)*. Burlington: Academic Press; 2006. p. 147-64.
148. Iacobini C, Pugliese G, Blasetti Fantauzzi C, Federici M, Menini S. Metabolically healthy versus metabolically unhealthy obesity. *Metabolism*. 2019;92:51-60.
149. Hall JE, do Carmo JM, da Silva AA, Wang Z, Hall ME. Obesity, kidney dysfunction and hypertension: mechanistic links. *Nat Rev Nephrol*. 2019;15(6):367-85.
150. Skilton MR, Celermajer DS. Endothelial dysfunction and arterial abnormalities in childhood obesity. *International Journal of Obesity*. 2006;30(7):1041-9.
151. La Favor JD, Dubis GS, Yan H, White JD, Nelson MAM, Anderson EJ, et al. Microvascular Endothelial Dysfunction in Sedentary, Obese Humans Is Mediated by NADPH Oxidase: Influence of Exercise Training. *Arteriosclerosis, thrombosis, and vascular biology*. 2016;36(12):2412-20.
152. Bramlage P, Pittrow D, Wittchen HU, Kirch W, Boehler S, Lehnert H, et al. Hypertension in overweight and obese primary care patients is highly prevalent and poorly controlled. *Am J Hypertens*. 2004;17(10):904-10.
153. Steinberg HO, Chaker H, Leaming R, Johnson A, Brechtel G, Baron AD. Obesity/insulin resistance is associated with endothelial dysfunction. Implications for

the syndrome of insulin resistance. *The Journal of clinical investigation*. 1996;97(11):2601-10.

154. Creager MA, Cooke JP, Mendelsohn ME, Gallagher SJ, Coleman SM, Loscalzo J, et al. Impaired vasodilation of forearm resistance vessels in hypercholesterolemic humans. *The Journal of clinical investigation*. 1990;86(1):228-34.

155. Lewis TV, Dart AM, Chin-Dusting JPF. Endothelium-dependent relaxation by acetylcholine is impaired in hypertriglyceridemic humans with normal levels of plasma LDL cholesterol. *Journal of the American College of Cardiology*. 1999;33(3):805.

156. Sinn DH, Gwak GY, Park HN, Kim JE, Min YW, Kim KM, et al. Ultrasonographically detected non-alcoholic fatty liver disease is an independent predictor for identifying patients with insulin resistance in non-obese, non-diabetic middle-aged Asian adults. *Am J Gastroenterol*. 2012;107(4):561-7.

157. Starley BQ, Calcagno CJ, Harrison SA. Nonalcoholic fatty liver disease and hepatocellular carcinoma: A weighty connection. *Hepatology (Baltimore, Md)*. 2010;51(5):1820-32.

158. Ter Horst KW, Serlie MJ. Fructose Consumption, Lipogenesis, and Non-Alcoholic Fatty Liver Disease. *Nutrients*. 2017;9(9).

159. Basaranoglu M, Basaranoglu G, Bugianesi E. Carbohydrate intake and nonalcoholic fatty liver disease: fructose as a weapon of mass destruction. *Hepatobiliary Surg Nutr*. 2015;4(2):109-16.

160. Strable MS, Ntambi JM. Genetic control of de novo lipogenesis: role in diet-induced obesity. *Crit Rev Biochem Mol Biol*. 2010;45(3):199-214.

161. Parks EJ, Skokan LE, Timlin MT, Dingfelder CS. Dietary sugars stimulate fatty acid synthesis in adults. *J Nutr*. 2008;138(6):1039-46.

162. Dowman JK, Tomlinson JW, Newsome PN. Pathogenesis of non-alcoholic fatty liver disease. *QJM*. 2010;103(2):71-83.
163. Williams B, Mancia G, Spiering W, Agabiti Rosei E, Azizi M, Burnier M, et al. 2018 ESC/ESH Guidelines for the management of arterial hypertension. *Eur Heart J*. 2018;39(33):3021-104.
164. García-Prieto CF, Pulido-Olmo H, Ruiz-Hurtado G, Gil-Ortega M, Aranguéz I, Rubio MA, et al. Mild caloric restriction reduces blood pressure and activates endothelial AMPK-PI3K-Akt-eNOS pathway in obese Zucker rats. *Vascul Pharmacol*. 2015;65-66:3-12.
165. Ketonen J, Pilvi T, Mervaala E. Caloric restriction reverses high-fat diet-induced endothelial dysfunction and vascular superoxide production in C57Bl/6 mice. *Heart Vessels*. 2010;25(3):254-62.
166. Gao Q, Jia Y, Yang G, Zhang X, Boddu PC, Petersen B, et al. PPAR α -Deficient ob/ob Obese Mice Become More Obese and Manifest Severe Hepatic Steatosis Due to Decreased Fatty Acid Oxidation. *Am J Pathol*. 2015;185(5):1396-408.
167. Poirier P, Giles TD, Bray GA, Hong Y, Stern JS, Pi-Sunyer FX, et al. Obesity and cardiovascular disease: pathophysiology, evaluation, and effect of weight loss: an update of the 1997 American Heart Association Scientific Statement on Obesity and Heart Disease from the Obesity Committee of the Council on Nutrition, Physical Activity, and Metabolism. *Circulation*. 2006;113(6):898-918.
168. Arkin JM, Alsdorf R, Bigornia S, Palmisano J, Beal R, Istfan N, et al. Relation of Cumulative Weight Burden to Vascular Endothelial Dysfunction in Obesity. *Am J Cardiol*. 2008;101(1):98-101.
169. Mehdad S, Hamrani A, El Kari K, El Hamdouchi A, El Mzibri M, Barkat A, et al. Prevalence of elevated blood pressure and its relationship with fat mass, body

mass index and waist circumference among a group of Moroccan overweight adolescents. *Obes Res Clin Pract*. 2013;7(4):e284-9.

170. Fantin F, Giani A, Zoico E, Rossi AP, Mazzali G, Zamboni M. Weight Loss and Hypertension in Obese Subjects. *Nutrients*. 2019;11(7):1667.

171. NADERALI EK, PICKAVANCE LC, WILDING JPH, WILLIAMS G. Diet-induced endothelial dysfunction in the rat is independent of the degree of increase in total body weight. *Clinical Science*. 2001;100(6):635-41.

172. Naderali EK, Brown MJ, Pickavance LC, Wilding JP, Doyle PJ, Williams G. Dietary obesity in the rat induces endothelial dysfunction without causing insulin resistance: a possible role for triacylglycerols. *Clinical science (London, England : 1979)*. 2001;101(5):499-506.

173. Steinberg HO, Tarshoby M, Monestel R, Hook G, Cronin J, Johnson A, et al. Elevated circulating free fatty acid levels impair endothelium-dependent vasodilation. *The Journal of clinical investigation*. 1997;100(5):1230-9.

174. Naderali EK, Williams G. Prolonged endothelial-dependent and -independent arterial dysfunction induced in the rat by short-term feeding with a high-fat, high-sucrose diet. *Atherosclerosis*. 2003;166(2):253-9.

175. Chinen I, Shimabukuro M, Yamakawa K, Higa N, Matsuzaki T, Noguchi K, et al. Vascular lipotoxicity: endothelial dysfunction via fatty-acid-induced reactive oxygen species overproduction in obese Zucker diabetic fatty rats. *Endocrinology*. 2007;148(1):160-5.

176. Shankar K, Mehendale HM. Oxidative Stress. In: Wexler P, editor. *Encyclopedia of Toxicology (Third Edition)*. Oxford: Academic Press; 2014. p. 735-7.

177. Kim J-a, Montagnani M, Chandrasekran S, Quon MJ. Role of lipotoxicity in endothelial dysfunction. *Heart failure clinics*. 2012;8(4):589-607.

178. Joris PJ, Plat J, Kusters YH, Houben AJ, Stehouwer CD, Schalkwijk CG, et al. Diet-induced weight loss improves not only cardiometabolic risk markers but also markers of vascular function: a randomized controlled trial in abdominally obese men. *The American journal of clinical nutrition*. 2017;105(1):23-31.
179. Naderali EK, Fatani S, Williams G. Chronic withdrawal of a high-palatable obesity-inducing diet completely reverses metabolic and vascular abnormalities associated with dietary-obesity in the rat. *Atherosclerosis*. 2004;172(1):63-9.
180. Maiorana A, O'Driscoll G, Taylor R, Green D. Exercise and the Nitric Oxide Vasodilator System. *Sports Medicine*. 2003;33(14):1013-35.
181. Chou SH, Lee YC, Huang CF, Wang YR, Yu HP, Lau YT. Gender-specific effects of caloric restriction on the balance of vascular nitric oxide and superoxide radical. *Cardiovasc Res*. 2010;87(4):751-9.
182. Minamiyama Y, Bito Y, Takemura S, Takahashi Y, Kodai S, Mizuguchi S, et al. Calorie restriction improves cardiovascular risk factors via reduction of mitochondrial reactive oxygen species in type II diabetic rats. *J Pharmacol Exp Ther*. 2007;320(2):535-43.
183. Francque S, Verrijken A, Mertens I, Hubens G, Van Marck E, Pelckmans P, et al. Visceral adiposity and insulin resistance are independent predictors of the presence of non-cirrhotic NAFLD-related portal hypertension. *International journal of obesity (2005)*. 2011;35(2):270-8.
184. Cedo L, Santos D, Roglans N, Julve J, Pallares V, Rivas-Urbina A, et al. Human hepatic lipase overexpression in mice induces hepatic steatosis and obesity through promoting hepatic lipogenesis and white adipose tissue lipolysis and fatty acid uptake. *PLoS One*. 2017;12(12):e0189834.
185. Fracanzani AL, Valenti L, Bugianesi E, Andreoletti M, Colli A, Vanni E, et al. Risk of severe liver disease in nonalcoholic fatty liver disease with normal

aminotransferase levels: a role for insulin resistance and diabetes. *Hepatology* (Baltimore, Md). 2008;48(3):792-8.

186. Neuman MG, Cohen LB, Nanau RM. Biomarkers in nonalcoholic fatty liver disease. *Can J Gastroenterol Hepatol*. 2014;28(11):607-18.

187. Ferramosca A, Conte A, Damiano F, Siculella L, Zara V. Differential effects of high-carbohydrate and high-fat diets on hepatic lipogenesis in rats. *European journal of nutrition*. 2014;53(4):1103-14.

188. Mamun MAA, Faruk M, Rahman MM, Nahar K, Kabir F, Alam MA, et al. High Carbohydrate High Fat Diet Induced Hepatic Steatosis and Dyslipidemia Were Ameliorated by Psidium guajava Leaf Powder Supplementation in Rats. *Evid Based Complement Alternat Med*. 2019;2019:1897237.

189. Trovato FM, Castrogiovanni P, Szychlinska MA, Purrello F, Musumeci G. Early effects of high-fat diet, extra-virgin olive oil and vitamin D in a sedentary rat model of non-alcoholic fatty liver disease. *Histol Histopathol*. 2018;33(11):1201-13.

190. Mamikutty N, Thent ZC, Haji Suhaimi F. Fructose-Drinking Water Induced Nonalcoholic Fatty Liver Disease and Ultrastructural Alteration of Hepatocyte Mitochondria in Male Wistar Rat. *BioMed research international*. 2015;2015:895961.

191. Sun YY, Li XF, Meng XM, Huang C, Zhang L, Li J. Macrophage Phenotype in Liver Injury and Repair. *Scand J Immunol*. 2017;85(3):166-74.

192. Neuschwander-Tetri BA, Ford DA, Acharya S, Gilkey G, Basaranoglu M, Tetri LH, et al. Dietary trans-fatty acid induced NASH is normalized following loss of trans-fatty acids from hepatic lipid pools. *Lipids*. 2012;47(10):941-50.

193. Hazarika A, Kalita H, Chandra Boruah D, Chandra Kalita M, Devi R. Pathophysiology of metabolic syndrome: The onset of natural recovery on withdrawal of a high-carbohydrate, high-fat diet. *Nutrition*. 2016;32(10):1081-91.

194. Ipsen DH, Lykkesfeldt J, Tveden-Nyborg P. Molecular mechanisms of hepatic lipid accumulation in non-alcoholic fatty liver disease. *Cell Mol Life Sci*. 2018;75(18):3313-27.
195. Fuchs M, Sanyal AJ. Non-Alcoholic Fatty Liver Disease: A Pathophysiological Perspective. *The Liver* 2009. p. 719-41.
196. Solinas G, Borén J, Dulloo AG. De novo lipogenesis in metabolic homeostasis: More friend than foe? *Molecular metabolism*. 2015;4(5):367-77.
197. Softic S, Cohen DE, Kahn CR. Role of Dietary Fructose and Hepatic De Novo Lipogenesis in Fatty Liver Disease. *Dig Dis Sci*. 2016;61(5):1282-93.
198. Horton JD, Goldstein JL, Brown MS. SREBPs: activators of the complete program of cholesterol and fatty acid synthesis in the liver. *The Journal of clinical investigation*. 2002;109(9):1125-31.
199. Perfield JW, 2nd, Ortinau LC, Pickering RT, Ruebel ML, Meers GM, Rector RS. Altered hepatic lipid metabolism contributes to nonalcoholic fatty liver disease in leptin-deficient Ob/Ob mice. *Journal of obesity*. 2013;2013:296537.
200. Shimomura I, Bashmakov Y, Horton JD. Increased levels of nuclear SREBP-1c associated with fatty livers in two mouse models of diabetes mellitus. *J Biol Chem*. 1999;274(42):30028-32.
201. Sanders FWB, Griffin JL. De novo lipogenesis in the liver in health and disease: more than just a shunting yard for glucose. *Biol Rev Camb Philos Soc*. 2016;91(2):452-68.
202. Iizuka K, Bruick RK, Liang G, Horton JD, Uyeda K. Deficiency of carbohydrate response element-binding protein (ChREBP) reduces lipogenesis as well as glycolysis. *Proceedings of the National Academy of Sciences of the United States of America*. 2004;101(19):7281-6.

203. Iizuka K, Horikawa Y. ChREBP: A Glucose-activated Transcription Factor Involved in the Development of Metabolic Syndrome. *Endocrine Journal*. 2008;55(4):617-24.
204. Kim MS, Krawczyk SA, Doridot L, Fowler AJ, Wang JX, Trauger SA, et al. ChREBP regulates fructose-induced glucose production independently of insulin signaling. *The Journal of clinical investigation*. 2016;126(11):4372-86.
205. Mashek DG. Hepatic fatty acid trafficking: multiple forks in the road. *Adv Nutr*. 2013;4(6):697-710.
206. Skat-Rørdam J, Højland Ipsen D, Lykkesfeldt J, Tveden-Nyborg P. A role of peroxisome proliferator-activated receptor γ in non-alcoholic fatty liver disease. *Basic Clin Pharmacol Toxicol*. 2019;124(5):528-37.
207. Mashek DG. Hepatic fatty acid trafficking: multiple forks in the road. *Adv Nutr*. 2013;4(6):697-710.
208. Wang G, Bonkovsky HL, de Lemos A, Burczynski FJ. Recent insights into the biological functions of liver fatty acid binding protein 1. *Journal of lipid research*. 2015;56(12):2238-47.
209. Mukai T, Egawa M, Takeuchi T, Yamashita H, Kusudo T. Silencing of FABP1 ameliorates hepatic steatosis, inflammation, and oxidative stress in mice with nonalcoholic fatty liver disease. *FEBS Open Bio*. 2017;7(7):1009-16.
210. Charlton M, Viker K, Krishnan A, Sanderson S, Veldt B, Kaalsbeek AJ, et al. Differential expression of lumican and fatty acid binding protein-1: New insights into the histologic spectrum of nonalcoholic fatty liver disease. *Hepatology (Baltimore, Md)*. 2009;49(4):1375-84.
211. Stremmel W, Staffer S, Wannhoff A, Pathil A, Chamulitrat W. Plasma membrane phospholipase A2 controls hepatocellular fatty acid uptake and is

responsive to pharmacological modulation: implications for nonalcoholic steatohepatitis. *Faseb j.* 2014;28(7):3159-70.

212. Alves-Bezerra M, Cohen DE. Triglyceride Metabolism in the Liver. *Compr Physiol.* 2017;8(1):1-8.

213. Lavoie JM, Gauthier MS. Regulation of fat metabolism in the liver: link to non-alcoholic hepatic steatosis and impact of physical exercise. *Cellular and Molecular Life Sciences CMLS.* 2006;63(12):1393-409.

214. Reddy JK, Hashimoto T. Peroxisomal beta-oxidation and peroxisome proliferator-activated receptor alpha: an adaptive metabolic system. *Annu Rev Nutr.* 2001;21:193-230.

215. Francque S, Verrijken A, Caron S, Prawitt J, Paumelle R, Derudas B, et al. PPAR α gene expression correlates with severity and histological treatment response in patients with non-alcoholic steatohepatitis. *J Hepatol.* 2015;63(1):164-73.

216. Strable MS, Ntambi JM. Genetic control of de novo lipogenesis: role in diet-induced obesity. *Critical reviews in biochemistry and molecular biology.* 2010;45(3):199-214.

217. Fabbrini E, Mohammed BS, Magkos F, Korenblat KM, Patterson BW, Klein S. Alterations in adipose tissue and hepatic lipid kinetics in obese men and women with nonalcoholic fatty liver disease. *Gastroenterology.* 2008;134(2):424-31.

218. Mato JM, Alonso C, Nouredin M, Lu SC. Biomarkers and subtypes of deranged lipid metabolism in non-alcoholic fatty liver disease. *World journal of gastroenterology.* 2019;25(24):3009-20.

219. Li H, Ge J. Cardiovascular diseases in China: Current status and future perspectives. *IJC Heart & Vasculature.* 2015;6:25-31.

220. Ferre T, Riu E, Franckhauser S, Agudo J, Bosch F. Long-term overexpression of glucokinase in the liver of transgenic mice leads to insulin resistance. *Diabetologia*. 2003;46(12):1662-8.
221. Foretz M, Guichard C, Ferré P, Foufelle F. Sterol regulatory element binding protein-1c is a major mediator of insulin action on the hepatic expression of glucokinase and lipogenesis-related genes. *Proceedings of the National Academy of Sciences of the United States of America*. 1999;96(22):12737-42.
222. Brown MS, Goldstein JL. The SREBP pathway: regulation of cholesterol metabolism by proteolysis of a membrane-bound transcription factor. *Cell*. 1997;89(3):331-40.
223. Knebel B, Haas J, Hartwig S, Jacob S, Köllmer C, Nitzgen U, et al. Liver-specific expression of transcriptionally active SREBP-1c is associated with fatty liver and increased visceral fat mass. *PloS one*. 2012;7(2):e31812-e.
224. Xie Z, Li H, Wang K, Lin J, Wang Q, Zhao G, et al. Analysis of transcriptome and metabolome profiles alterations in fatty liver induced by high-fat diet in rat. *Metabolism*. 2010;59(4):554-60.
225. Giudetti AM, Micioni Di Bonaventura MV, Ferramosca A, Longo S, Micioni Di Bonaventura E, Friuli M, et al. Brief daily access to cafeteria-style diet impairs hepatic metabolism even in the absence of excessive body weight gain in rats. *Faseb j*. 2020;34(7):9358-71.
226. Higuchi N, Kato M, Shundo Y, Tajiri H, Tanaka M, Yamashita N, et al. Liver X receptor in cooperation with SREBP-1c is a major lipid synthesis regulator in nonalcoholic fatty liver disease. *Hepatol Res*. 2008;38(11):1122-9.
227. Yellaturu CR, Deng X, Park EA, Raghov R, Elam MB. Insulin enhances the biogenesis of nuclear sterol regulatory element-binding protein (SREBP)-1c by posttranscriptional down-regulation of Insig-2A and its dissociation from SREBP

cleavage-activating protein (SCAP).SREBP-1c complex. The Journal of biological chemistry. 2009;284(46):31726-34.

228. Foretz M, Guichard C, Ferré P, Foufelle F. Sterol regulatory element binding protein-1c is a major mediator of insulin action on the hepatic expression of glucokinase and lipogenesis-related genes. Proceedings of the National Academy of Sciences of the United States of America. 1999;96(22):12737-42.

229. Espenshade PJ, Hughes AL. Regulation of Sterol Synthesis in Eukaryotes. Annual Review of Genetics. 2007;41(1):401-27.

230. Engelking LJ, Kuriyama H, Hammer RE, Horton JD, Brown MS, Goldstein JL, et al. Overexpression of Insig-1 in the livers of transgenic mice inhibits SREBP processing and reduces insulin-stimulated lipogenesis. The Journal of clinical investigation. 2004;113(8):1168-75.

231. Ouyang S, Mo Z, Sun S, Yin K, Lv Y. Emerging role of Insig-1 in lipid metabolism and lipid disorders. Clinica Chimica Acta. 2020;508:206-12.

232. Fernández-Alvarez A, Alvarez MS, Gonzalez R, Cucarella C, Muntané J, Casado M. Human SREBP1c expression in liver is directly regulated by peroxisome proliferator-activated receptor alpha (PPARalpha). J Biol Chem. 2011;286(24):21466-77.

233. Lee C-H, Olson P, Evans RM. Minireview: Lipid Metabolism, Metabolic Diseases, and Peroxisome Proliferator-Activated Receptors. Endocrinology. 2003;144(6):2201-7.

234. Naguib G, Morris N, Yang S, Fryzek N, Haynes-Williams V, Huang W-CA, et al. Dietary fatty acid oxidation is decreased in non-alcoholic fatty liver disease: A palmitate breath test study. Liver International. 2020;40(3):590-7.

235. Hodson L, Frayn KN. Hepatic fatty acid partitioning. Curr Opin Lipidol. 2011;22(3):216-24.

236. Jensen-Urstad APL, Semenkovich CF. Fatty acid synthase and liver triglyceride metabolism: housekeeper or messenger? *Biochim Biophys Acta*. 2012;1821(5):747-53.
237. Sanyal AJ, Campbell-Sargent C, Mirshahi F, Rizzo WB, Contos MJ, Sterling RK, et al. Nonalcoholic steatohepatitis: association of insulin resistance and mitochondrial abnormalities. *Gastroenterology*. 2001;120(5):1183-92.
238. Kotronen A, Seppälä-Lindroos A, Vehkavaara S, Bergholm R, Frayn KN, Fielding BA, et al. Liver fat and lipid oxidation in humans. *Liver Int*. 2009;29(9):1439-46.
239. Croci I, Byrne NM, Choquette S, Hills AP, Chachay VS, Clouston AD, et al. Whole-body substrate metabolism is associated with disease severity in patients with non-alcoholic fatty liver disease. *Gut*. 2013;62(11):1625-33.
240. Simoes ICM, Janikiewicz J, Bauer J, Karkucinska-Wieckowska A, Kalinowski P, Dobrzyń A, et al. Fat and Sugar-A Dangerous Duet. A Comparative Review on Metabolic Remodeling in Rodent Models of Nonalcoholic Fatty Liver Disease. *Nutrients*. 2019;11(12):2871.
241. Renaud HJ, Cui JY, Lu H, Klaassen CD. Effect of diet on expression of genes involved in lipid metabolism, oxidative stress, and inflammation in mouse liver- insights into mechanisms of hepatic steatosis. *PLoS One*. 2014;9(2):e88584.
242. Reilich P, Horvath R, Krause S, Schramm N, Turnbull DM, Trenell M, et al. The phenotypic spectrum of neutral lipid storage myopathy due to mutations in the PNPLA2 gene. *Journal of Neurology*. 2011;258(11):1987-97.
243. Wang C, Tao Q, Wang X, Wang X, Zhang X. Impact of high-fat diet on liver genes expression profiles in mice model of nonalcoholic fatty liver disease. *Environmental Toxicology and Pharmacology*. 2016;45:52-62.

244. Huang H, Xie Z, Yokoyama W, Yu L, Wang TTY. Identification of liver CYP51 as a gene responsive to circulating cholesterol in a hamster model. *J Nutr Sci.* 2016;5:e16-e.
245. Boone LR, Brooks PA, Niesen MI, Ness GC. Mechanism of resistance to dietary cholesterol. *J Lipids.* 2011;2011:101242.
246. Dorn C, Engelmann JC, Saugspier M, Koch A, Hartmann A, Müller M, et al. Increased expression of c-Jun in nonalcoholic fatty liver disease. *Laboratory Investigation.* 2014;94(4):394-408.
247. Vanden Berghe W, Vermeulen L, Delerive P, De Bosscher K, Staels B, Haegeman G. A paradigm for gene regulation: inflammation, NF-kappaB and PPAR. *Adv Exp Med Biol.* 2003;544:181-96.
248. Stienstra R, Mandard S, Patsouris D, Maass C, Kersten S, Müller M. Peroxisome proliferator-activated receptor alpha protects against obesity-induced hepatic inflammation. *Endocrinology.* 2007;148(6):2753-63.
249. Roberts MD, Mobley CB, Toedebush RG, Heese AJ, Zhu C, Krieger AE, et al. Western diet-induced hepatic steatosis and alterations in the liver transcriptome in adult Brown-Norway rats. *BMC Gastroenterol.* 2015;15:151.
250. Schulien I, Hockenjos B, Schmitt-Graeff A, Perdekamp MG, Follo M, Thimme R, et al. The transcription factor c-Jun/AP-1 promotes liver fibrosis during non-alcoholic steatohepatitis by regulating Osteopontin expression. *Cell Death & Differentiation.* 2019;26(9):1688-99.
251. Li Z, Yu P, Wu J, Tao F, Zhou J. Transcriptional Regulation of Early Growth Response Gene-1 (EGR1) is Associated with Progression of Nonalcoholic Fatty Liver Disease (NAFLD) in Patients with Insulin Resistance. *Med Sci Monit.* 2019;25:2293-3004.

252. Bali DS, Goldstein JL, Fredrickson K, Rehder C, Boney A, Austin S, et al. Variability of disease spectrum in children with liver phosphorylase kinase deficiency caused by mutations in the PHKG2 gene. *Molecular Genetics and Metabolism*. 2014;111(3):309-13.
253. Burwinkel B, Rootwelt T, Kvittingen EA, Chakraborty PK, Kilimann MW. Severe Phenotype of Phosphorylase Kinase-Deficient Liver Glycogenosis with Mutations in the PHKG2 Gene. *Pediatric Research*. 2003;54(6):834-9.
254. Foretz M, Pacot C, Dugail I, Lemarchand P, Guichard C, Le Lièpvre X, et al. ADD1/SREBP-1c is required in the activation of hepatic lipogenic gene expression by glucose. *Mol Cell Biol*. 1999;19(5):3760-8.
255. Jang J, Jung Y, Chae S, Cho SH, Yoon M, Yang H, et al. Gangjihwan, a polyherbal composition, inhibits fat accumulation through the modulation of lipogenic transcription factors SREBP1C, PPAR γ and C/EBP α . *J Ethnopharmacol*. 2018;210:10-22.
256. Meng Q, Duan XP, Wang CY, Liu ZH, Sun PY, Huo XK, et al. Alisol B 23-acetate protects against non-alcoholic steatohepatitis in mice via farnesoid X receptor activation. *Acta Pharmacol Sin*. 2017;38(1):69-79.
257. Song H, Zheng Z, Wu J, Lai J, Chu Q, Zheng X. White Pitaya (*Hylocereus undatus*) Juice Attenuates Insulin Resistance and Hepatic Steatosis in Diet-Induced Obese Mice. *PloS one*. 2016;11(2):e0149670-e.
258. Stone SJ, Myers HM, Watkins SM, Brown BE, Feingold KR, Elias PM, et al. Lipopenia and skin barrier abnormalities in DGAT2-deficient mice. *J Biol Chem*. 2004;279(12):11767-76.
259. Li J, Jiang R, Cong X, Zhao Y. UCP2 gene polymorphisms in obesity and diabetes, and the role of UCP2 in cancer. *FEBS Letters*. 2019;593(18):2525-34.

260. Lindquist C, Bjørndal B, Rossmann CR, Tusubira D, Svardal A, Røslund GV, et al. Increased hepatic mitochondrial FA oxidation reduces plasma and liver TG levels and is associated with regulation of UCPs and APOC-III in rats. *Journal of lipid research*. 2017;58(7):1362-73.
261. Yamazaki T, Okawa S, Takahashi M. The effects on weight loss and gene expression in adipose and hepatic tissues of very-low carbohydrate and low-fat isoenergetic diets in diet-induced obese mice. *Nutr Metab (Lond)*. 2016;13:78-.
262. Mardinoglu A, Wu H, Bjornson E, Zhang C, Hakkarainen A, Räsänen SM, et al. An Integrated Understanding of the Rapid Metabolic Benefits of a Carbohydrate-Restricted Diet on Hepatic Steatosis in Humans. *Cell metabolism*. 2018;27(3):559-71.e5.
263. Kennedy MA, Barrera GC, Nakamura K, Baldán A, Tarr P, Fishbein MC, et al. ABCG1 has a critical role in mediating cholesterol efflux to HDL and preventing cellular lipid accumulation. *Cell metabolism*. 2005;1(2):121-31.
264. Cui R, Gao M, Qu S, Liu D. Overexpression of superoxide dismutase 3 gene blocks high-fat diet-induced obesity, fatty liver and insulin resistance. *Gene Ther*. 2014;21(9):840-8.
265. Naik A, Košir R, Rozman D. Genomic aspects of NAFLD pathogenesis. *Genomics*. 2013;102(2):84-95.
266. Zhang L, Xu P, Cheng Y, Wang P, Ma X, Liu M, et al. Diet-induced obese alters the expression and function of hepatic drug-metabolizing enzymes and transporters in rats. *Biochemical Pharmacology*. 2019;164:368-76.
267. Liao Y, Shikapwashya ON, Shteyer E, Dieckgraefe BK, Hruz PW, Rudnick DA. Delayed hepatocellular mitotic progression and impaired liver regeneration in early growth response-1-deficient mice. *J Biol Chem*. 2004;279(41):43107-16.

268. Biesiada E, Krawczyk Z, Chorazy M. Expression of c-jun and Egr-1 genes in rat liver in response to partial hepatectomy, and injection of turpentine. *Cell Biol Int Rep*. 1992;16(1):53-62.
269. Diehl AM, Yin M, Fleckenstein J, Yang SQ, Lin HZ, Brenner DA, et al. Tumor necrosis factor-alpha induces c-jun during the regenerative response to liver injury. *American Journal of Physiology-Gastrointestinal and Liver Physiology*. 1994;267(4):G552-G61.
270. Seki E, Brenner DA, Karin M. A Liver Full of JNK: Signaling in Regulation of Cell Function and Disease Pathogenesis, and Clinical Approaches. *Gastroenterology*. 2012;143(2):307-20.
271. Kamata H, Honda S-i, Maeda S, Chang L, Hirata H, Karin M. Reactive Oxygen Species Promote TNF α -Induced Death and Sustained JNK Activation by Inhibiting MAP Kinase Phosphatases. *Cell*. 2005;120(5):649-61.
272. Dorn C, Engelmann JC, Saugspier M, Koch A, Hartmann A, Müller M, et al. Increased expression of c-Jun in nonalcoholic fatty liver disease. *Lab Invest*. 2014;94(4):394-408.
273. Fingerle-Rowson GR, Bucala R. Neuroendocrine properties of macrophage migration inhibitory factor (MIF). *Immunology & Cell Biology*. 2001;79(4):368-75.
274. Moon HY, Song P, Choi CS, Ryu SH, Suh P-G. Involvement of exercise-induced macrophage migration inhibitory factor in the prevention of fatty liver disease. *The Journal of endocrinology*. 2013;218(3):339-48.
275. Keinicke H, Sun G, Mentzel CMJ, Fredholm M, John LM, Andersen B, et al. FGF21 regulates hepatic metabolic pathways to improve steatosis and inflammation. *Endocr Connect*. 2020;9(8):755-68.

276. Coskun T, Bina HA, Schneider MA, Dunbar JD, Hu CC, Chen Y, et al. Fibroblast growth factor 21 corrects obesity in mice. *Endocrinology*. 2008;149(12):6018-27.
277. Laurila JP, Castellone MD, Curcio A, Laatikainen LE, Haaparanta-Solin M, Gronroos TJ, et al. Extracellular superoxide dismutase is a growth regulatory mediator of tissue injury recovery. *Mol Ther*. 2009;17(3):448-54.
278. Abu-Farha M, Dehbi M, Noronha F, Tiss A, Alarouj M, Behbehani K, et al. Gender differences in ghrelin association with cardiometabolic risk factors in arab population. *Int J Endocrinol*. 2014;2014:730472.
279. Gerds E, Regitz-Zagrosek V. Sex differences in cardiometabolic disorders. *Nature medicine*. 2019;25(11):1657-66.
280. Schorr M, Dichtel LE, Gerweck AV, Valera RD, Torriani M, Miller KK, et al. Sex differences in body composition and association with cardiometabolic risk. *Biol Sex Differ*. 2018;9(1):28-.
281. Krotkiewski M, Björntorp P, Sjöström L, Smith U. Impact of obesity on metabolism in men and women. Importance of regional adipose tissue distribution. *The Journal of clinical investigation*. 1983;72(3):1150-62.
282. Dmitruk A, Czezelewski J, Czezelewska E, Golach J, Parnicka U. Body composition and fatty tissue distribution in women with various menstrual status. *Rocz Panstw Zakl Hig*. 2018;69(1):95-101.
283. Wang N, Liu Y, Ma Y, Wen D. High-intensity interval versus moderate-intensity continuous training: Superior metabolic benefits in diet-induced obesity mice. *Life Sci*. 2017;191:122-31.
284. Hasin Y, Seldin M, Lusk A. Multi-omics approaches to disease. *Genome Biology*. 2017;18(1):83.

285. Feder ME, Walser JC. The biological limitations of transcriptomics in elucidating stress and stress responses. *J Evol Biol.* 2005;18(4):901-10.
286. Vogel C, Marcotte EM. Insights into the regulation of protein abundance from proteomic and transcriptomic analyses. *Nat Rev Genet.* 2012;13(4):227-32.
287. da Silva-Santi LG, Antunes MM, Caparroz-Assef SM, Carbonera F, Masi LN, Curi R, et al. Liver Fatty Acid Composition and Inflammation in Mice Fed with High-Carbohydrate Diet or High-Fat Diet. *Nutrients.* 2016;8(11).

APPENDICES

Appendix 1: List of differentially expressed genes between CAF vs NC exported from TAC 4.0 software. Blue highlight represents upregulated genes and red highlight represents downregulated genes.

Gene Symbol	Fold Change	P-val	FDR P-val	Description
Tm7sf2	-18.25	2.03E-19	4.71E-15	transmembrane 7 superfamily member 2
Cyp51	-7.05	2.93E-17	3.40E-13	cytochrome P450, family 51
Tymp	11.19	6.13E-17	4.74E-13	thymidine phosphorylase
Fmo5	-35.93	2.71E-15	1.57E-11	flavin containing monooxygenase 5
Sqle	-12.19	1.11E-14	5.16E-11	squalene epoxidase
Msmo1	-9.36	1.49E-14	5.75E-11	methylsterol monooxygenase 1
Dhcr24	-5.48	1.32E-13	4.37E-10	24-dehydrocholesterol reductase
Cyp3a9	-11.21	4.57E-13	1.32E-09	cytochrome P450, family 3, subfamily a, polypeptide 9
Car2	-3.39	7.95E-13	2.05E-09	carbonic anhydrase 2
Gck	13.51	1.40E-12	2.97E-09	glucokinase
Ar	6.44	1.41E-12	2.97E-09	androgen receptor
Inhba	3.61	2.92E-12	5.64E-09	inhibin beta-A
Junb	-14.85	2.89E-11	5.15E-08	jun B proto-oncogene
Cyp8b1	-6.12	3.11E-11	5.15E-08	cytochrome P450, family 8, subfamily b, polypeptide 1
Hsd17b7	-4.06	2.20E-10	3.40E-07	hydroxysteroid (17-beta) dehydrogenase 7
Slc4a4	-3.47	3.96E-10	5.73E-07	solute carrier family 4, sodium bicarbonate cotransporter, member 4
G6pc	-5.4	5.13E-10	7.00E-07	glucose-6-phosphatase, catalytic subunit
Cyp1a2	-5.15	6.18E-10	7.96E-07	cytochrome P450, family 1, subfamily a, polypeptide 2
Idi1	-4.88	6.87E-10	8.39E-07	isopentenyl-diphosphate delta isomerase 1
Dap	-2.96	8.57E-10	9.93E-07	death-associated protein

Acnat2	2.98	1.05E-09	1.16E-06	acyl-coenzyme A amino acid N-acyltransferase 2
Fdft1	-3.48	1.22E-09	1.29E-06	farnesyl diphosphate farnesyl transferase 1
Hsd17b13	2.94	1.43E-09	1.43E-06	hydroxysteroid (17-beta) dehydrogenase 13
Ass1	-2.65	1.48E-09	1.43E-06	argininosuccinate synthase 1
Fdps	-3.53	5.10E-09	4.73E-06	farnesyl diphosphate synthase
Egr1	-6.28	6.65E-09	5.93E-06	early growth response 1
Otc	2.15	1.20E-08	1.00E-05	ornithine cTri3bamoyltransferase
Fzd4	-3.05	1.21E-08	1.00E-05	frizzled class receptor 4
Slc22a5	-3.2	1.36E-08	1.09E-05	solute carrier family 22 (organic cation/carnitine transporter), member 5
Prkcdp	-3.91	1.47E-08	1.13E-05	protein kinase C, delta binding protein
Ypel3	2.2	1.80E-08	1.35E-05	yippee-like 3
Car3	5.51	2.08E-08	1.51E-05	carbonic anhydrase 3
Ak4	2.55	3.17E-08	2.23E-05	adenylate kinase 4
Cxcl14	-4.81	4.14E-08	2.66E-05	chemokine (C-X-C motif) ligand 14
Amacr	-2.1	4.17E-08	2.66E-05	alpha-methylacyl-CoA racemase
Hsd17b6	-3.68	4.22E-08	2.66E-05	hydroxysteroid (17-beta) dehydrogenase 6
Agxt2	3.82	4.25E-08	2.66E-05	alanine-glyoxylate aminotransferase 2
LOC100362350	-3.51	4.42E-08	2.70E-05	hydroxysteroid 17-beta dehydrogenase 6-like [Source:RGD Symbol;Acc:2318336]; ENCODE a protein that exhibits nucleotide binding (inferred) AND oxidoreductase activity (inferred)
Loxl4	-2.14	5.11E-08	3.04E-05	lysyl oxidase-like 4
Fam210b	3.43	6.23E-08	3.61E-05	family with sequence similarity 210, member B
Asl	-5.69	8.97E-08	4.95E-05	argininosuccinate lyase
Ier3	-3.92	1.22E-07	6.59E-05	immediate early response 3

Nucb2	2.26	1.41E-07	7.42E-05	nucleobindin 2
Marco	-14.82	1.81E-07	9.10E-05	macrophage receptor with collagenous structure
Acot7	-2.41	1.84E-07	9.10E-05	acyl-CoA thioesterase 7
Papss2	-2.55	2.61E-07	0.0001	3-phosphoadenosine 5-phosphosulfate synthase 2
Cpt1a	-4.63	2.66E-07	0.0001	carnitine palmitoyltransferase 1a, liver
Ebp	-2.31	2.97E-07	0.0001	emopamil binding protein (sterol isomerase)
Gsta3	-3.62	3.26E-07	0.0001	glutathione S-transferase alpha 3
P2ry2	-2.02	3.81E-07	0.0002	purinergic receptor P2Y, G-protein coupled, 2
Sqrdl	-3.44	4.37E-07	0.0002	sulfide quinone reductase-like (yeast)
Phgdh	3.56	4.52E-07	0.0002	phosphoglycerate dehydrogenase
RGD1559600	2.62	5.28E-07	0.0002	RGD1559600
Dhcr7	-2.64	5.40E-07	0.0002	7-dehydrocholesterol reductase
Pfkfb1	6.95	5.54E-07	0.0002	6-phosphofructo-2-kinase/fructose-2,6-biphosphatase 1
Igfbp1	-6.4	5.91E-07	0.0002	insulin-like growth factor binding protein 1
Got1	-4.29	5.95E-07	0.0002	glutamic-oxaloacetic transaminase 1, soluble
Col14a1	-2.91	6.02E-07	0.0002	collagen, type XIV, alpha 1
Hmox1	-4.26	6.02E-07	0.0002	heme oxygenase 1
Srebf1	2.99	6.31E-07	0.0002	sterol regulatory element binding transcription factor 1
Chka	3.87	7.21E-07	0.0003	choline kinase alpha
Tprg1l	-2.07	7.48E-07	0.0003	tumor protein p63 regulated 1-like
Cyp3a62	3.49	7.99E-07	0.0003	cytochrome P450, family 3, subfamily a, polypeptide 62
Acsf2	-2.13	8.07E-07	0.0003	acyl-CoA synthetase family member 2

Hmgcs1	-3.67	8.23E-07	0.0003	3-hydroxy-3-methylglutaryl-CoA synthase 1 (soluble)
C1rl	-2.96	8.31E-07	0.0003	complement component 1, r subcomponent-like
Maob	2.04	9.07E-07	0.0003	monoamine oxidase B
Nnmt	-2.72	1.04E-06	0.0003	nicotinamide N-methyltransferase
Cyp2c22	2.78	1.07E-06	0.0003	cytochrome P450, family 2, subfamily c, polypeptide 22
RGD1309821	-2.04	1.42E-06	0.0005	similar to KIAA1161 protein
Agxt	-2.61	1.43E-06	0.0005	alanine-glyoxylate aminotransferase
Sez6	3.4	1.51E-06	0.0005	seizure related 6 homolog (mouse)
Cd14	-2.84	1.55E-06	0.0005	CD14 molecule
RGD1566035; LOC102547074	2.35	1.74E-06	0.0005	Protein tyrosine phosphatase type IVA 1; INTERACTS WITH (-)-demecolcine (ortholog) AND (-)-epigallocatechin 3-gallate (ortholog) AND (S)-colchicine (ortholog)
Slc38a3	-3.13	1.80E-06	0.0005	solute carrier family 38, member 3
Abcb1a	-3.28	1.91E-06	0.0006	ATP-binding cassette, sub-family B (MDR/TAP), member 1A
LOC500300	-3.44	2.29E-06	0.0007	similar to hypothetical protein MGC6835; FOUND IN mitochondrion (ortholog) AND INTERACTS WITH 1-naphthyl isothiocyanate (ortholog) AND 17beta-estradiol (ortholog) AND 2 3 7 8-tetrachlorodibenzodioxine (ortholog)
Ppp1r3b	2.4	2.31E-06	0.0007	protein phosphatase 1, regulatory subunit 3B
Slc17a4	-3.03	2.33E-06	0.0007	solute carrier family 17, member 4
Ido2	-2.77	2.42E-06	0.0007	indoleamine 2,3-dioxygenase 2 [Source:RGD Symbol;Acc:1596771]; indoleamine 2,3-dioxygenase 2; ENCODES a protein that exhibits indoleamine 2 3-dioxygenase activity (ortholog) AND tryptophan 2 3-dioxygenase activity (ortholog) AND INVOLVED IN oxidation-reduction process (ortholog) AND tryptophan catabolic process to kynurenine (ortholog) AND

				PARTICIPATES IN Trypanosoma brucei infection pathway AND tryptophan metabolic pathway AND FOUND IN cytoplasm (ortholog) AND INTERACTS WITH orphenadrine AND thioacetamide AND (2 4 5-trichlorophenoxy)acetic acid (ortholog)
Hba2; Hba1	-2.01	2.47E-06	0.0007	hemoglobin, alpha 2; hemoglobin, alpha 1
Spsb1	-2.33	2.48E-06	0.0007	splA/ryanodine receptor domain and SOCS box containing 1
Srebf2	-2.49	2.55E-06	0.0007	sterol regulatory element binding transcription factor 2
Kif21a	-2.05	2.61E-06	0.0007	kinesin family member 21A
Slc16a10	-4.79	2.95E-06	0.0008	solute carrier family 16 (aromatic amino acid transporter), member 10
Slc26a11	-2.31	3.14E-06	0.0008	solute carrier family 26 (anion exchanger), member 11 [Source:RGD Symbol;Acc:1306178]; ENCODES a protein that exhibits anion transmembrane transporter activity (ortholog) AND INVOLVED IN sulfate transport (ortholog) AND FOUND IN endoplasmic reticulum (ortholog) AND extracellular vesicular exosome (ortholog) AND Golgi apparatus (ortholog) AND INTERACTS WITH 17beta-estradiol (ortholog) AND 2-methylcholine (ortholog) AND 3 4-methylenedioxymethamphetamine (ortholog); solute carrier family 26 (anion exchanger), member 11
Il17rb	-3.93	3.60E-06	0.0009	interleukin 17 receptor B
RT1-DMb	-2.23	3.83E-06	0.001	RT1 class II, locus DMb
Acmsd	-3.27	3.99E-06	0.001	aminocarboxymuconate semialdehyde decarboxylase
Gstk1	-3.43	4.54E-06	0.0011	glutathione S-transferase kappa 1
Sh3gl3	-2.9	5.02E-06	0.0012	SH3-domain GRB2-like 3
Atp11c	-2.01	6.08E-06	0.0015	ATPase, class VI, type 11C
Cav2	2.43	6.38E-06	0.0015	caveolin 2
Psat1	3.34	7.00E-06	0.0017	phosphoserine aminotransferase 1

Hao1	2.13	7.26E-06	0.0017	hydroxyacid oxidase (glycolate oxidase) 1
Oat	-2.6	8.50E-06	0.002	ornithine aminotransferase
Ivns1abp	2.3	9.72E-06	0.0022	influenza virus NS1A binding protein
Socs3	-2.71	9.98E-06	0.0022	suppressor of cytokine signaling 3
LOC100910385	-2.05	1.15E-05	0.0025	peroxisomal acyl-coenzyme A oxidase 1-like
Prlr	-2.19	1.16E-05	0.0025	prolactin receptor
Upp2	-7.51	1.20E-05	0.0025	uridine phosphorylase 2
Ggct	2.24	1.26E-05	0.0027	gamma-glutamyl cyclotransferase
Comt	-3.07	1.28E-05	0.0027	catechol-O-methyltransferase
Aig1	-2.93	1.28E-05	0.0027	androgen-induced 1
Cyp2b2	5.22	1.41E-05	0.0029	cytochrome P450, family 2, subfamily b, polypeptide 2
Pnpla2; LOC100911615	-2.23	1.45E-05	0.0029	patatin-like phospholipase domain containing 2 (Pnpla2), mRNA; ENCODES a protein that exhibits triglyceride lipase activity (ortholog) AND INVOLVED IN lipid particle organization (ortholog) AND lipid storage (ortholog) AND negative regulation of sequestering of triglyceride (ortholog) AND ASSOCIATED WITH Neutral Lipid Storage Disease with Myopathy (ortholog) AND FOUND IN cytosol (ortholog) AND intracellular membrane-bounded organelle (ortholog) AND lipid particle (ortholog) AND INTERACTS WITH (+)-catechin AND 17alpha-ethynylestradiol AND 2 3 7 8-tetrachlorodibenzodioxine; patatin-like phospholipase domain containing 2; patatin-like phospholipase domain containing 2 (Pnpla2), mRNA.
Cyp2b1; LOC100909962	11.69	1.52E-05	0.003	cytochrome P450, family 2, subfamily b, polypeptide 1; ENCODES a protein that exhibits steroid hydroxylase activity AND INVOLVED IN drug metabolic process AND response to calcium ion AND response to drug AND PARTICIPATES IN arachidonic acid metabolic pathway AND phase I biotransformation pathway via cytochrome P450 AND retinol metabolic pathway AND ASSOCIATED WITH Acute Lung Injury AND Depressive Disorder

				AND Diabetes Mellitus Experimental AND FOUND IN intracellular membrane-bounded organelle AND INTERACTS WITH (+)-artemisinin AND (-)-cotinine AND (S)-nicotine; cytochrome P450 2B1-like
Aco1	-2.08	1.54E-05	0.003	aconitase 1, soluble
Itm2c	-2.05	1.65E-05	0.0032	integral membrane protein 2C
Hal	-2.13	1.67E-05	0.0032	histidine ammonia lyase
Gls2	-2.02	1.78E-05	0.0034	glutaminase 2 (liver, mitochondrial)
Pnpla7	-2.07	1.80E-05	0.0034	patatin-like phospholipase domain containing 7
Btg2	-2.74	1.90E-05	0.0036	BTG family, member 2
Tmem8a	-2.26	2.01E-05	0.0037	transmembrane protein 8A
Mt1f	-3.64	2.20E-05	0.004	metallothionein 1F
Mbnl3	-2.69	2.65E-05	0.0047	muscleblind-like splicing regulator 3
Cabp2	2.32	2.68E-05	0.0047	calcium binding protein 2
Sebox	2.39	2.80E-05	0.0048	SEBOX homeobox
Trib3	-6.88	2.81E-05	0.0048	tribbles pseudokinase 3
Abhd1	-2.3	2.92E-05	0.005	abhydrolase domain containing 1
A2m	2.93	3.02E-05	0.005	alpha-2-macroglobulin
Insig1	-2.98	3.11E-05	0.0051	insulin induced gene 1
Thbd	-2.02	3.34E-05	0.0054	thrombomodulin
Hbb	-2.8	3.67E-05	0.0058	hemoglobin, beta
Mt1a	-2.74	3.87E-05	0.0061	metallothionein 1a
Smco4	-2.06	3.98E-05	0.0062	single-pass membrane protein with coiled-coil domains 4
Gjb2	-2.23	4.04E-05	0.0062	gap junction protein, beta 2
Camk2n1	-3.22	4.17E-05	0.0064	calcium/calmodulin-dependent protein kinase II inhibitor 1

Afmid	3.02	4.33E-05	0.0066	arylformamidase
Ech1	-2.64	4.43E-05	0.0066	enoyl CoA hydratase 1, peroxisomal
Ifitm3	-2.09	4.50E-05	0.0066	interferon induced transmembrane protein 3; INVOLVED IN cardiac muscle cell differentiation AND heart development AND defense response to virus (ortholog) AND FOUND IN apical part of cell (ortholog) AND cell surface (ortholog) AND cytoplasm (ortholog) AND INTERACTS WITH 17alpha-ethynylestradiol AND 2 3 7 8-tetrachlorodibenzodioxine AND 3 4-dichloroaniline; interferon induced transmembrane protein 3 (Ifitm3), mRNA.
Slc1a2	-4.71	4.50E-05	0.0066	solute carrier family 1 (glial high affinity glutamate transporter), member 2
Ptgfrn	-2.04	4.51E-05	0.0066	prostaglandin F2 receptor inhibitor
Chd1l	-4.13	4.51E-05	0.0066	chromodomain helicase DNA binding protein 1-like
Mt1a	-3.02	4.63E-05	0.0067	metallothionein 1a
Aass	-2.21	4.84E-05	0.007	aminoadipate-semialdehyde synthase
RGD1310495	-2.1	4.92E-05	0.007	similar to KIAA1919 protein [Source:RGD Symbol;Acc:1310495]; INTERACTS WITH sodium dichromate AND thioacetamide AND diarsenic trioxide (ortholog)
Tmem97	-2.03	5.07E-05	0.0071	transmembrane protein 97
Ppp2r5e	2.02	5.08E-05	0.0071	protein phosphatase 2, regulatory subunit B, epsilon isoform
Dio1	2.91	5.10E-05	0.0071	deiodinase, iodothyronine, type I
Ptp4a1	2.22	5.41E-05	0.0074	protein tyrosine phosphatase type IVA, member 1; protein tyrosine phosphatase type IVA, member 1 [Source:RGD Symbol;Acc:61970]; ENCODES a protein that exhibits protein tyrosine phosphatase activity AND INVOLVED IN peptidyl-tyrosine dephosphorylation AND positive regulation of cell migration (ortholog) AND FOUND IN nucleus AND cytoplasm (ortholog) AND cytoplasmic side of plasma membrane (ortholog) AND INTERACTS WITH 2 3 7 8-tetrachlorodibenzodioxine AND 2-nitrofluorene AND 3H-1 2-dithiole-

				3-thione; Chalmel, et. al. AceView Annotation Ptp4a1.cSep08
Car8	2.65	5.46E-05	0.0075	carbonic anhydrase 8
Mapkapk2	-2.22	6.08E-05	0.008	mitogen-activated protein kinase-activated protein kinase 2
Ndnf	3.24	6.09E-05	0.008	neuron-derived neurotrophic factor [Source:RGD Symbol;Acc:1311080]; ENCODES a protein that exhibits glycosaminoglycan binding (ortholog) AND heparin binding (ortholog) AND INVOLVED IN cell growth (ortholog) AND extracellular matrix organization (ortholog) AND negative regulation of neuron apoptotic process (ortholog) AND FOUND IN extracellular matrix (ortholog) AND extracellular region (ortholog) AND INTERACTS WITH all-trans-retinoic acid AND cisplatin AND cocaine
Stox2	-2.03	6.16E-05	0.0081	storkhead box 2
Veph1	2.42	6.20E-05	0.0081	ventricular zone expressed PH domain- containing 1
Cyr61	-3.76	6.25E-05	0.0081	cysteine-rich, angiogenic inducer, 61
Gys2	-2.07	6.65E-05	0.0084	glycogen synthase 2
Oaf	-2.82	6.69E-05	0.0084	out at first homolog
Pepd	-2.04	6.71E-05	0.0084	peptidase D
Tmem163	-2.32	6.74E-05	0.0084	transmembrane protein 163
Dpp6	2.4	6.87E-05	0.0086	dipeptidylpeptidase 6
LOC688922; LOC100909424	-2.36	6.96E-05	0.0086	similar to Insulin-induced gene 1 protein (INSIG-1) (Insulin-induced growth response protein CL-6) (Immediate-early protein CL-6) [Source:RGD Symbol;Acc:1582985]; similar to Insulin- induced gene 1 protein (INSIG-1) (Insulin- induced growth response protein CL-6) (Immediate-early protein CL-6); uncharacterized LOC100909424
Bbs10	2.12	7.49E-05	0.0092	Bardet-Biedl syndrome 10
Ppm1k	-2.48	8.26E-05	0.0099	protein phosphatase, Mg2+/Mn2+ dependent, 1K

Nab1	-2.06	8.27E-05	0.0099	Ngfi-A binding protein 1
Slx1b	-2.04	8.70E-05	0.0102	SLX1 structure-specific endonuclease subunit homolog B (<i>S. cerevisiae</i>)
Asns	2.12	8.80E-05	0.0103	asparagine synthetase (glutamine-hydrolyzing)
Apopf	14.81	8.92E-05	0.0104	apolipoprotein F
Slc5a6	-2.62	9.57E-05	0.011	solute carrier family 5 (sodium/multivitamin and iodide cotransporter), member 6
Slc35c2	22.32	9.79E-05	0.0112	solute carrier family 35 (GDP-fucose transporter), member C2
Stard4	-2.04	0.0001	0.0113	StAR-related lipid transfer (START) domain containing 4
Rhob	2.67	0.0001	0.0115	ras homolog family member B
Sik2	-2.61	0.0001	0.012	salt inducible kinase 2 [Source:MGI Symbol;Acc:MGI:2445031]; salt-inducible kinase 2
Hsp90b1	2.24	0.0001	0.0145	heat shock protein 90, beta, member 1
Tmem135	-2.14	0.0001	0.0147	transmembrane protein 135
Leap2	2.41	0.0001	0.0151	liver-expressed antimicrobial peptide 2
Angptl4	-2.37	0.0001	0.0152	angiopoietin-like 4
5330417C22Rik; RGD1310209	2.36	0.0001	0.0152	RIKEN cDNA 5330417C22 gene [Source:MGI Symbol;Acc:MGI:1923930]; similar to KIAA1324 protein
Igfbp3	-2.02	0.0002	0.0156	insulin-like growth factor binding protein 3
Oplah	-2.05	0.0002	0.016	5-oxoprolinase (ATP-hydrolysing)
LOC102553917	2.35	0.0002	0.016	putative zinc finger protein 724-like
Zfp189	2.29	0.0002	0.0165	zinc finger protein 189
Adh6	-7.65	0.0002	0.0167	alcohol dehydrogenase 6 (class V)
LOC691828	2.11	0.0002	0.0175	uncharacterized LOC691828 [Source:RGD Symbol;Acc:7592549]
Pla2g16	-2.82	0.0002	0.0186	phospholipase A2, group XVI

RGD1562699	-2.67	0.0002	0.0186	RGD1562699
Gnmt	-2.13	0.0002	0.0194	glycine N-methyltransferase
Srd5a1	-2.15	0.0002	0.0209	steroid-5-alpha-reductase, alpha polypeptide 1 (3-oxo-5 alpha-steroid delta 4-dehydrogenase alpha 1)
RGD1307603	2.1	0.0002	0.0211	similar to hypothetical protein MGC37914
Tmcc2	-2.21	0.0002	0.0211	transmembrane and coiled-coil domain family 2
Fam213a	-2.46	0.0002	0.0214	family with sequence similarity 213, member A
Pdlim1	2.93	0.0003	0.022	PDZ and LIM domain 1
Ppp1r3c; PPP1R3C; LOC100910671	4.2	0.0003	0.0221	protein phosphatase 1, regulatory subunit 3C; Protein phosphatase 1 regulatory subunit 3; ENCODES a protein that exhibits enzyme binding AND phosphoprotein phosphatase activity AND protein phosphatase binding (ortholog) AND INVOLVED IN dephosphorylation AND regulation of glycogen biosynthetic process AND regulation of glycogen catabolic process AND PARTICIPATES IN glycogen biosynthetic pathway AND glycogen degradation pathway AND insulin signaling pathway AND FOUND IN glycogen granule AND intracellular membrane-bounded organelle AND INTERACTS WITH 17alpha-ethynylestradiol AND 2' 5' 5'-tetrachlorobiphenyl AND 2 3 7 8-tetrachlorodibenzodioxine; INTERACTS WITH 17beta-estradiol (ortholog) AND 2 3 7 8-tetrachlorodibenzodioxine (ortholog) AND 2-methylcholine (ortholog)
Cd4	-2.02	0.0003	0.0225	Cd4 molecule
Nim1k	2.33	0.0003	0.0229	NIM1 serine/threonine protein kinase
St6galnac4	-2.3	0.0003	0.0233	ST6 (alpha-N-acetyl-neuraminyl-2,3-beta-galactosyl-1,3)-N-acetylgalactosaminide alpha-2,6-sialyltransferase 4
Idh2	2.91	0.0003	0.0238	isocitrate dehydrogenase 2 (NADP+), mitochondrial
Odf3b	2.06	0.0003	0.0243	outer dense fiber of sperm tails 3B

LOC100134871	-2.25	0.0003	0.0243	beta globin minor gene
Uck2	-2.04	0.0003	0.0243	uridine-cytidine kinase 2
Pygl	2.29	0.0003	0.025	phosphorylase, glycogen, liver
Fos	-3.87	0.0003	0.025	FBJ osteosarcoma oncogene
Slc25a23	2.93	0.0003	0.025	solute carrier family 25 (mitochondrial carrier; phosphate carrier), member 23
Ctss	-2.15	0.0003	0.0253	cathepsin S
Cyp4a1	-3.82	0.0003	0.0253	cytochrome P450, family 4, subfamily a, polypeptide 1
Klb	2.01	0.0004	0.0265	klotho beta [Source:RGD Symbol;Acc:1308227]; klotho beta; ENCODES a protein that exhibits fibroblast growth factor binding (ortholog) AND INVOLVED IN fibroblast growth factor receptor signaling pathway (ortholog) AND positive regulation of cell proliferation (ortholog) AND positive regulation of MAPKKK cascade by fibroblast growth factor receptor signaling pathway (ortholog) AND PARTICIPATES IN fibroblast growth factor signaling pathway AND INTERACTS WITH 2 3 7 8-tetrachlorodibenzodioxine (ortholog) AND aflatoxin B1 (ortholog) AND benzo[a]pyrene (ortholog)
Sc5d	-2.23	0.0004	0.0276	sterol-C5-desaturase
Hbb-b1	-2.39	0.0004	0.0278	hemoglobin, beta adult major chain
LOC102550314; LOC100360124	2.23	0.0004	0.0314	similar to glutaredoxin 1 (thioltransferase); glutaredoxin (LOC305806), mRNA; uncharacterized LOC102550314 [Source:RGD Symbol;Acc:7600849]; uncharacterized LOC102550314; ENCODES a protein that exhibits electron carrier activity (inferred) AND protein disulfide oxidoreductase activity (inferred) AND transferase activity (inferred) AND INVOLVED IN cell redox homeostasis (inferred) AND oxidation-reduction process (inferred)
Amdhd1	-2.69	0.0005	0.0321	amidohydrolase domain containing 1
Thrsp	6.84	0.0005	0.0324	thyroid hormone responsive

Cylc2	2.18	0.0005	0.0336	cylicin, basic protein of sperm head cytoskeleton 2
Tmem30b	-2.12	0.0005	0.0338	transmembrane protein 30B
Lhpp	-2.42	0.0005	0.0342	phospholysine phosphohistidine inorganic pyrophosphate phosphatase
Akr7a3	-3.26	0.0005	0.0355	aldo-keto reductase family 7, member A3 (aflatoxin aldehyde reductase)
Syne2	-2.25	0.0005	0.0355	Uncharacterized protein; spectrin repeat containing, nuclear envelope 2; ENCODES a protein that exhibits actin binding (ortholog) AND INVOLVED IN centrosome localization (ortholog) AND cytoskeletal anchoring at nuclear membrane (ortholog) AND establishment or maintenance of cell polarity (ortholog) AND ASSOCIATED WITH Muscular Dystrophy Emery-Dreifuss (ortholog) AND FOUND IN aggresome (ortholog) AND cytoplasm (ortholog) AND filopodium membrane (ortholog) AND INTERACTS WITH cefaloridine AND (-)-demecolcine (ortholog) AND (-)-epigallocatechin 3-gallate (ortholog); PREDICTED: spectrin repeat containing, nuclear envelope 2 (Syne2), partial mRNA.
Glt1d1	2.09	0.0005	0.0356	glycosyltransferase 1 domain containing 1
Sema3c	-2.62	0.0006	0.0377	sema domain, immunoglobulin domain (Ig), short basic domain, secreted, (semaphorin) 3C
Ppara	2.32	0.0006	0.0377	peroxisome proliferator activated receptor alpha
Popdc2; Cox17	2.53	0.0006	0.0377	popeye domain containing 2; popeye domain containing 2 (Popdc2), mRNA; COX17 cytochrome c oxidase copper chaperonepopeye domain containing 2; ENCODES a protein that exhibits cAMP binding (ortholog) AND INVOLVED IN regulation of heart rate (ortholog) AND regulation of membrane potential (ortholog) AND sinoatrial node cell development (ortholog) AND FOUND IN membrane (ortholog) AND INTERACTS WITH 2 3 7 8-tetrachlorodibenzodioxine AND 2 6-dinitrotoluene AND C60 fullerene; popeye domain containing 2 (Popdc2), mRNA.
Fabp7	2.84	0.0007	0.0425	fatty acid binding protein 7, brain

Evc	-2.44	0.0007	0.0425	Ellis van Creveld protein
Mark4	-2.01	0.0007	0.0435	MAP/microtubule affinity-regulating kinase 4
Slc39a4	-2.05	0.0007	0.044	solute carrier family 39 (zinc transporter), member 4
Pigq; Nhlrc4	-2.25	0.0008	0.0455	phosphatidylinositol glycan anchor biosynthesis, class Q; NHL repeat containing 4
A2m; LOC100911545	2.16	0.0008	0.0467	alpha-2-macroglobulin (A2m), mRNA; alpha-2-macroglobulin-like [Source:RGD Symbol;Acc:6492449]; alpha-2- macroglobulin alpha-1-inhibitor III; alpha-2- macroglobulin, mRNA (cDNA clone MGC:114358 IMAGE:7458629), complete cds.; null; alpha-2-macroglobulin (A2m), mRNA.
Hba1	-2.25	0.0008	0.0468	hemoglobin, alpha 1

Appendix 2: List of differentially expressed genes in REV vs NC-REV exported from TAC 4.0 software. Blue highlight represents upregulated genes and red highlight represents downregulated genes.

Gene Symbol	Fold Change	P-val	FDR P-val	Description
RGD1561137	3.12	3.44E-12	7.25E-08	similar to 40S ribosomal protein S16 [Source:RGD Symbol;Acc:1561137]; ENCODES a protein that exhibits structural constituent of ribosome (inferred) AND INVOLVED IN translation (inferred) AND FOUND IN ribosome (inferred) AND INTERACTS WITH 17beta-estradiol (ortholog) AND 17beta-hydroxy-17-methylestra-4 9 11-trien-3-one (ortholog) AND acetylsalicylic acid (ortholog); similar to 40S ribosomal protein S16
Oxa1l	3.23	6.26E-12	7.25E-08	oxidase (cytochrome c) assembly 1-like
Dusp1	5.51	2.21E-11	1.54E-07	dual specificity phosphatase 1
Rpl36	3.89	2.65E-11	1.54E-07	ribosomal protein L36
Gdf15	4.57	4.02E-11	1.82E-07	growth differentiation factor 15
Ctc1	3.25	4.72E-11	1.82E-07	CTS telomere maintenance complex component 1
LOC102552540	-4.77	1.10E-10	3.64E-07	uncharacterized LOC102552540
Rpl36	3.53	2.08E-10	5.36E-07	ribosomal protein L36
RGD1564665; LOC100360856; LOC501224; LOC691414; LOC685598; MGC116197	-3.14	2.76E-10	5.89E-07	Protein LOC100360856; hypothetical protein LOC100360856 [Source:RGD Symbol;Acc:2321302]; similar to RIKEN cDNA 2610042L04; hypothetical protein LOC691414; hypothetical protein LOC685598; INTERACTS WITH bilirubin (ortholog) AND bisphenol A (ortholog) AND copper atom (ortholog)
LOC100361060	3.84	2.79E-10	5.89E-07	ribosomal protein L36-like [Source:RGD Symbol;Acc:2320900]; ENCODES a protein that exhibits structural constituent of ribosome (inferred) AND INVOLVED IN translation (inferred) AND FOUND IN ribosome (inferred) AND INTERACTS WITH 17beta-estradiol (ortholog) AND

				cisplatin (ortholog) AND cyclosporin A (ortholog)
Dad1	2.42	4.42E-10	8.37E-07	defender against cell death 1
Tecr	3.44	4.69E-10	8.37E-07	trans-2,3-enoyl-CoA reductase
Ar	3.41	5.34E-10	8.85E-07	androgen receptor
Nfam1	3.17	7.01E-10	1.08E-06	NFAT activating protein with ITAM motif 1
LOC102556351	-2.12	1.23E-09	1.78E-06	uncharacterized LOC102556351
Wars	2.43	1.61E-09	2.07E-06	tryptophanyl-tRNA synthetase
Pspc1	-2.58	2.19E-09	2.46E-06	paraspeckle component 1
Tmem63b	2.16	2.20E-09	2.46E-06	transmembrane protein 63B
LOC501421; LOC690568	-4.43	2.22E-09	2.46E-06	Protein LOC501421; INTERACTS WITH bilirubin (ortholog) AND bisphenol A (ortholog) AND copper atom (ortholog); similar to RIKEN cDNA 5031410I06
Srcap	2.64	2.39E-09	2.51E-06	Snf2-related CREBBP activator protein
Insig1	4.71	2.99E-09	3.02E-06	insulin induced gene 1
Amdhd1	-3.86	3.85E-09	3.72E-06	amidohydrolase domain containing 1
Aqp8	2.69	4.13E-09	3.83E-06	aquaporin 8
Tmem37	3.39	4.54E-09	4.05E-06	transmembrane protein 37
Egr1	14.49	5.13E-09	4.25E-06	early growth response 1
Cdkn1a	5.7	5.98E-09	4.79E-06	cyclin-dependent kinase inhibitor 1A
Dhcr24	3.19	6.88E-09	5.10E-06	24-dehydrocholesterol reductase
Atp6v1f	2.36	7.04E-09	5.10E-06	ATPase, H ⁺ transporting, lysosomal V1, subunit F
Ergic1	2.55	7.33E-09	5.13E-06	endoplasmic reticulum-golgi intermediate compartment 1
Lrp10	4.79	7.53E-09	5.13E-06	low-density lipoprotein receptor-related protein 10

Orai1	3.7	8.11E-09	5.25E-06	ORAI calcium release-activated calcium modulator 1
Hsd17b2	-7.39	8.15E-09	5.25E-06	hydroxysteroid (17-beta) dehydrogenase 2
Crkl	2.12	9.69E-09	5.76E-06	v-crk avian sarcoma virus CT10 oncogene homolog-like
Slc6a9	5.47	1.42E-08	8.17E-06	solute carrier family 6 (neurotransmitter transporter, glycine), member 9
Kxd1	2.01	1.45E-08	8.17E-06	KxDL motif containing 1
Pdk2	2.46	1.71E-08	9.45E-06	pyruvate dehydrogenase kinase, isozyme 2
Masp2	4.94	1.87E-08	1.01E-05	mannan-binding lectin serine peptidase 2
Tp53inp2	2.55	1.98E-08	1.03E-05	tumor protein p53 inducible nuclear protein 2
LOC100911319	2.9	2.00E-08	1.03E-05	zinc finger protein 36, C3H1 type-like 2-like [Source:RGD Symbol;Acc:6493373]; ENCODES a protein that exhibits metal ion binding (inferred) AND INTERACTS WITH (-)-epigallocatechin 3-gallate (ortholog) AND 17beta-estradiol (ortholog) AND 2 3 7 8-tetrachlorodibenzodioxine (ortholog)
Rpl34	2.55	2.24E-08	1.08E-05	ribosomal protein L34
LOC102550466	-2.62	2.24E-08	1.08E-05	disks large homolog 5-like
LOC690700; LOC685792; LOC301748	-2.96	2.82E-08	1.28E-05	similar to similar to RIKEN cDNA 1700001E04 [Source:RGD Symbol;Acc:1592262]; similar to Discs large homolog 5 (Placenta and prostate DLG) (Discs large protein P-dlg); similar to RIKEN cDNA 1700001E04
LOC363337	-2.75	3.54E-08	1.58E-05	similar to RIKEN cDNA 1700081O22
Rpl28	2.44	3.74E-08	1.64E-05	ribosomal protein L28
Trmt112	2.67	4.69E-08	2.01E-05	tRNA methyltransferase 11-2 homolog (S. cerevisiae)
Rps15	2.36	5.76E-08	2.38E-05	ribosomal protein S15
Mlec	3.05	5.96E-08	2.38E-05	malectin
Ppp1r37; Lrrc68	2.22	5.96E-08	2.38E-05	protein phosphatase 1, regulatory subunit 37; ENCODES a protein that exhibits

				phosphatase binding (ortholog) AND INVOLVED IN negative regulation of phosphatase activity (ortholog) AND INTERACTS WITH C60 fullerene AND cadmium dichloride AND diuron; protein phosphatase 1, regulatory subunit 37 (Ppp1r37), mRNA. NM_001107482; leucine rich repeat containing 68 (Lrrc68), mRNA.
Apol3	-3.11	6.19E-08	2.43E-05	apolipoprotein L, 3
LOC100909441	2.15	6.45E-08	2.49E-05	FOUND IN cytoplasmic microtubule (ortholog) AND nucleus (ortholog) AND INTERACTS WITH 2 3 7 8-tetrachlorodibenzodioxine AND bis(2-ethylhexyl) phthalate AND ketamine
Araf	2.19	8.58E-08	3.14E-05	A-Raf proto-oncogene, serine/threonine kinase
Rela	2.21	8.59E-08	3.14E-05	v-rel avian reticuloendotheliosis viral oncogene homolog A
Ucp2	2.33	8.69E-08	3.14E-05	uncoupling protein 2 (mitochondrial, proton carrier)
Dgcr2	2.64	8.73E-08	3.14E-05	DiGeorge syndrome critical region gene 2
Tab2	2.07	8.79E-08	3.14E-05	TGF-beta activated kinase 1/MAP3K7 binding protein 2
Itgb5	2.43	1.19E-07	4.07E-05	integrin, beta 5
Anp32a	-2.1	1.27E-07	4.26E-05	acidic (leucine-rich) nuclear phosphoprotein 32 family, member A
Serinc3	2.07	1.31E-07	4.33E-05	serine incorporator 3
Lpcat3	2.77	1.35E-07	4.40E-05	lysophosphatidylcholine acyltransferase 3
Angptl8	3.16	1.39E-07	4.47E-05	angiopoietin-like 8
N4bp1	2.36	1.46E-07	4.63E-05	Nedd4 binding protein 1
Alg3	2.99	1.51E-07	4.69E-05	ALG3, alpha-1,3- mannosyltransferase
Colgalt1	2.2	1.53E-07	4.69E-05	collagen beta(1-O)galactosyltransferase 1
Slc16a2	3.11	1.54E-07	4.69E-05	solute carrier family 16, member 2 (thyroid hormone transporter)

Sdhc	2.75	1.57E-07	4.73E-05	succinate dehydrogenase complex, subunit C, integral membrane protein
Scd2	2.99	1.60E-07	4.76E-05	stearoyl-Coenzyme A desaturase 2
Pld3	2.71	1.70E-07	4.99E-05	phospholipase D family, member 3
LOC100360439	2.3	2.21E-07	6.21E-05	ribosomal protein L36-like [Source:RGD Symbol;Acc:2322117]; ENCODES a protein that exhibits structural constituent of ribosome (inferred) AND INVOLVED IN translation (inferred) AND FOUND IN cytosolic large ribosomal subunit (inferred) AND nucleolus (inferred) AND INTERACTS WITH 17beta-estradiol (ortholog) AND cisplatin (ortholog) AND cyclosporin A (ortholog)
LOC501224	-2.37	2.22E-07	6.21E-05	similar to RIKEN cDNA 2610042L04, mRNA (cDNA clone MGC:94005 IMAGE:7115745), complete cds.
LgalsI	2.42	2.33E-07	6.42E-05	lectin, galactoside-binding-like
Tpp1	2.04	2.56E-07	6.99E-05	tripeptidyl peptidase I
MGC116197	-2.97	2.64E-07	7.12E-05	similar to RIKEN cDNA 1700001E04; similar to RIKEN cDNA 1700001E04 [Source:RGD Symbol;Acc:1560404]; INTERACTS WITH bilirubin (ortholog) AND bisphenol A (ortholog) AND copper atom (ortholog)
Tkt	2.12	2.73E-07	7.24E-05	transketolase
LOC100359616	3.13	2.75E-07	7.24E-05	60S ribosomal protein L36; ENCODES a protein that exhibits structural constituent of ribosome (inferred) AND INVOLVED IN translation (inferred) AND FOUND IN ribosome (inferred) AND INTERACTS WITH 17beta-estradiol (ortholog) AND cisplatin (ortholog) AND cyclosporin A (ortholog)
Hmgb2	-2.03	2.80E-07	7.24E-05	high mobility group box 2
Aff1	2.19	2.81E-07	7.24E-05	AF4/FMR2 family, member 1
Fech	2.13	2.84E-07	7.24E-05	ferrochelatase
LOC102554663	-3.05	2.90E-07	7.31E-05	sodium/nucleoside cotransporter 2-like

Tbx20	2.3	3.10E-07	7.65E-05	T-box 20
Gaa	3.27	3.35E-07	8.18E-05	glucosidase, alpha, acid
Sod3	2.27	3.54E-07	8.46E-05	superoxide dismutase 3, extracellular
Lrrc58	2.05	3.82E-07	9.04E-05	leucine rich repeat containing 58
Rhog	2.31	3.95E-07	9.24E-05	ras homolog family member G
Dio1	3.49	3.99E-07	9.24E-05	deiodinase, iodothyronine, type I
Gstk1	4.11	4.48E-07	0.0001	glutathione S-transferase kappa 1
Ssr4	2.06	4.67E-07	0.0001	signal sequence receptor, delta
Dusp7	4.65	4.72E-07	0.0001	dual specificity phosphatase 7
LOC100361854	2.25	4.77E-07	0.0001	ribosomal protein S26-like [Source:RGD Symbol;Acc:2319323]; ENCODES a protein that exhibits structural constituent of ribosome (inferred) AND INVOLVED IN translation (inferred) AND FOUND IN ribosome (inferred) AND INTERACTS WITH 17beta-hydroxy-17-methylestra-4 9 11-trien-3-one (ortholog) AND 5-fluorouracil (ortholog) AND copper(2+) sulfate (ortholog)
Psenen	2.51	4.78E-07	0.0001	presenilin enhancer gamma secretase subunit
Ubqln4	2.15	4.93E-07	0.0001	ubiquilin 4
Slc48a1	2.17	5.07E-07	0.0001	solute carrier family 48 (heme transporter), member 1
Thrsp	6.86	5.59E-07	0.0001	thyroid hormone responsive
RGD1561667	-2.3	6.24E-07	0.0001	INTERACTS WITH indole-3-methanol AND thioacetamide
LOC688922; LOC100909424	2.35	8.07E-07	0.0002	similar to Insulin-induced gene 1 protein (INSIG-1) (Insulin-induced growth response protein CL-6) (Immediate-early protein CL-6) [Source:RGD Symbol;Acc:1582985]; similar to Insulin-induced gene 1 protein (INSIG-1) (Insulin-induced growth response protein CL-6) (Immediate-early protein CL-6); uncharacterized LOC100909424

Nfic	2.77	8.21E-07	0.0002	nuclear factor I/C
Arhgdib	2.42	9.09E-07	0.0002	Rho, GDP dissociation inhibitor (GDI) beta
Rpl10a	2.09	9.45E-07	0.0002	ribosomal protein L10A [Source:RGD Symbol;Acc:620497]; ENCODES a protein that exhibits poly(A) RNA binding (ortholog) AND INVOLVED IN translation (inferred) AND FOUND IN cytoplasm (ortholog) AND cytosolic large ribosomal subunit (ortholog) AND extracellular vesicular exosome (ortholog) AND INTERACTS WITH 1-naphthyl isothiocyanate AND 2 4 6-trinitrotoluene AND 2 4-dinitrotoluene; ribosomal protein L10A; Chalmel, et. al. AceView Annotation Rpl10a.bSep08
Lmf2	2.11	9.55E-07	0.0002	lipase maturation factor 2
LOC102547093	-2.69	1.02E-06	0.0002	uncharacterized LOC102547093
Bhlhe40	2.97	1.02E-06	0.0002	basic helix-loop-helix family, member e40
Ostm1	2.57	1.06E-06	0.0002	osteopetrosis associated transmembrane protein 1
Megf9	4.45	1.09E-06	0.0002	multiple EGF-like-domains 9
Ttyh2	2.25	1.13E-06	0.0002	tweety family member 2
Slc50a1	2.34	1.16E-06	0.0002	solute carrier family 50 (sugar efflux transporter), member 1
Pura	2.32	1.17E-06	0.0002	purine rich element binding protein A [Source:RGD Symbol;Acc:1308543]; ENCODES a protein that exhibits DNA binding (ortholog) AND double-stranded DNA binding (ortholog) AND double-stranded telomeric DNA binding (ortholog) AND INVOLVED IN DNA unwinding involved in DNA replication (ortholog) AND negative regulation of transcription DNA-templated (ortholog) AND negative regulation of translation (ortholog) AND FOUND IN nucleus AND cytoplasm (ortholog) AND dendrite (ortholog) AND INTERACTS WITH 2 3 7 8-tetrachlorodibenzodioxine AND 3H-1 2-dithiole-3-thione AND acetylsalicylic acid; purine rich element binding protein A;

				PREDICTED: purine rich element binding protein A (Pura), mRNA.
Vkorc1	3.3	1.18E-06	0.0002	vitamin K epoxide reductase complex, subunit 1
Clptm1	2.17	1.19E-06	0.0002	cleft lip and palate associated transmembrane protein 1
Myadm	2.48	1.21E-06	0.0002	myeloid-associated differentiation marker
Syngn2	2.28	1.41E-06	0.0002	synaptogyrin 2
Desi1	2.19	1.48E-06	0.0003	desumoylating isopeptidase 1
Mapk1ip1l	3.15	1.56E-06	0.0003	mitogen-activated protein kinase 1 interacting protein 1-like
Pcdhgb7; Pcdhga7; Pcdhga10; Pcdhga5; Pcdhga2; Pcdhga1; Pcdhga11; Pcdhga8; Pcdhga9; Pcdhgb8; Pcdhgc3; Pcdhga6	2.35	1.78E-06	0.0003	protocadherin gamma subfamily B, 7; protocadherin gamma subfamily A, 7; protocadherin gamma subfamily A, 10; protocadherin gamma subfamily A, 5; protocadherin gamma subfamily A, 2; protocadherin gamma subfamily A, 1; protocadherin gamma subfamily A, 11; protocadherin gamma subfamily A, 8; protocadherin gamma subfamily A, 9; protocadherin gamma subfamily B, 8; protocadherin gamma subfamily C, 3; protocadherin gamma subfamily A, 6
Pigt	2.09	1.94E-06	0.0003	phosphatidylinositol glycan anchor biosynthesis, class T
LOC102557302	-2.11	1.96E-06	0.0003	uncharacterized LOC102557302 [Source:RGD Symbol;Acc:7730632]
Slc17a5	2.9	1.96E-06	0.0003	solute carrier family 17 (acidic sugar transporter), member 5
Krt18	-2.12	1.97E-06	0.0003	keratin 18, type I
Ier2	2.12	1.97E-06	0.0003	immediate early response 2
Zfp524	2.65	2.15E-06	0.0003	zinc finger protein 524
Fam53a	2.19	2.21E-06	0.0003	family with sequence similarity 53, member A
Mettl22	2.02	2.22E-06	0.0003	methyltransferase like 22

LOC367516	-2.05	2.43E-06	0.0004	hypothetical LOC367516
Cyp8b1	-3.88	2.44E-06	0.0004	cytochrome P450, family 8, subfamily b, polypeptide 1
Hbb	-2.32	2.46E-06	0.0004	hemoglobin, beta
Zfp36	2.79	2.47E-06	0.0004	zinc finger protein 36
Acp2	2.16	2.54E-06	0.0004	acid phosphatase 2, lysosomal
Eci1	-2.21	2.57E-06	0.0004	enoyl-CoA delta isomerase 1
Use1	2.17	2.75E-06	0.0004	unconventional SNARE in the ER 1 homolog (S. cerevisiae)
Ninj1	3.12	2.77E-06	0.0004	ninjurin 1
LOC102551050	-2.08	2.88E-06	0.0004	disks large homolog 5-like
Ost4	2.28	3.32E-06	0.0004	oligosaccharyltransferase complex subunit 4
Mpdu1	2.07	3.36E-06	0.0004	mannose-P-dolichol utilization defect 1
Sppl3	2.22	3.61E-06	0.0005	signal peptide peptidase like 3
Phc2	2.23	3.71E-06	0.0005	polyhomeotic homolog 2 (Drosophila)
RGD1309079	4.04	3.73E-06	0.0005	similar to Ab2-095
LOC100911173	-2.37	3.74E-06	0.0005	afadin-like
Abhd6	2.31	3.78E-06	0.0005	abhydrolase domain containing 6
Epas1	2.09	3.85E-06	0.0005	endothelial PAS domain protein 1
LOC102547811	-2.06	3.88E-06	0.0005	uncharacterized LOC102547811; INTERACTS WITH bilirubin (ortholog) AND bisphenol A (ortholog) AND copper atom (ortholog)
LOC100360856	-2.67	3.88E-06	0.0005	INTERACTS WITH bilirubin (ortholog) AND bisphenol A (ortholog) AND copper atom (ortholog)
Wsb2	2.66	4.27E-06	0.0005	WD repeat and SOCS box-containing 2
Fasn	4.08	4.33E-06	0.0005	fatty acid synthase

Parp16	2.22	4.56E-06	0.0006	poly (ADP-ribose) polymerase family, member 16
Txnip	2.06	4.56E-06	0.0006	thioredoxin interacting protein
Gm2a	2.4	4.61E-06	0.0006	GM2 ganglioside activator
Fcgr2a	2.81	4.72E-06	0.0006	Fc fragment of IgG, low affinity IIa, receptor
B9d1	2.57	4.89E-06	0.0006	B9 protein domain 1
Tuba4a	2.41	5.02E-06	0.0006	tubulin, alpha 4A
Rpl18a	2.46	5.28E-06	0.0006	ribosomal protein L18A
RGD1565131	2.67	5.37E-06	0.0006	similar to ribosomal protein L15
LOC689743; LOC679663; RGD1561891_predicted	-2.11	5.67E-06	0.0006	similar to transcription elongation factor B (SIII), polypeptide 1; INTERACTS WITH 2 3 7 8-tetrachlorodibenzodioxine (ortholog) AND 4-hydroxynon-2-enal (ortholog) AND copper(2+) sulfate (ortholog); similar to transcription elongation factor B (SIII), polypeptide 1 (predicted)
Hnrnpdl	-2.14	5.68E-06	0.0006	heterogeneous nuclear ribonucleoprotein D-like
Ubl7	2.67	6.22E-06	0.0007	ubiquitin-like 7
Rpl15	3.06	6.22E-06	0.0007	ribosomal protein L15
Ubp2	2.77	6.37E-06	0.0007	ubiquitin-associated protein 2
Gstt1	2.1	6.64E-06	0.0007	glutathione S-transferase theta 1
LOC102550188	-2.04	7.35E-06	0.0008	Protein LOC681380; disks large homolog 5-like
Zrsr2	-2.44	7.40E-06	0.0008	zinc finger (CCCH type), RNA binding motif and serine/arginine rich 2
Slc25a39	2.28	7.54E-06	0.0008	solute carrier family 25, member 39
Thap7	2.72	7.61E-06	0.0008	THAP domain containing 7
Ppt2	2.02	7.79E-06	0.0008	palmitoyl-protein thioesterase 2
Emd	2.72	8.08E-06	0.0008	emerin

Tmem86b	2.89	8.12E-06	0.0008	transmembrane protein 86B
Ppp1r3c; PPP1R3C; LOC100910671	2.23	8.27E-06	0.0008	protein phosphatase 1, regulatory subunit 3C; Protein phosphatase 1 regulatory subunit 3; ENCODES a protein that exhibits enzyme binding AND phosphoprotein phosphatase activity AND protein phosphatase binding (ortholog) AND INVOLVED IN dephosphorylation AND regulation of glycogen biosynthetic process AND regulation of glycogen catabolic process AND PARTICIPATES IN glycogen biosynthetic pathway AND glycogen degradation pathway AND insulin signaling pathway AND FOUND IN glycogen granule AND intracellular membrane-bounded organelle AND INTERACTS WITH 17alpha-ethynylestradiol AND 2 2' 5 5'-tetrachlorobiphenyl AND 2 3 7 8-tetrachlorodibenzodioxine; INTERACTS WITH 17beta-estradiol (ortholog) AND 2 3 7 8-tetrachlorodibenzodioxine (ortholog) AND 2-methylcholine (ortholog)
Gpm6a	3	8.80E-06	0.0009	glycoprotein m6a
LOC685989	-2.73	8.89E-06	0.0009	hypothetical protein LOC685989
Akr1c1	-2.85	9.11E-06	0.0009	aldo-keto reductase family 1, member C1
Hyal2	2.42	9.13E-06	0.0009	hyaluronoglucosaminidase 2
Gltpd2	2.73	9.52E-06	0.0009	glycolipid transfer protein domain containing 2
LOC679711	-2.73	9.55E-06	0.0009	similar to RIKEN cDNA 5031410I06
Cry1	2.04	1.00E-05	0.0009	cryptochrome circadian clock 1
Srebf1	3.42	1.04E-05	0.001	sterol regulatory element binding transcription factor 1
LOC684841	2.19	1.05E-05	0.001	ENCODES a protein that exhibits DNA binding (inferred) AND protein heterodimerization activity (inferred) AND INVOLVED IN nucleosome assembly (inferred) AND FOUND IN extracellular vesicular exosome (ortholog) AND nucleus (ortholog) AND INTERACTS WITH 17beta-estradiol (ortholog) AND 2 3 7 8-

				tetrachlorodibenzodioxine (ortholog) AND 2-methylcholine (ortholog)
Atp6v0e1	2	1.08E-05	0.001	ATPase, H ⁺ transporting, lysosomal, V0 subunit e1
Mrpl38	2.35	1.08E-05	0.001	mitochondrial ribosomal protein L38
G6pd	2.2	1.17E-05	0.0011	glucose-6-phosphate dehydrogenase
Slc46a1	3.07	1.20E-05	0.0011	solute carrier family 46 (folate transporter), member 1
LOC102555131	-2.39	1.23E-05	0.0011	afadin-like
Hist2h4	2.46	1.23E-05	0.0011	histone cluster 2, H4
Dao	2.23	1.30E-05	0.0011	D-amino-acid oxidase
Hmox1	2.02	1.31E-05	0.0011	heme oxygenase 1
LOC367485; LOC501467	-3.09	1.38E-05	0.0012	Protein LOC367485; similar to spermatogenesis associated glutamate (E)-rich protein 4d [Source:RGD Symbol;Acc:1588462]; similar to spermatogenesis associated glutamate (E)-rich protein 4d
Cylc2	-2.35	1.41E-05	0.0012	cylicin, basic protein of sperm head cytoskeleton 2
Grina	2.99	1.44E-05	0.0012	glutamate receptor, ionotropic, N-methyl D-aspartate-associated protein 1 (glutamate binding)
Slco2a1	2.9	1.48E-05	0.0013	solute carrier organic anion transporter family, member 2a1
Cxcl14	-3.11	1.54E-05	0.0013	chemokine (C-X-C motif) ligand 14
Urad	2.75	1.55E-05	0.0013	ureidoimidazoline (2-oxo-4-hydroxy-4-carboxy-5-) decarboxylase [Source:RGD Symbol;Acc:1595191]; ENCODES a protein that exhibits carboxy-lyase activity (ortholog) AND INVOLVED IN allantoin biosynthetic process (inferred) AND INTERACTS WITH bis(2-ethylhexyl) phthalate (ortholog) AND pirinixic acid (ortholog)
LOC103690018; Gorasp2	2.11	1.58E-05	0.0013	Golgi reassembly-stacking protein 2-like; golgi reassembly stacking protein 2;

				INVOLVED IN Golgi organization AND organelle organization (ortholog) AND FOUND IN Golgi apparatus AND Golgi medial cisterna AND plasma membrane (ortholog) AND INTERACTS WITH ammonium chloride AND 17alpha-ethynylestradiol (ortholog) AND 2 3 7 8-tetrachlorodibenzodioxine (ortholog)
Atp6v0a2	2.24	1.65E-05	0.0013	ATPase, H+ transporting, lysosomal V0 subunit A2
Fgf1	2.61	1.66E-05	0.0013	fibroblast growth factor 1 (acidic)
LOC681198; LOC102549465	-2.51	1.73E-05	0.0014	similar to Spetex-2F protein [Source:RGD Symbol;Acc:1583493]; disks large homolog 5-like
Hbb-b1	-2.03	1.74E-05	0.0014	hemoglobin, beta adult major chain
Dgat2	2.84	1.76E-05	0.0014	diacylglycerol O-acyltransferase 2
Afmid	2.38	1.79E-05	0.0014	arylformamidase
Hfe2	2.66	1.85E-05	0.0014	hemochromatosis type 2 (juvenile)
Hes1	2.31	1.86E-05	0.0014	hes family bHLH transcription factor 1
LOC679973	-2.01	1.87E-05	0.0015	similar to Heat shock protein HSP 90-beta (HSP 84) (Tumor-specific transplantation 84 kDa antigen) (TSTA)
Upp2	-2.52	1.89E-05	0.0015	uridine phosphorylase 2
Lrrc8a	2.3	1.94E-05	0.0015	leucine rich repeat containing 8 family, member A
Jun	2.89	1.95E-05	0.0015	jun proto-oncogene
Zfp36l1	2.28	2.00E-05	0.0015	zinc finger protein 36, C3H type-like 1
Steap3	2.81	2.13E-05	0.0016	STEAP family member 3, metalloredutase
Tmem259	2.31	2.14E-05	0.0016	transmembrane protein 259
Man2b2	2.49	2.20E-05	0.0016	mannosidase, alpha, class 2B, member 2
Mmachc	2.54	2.20E-05	0.0016	methylmalonic aciduria (cobalamin deficiency) cbIC type, with homocystinuria

Fxyd1	2.15	2.22E-05	0.0016	FXYD domain-containing ion transport regulator 1
Nfix	2.9	2.24E-05	0.0016	nuclear factor I/X (CCAAT-binding transcription factor)
Tnfrsf1a	2.19	2.26E-05	0.0016	tumor necrosis factor receptor superfamily, member 1a
Mx2	-2.29	2.37E-05	0.0017	myxovirus (influenza virus) resistance 2
Klf10	2.65	2.43E-05	0.0017	Kruppel-like factor 10
Leprot	2.38	2.44E-05	0.0017	leptin receptor overlapping transcriptleptin receptor
Tmem205	3.42	2.52E-05	0.0018	transmembrane protein 205
Fgf21	4.05	2.57E-05	0.0018	fibroblast growth factor 21
Ppp1r3b	2.11	2.58E-05	0.0018	protein phosphatase 1, regulatory subunit 3B
Nadk	2.14	2.66E-05	0.0019	NAD kinase; ENCODES a protein that exhibits NAD+ kinase activity (ortholog) AND INVOLVED IN NAD metabolic process (inferred) AND NADP biosynthetic process (inferred) AND PARTICIPATES IN monoterpenoid biosynthetic pathway AND niacin metabolic pathway AND INTERACTS WITH dibutyl phthalate AND 2 3 7 8-tetrachlorodibenzodioxine (ortholog) AND 4 4'-diaminodiphenylmethane (ortholog); NAD kinase [Source:RefSeq peptide;Acc:NP_001103148]
Bmp6	2.66	2.72E-05	0.0019	bone morphogenetic protein 6
Vac14	2.38	2.80E-05	0.0019	Vac14 homolog (S. cerevisiae)
Tubb5	2.08	2.87E-05	0.002	tubulin, beta 5 class I
Tsc22d3	2.29	3.04E-05	0.002	TSC22 domain family, member 3
Plbd1	2.07	3.07E-05	0.0021	phospholipase B domain containing 1
F11r	2.74	3.14E-05	0.0021	F11 receptor
C8g	2.49	3.17E-05	0.0021	complement component 8, gamma polypeptide

Lynx1	2.94	3.33E-05	0.0022	Ly6/neurotoxin 1
Mtch2	2.75	3.36E-05	0.0022	mitochondrial carrier 2
Eftud2	2.17	3.51E-05	0.0023	elongation factor Tu GTP binding domain containing 2
Dpagt1	2.21	3.57E-05	0.0023	dolichyl-phosphate (UDP-N-acetylglucosamine) N-acetylglucosaminophosphotransferase 1 (GlcNAc-1-P transferase)
Stard3	2.06	3.58E-05	0.0023	StAR-related lipid transfer (START) domain containing 3
Zdhc1	2.23	3.64E-05	0.0023	zinc finger, DHHC-type containing 1
Ceacam1	2.01	3.81E-05	0.0024	carcinoembryonic antigen-related cell adhesion molecule 1 (biliary glycoprotein)
Cnppd1	2.02	3.87E-05	0.0024	cyclin Pas1/PHO80 domain containing 1
Ccl5	2.39	3.90E-05	0.0024	chemokine (C-C motif) ligand 5
LOC100912852; LOC100360712; LOC360998	-2.66	4.37E-05	0.0027	disks large homolog 5-like [Source:RGD Symbol;Acc:6485354]; rCG43589-like; hypothetical LOC360998
Tm6sf2	2.09	4.46E-05	0.0027	transmembrane 6 superfamily member 2
Foxa3	2.85	4.53E-05	0.0028	forkhead box A3
Snrnp70	-2.25	4.96E-05	0.0029	small nuclear ribonucleoprotein 70 (U1)
LOC100909409; LOC688649	-2.76	5.13E-05	0.003	disks large homolog 5-like [Source:RGD Symbol;Acc:6504293]; similar to spermatogenesis associated glutamate (E)-rich protein 4d
Slc27a1	2.47	5.18E-05	0.003	solute carrier family 27 (fatty acid transporter), member 1
Car3	2.55	5.22E-05	0.003	carbonic anhydrase 3
Srm	3.03	5.87E-05	0.0033	spermidine synthase
Hs3st3b1	2.45	5.87E-05	0.0033	heparan sulfate (glucosamine) 3-O-sulfotransferase 3B1

Cyp4a1	-2.3	5.97E-05	0.0034	cytochrome P450, family 4, subfamily a, polypeptide 1
Ccnd3	2.01	6.25E-05	0.0035	cyclin D3
Pink1	2.73	6.54E-05	0.0037	PTEN induced putative kinase 1
Rnf5	3.67	6.71E-05	0.0037	ring finger protein 5, E3 ubiquitin protein ligase
LOC685828	-2.05	6.89E-05	0.0038	hypothetical protein LOC685828
Aph1b	2.12	6.98E-05	0.0038	APH1B gamma secretase subunit (Aph1b), mRNA; APH1B gamma secretase subunit; anterior pharynx defective 1 homolog B (C. elegans), mRNA (cDNA clone MGC:188357 IMAGE:7929867), complete cds.; INVOLVED IN positive regulation of catalytic activity (inferred) AND protein processing (inferred) AND PARTICIPATES IN Notch signaling pathway AND syndecan signaling pathway AND Alzheimer disease pathway AND FOUND IN integral component of membrane (inferred); anterior pharynx defective 1 homolog B (C. elegans) (Aph1b), mRNA.
Hs3st3a1	2.07	7.06E-05	0.0038	heparan sulfate (glucosamine) 3-O-sulfotransferase 3A1
Heg1	2.04	7.10E-05	0.0038	heart development protein with EGF-like domains 1
LOC100912377; Ttc6; TPR_1.2	-2.46	7.12E-05	0.0038	uncharacterized LOC100912377; Chalmel, et. al. AceView Annotation Ttc6.cSep08; Chalmel, et. al. AceView Annotation TPR_1.2.aSep08; tetratricopeptide repeat domain 6
Jmjd8	2.41	7.29E-05	0.0039	jumonji domain containing 8
Mospd3	3.71	7.48E-05	0.0039	motile sperm domain containing 3
Aph1b	2.12	7.60E-05	0.004	APH1B gamma secretase subunit
Shisa5	2.22	7.76E-05	0.004	shisa family member 5
Oat	-2.19	7.76E-05	0.004	ornithine aminotransferase

AcsM3	-3.27	7.99E-05	0.0041	acyl-CoA synthetase medium-chain family member 3
Tmem223	2.06	8.26E-05	0.0042	transmembrane protein 223
Ugt2b	3329.24	8.35E-05	0.0043	UDP glycosyltransferase 2 family, polypeptide B; ENCODES a protein that exhibits glucuronosyltransferase activity AND INVOLVED IN metabolic process (inferred) AND PARTICIPATES IN ascorbate and aldarate metabolic pathway AND O-linked glycan biosynthetic pathway AND pentose and glucuronate interconversion pathway AND FOUND IN endoplasmic reticulum membrane (inferred) AND integral component of membrane (inferred) AND INTERACTS WITH 17alpha-ethynylestradiol AND 2 3 7 8-tetrachlorodibenzodioxine AND 3 3' 4 4' 5-pentachlorobiphenyl
Paqr3	2.68	8.41E-05	0.0043	progesterin and adipoQ receptor family member III
Sys1	3.41	8.43E-05	0.0043	Sys1 golgi trafficking protein
Thumpd1	-2.3	8.79E-05	0.0045	THUMP domain containing 1
Bace1	2.47	8.95E-05	0.0045	beta-site APP cleaving enzyme 1
Arl11	2.28	9.38E-05	0.0046	ADP-ribosylation factor-like 11
Slc15a4	2.27	9.40E-05	0.0046	solute carrier family 15 (oligopeptide transporter), member 4
Yipf2	2.32	9.60E-05	0.0047	Yip1 domain family, member 2
Slc30a6	2.22	0.0001	0.0049	solute carrier family 30 (zinc transporter), member 6
Abcg1	2.01	0.0001	0.0051	ATP-binding cassette, subfamily G (WHITE), member 1
LOC100909409	-2.22	0.0001	0.0052	INTERACTS WITH bilirubin (ortholog) AND bisphenol A (ortholog) AND copper atom (ortholog)
Tmem189	2.54	0.0001	0.0052	transmembrane protein 189
Pxdc1	2.22	0.0001	0.0054	PX domain containing 1

Oaz1	2.65	0.0001	0.0054	ornithine decarboxylase antizyme 1
Msra	2.05	0.0001	0.0054	methionine sulfoxide reductase A
Trim8	2.05	0.0001	0.0056	tripartite motif-containing 8
LOC100363509; Tmem125	3.98	0.0001	0.0058	transmembrane protein 125-like [Source:RGD Symbol;Acc:2322838]; INTERACTS WITH (S)-nicotine (ortholog) AND 3 4-methylenedioxymethamphetamine (ortholog) AND all-trans-retinoic acid (ortholog); transmembrane protein 125
Lrrc32	2.24	0.0001	0.006	leucine rich repeat containing 32
Fbxl12	2.36	0.0001	0.0061	F-box and leucine-rich repeat protein 12
Irf2bp2	2.12	0.0001	0.0062	interferon regulatory factor 2 binding protein 2
LOC689064	-2.17	0.0002	0.0068	beta-globin
Pofut1	2.06	0.0002	0.0068	protein O-fucosyltransferase 1
Rnpepl1	2.22	0.0002	0.007	arginyl aminopeptidase (aminopeptidase B)- like 1
LOC681180	-2.08	0.0002	0.007	INTERACTS WITH bilirubin (ortholog) AND bisphenol A (ortholog) AND copper atom (ortholog)
LOC302192	-2.08	0.0002	0.007	similar to RIKEN cDNA 1700001E04
Mfsd13a	2.53	0.0002	0.007	major facilitator superfamily domain containing 13A
Csf2ra	2.81	0.0002	0.0072	colony stimulating factor 2 receptor, alpha, low-affinity (granulocyte-macrophage)
Lypla2	2.29	0.0002	0.0072	lysophospholipase II
Gemin8	2.26	0.0002	0.0073	gem (nuclear organelle) associated protein 8
Rplp0	2.02	0.0002	0.0074	ribosomal protein, large, P0
Fus	-2.29	0.0002	0.0074	fused in sarcoma RNA binding protein
Cers2	2.26	0.0002	0.0074	ceramide synthase 2
Tkfc	2.53	0.0002	0.0074	trio kinase/FMN cyclase

Hist1h1d	2.27	0.0002	0.0075	histone cluster 1, H1d
Luc7l2	-2.69	0.0002	0.0076	LUC7-like 2 pre-mRNA splicing factor
Tsku	4.98	0.0002	0.0077	tsukushi, small leucine rich proteoglycan
Herc1	2.35	0.0002	0.008	HECT and RLD domain containing E3 ubiquitin protein ligase family member 1; PREDICTED: hect (homologous to the E6-AP (UBE3A) carboxyl terminus) domain and RCC1 (CHC1)-like domain (RLD) 1 (Herc1), mRNA.
Borcs8	2.3	0.0002	0.0082	BLOC-1 related complex subunit 8
Ethe1	2.1	0.0002	0.0083	ethylmalonic encephalopathy 1
Slc35b1	2.08	0.0002	0.0083	solute carrier family 35, member B1
Mpv17l	2.09	0.0002	0.0084	MPV17 mitochondrial membrane protein-like
Srm	2.57	0.0002	0.0085	ENCODES a protein that exhibits spermidine synthase activity AND protein homodimerization activity (ortholog) AND INVOLVED IN spermidine biosynthetic process AND PARTICIPATES IN spermidine metabolic pathway AND methionine cycle/metabolic pathway AND polyamine metabolic pathway AND INTERACTS WITH 2 3 7 8-tetrachlorodibenzodioxine AND 2 4 6-trinitrotoluene AND 2 4-dinitrotoluene; spermidine synthase; spermidine synthase (Srm), mRNA.
Abhd17c	2.15	0.0002	0.0089	abhydrolase domain containing 17C
Dnajc30	2.2	0.0002	0.0089	DnaJ (Hsp40) homolog, subfamily C, member 30
Amph	-2.12	0.0002	0.009	amphiphysin; Uncharacterized protein; ENCODES a protein that exhibits protein C-terminus binding AND protein complex binding AND protein heterodimerization activity AND INVOLVED IN positive regulation of endocytosis AND positive regulation of GTPase activity AND PARTICIPATES IN Fc gamma receptor mediated signaling pathway AND FOUND IN axon terminus AND INTERACTS WITH 4-hydroxynon-2-enal (ortholog) AND all-

				trans-retinoic acid (ortholog) AND cyclosporin A (ortholog)
Siah2	2.13	0.0002	0.009	siah E3 ubiquitin protein ligase 2
Hyi	2.6	0.0003	0.0093	hydroxypyruvate isomerase
Zfp385a	2.05	0.0003	0.0093	zinc finger protein 385A
LOC100912007	-2.07	0.0003	0.0094	INTERACTS WITH 2 3 7 8-tetrachlorodibenzodioxine (ortholog) AND 4-hydroxynon-2-enal (ortholog) AND copper(2+) sulfate (ortholog)
Ephx1	2.73	0.0003	0.0095	epoxide hydrolase 1, microsomal (xenobiotic)
Rbpms2	2.2	0.0003	0.0098	RNA binding protein with multiple splicing 2
Fmo5	-2.68	0.0003	0.0099	flavin containing monooxygenase 5
Asl	-2.35	0.0003	0.0099	argininosuccinate lyase
Tmem53	2.01	0.0003	0.01	transmembrane protein 53
Avpr1a	2.81	0.0003	0.0101	arginine vasopressin receptor 1A
Peak1	2.19	0.0003	0.0103	pseudopodium-enriched atypical kinase 1
LOC100125368; LOC100360514; LOC102551539	-4.14	0.0003	0.0104	zinc finger protein LOC100125368 (LOC100125368), mRNA; zinc finger protein LOC100125368; zinc finger-like protein-like; zinc finger protein 709-like
Il1rap	2.03	0.0003	0.0106	interleukin 1 receptor accessory protein
RGD1565590	-2.24	0.0003	0.0107	INTERACTS WITH thioacetamide; similar to Wolf-Hirschhorn syndrome candidate 1 protein isoform 3
Reep6	4.6	0.0003	0.011	receptor accessory protein 6
Vom2r4	-2.27	0.0003	0.0111	vomeroneasal 2 receptor, 4
Pemt	2.67	0.0004	0.0112	phosphatidylethanolamine N-methyltransferase
Ehd3	2.26	0.0004	0.0113	EH-domain containing 3
LOC102551451	-2.19	0.0004	0.0115	zinc finger protein 665-like

Tubb2a	2.26	0.0004	0.0118	tubulin, beta 2A class IIa
Slc9a9	2.21	0.0004	0.012	solute carrier family 9, subfamily A (NHE9, cation proton antiporter 9), member 9
RGD1563941	2.58	0.0004	0.0122	similar to hypothetical protein FLJ20010
Sntb1	2.2	0.0004	0.0125	syntrophin, beta 1
Llgl2	2.19	0.0004	0.0127	lethal giant larvae homolog 2 (Drosophila)
B9d1	2.12	0.0004	0.0128	B9 protein domain 1 (B9d1), mRNA; B9 protein domain 1, mRNA (cDNA clone MGC:189582 IMAGE:6889289), complete cds.; ENCODES a protein that exhibits hedgehog receptor activity (ortholog) AND INVOLVED IN camera-type eye development (ortholog) AND cilium assembly (ortholog) AND cilium morphogenesis (ortholog) AND FOUND IN centrosome (ortholog) AND ciliary basal body (ortholog) AND ciliary transition zone (ortholog) AND INTERACTS WITH indole-3-methanol AND 17alpha-ethynylestradiol (ortholog) AND 2 3 7 8-tetrachlorodibenzodioxine (ortholog)
Lingo4; Rorc	2.02	0.0004	0.0129	leucine rich repeat and Ig domain containing 4; RAR-related orphan receptor C
S1pr1	2.24	0.0005	0.0132	sphingosine-1-phosphate receptor 1
Rac2	2.04	0.0005	0.0134	ras-related C3 botulinum toxin substrate 2 (rho family, small GTP binding protein Rac2)
Fam216a	2.56	0.0005	0.0135	family with sequence similarity 216, member A
Parvb	2.04	0.0005	0.0135	parvin, beta
LOC102549812	2.8	0.0005	0.0137	serum response factor homolog A-like
LOC100910177	2.06	0.0005	0.0139	ENCODES a protein that exhibits dolichyl-phosphate beta-D-mannosyltransferase activity (ortholog) AND INVOLVED IN GPI anchor biosynthetic process (ortholog) AND regulation of protein stability (ortholog) AND ASSOCIATED WITH Congenital Disorder of Glycosylation Type Ie (ortholog) AND FOUND IN dolichol-phosphate-mannose synthase complex (ortholog) AND

				endoplasmic reticulum (ortholog) AND integral component of endoplasmic reticulum membrane (ortholog) AND INTERACTS WITH toluene AND 17beta-estradiol (ortholog) AND 2 3 7 8-tetrachlorodibenzodioxine (ortholog)
Btg2	2.67	0.0005	0.0143	BTG family, member 2
Dalrd3	2.04	0.0005	0.0145	DALR anticodon binding domain containing 3
Srxn1	2.47	0.0006	0.0152	sulfiredoxin 1
Paqr9	3.28	0.0006	0.0158	progesterin and adipoQ receptor family member IX
Stard10	2.03	0.0006	0.016	StAR-related lipid transfer domain containing 10
Fastk	2.04	0.0006	0.0161	Fas-activated serine/threonine kinase
Myct1	2.17	0.0006	0.0161	myc target 1
Zdhhc4	2.33	0.0006	0.0162	zinc finger, DHHC-type containing 4
LOC100125368	-3.14	0.0007	0.0166	zinc finger protein LOC100125368; zinc finger protein LOC100125368 [Source:RGD Symbol;Acc:1642422]; zinc finger protein LOC100125368, mRNA (cDNA clone MGC:156774 IMAGE:7123097), complete cds.; ENCODES a protein that exhibits metal ion binding (inferred) AND nucleic acid binding (inferred) AND INVOLVED IN regulation of transcription DNA-templated (inferred) AND FOUND IN intracellular (inferred) AND INTERACTS WITH (-)-epigallocatechin 3-gallate (ortholog) AND 2 3 7 8-tetrachlorodibenzodioxine (ortholog) AND 5-aza-2'-deoxycytidine (ortholog); zinc finger protein LOC100125368 (LOC100125368), mRNA.
Bco1	2.54	0.0007	0.0169	beta-carotene oxygenase 1
Plid4	2.13	0.0007	0.0171	phospholipase D family, member 4
Cpt1a	-2.05	0.0007	0.0173	carnitine palmitoyltransferase 1a, liver
Agpat2	2.6	0.0007	0.0176	1-acylglycerol-3-phosphate O-acyltransferase 2

Akr7a2	2.08	0.0007	0.0176	aldo-keto reductase family 7, member A2
Slc19a1	2.11	0.0008	0.0181	solute carrier family 19 (folate transporter), member 1
Ktn1	-2.22	0.0008	0.0188	kinectin 1 (kinesin receptor)
Il6r	2.72	0.0008	0.0191	interleukin 6 receptor
Cldn3	3.31	0.0008	0.0194	claudin 3
Mgat4b	2.11	0.0008	0.0197	mannosyl (alpha-1,3-)-glycoprotein beta-1,4-N-acetylglucosaminyltransferase, isozyme B
Sds	-4.19	0.0009	0.0201	serine dehydratase
Cyhr1	2.52	0.0009	0.0201	cysteine/histidine-rich 1
Asnsd1	2.04	0.0009	0.0202	asparagine synthetase domain containing 1
Hist2h2ab	2.2	0.0009	0.0204	histone cluster 2, H2ab
C5ar2	2.5	0.0009	0.0209	complement component 5a receptor 2
Slc28a2	-3.04	0.0009	0.0211	solute carrier family 28 (concentrative nucleoside transporter), member 2
Ubald1	2.14	0.001	0.0212	UBA-like domain containing 1
Shmt2	2.04	0.001	0.0214	serine hydroxymethyltransferase 2 (mitochondrial)
Ak4	2.24	0.001	0.0217	adenylate kinase 4
Dgcr6	2.01	0.001	0.0223	DiGeorge syndrome critical region gene 6
Cdk4; LOC100362034	2.38	0.001	0.0224	cyclin-dependent kinase 4; ENCODES a protein that exhibits cyclin binding AND cyclin-dependent protein serine/threonine kinase activity AND protein complex binding AND INVOLVED IN circadian rhythm AND lens development in camera-type eye AND organ regeneration AND PARTICIPATES IN G1/S transition pathway AND bladder cancer pathway AND cell cycle pathway mitotic AND ASSOCIATED WITH tumorigenesis AND ASSOCIATED WITH Hyperoxia AND Liver Cirrhosis Experimental AND Mammary Neoplasms Experimental AND FOUND IN nucleus AND perinuclear region of cytoplasm AND

				chromatin (ortholog) AND INTERACTS WITH (Z)-3-butylidenephthalide AND 1 3-dinitrobenzene AND 17alpha-ethynylestradiol; cyclin-dependent kinase 4 (Cdk4), mRNA.
Zfp958	-2.02	0.0011	0.0227	zinc finger protein 958
Entpd4	2.21	0.0011	0.0227	ectonucleoside triphosphate diphosphohydrolase 4
Zfp354a	2.74	0.0012	0.0243	zinc finger protein 354A
Anpep	2.11	0.0012	0.0249	alanyl (membrane) aminopeptidase
Slc25a23	2.02	0.0013	0.0252	solute carrier family 25 (mitochondrial carrier; phosphate carrier), member 23
Ier3	3.34	0.0013	0.026	immediate early response 3
Phkg2; PHKG2; LOC100909429	2.28	0.0013	0.026	phosphorylase kinase, gamma 2 (testis); Phosphorylase b kinase gamma catalytic chain, liver/testis isoform; ENCODES a protein that exhibits ATP binding AND calmodulin binding AND enzyme binding AND INVOLVED IN glycogen metabolic process AND protein phosphorylation AND PARTICIPATES IN glycogen degradation pathway AND calcium/calcium-mediated signaling pathway AND insulin signaling pathway AND ASSOCIATED WITH Glycogen Storage Disease AND Fibrosis (ortholog) AND Glycogen Storage Disease IXC (ortholog) AND FOUND IN phosphorylase kinase complex AND INTERACTS WITH (-)-epigallocatechin 3-gallate (ortholog) AND 17alpha-ethynylestradiol (ortholog) AND 2 3 7 8-tetrachlorodibenzodioxine (ortholog); ASSOCIATED WITH Glycogen Storage Disease IXC (ortholog) AND INTERACTS WITH 3H-1 2-dithiole-3-thione AND ammonium chloride AND cocaine; phosphorylase kinase, gamma 2 (testis) (Phkg2), mRNA.
Nr1h3	2.01	0.0013	0.0263	nuclear receptor subfamily 1, group H, member 3
St5; LOC102554209	2.3	0.0014	0.0269	suppression of tumorigenicity 5; ENCODES a protein that exhibits Rab guanyl-nucleotide exchange factor activity (ortholog) AND

				INVOLVED IN positive regulation of ERK1 and ERK2 cascade (ortholog) AND positive regulation of Rab GTPase activity (ortholog) AND INTERACTS WITH 2 3 7 8-tetrachlorodibenzodioxine AND benzo[a]pyrene AND ketamine; uncharacterized LOC102554209; suppression of tumorigenicity 5 protein [Source:RefSeq peptide;Acc:NP_001101017]
Cenpj	-2.91	0.0014	0.0273	centromere protein J
Akr7a3	2.56	0.0015	0.0277	aldo-keto reductase family 7, member A3 (aflatoxin aldehyde reductase)
Nde1	2.25	0.0015	0.028	nudE neurodevelopment protein 1
Aspdh	2.13	0.0015	0.028	aspartate dehydrogenase domain containing
Garem	2.18	0.0015	0.0282	Protein LOC679154; ENCODES a protein that exhibits proline-rich region binding (ortholog) AND INVOLVED IN cellular response to epidermal growth factor stimulus (ortholog) AND epidermal growth factor receptor signaling pathway (ortholog) AND positive regulation of cell proliferation (ortholog) AND INTERACTS WITH 2 3 7 8-tetrachlorodibenzodioxine (ortholog) AND aflatoxin B1 (ortholog) AND all-trans-retinoic acid (ortholog)
LOC367746	-2.04	0.0015	0.0284	similar to Spindlin-like protein 2 (SPIN-2) [Source:RGD Symbol;Acc:1584901]; similar to Spindlin-like protein 2 (SPIN-2); INVOLVED IN gamete generation (inferred) AND INTERACTS WITH (-)-demecolcine (ortholog) AND 17beta-estradiol (ortholog) AND 17beta-hydroxy-17-methylestra-4 9 11-trien-3-one (ortholog)
Sh3bgrl3	2.32	0.0015	0.0286	SH3 domain binding glutamate-rich protein like 3
Proser1	2.09	0.0016	0.0291	proline and serine rich 1
Mid1ip1	2.05	0.0017	0.0301	MID1 interacting protein 1
Csf1r	2.1	0.0017	0.0308	colony stimulating factor 1 receptor
Rnaseh2c	2.08	0.0017	0.031	ribonuclease H2, subunit C

Slc43a1	2.45	0.0018	0.0313	solute carrier family 43 (amino acid system L transporter), member 1
Vamp5	2.01	0.0018	0.0316	vesicle-associated membrane protein 5
Polr2k	-2.04	0.0018	0.0318	polymerase (RNA) II (DNA directed) polypeptide K
Prr16	2.2	0.0018	0.0318	proline rich 16
Gmcl1	2.01	0.0019	0.0323	germ cell-less, spermatogenesis associated 1
Pklr	2.45	0.0019	0.0326	pyruvate kinase, liver and RBC
Aqp11	2.21	0.0019	0.0327	aquaporin 11
Ppan	2.23	0.002	0.0333	peter pan homolog (Drosophila)
Noct	2.54	0.002	0.0336	nocturnin
Vipr1	2.23	0.002	0.0338	vasoactive intestinal peptide receptor 1
LOC100910833	2.06	0.0022	0.0354	histone-lysine N-methyltransferase setd3-like; ENCODES a protein that exhibits histone methyltransferase activity (H3-K36 specific) (ortholog) AND histone methyltransferase activity (H3-K4 specific) (ortholog) AND RNA polymerase II activating transcription factor binding (ortholog) AND INVOLVED IN histone H3-K36 methylation (ortholog) AND histone H3-K4 methylation (ortholog) AND peptidyl-lysine methylation (ortholog) AND FOUND IN nuclear chromatin (ortholog) AND INTERACTS WITH 17alpha-ethynylestradiol (ortholog) AND 2 3 7 8-tetrachlorodibenzodioxine (ortholog) AND Aroclor 1254 (ortholog)
Cox16	2.57	0.0022	0.0359	cytochrome c oxidase assembly protein 16
Slc25a10	2.45	0.0024	0.0372	solute carrier family 25 (mitochondrial carrier; dicarboxylate transporter), member 10
Kcnn2	2.08	0.0024	0.038	Uncharacterized protein; ENCODES a protein that exhibits calmodulin binding AND small conductance calcium-activated potassium channel activity AND alpha-actinin binding (ortholog) AND INVOLVED

				IN potassium ion transmembrane transport AND potassium ion transport AND regulation of neuronal synaptic plasticity AND PARTICIPATES IN calcium/calcium-mediated signaling pathway AND bile acid transport pathway AND FOUND IN dendritic spine AND integral component of membrane AND neuronal cell body AND INTERACTS WITH (+)-pilocarpine AND 2 3 7 8-tetrachlorodibenzodioxine AND amitriptyline
Mif	2.13	0.0024	0.0381	macrophage migration inhibitory factor (glycosylation-inhibiting factor) [Source:RGD Symbol;Acc:621163]; macrophage migration inhibitory factor (glycosylation-inhibiting factor); ENCODES a protein that exhibits protein complex binding AND chemoattractant activity (ortholog) AND cytokine activity (ortholog) AND INVOLVED IN aging AND brain development AND brain renin-angiotensin system AND PARTICIPATES IN phenylalanine metabolic pathway AND tyrosine metabolic pathway AND ASSOCIATED WITH Anti-Glomerular Basement Membrane Disease AND Arthritis Experimental AND Asthma AND FOUND IN cytoplasm AND extracellular space AND nucleus AND INTERACTS WITH 1 2 4-trimethylbenzene AND 17alpha-ethynylestradiol AND 2 4 6-trinitrotoluene; macrophage migration inhibitory factor (Mif), mRNA.
RT1-CE5	2.01	0.0026	0.0397	RT1 class I, locus CE5
Tm9sf1	2.03	0.0027	0.0406	transmembrane 9 superfamily member 1
A2ml1	2.21	0.0028	0.0412	alpha-2-macroglobulin-like 1
LOC102553249	-2.11	0.0028	0.0417	zinc finger protein 120-like [Source:RGD Symbol;Acc:7545273]
Mafb	2.26	0.0028	0.0419	v-maf avian musculoaponeurotic fibrosarcoma oncogene homolog B
Myeov2	2.57	0.0028	0.0419	myeloma overexpressed 2
Scimp	2.17	0.0031	0.0445	SLP adaptor and CSK interacting membrane protein

Pdpf	2.11	0.0032	0.0448	pancreatic progenitor cell differentiation and proliferation factor
Dgcr2	2.04	0.0032	0.0454	DiGeorge syndrome critical region gene 2
Il34	2.1	0.0033	0.0456	interleukin 34
Sema4b	2.18	0.0033	0.0456	sema domain, immunoglobulin domain (Ig), transmembrane domain (TM) and short cytoplasmic domain, (semaphorin) 4B
Junb	2.42	0.0034	0.0464	jun B proto-oncogene
LOC498446	-2	0.0036	0.0478	similar to Spetex-2C protein
Rcan1	2.34	0.0036	0.048	regulator of calcineurin 1
Rcan2	2.09	0.0037	0.0486	regulator of calcineurin 2
Ndufa5	-2.17	0.0037	0.0491	NADH dehydrogenase (ubiquinone) 1 alpha subcomplex 5
Dolk	2.05	0.0037	0.0492	dolichol kinase